



NBS SPECIAL PUBLICATION 563

U.S. DEPARTMENT OF COMMERCE / National Bureau of Standards

Advanced Composites: Design and Applications

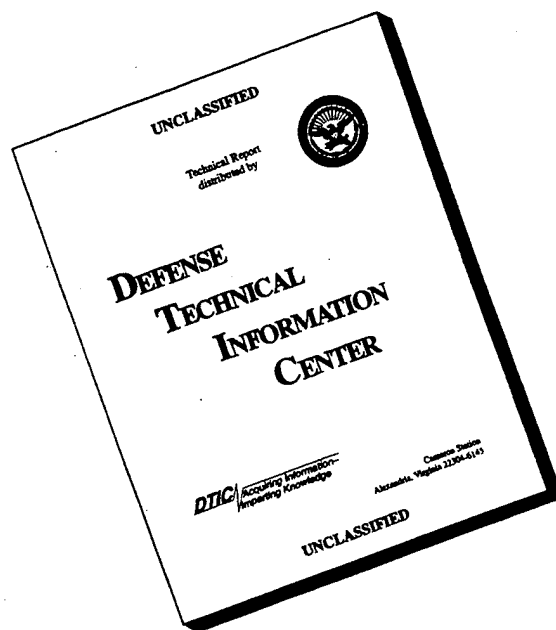
19960321 004

MFPG
29th Meeting

DEPARTMENT OF DEFENSE
PLASTICS TECHNICAL EVALUATION CENTER
ARRADCOM, ROVER, N. J. 07864

PLASTEC 35647

DISCLAIMER NOTICE



THIS DOCUMENT IS BEST QUALITY AVAILABLE. THE COPY FURNISHED TO DTIC CONTAINED A SIGNIFICANT NUMBER OF PAGES WHICH DO NOT REPRODUCE LEGIBLY.

Add 430021 -
430042

MFPG

Advanced Composites: Design and Applications

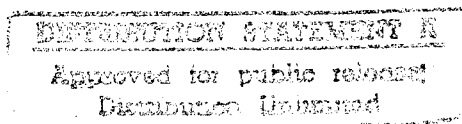
Proceedings of the 29th Meeting of the
Mechanical Failures Prevention Group,
held at the National Bureau of Standards,
Gaithersburg, Maryland, May 23-25, 1979.

Edited by

T. Robert Shives and William A. Willard

Center for Materials Science
National Measurement Laboratory
National Bureau of Standards
Washington, DC 20234

The 29th meeting of the MFPG and these proceedings were sponsored by
the Center for Materials Science of the National Bureau of Standards,
Washington, DC 20234; the Office of Naval Research, Department of the
Navy, Arlington, VA 22217; the Naval Air Systems Command, A. J. Koury,
Washington, DC 20360; the National Aeronautics and Space Administra-
tion, Goddard Space Flight Center, Greenbelt, MD 20771; and the
Department of Energy - Fossil Energy, Washington, DC 20545.



U.S. DEPARTMENT OF COMMERCE, Juanita M. Kreps, Secretary

Luther H. Hodges, Jr., Under Secretary

Jordan J. Baruch, Assistant Secretary for Science and Technology

NATIONAL BUREAU OF STANDARDS, Ernest Ambler, Director

Issued October 1979

DTIC QUALITY INSPECTED 1

Library of Congress Catalog Card Number: 79-600151

National Bureau of Standards Special Publication 563

Nat. Bur. Stand. (U.S.), Spec. Publ. 563, 304 pages (Oct. 1979)

CODEN: XNBSAV

U.S. GOVERNMENT PRINTING OFFICE
WASHINGTON: 1979

For sale by the Superintendent of Documents, U.S. Government Printing Office, Washington, D.C. 20402

Stock No. 003-003-02120-2 Price \$7.00
(Add 25 percent additional for other than U.S. mailing)

FOREWORD

The 29th meeting of the Mechanical Failures Prevention Group was held May 23-25, 1979, at the National Bureau of Standards in Gaithersburg, Maryland. The program was organized by the Design Committee under the chairmanship of Jesse E. Stern of the Goddard Space Flight Center. The committee, the session chairmen, and especially the speakers are to be commended for the excellent program. Special appreciation is extended to Harriet Gordon of the Goddard Space Flight Center for her expert coordination and preparation of the many items of correspondence that were generated in order to develop the technical program into its final form.

The symposium opened with a welcome to the National Bureau of Standards by Dr. Elio Passaglia, Deputy Director of the Center for Materials Science. Dr. Passaglia's comments centered on the continuing need for standards and accuracy of measurements especially in the design and application of new materials such as those to be discussed at the symposium.

Appreciation is extended to the following members of the NBS Fracture and Deformation Division: T. Robert Shives and William A. Willard for their editing, organization and preparation of the proceedings, and Joel C. Sauter for photographic work. Most of the papers in the proceedings are presented as submitted by the authors on camera ready copy. Some moderate editorial changes were required.

Gratitude is expressed to the following members of the NBS Center for Materials Science: Marian L. Slusser for handling financial matters, Delores J. Covey for typing, and Larry W. Ketron for drafting work.

Special thanks is extended to Jo Ann Lorden of the NBS Public Information Division for the meeting, hotel and banquet arrangements.

HARRY C. BURNETT
Executive Secretary, MFPG

Center for Materials Science
National Bureau of Standards

TABLE OF CONTENTS

Page

III

FOREWARD

SESSION 1: AEROSPACE AND AIRCRAFT APPLICATIONS AND DESIGN

- A. Characterization and Application of Advanced Composite Materials (abstract only). Max Waddoups 3
- B. Physical and Mechanical Response of Graphite/ Polyimide Materials to Long Term Exposure in a Space Environment; Material Preparation and Control Testing. J. H. Powell 35648 (4)
- C. Effects of Room-Temperature Aging on Composite Prepregs. H. C. Nash, C. F. Poranski, Jr.*, and R. Y. Ting 35649 (17)

SESSION 2: AEROSPACE AND AIRCRAFT APPLICATIONS AND DESIGN

- A. Application of Instrumental Techniques to the Study of the Cure of Phthalocyanine/Graphite Composites. Robert Y. Ting 35650 (25)
- B. Moisture Diffusion Analysis for Composite Micro-damage. C. L. Leung* and D. H. Kaelble 35651 (32)
- C. Recent Work on Techniques and Applications of Moisture Barriers to Graphite Epoxy Composites. James F. Haskins 35652 (47)

SESSION 3: AEROSPACE AND AIRCRAFT APPLICATIONS AND DESIGN

- A. In-Service Ultrasonic Inspection System for Composites (abstract only). F. H. Chang*, J. R. Bell, A. H. Gardner, C. P. Fisher and G. P. Handley 35653 59
- B. Design Considerations for Graphite-Epoxy Laminates of Low Thermal Expansivity. Dennis D. Smith 35654 (60)

- guy
- C. Aircraft Composite Materials Selection and Application. V. L. Reneau 35655

72

- D. Composite Structures in Rotors and Propellers. David F. Thompson 35656

80

SESSION 4: AEROSPACE AND AIRCRAFT APPLICATIONS AND DESIGN

- A. Development of a Library Module for the Analysis of Advanced Composite Materials. Karyn T. Knoll 35657

91

- B. Structural SMC - Material, Process and Performance Review. Ralph B. Jutte (presented by Joseph D. Feko, Owens-Corning Fiberglas Corporation) 35658

108

- C. Development of a Graphite-Epoxy Spacecraft Precision Mounting Platform (abstract only). Kathleen S. Budlong and Alvin W. Sheffler 130

SESSION 5: AUTOMOTIVE APPLICATIONS AND DESIGN

- A. Design Analysis of Automotive Composite Structures (abstract only). M. F. Kowalski, D. S. Fine*, and R. K. Herrman 133

- B. Fiberglass Reinforced Plastics Use in Transportation Vehicles (abstract only). R. D. Pistole 134

- guy
- C. Designing Automotive Components with Continuous Fiber Composites. H. T. Kulkarni* and P. Beardmore 35659

135

SESSION 6: INDUSTRIAL APPLICATIONS AND DESIGN

- guy
- A. Fabrication of Large Composite Spars and Blades. O. Weingart (presented by Robert Gordon, Structural Composite Industries, Inc.) 12-31/83

155

- B. The Effect of Fiber Orientation on the Design Parameters of Reinforced and Filled Thermoplastic Compounds (abstract only). Peter J. Cloud* and Robert T. Alvord 173

- C. Quality Assurance of Manufactured Components 174
(abstract only). R. D. Margolis

SESSION 7: INDUSTRIAL APPLICATIONS AND DESIGN

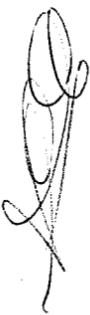
- A. Degradation Data of Kevlar Pressure Vessels. 35660 177
W. D. Humphrey
- B. Design Assurance of a Leak Failure Mode for 35661 198
Composite Overwrapped Metal Tankage. W. W. Schmidt
- C. Composite Materials in Recreational Equipment 208
(abstract only). David Ratchford

SESSION 8: INDUSTRIAL APPLICATIONS AND DESIGN

- A. Holographic Nondestructive Evaluation of Spherical 211
Kevlar/Epoxy Pressure Vessels. D. M. Boyd* and
B. W. Maxfield
- B. The Air Force "Manufacturing Cost/Design Guide 226
(MC/DG)" (abstract only). Bryan R. Noton* and Captain
Dan L. Shunk
- C. Tensile Strength and Failure Modes of Boron-Epoxy 228
Composites with a Notch. Charles E. S. Ueng

SESSION 9: FAILURE MODES IN ADVANCED COMPOSITES

- A. Failure Criteria for Composites under Complex 241
Loading (abstract only). P. W. Mast*, L. A. Beaubien,
D. R. Mulville, S. A. Sutton, R. W. Thomas, J. Tirosh
and I. Wolock
- B. Failure Analysis of an Idealized Composite Damage 242
Zone. Carl T. Herakovich* and David A. O'Brien
- C. Interlaminar Failure in Epoxy Based Composite 255
Laminates. A. S. Wang*, F. W. Crossman and
G. E. Law, Jr.



SESSION 10: MARINE APPLICATIONS AND DESIGN

- 38666
- A. Current Developments in Advanced Composites for Naval Ship Application. J. J. Kelly* and H. H. Vanderveldt
- 267
- B. Environmental Effects on Fiber Reinforced Organic Matrix Composites. M. Silvergleit*, A. B. Macander, F. A. Brauer, and H. P. Edelstein
- 276
- C. Composite Technology for Marine Application.
- 286
- W. P. Couch

APPENDIX

List of Registrants for the 29th MFPG Meeting.	301
MFPG Publications	307

*Indicates speaker when a paper had more than one author.

ABSTRACT

These proceedings consist of a group of thirty one submitted entries (twenty one papers and ten abstracts) from the 29th meeting of the Mechanical Failures Prevention Group which was held at the National Bureau of Standards in Gaithersburg, Maryland, May 23-25, 1979. The subject of the symposium was the design and application of advanced composites. Special emphasis was directed to aerospace, aircraft, automotive, marine, and industrial applications and design. Failure modes in advanced composites were also discussed.

Key words: Advanced composites; applications of composites; composites; composite structures; design using composites; fiber composites; fiber glass; filament wound composites.

UNITS AND SYMBOLS

Customary United States units and symbols appear in some of the papers in these proceedings. The participants in the 29th meeting of the Mechanical Failures Prevention Group have used the established units and symbols commonly employed in their professional fields. However, as an aid to the reader in increasing familiarity with the usage of the metric system of units (SI), the following references are given:

NBS Special Publication, SP330, 1977 Edition, "The International System of Units."
ISO International Standard 1000 (1973 Edition), "SI Units and Recommendations for Use of Their Multiples."
E380-76 ASTM/IEEE Standard Metric Practice (Institute of Electrical and Electronics Engineers, Inc., Standard 268-1976).

Disclaimer:

Certain trade names and company products are identified in order to adequately specify the experimental procedure. In no case does such identification imply recommendation or endorsement by the National Bureau of Standards, nor does it imply that the products are necessarily the best available for the purpose. Views expressed by the various authors are their own and do not necessarily represent those of the National Bureau of Standards.

SESSION 1

AEROSPACE AND AIRCRAFT APPLICATIONS AND DESIGN

Chairman: J. E. Stern

Goddard Space Flight Center

Characterization and Application of Advanced Composite Materials

Max Waddoups
General Dynamics, Fort Worth Division
Fort Worth, Texas 76101

Abstract

A technical understanding of the structural characteristics of composite materials and the critical issues in aircraft structural component development have been simultaneously generated. It is established that the strengthening concept, structural characteristics, and fabrication techniques are distinct from metals. These differences and the resultant structural implications are the subject of this lecture.

For practical purposes, composites are linear elastic. Tensile failure modes are brittle fracture governed, and compressive failure modes are micro and macro stability governed. Even though composites have no classical ductility, they are surprisingly tough materials. In most full-scale structures currently developed, tensile fracture constitutes the critical strength failure mode.

While generally tensile fracture governs strength, an equivalent-to-crack coalescence and monotonic growth in tension are not observed in composites (except glass-fiber-reinforced plastics). In fact, tension-dominated cracking is not of serious consequence in advanced laminates. Weak plane (intralaminar and interlaminar) flaw propagation, predominantly in compressive and shear loadings, yields the lift limiting failure modes for composites. When modeled as strain-energy release-rate-driven flaw-growth processes, different growth rates and initial strengths generate competing failure modes in full-scale structures.

Simple structural forms that control the life-limiting failure processes will become the rule for successful structures. Only on stiffness critical or fairing type of structure will the complex shape moldability advantages of composites be used.

Because of the scale effects in the fracture process zone and the ability to react significant out-of-plane loads, simple mechanical fastening will dominate highly loaded, strength-critical structure. Secondary adhesive bonding will not be very successful in highly loaded fracture critical structure.

PHYSICAL AND MECHANICAL RESPONSE OF
GRAPHITE/POLYIMIDE MATERIALS TO LONG TERM EXPOSURE
IN A SPACE ENVIRONMENT; MATERIAL PREPARATION AND
CONTROL TESTING

J. H. Powell
Rockwell International
Tulsa, Oklahoma 74151

Abstract: Graphite/polyimide (Gr/PI) composite laminates are currently being prepared for deployment on NASA Langley Research Center's Long Duration Exposure Facility (LDEF). The experiment is intended to provide scientific and engineering design information on the response of Gr/PI composites to an actual exoatmospheric environment. Material systems to be exposed are a bismaleimide PI (Hexcel F-178) on Thorne1 300 graphite fibers and a condensation PI (Monsanto Skybond 703) on HT-S graphite fibers, including both "precured" and "cocured" laminates. Initial physical characteristics determined on both exposure and simultaneously processed control panels include flatness, microcracking, void content, dry weight, and general appearance. Mechanical tests performed to date (on control panels only) are the basis for strength and elastic properties in tension, compression, and (rail) shear at ambient and elevated temperatures. Following in-space exposure of test panels and return to earth, identical physical and mechanical determinations will be made. Data generated before and after exposure will be compared to identify any changes in physical or mechanical characteristics, particularly any unexpected changes. The ultimate output of the experiment will be either confirmation of predicted material behavior or the basis for revised prediction methods.

Key Words: Exoatmospheric exposure of composites; polyimide/graphite mechanical properties; polyimide composite stability in space; Long Duration Exposure Facility (LDEF); ultrasonic inspection; cocured and precured laminates.

The essentially universal organic matrix material currently used in aerospace advanced composite structures is that based upon epoxide chemical polymerization mechanisms -- for several excellent reasons. As a class, epoxy resin systems are well characterized, allowables are established for many of them, processing procedures are essentially trouble free, well developed, reproducible and compatible with existing industry processing equipment. The Space Shuttle Vehicle employs epoxy/graphite composite in two major structural components -- the payload bay doors and orbital maneuvering system (OMS) pods, both

applications resulting in substantial weight savings even though requiring external insulation. Epoxies are, however, approaching their upper temperature capability for efficient operation; in addition to which their capability is further limited by absorbed moisture at elevated temperatures.

Appreciable gains in high temperature performance must therefore be sought in the higher temperature resistant systems, the more promising current materials belonging to the polyimide family. Increasing temperature capability by 100 to 250F over the present 250 to 350F maximum operating range of epoxies potentially saves critical weight through higher operating allowables or reduced insulation requirements. Under discretionary company funding, Rockwell International's Tulsa Division had previously investigated two interim, conventionally processible polyimide systems, one suitable for 450F use, the other for 550 to 600F use. When the Long Duration Exposure Facility (LDEF) project solicited proposals for experiments, Rockwell-Tulsa responded and was awarded a contract¹ to test these two materials.

Objective: The experiment is intended to accumulate design and scientific data associated with long term exposure in a space environment, including any evidence of changes in mechanical properties, weight loss, dimensional instability, microcrack growth, delamination, or other degradation due to hitherto "unknowns". An addition polyimide (API) and a conventional condensation polyimide (CPI) will be evaluated both in the "precured" and "cocured" laminate form. By comparing post-exposure with control data, previous assumptions and prediction tools will be verified or corrected as necessary.

Experiment description: Essential elements of the experiment are described sequentially below under the enumerated headings: (1) test vehicle, (2) general experiment flow, (3) materials, (4) panel design, (5) processing, (6) non-destructive examination, (7) specimens preparation and testing, (8) test evaluation and analysis, and (9) loading and shipment of experiment.

(1) The test vehicle is the LDEF structure (Figure 1) which is currently estimated to be launched between late 1980 and late 1981 during one of the regular Space Shuttle missions. Test panels are mounted in one of two trays, the arrangement of that for 3 panels shown in Figure 2. The LDEF is released from the orbiting Space Shuttle at an extremely low acceleration and put into its own independent orbit at an average distance of 235 nautical miles above the earth's surface. The orbital period will be about 92 minutes, or 15.6 revolutions per 24 hours. In stabilized flight, the LDEF will maintain a fixed attitude, the projection of its longitudinal axis passing through the center of the earth. Initial oscillatory motions experienced during release will

¹NASA Langley Research Center Contract NAS1-15309, March 1978.

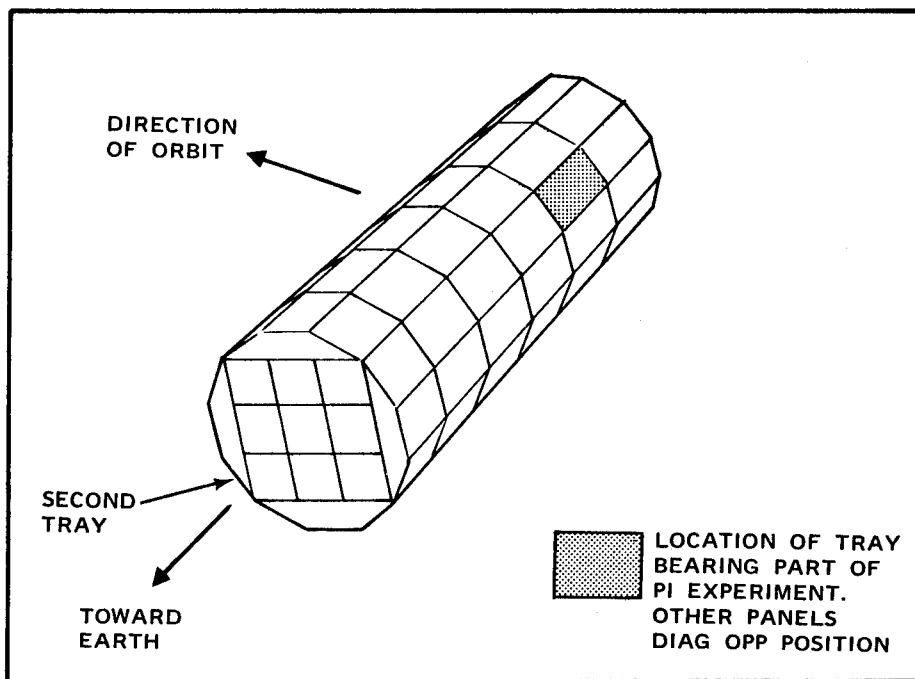


Figure 1. Long Duration Exposure Facility (LDEF);
Dimensions 30 Feet Long x 13.5 Feet In
Diameter

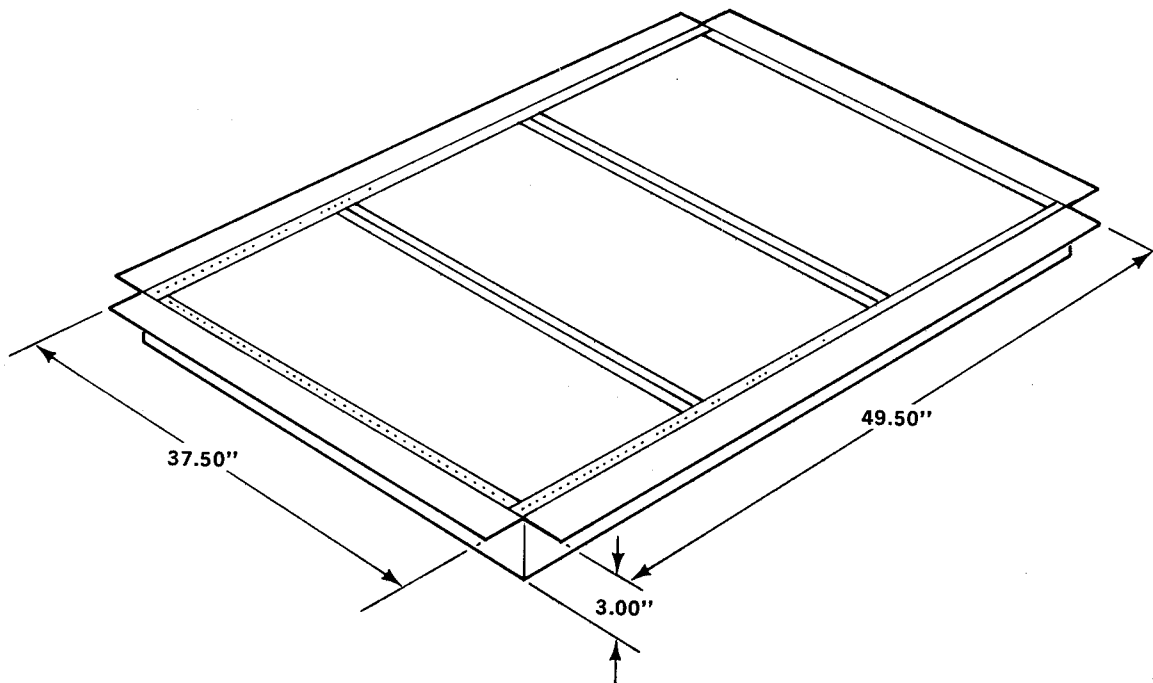


Figure 2. LDEF Tray Conceptual Sketch Showing
3-Panel Arrangement

dampen out within a few days. After 6 to 12 months in orbit, the LDEF will be retrieved during a subsequent Shuttle mission and returned to earth. During this period, the test panels will be exposed to alternating low and high temperatures, calculated to range between -109F and +236F, and various types and levels of radiation endemic to the space environment. Ambient pressure is assumed to be on the order of 1×10^{-10} torr. While the Gr/PI experiments are completely passive, the LDEF vehicle will be equipped to acquire and record certain information, e.g. temperatures and impinging radiation at various locations on the structure. The position of each experiment will also be ascertained after the fact. Through use of applicable analysis techniques, the exposure environment for each experiment can be reconstructed.

(2) General experiment flow is shown in Figure 3. Two matched sets of panels are subjected to an identical series of operations, excepting of course that one set is exposed on the LDEF. Both "precured" and "co-cured" laminates are prepared for each material type (condensation and addition). All panels are nondestructively inspected, employing ultrasonic through transmission, microscopy, and physical measurement techniques. Finally, panels are sectioned and mechanically tested. Data from the two sets of panels are analyzed and compared, and the effects of exposure to the space environment assessed.

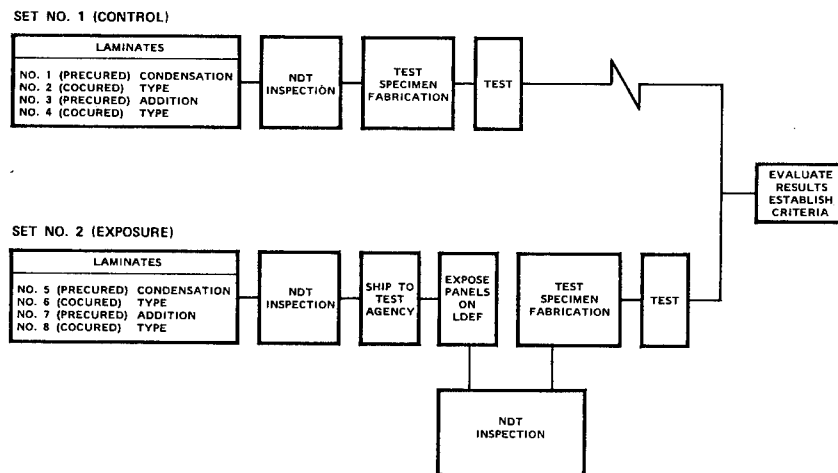


Figure 3. General Experiment Flow

(3) Material systems used in the experiment are representative of two polyimides, the standard vacuum bag/autoclave processible condensation PI's and the more recent intermediate temperature vacuum bag/autoclave processible addition PI's. Neither system requires pressure in excess of 100 psi nor curing temperature in excess of 350F. The condensation system (CPI) selected is Ferro Corporation's CPI - 2249 (Monsanto Sky-bond 703)/HT-S collimated tape, molding to a ply thickness of .0055 inch at 63% fiber volume. This system was selected on the basis of past successes in IR&D projects where both tape and fabric systems

were conventionally autoclave processed, yielding good mechanical properties in tension and compression at room temperature and 600F. The system is considered an interim material, ultimately to be replaced by advanced systems, but still having many potential applications at an economical cost. The addition system (API) is Hexcel's F-178 bismaleimide on Thornel 300 fibers, supplied in tape form and molding to a ply thickness of .005 inch at 65% fiber volume. This system processes much like epoxies, exhibits superior moisture resistance and offers about 100F more temperature resistance. It and similar emerging API systems offer excellent potential for application in the 400 to 450F temperature regime at an economical processing cost.

(4) Panels were designed to represent a commonly applied fiber orientation, i.e. quasi-isotropic $(0, +45, 90)_n$ construction. The specific panel geometry, i.e. planform dimensions and thickness were analyzed to verify ability to withstand environmental requirements of the governing NASA document.¹ Table I summarizes the key elements of the dynamic environment that were considered in designing panels. The critical design condition was a natural frequency of 50 Hertz, minimum, for each panel when simply supported along its four edges. Overall panel sizes were determined by LDEF tray geometry and the number of specimens needed to provide 5 replicates of each specimen type and test condition (Figure 4). Thickness was determined by minimum panel stiffness requirements.

Panels are mounted in trays on specially designed support structures which are unique to these particular experiments. Figure 5 conceptually illustrates tray support structure and test panel. Both tray and support are constructed from aluminum alloy, thus have high coefficients of thermal expansion. Graphite laminates, on the other hand, have very low thermal expansion. Panels are therefore attached by clamping, allowing surrounding structure to expand and contract freely with temperature change without loading or buckling test panels. A thermal isolation septum is placed between the experiments and interior of the LDEF to minimize interaction between the internal and external environments.

(5) Test panels are processed in a conventional autoclave at 85-100 psig and 350F. Both polyimide types are prebled prior to final cure, using part of the calculated bleeder material during prebleeding and the remainder during cure. The API is processed much like epoxy, being essentially a volatile-free prepreg. The CPI, on the other hand, requires a relatively long, 200F dwell under full vacuum to release a large part of the N-methyl pyrrolidone (NMP) solvent. Autoclave pressure is applied at the beginning of heat up, and curing completed at 350F. The API is postcured without restraint in an oven at 450F for 16-20 hours, the CPI for 96 hours at temperatures progressing from

¹Long Duration Exposure Facility (LDEF) Experimenter Users Handbook, LDEF No. 840-2, LDEF Project Office, Langley Research Center, Hampton, Virginia

Table I. Summary of General Environmental Conditions, Dynamic Environments

	ACCELERATION	VIBRATION	ACOUSTIC	SHOCK										
<u>GROUND HANDLING</u>	<u>1.0g Steady State</u> (Gravity) <u>Hoisting Operations:</u> Up to 2g short term (≥ 0.1 Sec) with directions up to 20° away from the local vertical	<u>Transportation: Sinusoidal</u> <u>Equivalent</u> 4 Sweeps, 0.5 oct/min 2-5 Hz: 1.0 inch, d.a. 5-26 Hz: 1.3g, 0 to Peak 26-50 Hz: 0.036 inch d.a. 50-1000 Hz: 5g, 0-to-peak (d.a. is double amplitude)		<u>Bench Handling</u> 20g terminal peak Sawtooth; 11 millisecond pulses Both directions along 3 mutually perpendicular axes										
<u>LAUNCH AND POWERED FLIGHT</u>	<u>L</u> <u>N&M</u> Liftoff ± 2.90g ± 1.80g High Q ± 2.00g ± 0.80g Max Boost ± 3.30g ± 0.36g Shuttle Max ± 3.30g ± 1.10g End Trays Apply L Values in all 3 directions	<u>Random (FAT)</u> 7.31 grms, 3 axes, 30 sec/axis 16-1000 Hz: Shaped Spectrum 16-60 Hz: 6 db/oct, roll up 60-300 Hz: 0.1g ² /Hz Flat 300-100 Hz: 6 db/oct, roll off <u>Sinusoidal (FAT)</u> Sweep 4 octaves/min 5-14 Hz: 0.5 inch d.a. 14-20 Hz: 5.0g 0-to-peak 20-35 Hz: 1.0g 0-to-peak	Overall: 145 db Maximum Acoustic Exposure Spectrum;	<u>Emergency Landing</u> as defined for Retrieval Acceleration										
<u>ORBIT, FREE FLYING</u>	Transients after deployment: 1 X 10 ⁻³ g Steady State: 1 x 10 ⁻⁶ g													
<u>RETRIEVAL-RE-ENTRY AND LANDING</u>	<u>L</u> <u>N&M</u> Entry (Pitch) ± 1.06g ± 2.80g Entry (Yaw) ± 0.75g ± 1.80g Landing ± 1.00g ± 2.84g Emergency Landing ± 4.50g ± 4.50g Emergency Landing applies to Ultimate Stress Conditions		Overall reaches 135 db Max in 1 percent of Entry Cases <table><tr><td>Landing Shock Applications</td></tr><tr><td><u>g peak</u> <u>m sec</u> <u>occurs</u></td></tr><tr><td>0.23 170 22</td></tr><tr><td>0.28 280 37</td></tr><tr><td>0.35 360 20</td></tr><tr><td>0.43 360 20</td></tr><tr><td>0.56 350 9</td></tr><tr><td>0.72 320 4</td></tr><tr><td>1.50 260 1</td></tr><tr><td>125</td></tr></table>	Landing Shock Applications	<u>g peak</u> <u>m sec</u> <u>occurs</u>	0.23 170 22	0.28 280 37	0.35 360 20	0.43 360 20	0.56 350 9	0.72 320 4	1.50 260 1	125	
Landing Shock Applications														
<u>g peak</u> <u>m sec</u> <u>occurs</u>														
0.23 170 22														
0.28 280 37														
0.35 360 20														
0.43 360 20														
0.56 350 9														
0.72 320 4														
1.50 260 1														
125														

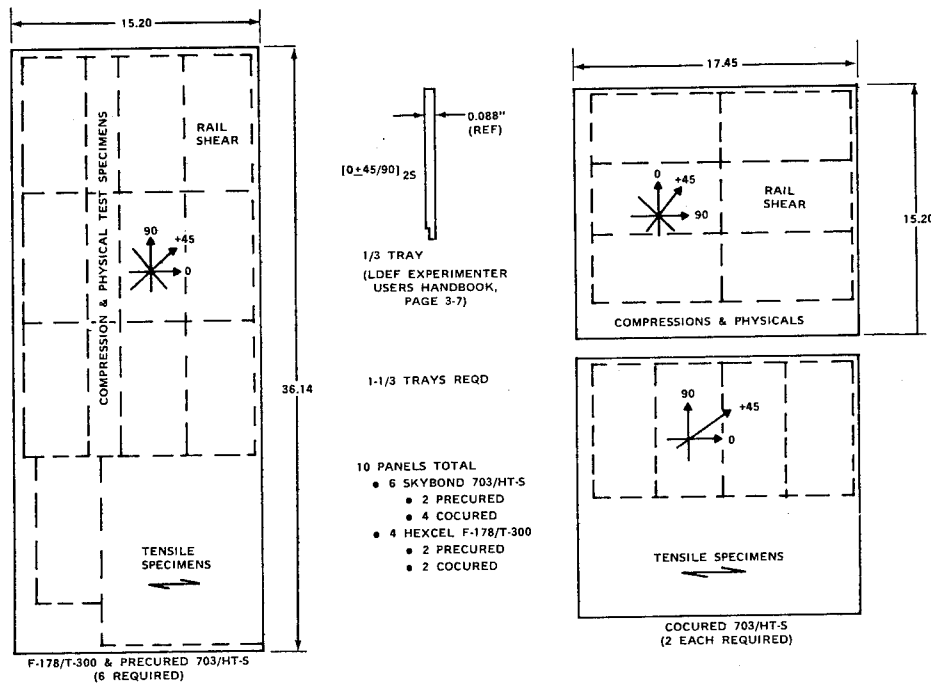


Figure 4. Test Laminate for Graphite/Polyimide Experiments Showing Layouts of Test Specimens

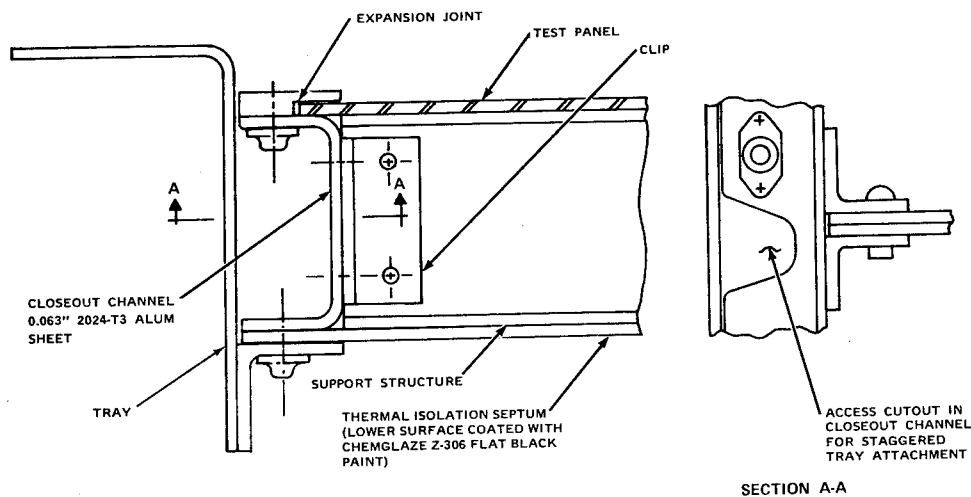


Figure 5. Support Structure Conceptually Shown Including Interface With LDEF Tray

350F to 600F. "Precured" panels are molded directly against a smooth platen, while "cocured" panels are molded over honeycomb core with a non-porous fluorocarbon film between core and laminate. The pattern of the honeycomb is thus imparted to one surface of the cocured laminate.

(6) Non-destructive examination is performed using ultrasonic through transmission, visual examination, photomicroscopy, and physical measurement. Ultrasonic measurements are made with the panel fully immersed in a water tank, and panel quality is assessed by transmitting an ultrasonic signal through the panel normal to its surface. Attenuation of the input signal indicates voids, discontinuities, or other anomalies and is evidenced by loss of received signal or blank regions in the closely spaced pen lines drawn by the recorder. Input signal can be adjusted to accommodate different panel thicknesses or uniformly dispersed voids by varying the signal frequency and gain. The inherent void containing CPI system can thus be measured to detect blistered and delaminated areas. Panels will be examined ultrasonically both before and after space exposure. Laminate surfaces and edges are examined with and without the aid of a low-powered lens for general uniformity in appearance, and for evidence of resin starving, roughness, fiber splintering, cracks, and other anomalies. Specimens representing typical regions of laminates will be potted in resin with edges normal to the surface, ground and polished, then examined under high magnification. Photo-micrographs of sound, microcracked, and porous areas will document the typical condition. Physical measurements determine cupping, bowing, and twisting. With three corners of a panel touching a surface table (i.e. in one plane), twist is easily determined by departure of the fourth corner from plane. With the panel placed concave upward on a surface, cupping and bowing are directly measurable with a straight edge.

(7) Specimens are cut from test panels according to the layout schemes shown in Figure 4. Test specimens have the geometries shown in Figure 6. In all panels, the zero degree (0) reference direction is defined by the fiber direction of surface plies. Hence, tension specimens are laid out with their long axes in the (0) direction, while rail shears and compression specimens have their long axes parallel to the (90) direction. Layout directions were dictated by specimen and panel dimensions, thus options for specimen orientations were limited. The grip regions of high temperature tensile specimens are tabbed with aluminum to produce the desired type of failure. A "gripper" strip about one and one-half inch wide is bonded to each surface of the long edges of rail shear specimens. This has been found necessary to prevent slippage of specimens in the test fixture. Slippage promotes premature bearing failures in specimens, thus not demonstrating full shear strength.

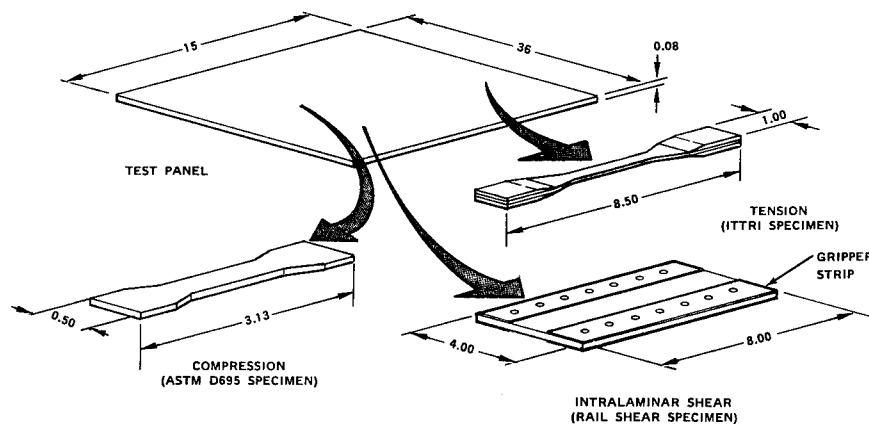


Figure 6. Mechanical Test Specimen Configurations

Table II presents the test matrix for control panels. The elevated temperature test condition for API (addition) specimens is 450F, for CPI (condensation) specimens, 600F. API control panels, laid out for specimen cutting are shown undergoing warp and twist measurement in Figure 7. Subsequent to space flight, exposure panels will be sectioned and tested in an identical manner.

Testing is performed in a 20,000 pound capacity Instron Testing Instrument equipped with automatic load vs. strain plotting capability and a high temperature Conrad-Missimers test chamber.

(8) Upon completion of control testing for each panel type, test data will be analyzed, compared with predictions made during the experiment design task, and compared with requirements. Upon verification of compliance with requirements, exposure panels will be ready for installation in LDEF trays.

(9) Exposure test panels will be trimmed to final dimensions on assembly in LDEF trays. The support structures will have been assembled in situ in trays prior to installing test panels. Edge retainers which clamp test laminates in place are made from aluminum shim stock, which can be stripped to accommodate variable panel thicknesses. Trays were received from NASA installed, shock mounted in reusable shipping containers, and will be returned in like manner. Figure 8 shows one of the two trays provided and support structure, which will contain the cocured CPI panels. This tray also contains graphite/epoxy test panels made under the "sister" experiment to the polyimide experiment, in addition to the two smaller cocured CPI panels.

Test results to date: The control testing phase of the experiment was incomplete at the time of this paper's issue; thus, only part of the control test data to be generated is reported herein. Exposure tests are not expected to be completed before the 1981-1982 time period.

Table II. Test Matrix for Control and Exposure Specimens

LAMINATE NUMBER	CURE PROCESS		SIZE	NO. REQD*	TEST	TEST TEMP		MATERIAL TYPE		INSTRUMENTATION
	PRECURED	COCURED				RT	ET	COND	ADDITION	
60-001	X		8.50 X 1.0	10	TENSION	X	X	X		EXTENSIONETER
60-005		X	8.50 X 1.0	10	TENSION	X	X	X		EXTENSIONETER
60-009	X		8.50 X 1.0	10	TENSION	X	X		X	EXTENSIONETER
60-003		X	8.50 X 1.0	10	TENSION	X	X		X	EXTENSIONETER
60-001	X		0.5 X 3.13	10	COMPRESSION	X	X	X		COMPRESSIONETER
60-005		X	0.5 X 3.13	10	COMPRESSION	X	X	X		COMPRESSIONETER
60-009	X		0.5 X 3.13	10	COMPRESSION	X	X		X	COMPRESSIONETER
60-007		X	0.5 X 3.13	10	COMPRESSION	X	X		X	COMPRESSIONETER
60-001	X		4.0 X 8.0	10	SHEAR	X	X	X		BI-AXIAL S/G
60-005		X	4.0 X 8.0	10	SHEAR	X	X	X		BI-AXIAL S/G
60-009	X		4.0 X 8.0	10	SHEAR	X	X		X	BI-AXIAL S/G
60-003		X	4.0 X 8.0	10	SHEAR	X	X		X	BI-AXIAL S/G
60-007		X	4.0 X 8.0	10	SHEAR	X	X		X	BI-AXIAL S/G

NOTES: *10 SPECIMENS PER LAMINATE - 5 PER TEST TEMPERATURE
 **ITRI SPECIMEN
 ***ASTM D695
 ****RAIL SHEAR

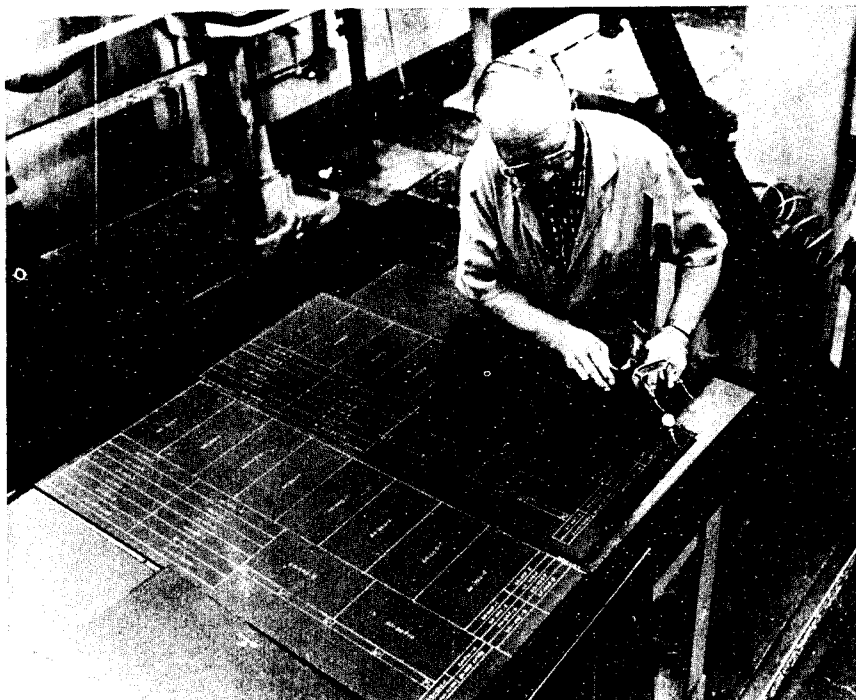


Figure 7. Measurement of Warp and Twist in API Control Panels

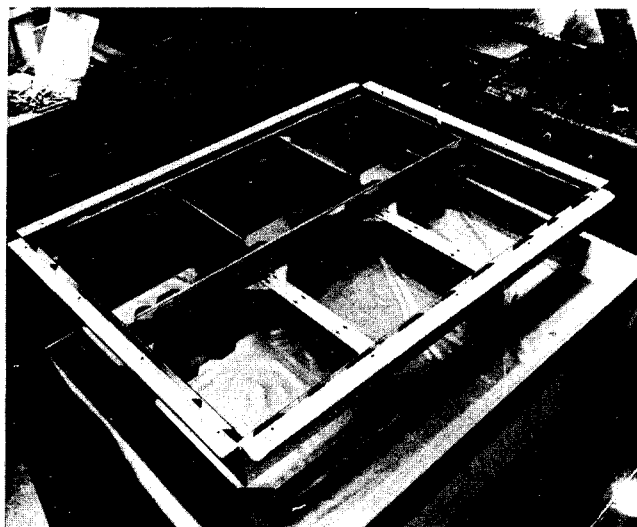


Figure 8. LDEF Tray and Support Structure

Thus, final evaluations will probably not be available until 1982. Control test data generated thus far are reported in Tables III and IV, and Figure 9.

While the major significance of the experiment will not be known until exposure panels are returned from space, some general impressions resulting from API panel fabrication and testing may be cited. First, the bis-maleimide/graphite prepreg molded readily without incident. Non-destructive testing indicated freedom from significant porosity and other flaws. Microscopic studies have not been performed to date, and will now probable be accomplished simultaneously with those done on exposed panels. Similarly, part of the control testing will be performed at this latter time, to accommodate possible diversion of some testing to other more significant investigation in the event of unanticipated exposure effects.

The API system retained about 80% of matrix critical room temperature properties at 450F. Bending (plate) stiffness of panels is high enough to meet natural frequency requirements during Space Shuttle launch and landing. Dimpling associated with cocuring tends to reduce properties 3-13% as shown in Figure 10.

Condensation polyimide control specimens will be tested in modes similar to those used in API testing upon availability of test panels. The elevated temperature will, of course, be 600F.

Acknowledgments: The author is indebted to Mr. D. W. Welch, co-investigator, for direction of the analytical activity associated with this experiment; to Mr. G. T. Smith for panel processing and test specimen preparation; and to Mr. R. E. Haak for direction of support structure fabrication and mechanical testing.

Table III. Physical and Mechanical Properties of
Bismaleimide/Graphite Modified Quasi-Isotropic
Laminates [0(0/+45/90)_{2s}0], Hexcel
F-178/T-300, Precured

PROPERTY	ROOM TEMPERATURE				450 F			
	NUMBER OF SPECIMENS	TEST VALUE			NUMBER OF SPECIMENS	TEST VALUE		
		LOW	HIGH	AVG		LOW	HIGH	AVG
TENSILE STR, ULT [0], KSI	5	61.2	71.6	66.5	3	69.7	73.6	71.7
TENSILE MOD [0], MSI	5	7.37	8.12	7.85	3	7.50	8.26	7.78
COMPRESSIVE STR, ULT [0], KSI	4	62.8	70.1	67.2				
COMPRESSIVE STR, ULT [90], KSI	4	44.5	51.8	47.7	3	37.7	45.4	40.9
COMPRESSIVE MOD [0], MSI	4	7.57	8.22	7.98				
COMPRESSIVE MOD [90], MSI	5	5.92	6.67	6.29	3	6.51	6.74	6.63
RAIL SHEAR STR, ULT [90/0], KSI	2	27.4	28.5	28.0	1			22.3
RAIL SHEAR MOD [90/0], MSI	2	2.21	2.40	2.30	1			2.38
FLEXURAL STR, ULT [0], KSI	4	152.6	159.2	156.9				
FLEXURAL MOD [0], MSI	4	11.20	11.59	11.32				
BENDING STIFFNESS, EI, LB-IN. ²	4	345	416	368				
INTERLAM SHEAR STR, ULT [0], KSI	5	5.46	6.50	5.99				
PHYSICAL PROPERTIES	SP GR 1.57, FIBER VOL FRAC 0.61, MOLDED PLY THICKNESS 0.0053 IN.							

Table IV. Physical and Mechanical Properties of
Bismaleimide Polyimide/Graphite Modified Quasi-
Isotropic Laminates [0(0/+45/90)_{2s}0], Hexcel
F-178/T-300, Cured

PROPERTY	ROOM TEMPERATURE				450 F			
	NUMBER OF SPECIMENS	TEST VALUE			NUMBER OF SPECIMENS	TEST VALUE		
		LOW	HIGH	AVG		LOW	HIGH	AVG
TENSILE STR, ULT [0], KSI	5	65.2	71.6	68.4	2	61.6	72.7	67.1
TENSILE MOD [0], MSI	5	7.18	7.95	7.64	3	7.90	8.54	8.20
COMPRESSIVE STR, ULT [0], KSI	3	52.2	60.7	56.3				
COMPRESSIVE STR, ULT [90], KSI	5	44.6	48.8	46.3	3	32.6	42.0	38.3
COMPRESSIVE MOD [0], MSI	3	9.11	9.25	9.18				
COMPRESSIVE MOD [90], MSI	5	5.57	6.45	6.03	3	6.17	7.17	6.57
RAIL SHEAR STR, ULT [90/0], KSI	2	24.7	24.8	24.75	1			19.4
RAIL SHEAR MOD [90/0], MSI	2	2.040	2.042	2.041				
FLEXURAL STR, ULT [0], KSI	4	121.3	155.3	139.7				
FLEXURAL MOD [0], MSI	4	10.53	11.82	11.07				
BENDING STIFFNESS, EI, LB-IN. ²	4	349	393	370				
INTERLAM SHEAR STR, ULT [0], KSI	5	5.51	6.39	5.93				
PHYSICAL PROPERTIES	SP GR 1.56, FIBER VOL FRAC 0.60, MOLDED PLY THICKNESS 0.0053 IN.							

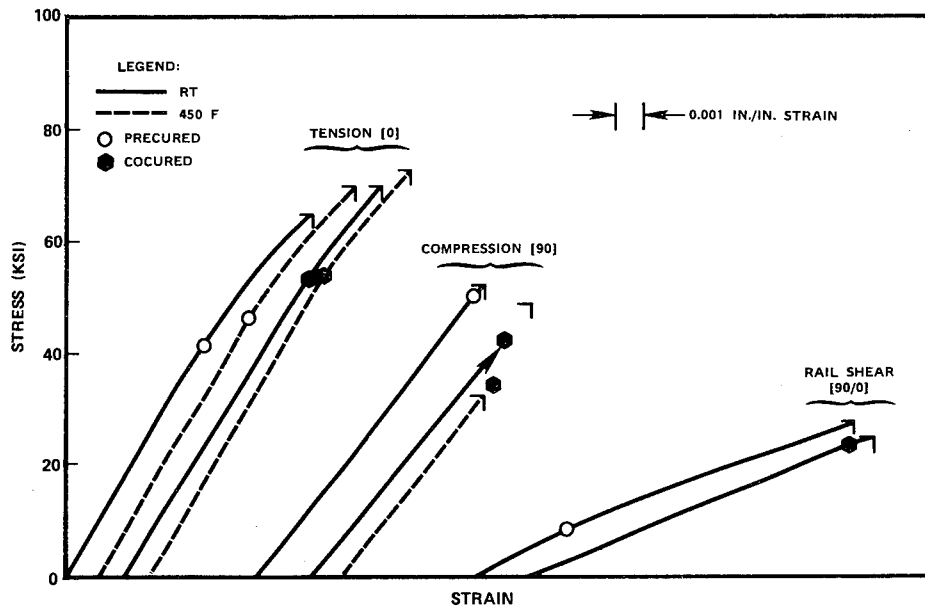


Figure 9. Typical Stress-Strain Curves for F178/T-300 Bismaleimide/Graphite Laminates [0(0/+45/90)_{2s}0]

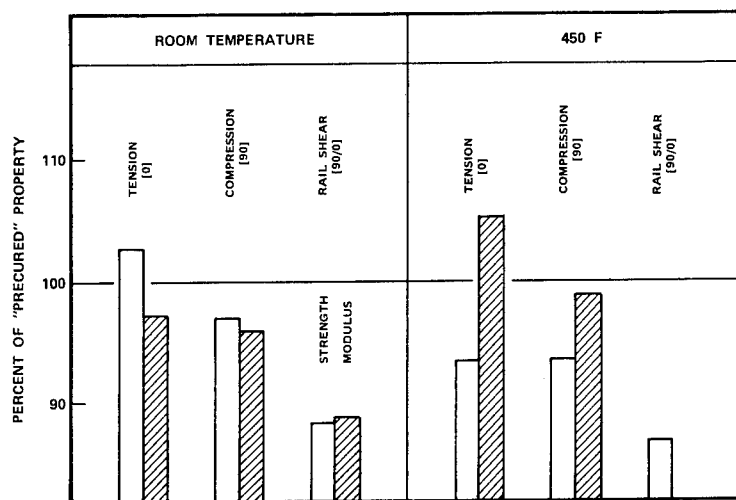


Figure 10. Summary of "Cocured" API Laminate Properties in [0(0/+45//90)_{2s}0] Construction, Expressed as Percent of "Precured" Properties

EFFECTS OF ROOM-TEMPERATURE AGING ON COMPOSITE PREPREGS

H. C. Nash, C. F. Poranski, Jr. and R. Y. Ting

Chemistry Division
Naval Research Laboratory
Washington, D. C. 20375

Abstract: Prepreg materials of organic-matrix composites have very limited shelf-life, even under the required cold-storage conditions. A prepreg aging study has been carried out by storing prepreg materials at room temperature under three different controlled humidity levels. Exposed samples were examined periodically by proton NMR spectroscopy, and unidirectional 16-ply laminates were fabricated. Prepreg appearance, curing behavior, and laminate properties were found to change with prepreg out-time.

Key words: Aging of polymer; prepreg; composite; NMR; mechanical properties; fiber; moisture.

As fiber-reinforced composite materials become increasingly important in many aerospace applications, the storage, handling and processing of composite prepreg materials are also receiving greater attention. A major difficulty in handling many prepregs is that the material must be stored at very low temperatures. The shelf life of these prepregs is generally only a few months at freezer temperatures. Presumably, continued B-staging occurs at room temperature and, at the same time, the resin may degrade by absorbing moisture from the atmosphere. Also, since the prepreg must warm up to room temperature before lay-up for fabrication, it could absorb moisture through condensation.

An aging study was therefore carried out to examine the effects of out-time and humidity at room temperature on the properties of a polyimide/graphite prepreg. Laminates were fabricated from material which had been exposed to various humidities at room temperature and the mechanical properties were evaluated as a function of prepreg out-time. Extracts of the aged prepreg were also analyzed using proton NMR spectroscopy to see if this technique could reveal any chemical change resulting from the aging process.

Experimental

Material: The polyimide/graphite prepreg (F-178/T300) was obtained directly from the manufacturer, Hexcel. The resin is described as a bismaleimide type of polyimide which cures through a free-radical addition mechanism. The glass transition temperature, determined by

torsional pendulum measurements, was 360°C for this resin compared to 260°C for an epoxy. Fresh prepreg material was cut, and stored at room temperature in three environmental chambers controlled at 16%, 50% and 95% relative humidity, respectively. Aging extended over a period of twenty-eight weeks. A 16-ply laminate was prepared every four weeks. An additional sheet of aged prepreg was used for proton NMR analysis.

Unidirectional 16-ply laminates were fabricated in a hydraulic press using conventional vacuum bag techniques. The processing included a full vacuum cycle at 121°C (250°F) and a pressure cycle at 177°C (350°F) with a pressure of 6.9×10^5 Pa (100 psi). Post cure was carried out at 249°C (480°F) for 10 hours. The curing cycle was kept the same for processing all aged samples.

Samples were cut from the laminate and tests were carried out to determine if any change occurred in their mechanical properties relative to composites prepared from unaged prepreg. The short-beam shear test (ASTM-D 2344) was chosen to determine the interlaminar shear strength, a resin-dominated property. The flexure test (ASTM-D 790) was selected to measure the laminate flexural strength and modulus, which are fiber-dominated properties. For proton NMR analysis, weighed 2 cm x 2 cm samples were extracted using acetone-d₆ for ~2 hours at room temperature. The resulting solutions were filtered directly into dry NMR sample tubes. The residues were dried and weighed. The spectra were obtained on a JOEL FX60 Q spectrometer system.

Results

Figure 1 shows the flexural strength of the graphite/polyimide composite plotted as a function of the prepreg aging period in weeks. It can be seen that laminate flexural property steadily decreases as aging continues. The effect is more pronounced at higher humidity levels. After twenty weeks of aging at 95% relative humidity, the flexural strength is reduced by nearly 30% from that of the original control sample. The same trend is followed by the flexural modulus data.

Figure 2 presents the interlaminar shear strength data as a function of prepreg aging period. In this case, the results show a rapid increase in shear strength initially as aging proceeds. Then it becomes constant at a level approximately 55% higher than that of the initial control. The increase seems to be independent of the humidity level at which prepreg samples were aged.

At first glance these results seemed surprising because any resin degradation taking place due to moisture absorption in the prepreg would lead to a poorer resin-dominated property such as interlaminar shear strength. The fact that interlaminar shear strength was improved and flexural properties deteriorated may be resolved by considering some physical changes to the prepreps which occurred during aging.

First of all, during the aging period the prepreg material clearly showed a steady loss of tackiness. As aging continued, the prepreg gradually became dry and brittle, making it difficult to keep all plies properly aligned and adhered during lay-up. Secondly, the bleeding during curing was greatly reduced for aged samples. Wetting of the bleeder plies became less and less, particularly around the corners of the square plies, as aging continued. These changes seem to suggest that the amount of resin flow was greatly reduced due to aging.

Figure 3 shows the proton NMR spectrum of the resin extracted from the control sample. Analysis of the spectrum showed that the extracted resin had two major components. The lines at 4, 7 and 7.2 ppm were assigned to the methylene, olefinic and aromatic protons of the bis-maleimide of methylene dianiline (see Figure 4A). The multiple peaks in the region from 4.1 to 6.1 ppm were due to the allyl protons in triallyl isocyanurate (see Figure 4B). However, it was surprising that there was no noticeable difference in the appearance of the spectra of the aged samples compared to that of the control sample. The most probable reason for this is that the initial products of the aging process were not soluble in acetone- d_6 , or that they did not reach a high enough concentration, before reacting further, to be detected. It was noticed, however, that the amount of extractable materials decreased with aging.

These observations suggest that exposure to high humidity caused little or no chemical degradation in the resin system. But room temperature storage produced a prepreg material that was excessively B-staged. The aged prepreps essentially had a higher degree of crosslinking than a fresh sample at the beginning of the fabrication process. This change in degree of crosslinking was not detected by proton NMR, but the material was essentially one with higher molecular weights having greater melt viscosities. This, therefore, lowered the flow when the sample was subjected to the processing cycle originally designed for the control sample. The result was a composite laminate having higher resin content, but poorer flexural properties. Laminate density measurements and fiber/matrix volume determination confirmed this. The result showed that the resin content in the laminates increased with increased age of the prepreg, resulting in decreased laminate density.

Reference

1. W. D. Bascom, J. L. Bitner and R. L. Cottingham, ACS Org. Coat. and Plast. Preprint, 38, 477 (1978).

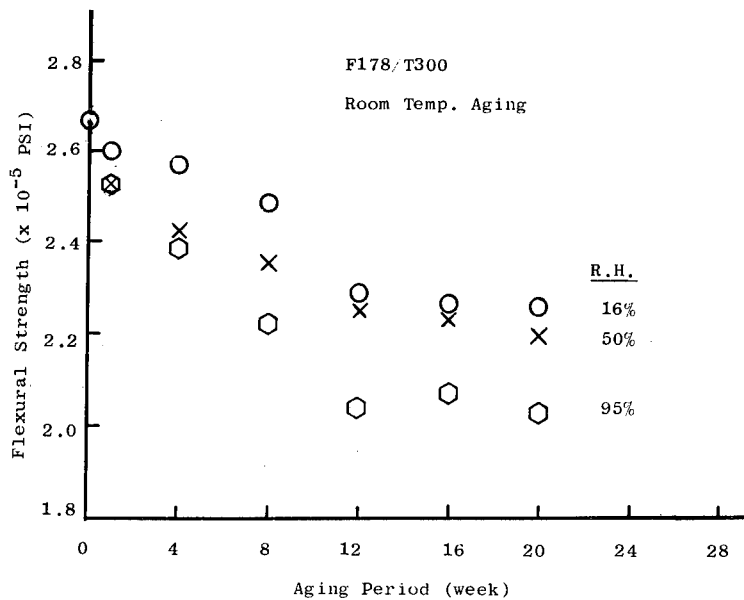


Figure 1. Laminate flexural strength as a function of aging period.

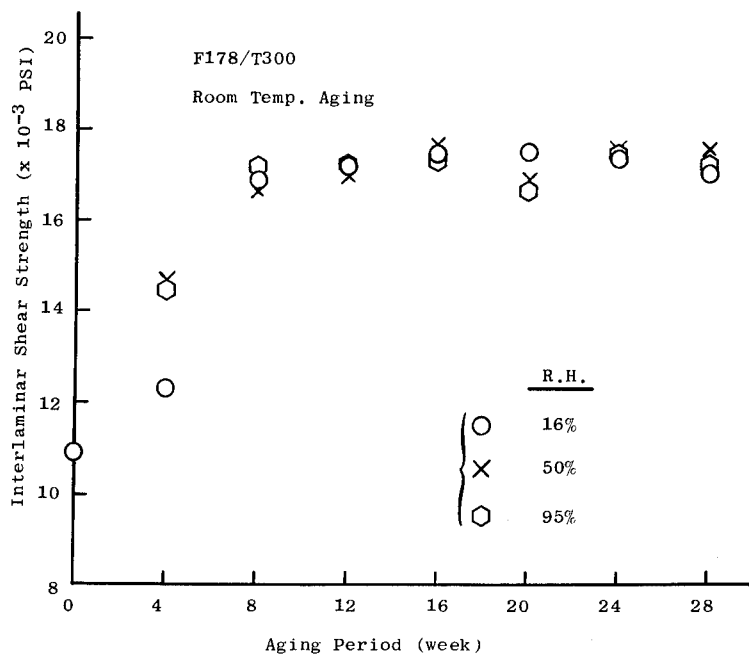


Figure 2. Interlaminar shear strength of aged samples.

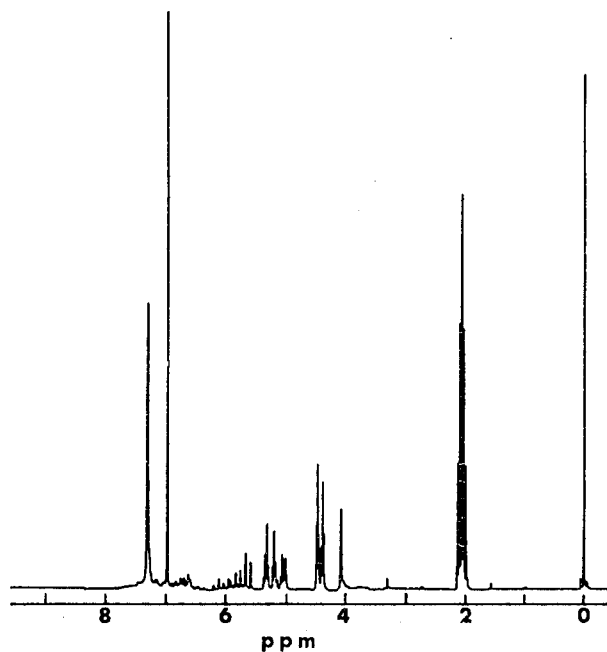


Figure 3. 60 MHz proton nmr spectrum of material extracted from unaged F-178/T-300 prepreg. The line at 0 ppm is that of the reference, tetramethylsilane. The multiplet at 2 ppm is due to the residual protons in the solvent, acetone -d₆.

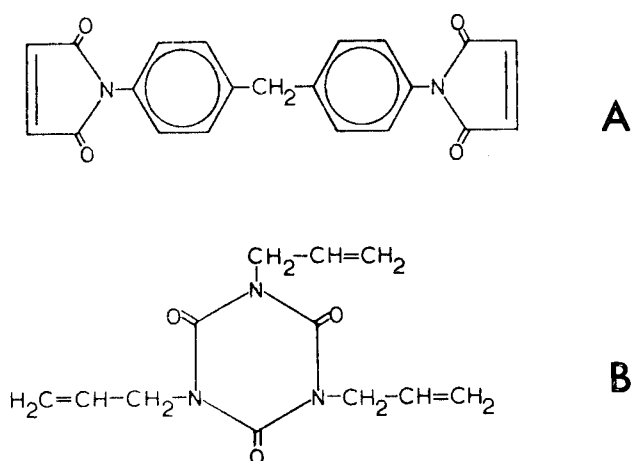


Figure 4. Chemical structures of components in Hexcel polyimide resin.

SESSION 2

AEROSPACE AND AIRCRAFT APPLICATIONS AND DESIGN

Chairman: S. E. J. Johnsen
Detroit Diesel Allison Division,
GMC

APPLICATION OF INSTRUMENTAL TECHNIQUES TO THE STUDY OF
THE CURE OF PHTHALOCYANINE/GRAPHITE COMPOSITES

Robert Y. Ting
Chemistry Division
Naval Research Laboratory
Washington, D. C. 20375

Abstract: Work on resin evaluation in the NRL V/STOL aircraft program is directed toward the development of high temperature resins for application as potential composite matrix materials. As successful prepregging of the polyphthalocyanine/graphite-fiber system has recently been demonstrated, the processability of this material is now under study. Instrumental techniques including differential scanning calorimetry (DSC), thermogravimetric analysis (TGA) and dynamic dielectric analysis are employed to examine the thermal properties of unidirectional prepregs and the fabrication of unidirectional laminates. Results of these studies have led to the development of a cure cycle for this new resin system.

Key words: V/STOL, polyphthalocyanine, graphite-fiber, DSC, TGA, dielectric analysis, cure, prepreg.

Introduction: Organic composite materials having high temperature capabilities are being evaluated for structural applications in advanced aircraft such as future vertical and short take-off and landing (V/STOL) aircraft. The basic concept is to replace much of the metallic structural components with organic composites for weight-saving purposes and consequently to increase the range and payload of the aircraft.

For such applications the presently available composite materials suffer many shortcomings, including moisture pick-up, chemical degradation and poor storage stability. Most of all, current matrix materials (epoxy resins) have a limiting use temperature around 135°C. Resins are therefore being sought which will meet operational requirements at temperatures in excess of 200°C, but will be relatively insensitive to moisture attack and will have the ease of fabrication of state-of-the-art epoxies. Phthalocyanine resins recently developed at NRL (1) seem to provide the desired features when properly cured (2). Figure 1 shows the network structure of these polymers. The phthalocyanine polymer based on the C-10 diamide resin is now being evaluated as a potential matrix material in fiber-reinforced composites.

Experimental: Thornel 300 graphite fibers were used in producing unidirectional prepreg tapes. Prepregging of the C-10/T-300 system was carried out by both the usual hot-melt method and a resin/solvent slurry method. In the hot-melt procedure the resin was staged at about 200°C to give a liquid intermediate state during which the fiber reinforcements were easily impregnated. The prepreg had the general appearance of being dry and brittle; however, the material could be briefly heated at 130°C to develop sufficient amount of tack for complex lay-up. In the slurry technique, dimethyl formamide (DMF) was used as the solvent, and the final product had an average resin content of ca. 40% and volatile content of ca. 6%. Prepregs prepared by the hot-melt technique, on the other hand, had ca. 33% resin content with practically no residual volatiles.

A Perkin-Elmer DSC-2 unit was used for the DSC cure study. The scanning was performed over the temperature range of 310°K (37°C) to 500°K (227°C) at a heating rate of 10°C/min under a dry nitrogen atmosphere. A DuPont 900 Series unit was also used to perform the TGA work on prepreg samples (~ 20 mg) over the temperature interval of 20°C to 350°C. Sample weight loss was determined as a function of temperature at a heating rate of 5° C/min, while purging with dry nitrogen.

A dynamic dielectric technique (3) was employed to monitor the curing of composite samples using an Audrey III Dielectrometer. Sixteen-ply unidirectional samples (15.2 cm x 15.2 cm in size) were laid up by hand between two aluminum-foil electrodes, 5.1 cm x 5.1 cm in size, for the dielectric monitoring. Sample capacitance and dissipation factors were continuously measured as a function of cure time and temperature at a fixed frequency of 10³ Hz. Conventional vacuum-bag technique was used for sample cure in a hydraulic press (4).

Results: The results of DSC scans on uncured polymer is shown in Figure 2. Trace B is a "null-reference" baseline. Trace E is from a pure, uncured C-10 phthalocyanine resin, which exhibits a melting peak at 180°C, and an exotherm at 197°C, related to the onset of cure. Trace D is that for the prepreg material prepared by using the slurry technique. The two sharp endotherms at low temperatures are perhaps related to the release of some unknown, low boiling volatiles. A peak at 145°C may be identified with the release of DMF added during prepregging. The other peaks at 134°C and 174°C are believed to be related to the melting of resin oligomers. These temperatures are lower than the melting point of pure C-10 resin. This phenomenon of melting-point depression by B-staging is well-known (4). Trace C in Figure 2 is that for a different batch of prepreg, presumably prepared according to the same procedure as the material of Trace D. It is noticed, however, that the thermal behavior of the C-10 resin is quite sensitive to its thermal history. Apparently, the two batches of prepregs were B-staged differently. In Trace C there is no endotherm peak at 124°C, but the solvent peak and higher temperature melting

peaks are more pronounced when compared with those in Trace D. Trace A in Figure 2 gives the record of hot-melt prepreg. Since no volatile release is expected from this material, the endotherm peaks again manifest the melting of oligomers of separate entities. This multiple melting behavior of B-staged phthalocyanine was also observed by Gillham recently in a torsion braid analysis of this resin (5).

In order to further identify the nature of the observed DSC endotherm peaks, TGA was also performed; Figure 3 shows this result for a slurry prepreg sample. Substantial weight loss is found in the temperature range of 50°C to 90°C, suggesting that the corresponding DSC endotherms are indeed related to release of volatiles and/or moisture. The further weight loss observed near 150°C shows DMF evaporation; the amount is nevertheless small. Rapid weight loss begins to take place beyond 275°C. This suggests a limit of initial cure temperature to no more than 260°C.

Figure 4 shows the dielectric dissipation curve of a slurry prepreg sample subjected to an isothermal cure at 225°C. Small peaks at ca. 100°C and 150°C show the release of moisture and DMF, respectively. As the temperature exceeded 200°C, the material quickly melted and polymerization to phthalocyanine was also activated thermally. This caused the dissipation to increase and reach a maximum, which was believed to be the gelation point (6). Beyond this point the sample gradually solidified, but a distinct cure-peak was not observed as in the case of epoxy-matrix materials (7).

Similar techniques may be applied to laminate samples during the fabrication in a press. In Figure 5, an example for in situ dynamic dielectric monitoring is given. In this case, a 16-ply laminate sample was placed in a vacuum bag, and initially heated to 145°C under vacuum. Temperature was subsequently raised to 260°C rapidly and kept for an extended period of time. The dissipation curve showed at first a broad melting (Figure 5A), followed by a rapid increase to reach the gel point. This would allow one to determine the exact time at which high pressure should be applied to the sample in order to fabricate laminates with very low void contents. Figure 5B shows the dissipation of a prepreg lay-up with raw resin powder sprinkled between the plies in an attempt to increase the sample resin content. As resin melting temperature was reached, one observed an excessive amount of resin flow accompanying the melting, as indicated by the first pronounced dissipation peak. It suggests that the control of this resin flow would be difficult since the melt viscosity of unstaged C-10 resin is apparently low.

In summary, it has been shown that studies of prepreg materials using DSC, TGA and dynamic dielectric techniques prior to laminate fabrication enable one to develop information concerning the thermal processes such as volatile release, melting and gelation. In situ

dynamic dielectric analysis during fabrication provides sample capacitance and dissipation data, which are related to the chemorheological changes in the curing of a thermosetting system. This information is useful in identifying the melting and gelation of laminate samples. Proper pressure application with respect to the gel point led to cured samples with desired resin content and minimum void content, which is critical for applications where fracture processes dominate in composite failure.

References

1. T. R. Walton, J. R. Griffith and J. G. O'Rear, ACS Advances in Chemistry Ser., 142, 458 (1975).
2. T. R. Walton, J. R. Griffith and J. G. O'Rear, ACS Org. Coat. Plast. Preprint, 34, 446 (1974).
3. N. G. McCrum, B. E. Read and G. Williams, Anelastic and Dielectric Effects in Polymeric Solids, John Wiley, New York, 1967.
4. J. V. Gauchel and H. C. Nash, in High Performance Composites and Adhesives for Advanced V/STOL Aircraft, ed. L. B. Lockhart and W. D. Bascom, NRL Memo. Report 3433, Washington, D. C., 1976.
5. J. V. Gillham, ACS Org. Coat. Plast. Preprint, 40, 866 (1979).
6. J. K. Gillham, J. A. Benci and A. Noshey, J. Polym. Sci., C46, 279 (1964).
7. C. A. May, D. K. Whearty and J. S. Fritzen, SAMPE Ser., 21, 803 (1976).

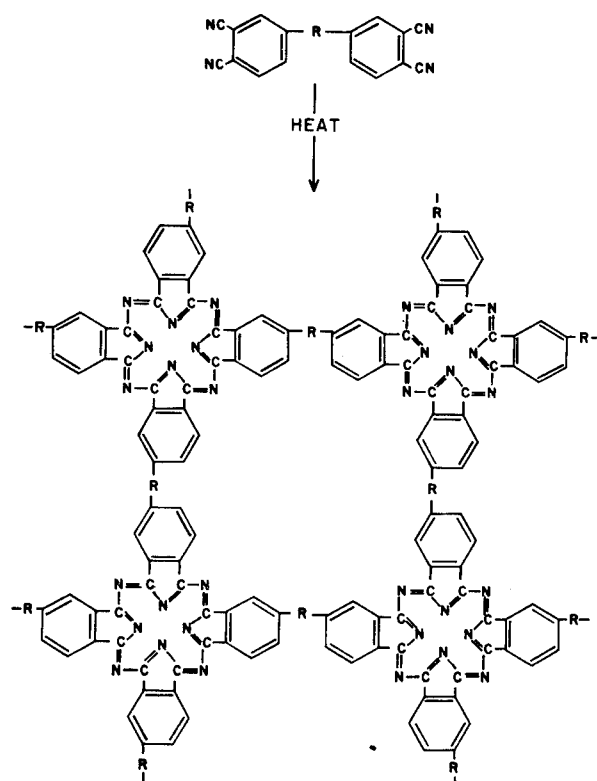


Fig. 1: Polyphthalocyanine network

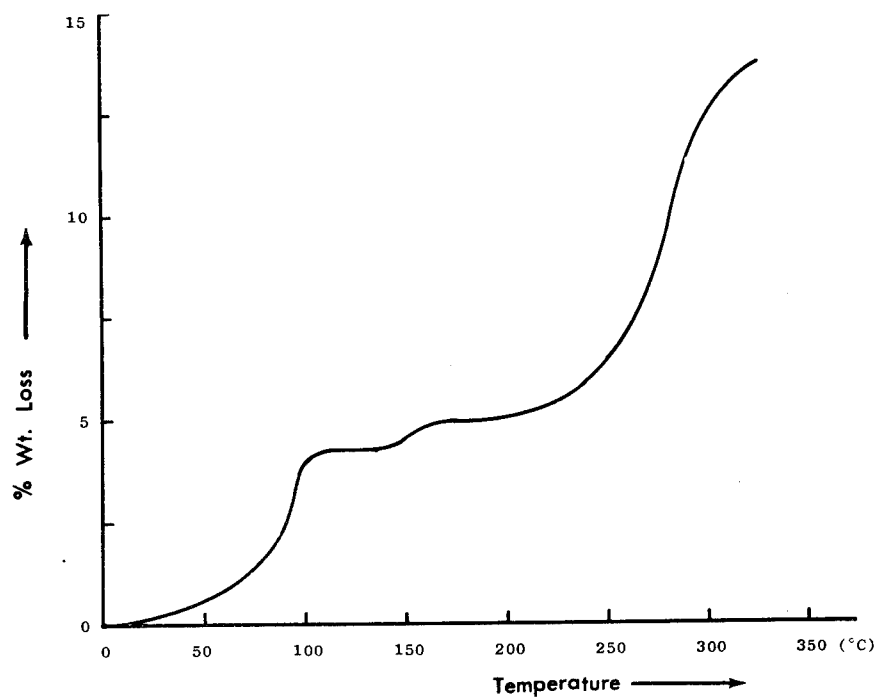


Fig. 3: Percent weight loss of C-10/T-300 prepreg as a function of temperature

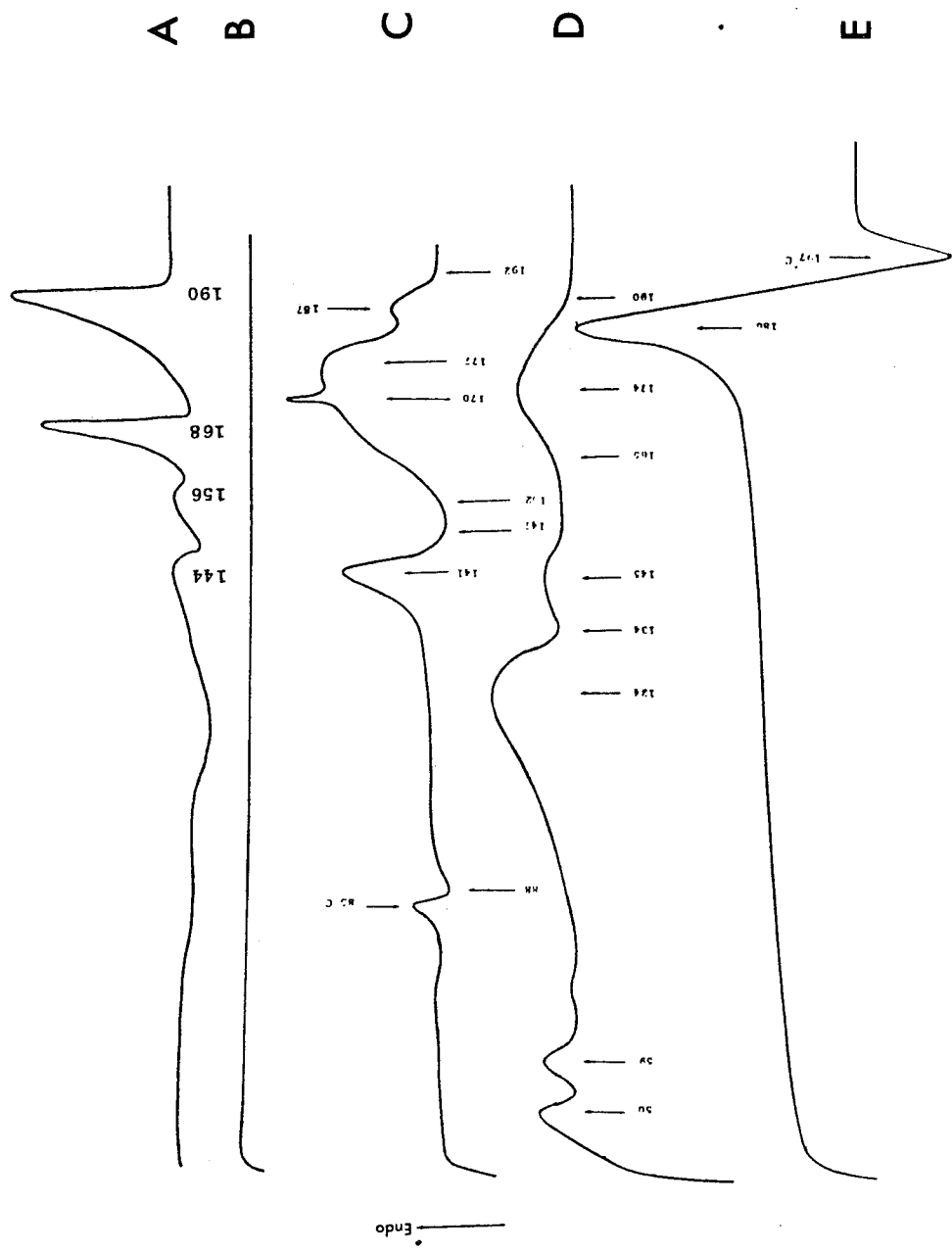


Fig. 2: DSC records of C-10 resin and prepregs

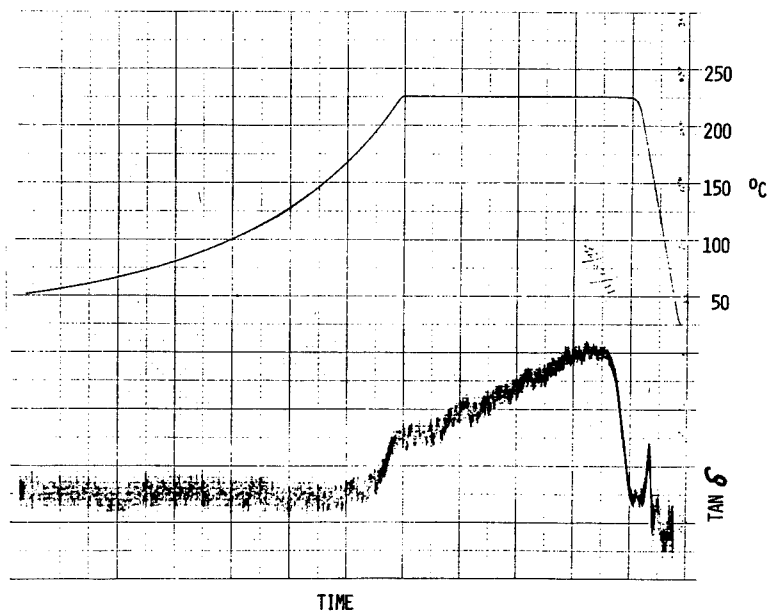


Fig. 4: Dielectric dissipation record of a prepreg sample under 225°C cure

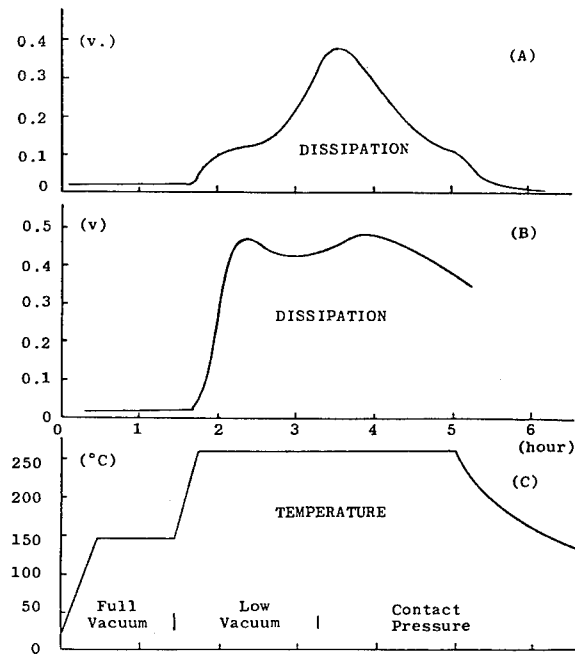


Fig. 5: Dynamic dielectric results of in-situ monitoring of a 16-ply C-10/T-300 laminate

MOISTURE DIFFUSION ANALYSIS FOR COMPOSITE MICRODAMAGE

C. L. Leung and D. H. Kaelble
Rockwell International Science Center
Thousand Oaks, California 91360

Abstract: Because of their favorable performance characteristics, advanced composites using graphite fibers as reinforcement are increasingly being used in aerospace and commercial applications. There has been much concern, however, about the extent and mechanisms of strength degradation of these composites when exposed to moisture for long periods of time. In this paper, methods to obtain directional diffusion coefficients, i.e., D_x , D_y and D_z for the principal axis of a unidirectional fibrous composite are described by moisture absorption and effusion measurements. Additionally, analytical models have been developed to calculate, using the previously established diffusion coefficients, the moisture profile of the composite after periods of moisture exposure. The feasibility of the integration of the effusion rate measurement, moisture profiling, and strength prediction into a computer-aided analyzer for composite microstructure damage or defect is discussed.

Key words: Diffusion coefficients, iteration, moisture profile modeling, nondestructive evaluation, statistical estimation.

INTRODUCTION

A number of reports show that the mechanical properties of graphite-epoxy composites are degraded by moisture [1-4]. Hydrothermal stresses generated by hydration-dehydration can cause microcracks and delaminations to occur within the composite. This paper outlines an iterative calculation method to isolate the coefficients of diffusion for the three axes of rotation. Using these coefficients, as well as the rates of water effusion from the composites, an inversion method which solves for the original moisture profile is also reported.

THEORY

1. Directional Diffusion Coefficients

Fick's second law of diffusion can be represented in terms of three principal axes of diffusion by the following relationship [5-7]:

$$\frac{\partial c}{\partial t} = D_x \frac{\partial^2 c}{\partial x^2} + D_y \frac{\partial^2 c}{\partial y^2} + D_z \frac{\partial^2 c}{\partial z^2} \quad (1)$$

The schematic of Fig. 1 identifies the orientation of the x, y, z coordinate system for Eq. (1) as centered within a unidirectionally reinforced composite. Recent studies show that for undamaged composites, Eq. (1) is obeyed and appears to provide a valid basis for diffusional kinetics analysis [3]. Uniaxially reinforced composites can be rotated relative to the x, y and z coordinates to isolate the diffusion coefficients D_x , D_y and D_z as shown in Fig. 2. In the limit of short times for moisture absorption, the following relationship for the initial ϕ vs $t^{1/2}$ was derived [5]:

$$\phi = \frac{M_t - M_0}{M_\infty - M_0} = 4 \left(\frac{t}{\pi} \right)^{1/2} \left[\frac{D_x^{1/2}}{x_x} + \frac{D_y^{1/2}}{x_y} + \frac{D_z^{1/2}}{x_z} \right] \quad (2)$$

In Eq. (2), it is assumed that each of the six sides of the composite absorbs and desorbs moisture independently. An alternative expression for Eq. (2) is [5,7]:

$$\phi_{i=x,y,z} = \frac{4}{x_i} \left[\frac{\bar{D}_i t}{\pi} \right]^{1/2} \quad (3)$$

where \bar{D}_i is the apparent experimental diffusion coefficients as determined from the initial slopes of the ϕ_i vs $t^{1/2}$ curves.

This averaged experimental diffusion coefficient \bar{D}_i can be reexpressed as [5,7]:

$$\bar{D}_i = D_i \left[1 + \frac{x_i}{x_j} \sqrt{\frac{D_j}{D_i}} + \frac{x_i}{x_k} \sqrt{\frac{D_k}{D_i}} \right]^2 \quad (4)$$

where by definition, the following axis transformations would apply:

when $i = x$, then $j = y$, $k = z$

when $i = y$, then $j = x$, $k = z$

when $i = z$, then $j = x$, $k = y$

Inspection of Eq. (4) shows that the measured values of $D_{i=x,y,z}$ must be further analyzed by an iterative calculation to isolate precise values of D_x , D_y and D_z . Rearrangement of Eq. (4) provides the following

$$(\tilde{D}_i)_n = \bar{D}_i \left[1 + \frac{x_i}{x_j} \sqrt{\frac{(\tilde{D}_j)_{n-1}}{(\tilde{D}_i)_{n-1}}} + \frac{x_i}{x_k} \sqrt{\frac{(\tilde{D}_k)_{n-1}}{(\tilde{D}_i)_{n-1}}} \right]^{-2} \quad (5)$$

where n = number of iterations. This iterative calculation continues until an appropriate convergence test condition is satisfied such as [8]:

$$0 \leq \left| \frac{\{(\tilde{D}_i)_n - (\tilde{D}_i)_{n-1}\}^2}{\{(\tilde{D}_i)_n - (\tilde{D}_i)_{n-2}\}} \right| < \epsilon_n \quad (6)$$

When Eq. (6) is satisfied, the diffusion coefficient will be:

$$D_{i=x,y,z} = (\tilde{D}_i)_n \pm \epsilon_n \quad (7)$$

For the first iteration where $n=1$, the initial inputs for iteration are the measured coefficients of diffusion in the three principal axes as follows:

$$\begin{aligned} (\tilde{D}_i)_{n-1} &= \bar{D}_i = x,y,z \\ (\tilde{D}_n)_{n-1} &= \bar{D}_j = y,x,z \\ (\tilde{D}_k)_{n-1} &= \bar{D}_k = z,x,y \end{aligned} \quad (8)$$

Equation (5) is thus solved for the principal axis $i = x,y,z$ to compute $(D_x)_{n=1}$, $(D_y)_{n=1}$ and $(D_z)_{n=1}$. Successively higher iterations of $n=2, 3, 4...$ can thus be calculated using the appropriate $(n-1)$ values.

Moisture absorption and desorption experiments in the principal axis $i = x,y,z$ of a uniaxial composite followed by iterative calculations leading to Eq. (7) are therefore proposed as a useful approach to isolate the principal axis components of moisture diffusion kinetics in these uniaxial composites.

2. Moisture Profile Modeling

Subsequent to the determination of the directional diffusion coefficients as discussed above, the depth/concentration profile of moisture

in the composite can be obtained by a series of mathematical analyses and experiments. The experiment involves the heating of the composite to a desired temperature followed by measurement of the rate of moisture effusion as a function of time. The analytical problem is then to determine the initial distribution of water, i.e., the concentration $c_0(x) = c(x,0)$ as a function of x (where x is the distance into the thickness of the composite), from the subsequent history of effusion rate measurements. The attempt to treat this as a deterministic problem leads to difficulties. One of these difficulties is associated with the inevitable incompleteness of the experimental data: any real experiment can yield only a finite set of numbers. A particularly convenient way is to apply statistical estimation theory to the analysis. This analytical methodology is termed inverse-diffusion.

The inverse-diffusion system is illustrated more explicitly in Fig. 3. The material is assumed to be a rectangular block of composite occupying a region of space defined by the inequalities

$$\begin{aligned} 0 &< x < L_x \\ 0 &< y < L_y \\ 0 &< z < L_z \end{aligned} \quad (9)$$

where x, y, z are the usual Cartesian coordinates. The principal values of the diffusion tensor are denoted by D_x, D_y and D_z . The initial concentration is assumed to depend only on x , i.e.,

$$c(x,y,z, t=0) = c_0(x) \quad (10)$$

It is further assumed that the measurements involve the total diffusion rate from the entire surface at a specific set of later times. The inversion problem, therefore, involves a theoretical solution of the above diffusion problem with an arbitrary $c_0(x)$ and dry boundary conditions ($c_1 = 0$) [9]. The matrix L_{mn} shown in Fig. 3 is then used to obtain from the measured J_m (the experimental total diffusion rate) at times t_m estimates \hat{a}_n of the coefficients of $\sin(n\pi x/L_x)$, i.e.,

$$c_0(x) = c_1 + \sum_{n=1}^n \hat{a}_n \sin \frac{n\pi x}{L_x} \quad (11)$$

This process of going from the experimental J_m to the estimates \hat{a}_n is incorporated in the box labelled "estimator" in Fig. 3. The final result of the entire estimation process is presented as a plot of the original moisture concentration at time $t=0$ on the ordinate and the depth of moisture penetration on the abscissa.

To establish the validity and accuracy of the estimator, called the Inverse Diffusion Model, a Direct Model is independently developed [10], which is based on a numerical solution of Fickian diffusion equations. The Direct Model gives data for:

- (a) Moisture profile at any specific time,
- (b) Moisture diffusion rate at each time interval,
- (c) Moisture content at each time interval.

Moisture effusion rates obtained from the Direct Model, item (b), can, therefore, be analyzed by the Inverse Diffusion Model, yielding moisture profiles which should correlate to those generated from Fick's Law, item (a), thus validating the Inverse Diffusion Model.

EXPERIMENTAL

A 48-ply unidirectionally reinforced composite panel (Hercules 3501-5 epoxy reinforced with Hercules Type AS graphite fiber) was fabricated and cured by standard production procedures. The composite has a fiber volume $V_f = 0.60$ and void volume $V_v \leq 0.01$.

Moisture absorption kinetics were evaluated by measurements of weight change as a function of moisture exposure using an analytical balance sensitive to 10^{-5} g. Moisture effusion kinetics were evaluated on the Moisture Evolution Analyzer (DuPont Model 902H) supplemented by weight change measurements.

Thin plate specimens were cut to provide dimensions of length \times width \times thickness = $(20 \times 5 \times 1) \times 10^{-3}$ m. They were completely dried in a desiccator prior to moisture exposure.

RESULTS AND DISCUSSION

The results of moisture diffusional analysis for successive cycles of absorption $(D)_A$ and desorption $(D)_D$ are summarized in Table I. The results in Table I show that each additional cycle of full hydration and subsequent drying produces large increases in diffusional coefficients for moisture absorption $(D_i)_A$. However, the coefficients for moisture desorption $(D_i)_D$ are essentially constant over the three hydration-dehydration cycles. The results are indicative of a damage mechanism in the composite microstructure which enhances moisture uptake from the dry state, but does not affect moisture release from the wet state.

Using the coefficients of diffusion tabulated in Table I, a series of the profiles generated by the estimation process of the Inverse Diffusion Model are compared against the profiles from a Direct (Fickian) Model, as discussed previously. For the sake of argument,

the composite was assumed to be completely saturated with water prior to effusion measurements and the moisture profiles were calculated at times of 20 and 100 minutes after effusion started. The moisture profiles as calculated from the Inverse Diffusion Model were compared against a numerical solution of Fick's Law, as shown in Fig. 4.

A much more severe test of the estimator of the Inverse Diffusion Model is for the case of varying boundary concentrations, in which case the specimen is hypothetically partially saturated, removed from moisture and the moisture penetration mapped after varying lengths of drying times. Again using the coefficients of diffusion tabulated in Table I, analytical solutions of moisture profiles solved for 20 and 100 minutes of absorption and various drying times are shown in Fig. 5.

Several important conclusions can be drawn from the results shown in Figs. 4 and 5. In each case, there is excellent agreement between the Direct and Inverse solutions, thus validating the Estimator of the Inverse Diffusion Model. Particularly for Figs. 5a and 5b, after dehydration has begun, a ridge of high moisture content is present immediately beneath the surface which is dry. It is feasible that there exist different states of stress to the right (into the center) and to the left (on the surface) of the ridge of water beneath the surface. If a thermal spike is applied to the composite at this time, the different stress states can cause microcracks or delamination beneath the surface of the composite.

Such subsurface microcracks can be detected by measuring the moisture effusion rates and analyzing the data by the Inverse Diffusion Model. Figure 6 shows the estimated moisture profile of a partially saturated composite which contains two layers of air voids, as shown in Fig. 7. The discontinuities at X/L values of 0.1 and 0.9 as shown in Fig. 6 are correlated to defects within the sample.

SUMMARY AND CONCLUSIONS

This report describes and applies a quantitative methodology to the diffusion kinetics analysis for moisture degradation in graphite-epoxy composites. An Inverse Diffusion Model has been developed by an estimation process. This model has been shown to give correct moisture profile at $t=0$, given a set of effusion rates at later times. It can also serve as a sensitive, nondestructive analytical methodology for subsurface microdamage and defects.

ACKNOWLEDGEMENTS

This research was sponsored by the Center for Advanced NDE operated by the Rockwell International Science Center for the Advanced Research Projects Agency and the Air Force Materials Laboratory under Contract F33615-74-C-5180.

REFERENCES

- (1) Transactions on the Workshop on "The Effects of Relative Humidity and Elevated Temperature on Composite Structures," Ed. J. R. Vinson, R. B. Pipes, W. J. Walker and D. R. Ulrich, Air Force Office of Scientific Research Tech. Report AFOSR 770030.
- (2) C. E. Browning and J. T. Hartness, "Effect of Moisture on the Properties of High Performance Resins and Composites," ASTM STP 546, American Society for Testing and Materials, Philadelphia, 1974, pp. 284-302.
- (3) D. H. Kaelble, P. J. Dynes and L. Maus, "Kinetics of Environmental Degradation in Graphite-Epoxy Laminates," ASTM STP 580, American Society for Testing and Materials, 1975, pp. 247-262.
- (4) E. L. McKague, J. E. Halkais and J. D. Reynolds, J. Comp. Materials, 9, 2 (1975).
- (5) W. Jost, "Diffusion in Solids, Liquids and Gases," Academic Press, New York, 1960.
- (6) J. Crank, "The Mathematics of Diffusion," 2nd Ed. Oxford University Press, 1975.
- (7) C. H. Shen and G. S. Springer, J. Composite Materials, 10, 2 (1976).
- (8) A. Ralston, "A First Course in Numerical Analysis," McGraw Hill, New York, 1955, p. 328-332.
- (9) J. M. Richardson, "The Inverse Diffusion Problems," Internal Letter: "Diffusion With Arbitrary Boundary Concentrations," Feb. 1978.
- (10) J. M. Richardson, "Diffusion with Arbitrary Boundary Concentrations," Feb. 1978.

TABLE I. Moisture Diffusion Kinetics

<u>Experimental Diffusion Coefficients (cm^2/sec) $\times 10^8$</u>				
<u>Adsorption</u> <u>Cycle</u>	<u>Resin</u>	<u>Transfibrous</u>	<u>Translaminar</u>	<u>Interlaminar</u>
1	2.37	1.62	0.68	0.63
2	3.4	4.89	1.32	1.36
3		7.14	1.77	1.75
<u>Desorption</u> <u>Cycle</u>				
1	3.14	22.0	5.18	4.90
2	5.03	16.0	4.67	4.90
3		18.6	5.18	4.90

<u>Iteratively Calculated Diffusion Coefficients, (cm^2/sec) $\times 10^8$</u>				
<u>Absorption</u> <u>Cycle</u>	<u>Resin</u>	<u>Transfibrous</u>	<u>Translaminar</u>	<u>Interlaminar</u>
1	2.08	1.30	0.44	0.39
2	2.98	3.94	0.81	0.85
3		5.81	1.08	1.07
<u>Desorption</u> <u>Cycle</u>				
1	2.75	18.0	3.18	2.95
2	4.87	12.9	2.87	3.06
3		15.0	3.54	3.39

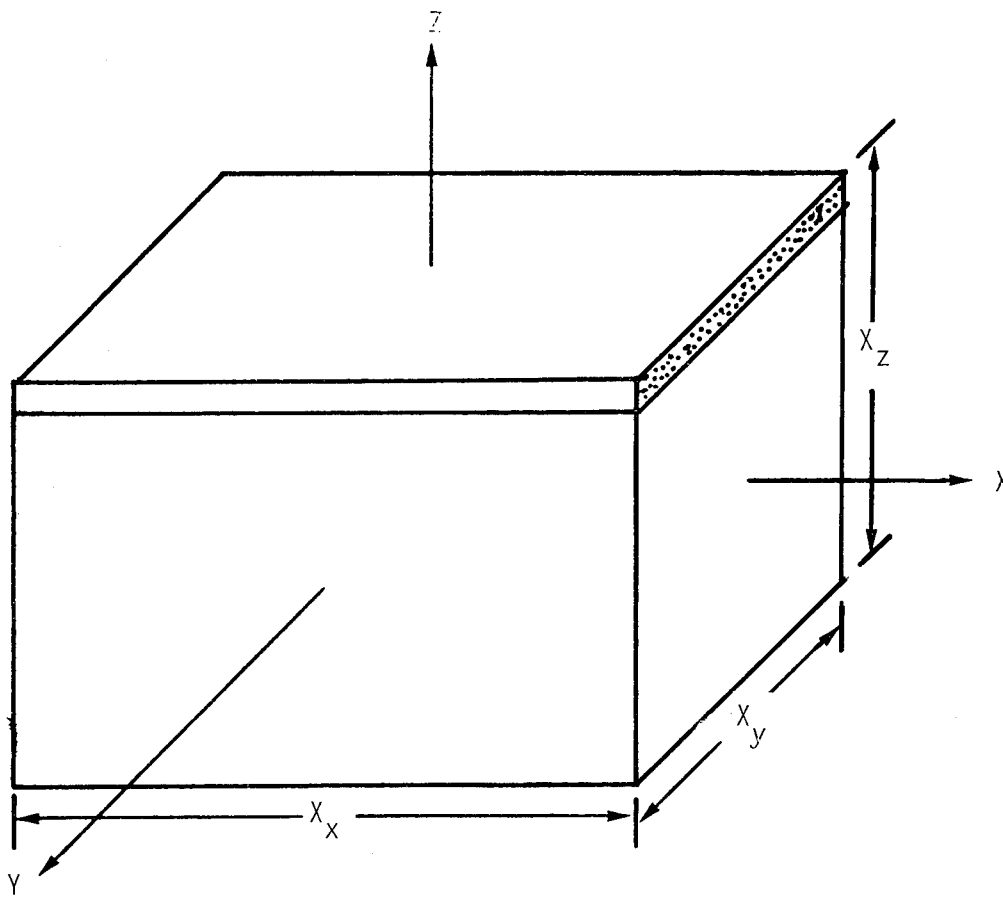


FIGURE 1

Orientations of fibers and plies within a unidirectionally reinforced composite (fibers parallel to x -axis, plies parallel to xy plane).

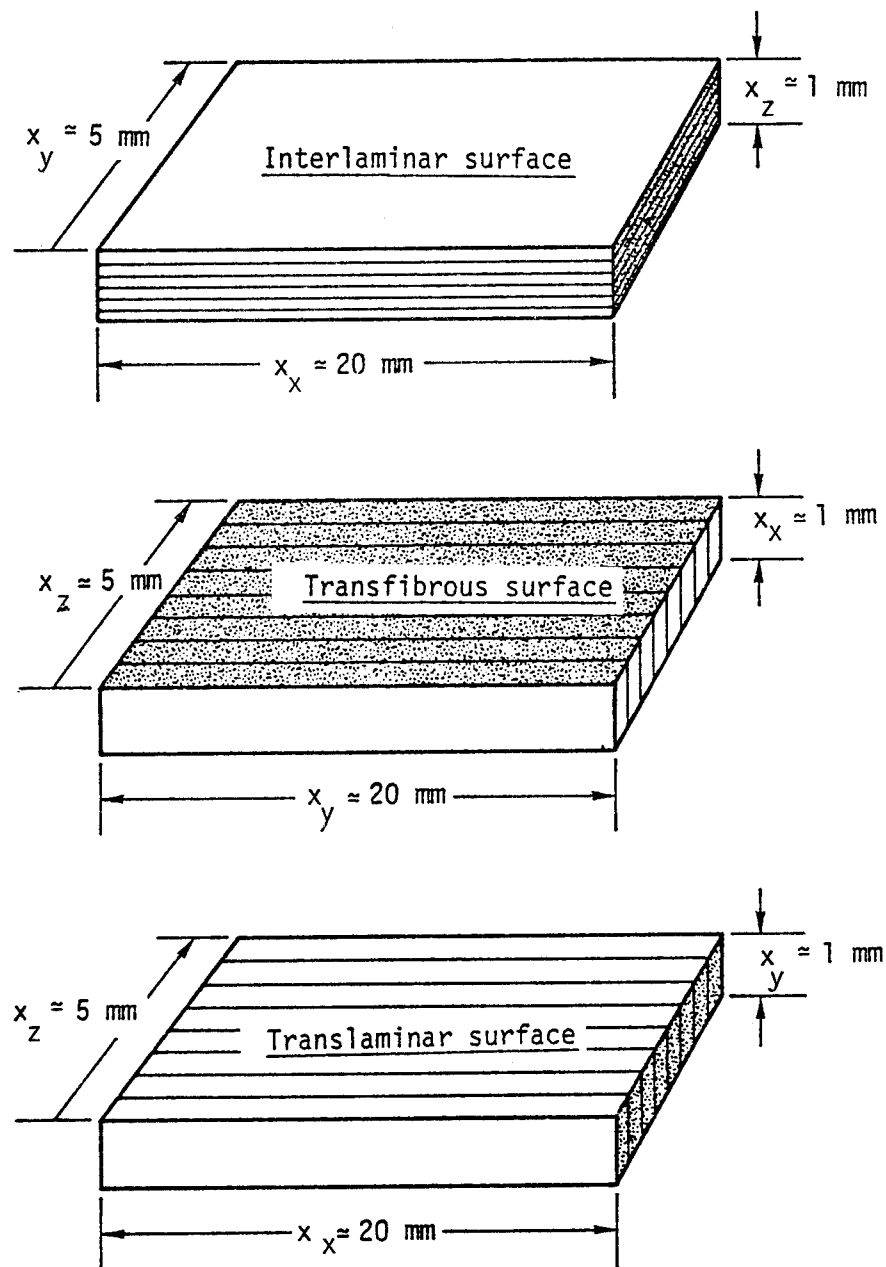


Figure 2.

Specimen orientations and geometry for kinetics of adsorption and desorption in interlaminar, transfibrous, and translaminar directions of uniaxial reinforced composite (layers represent plies and dots fiber ends).

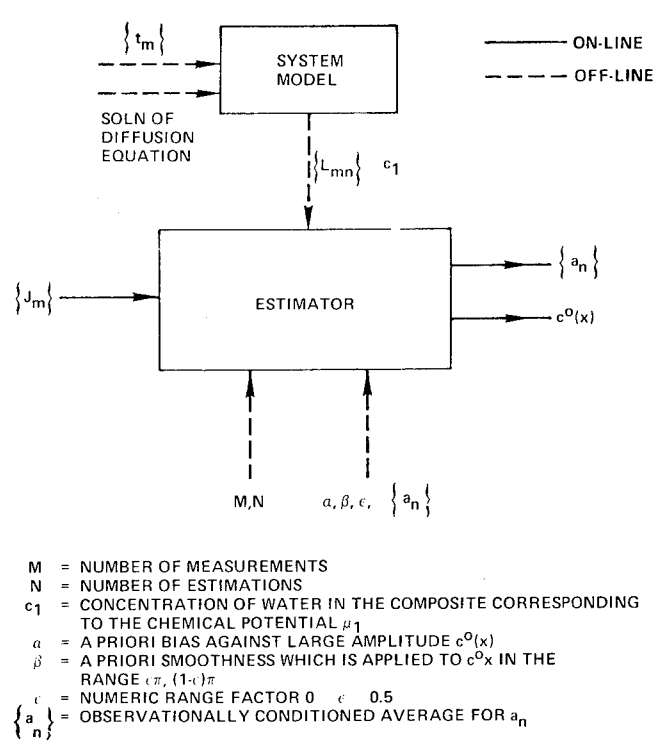
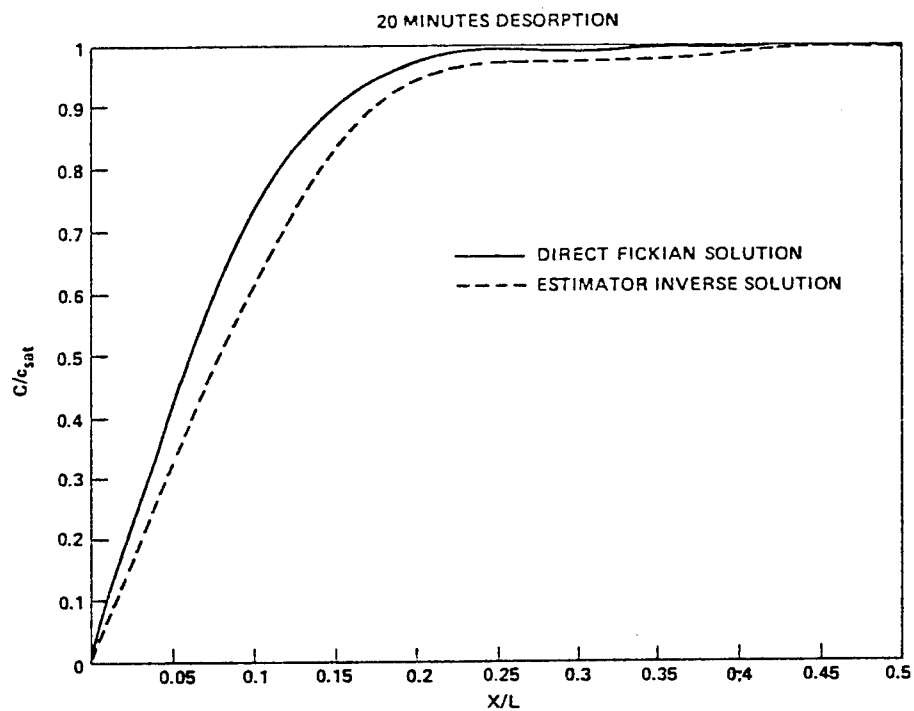
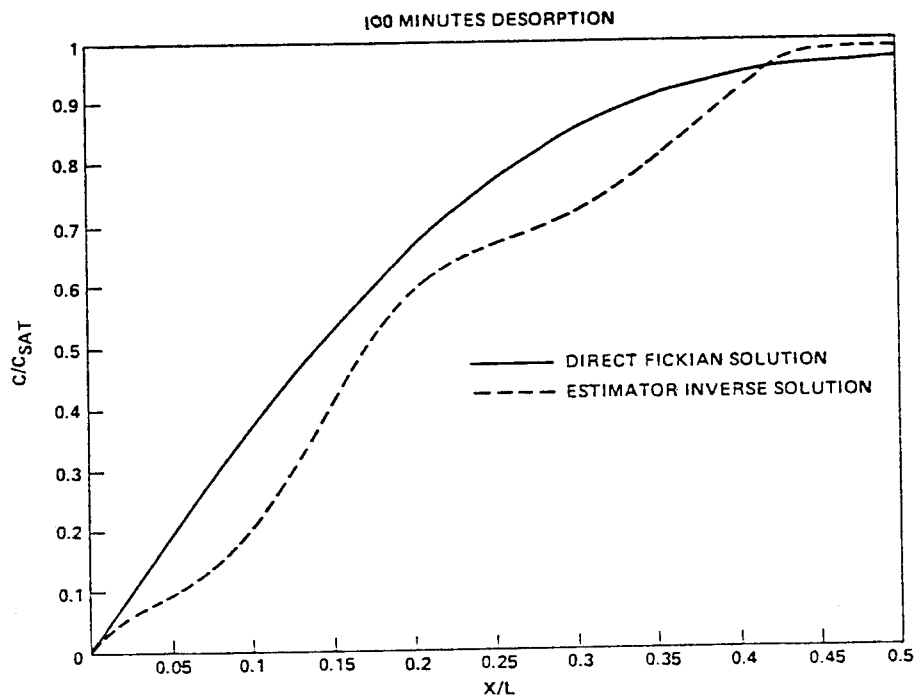


FIGURE 3

Schematic representation of the estimation process.



(a)



(b)

FIGURE 4

Moisture profiles via analytical modeling of a fully saturated composite after (a) 20 minutes desorption, (b) 100 minutes desorption.

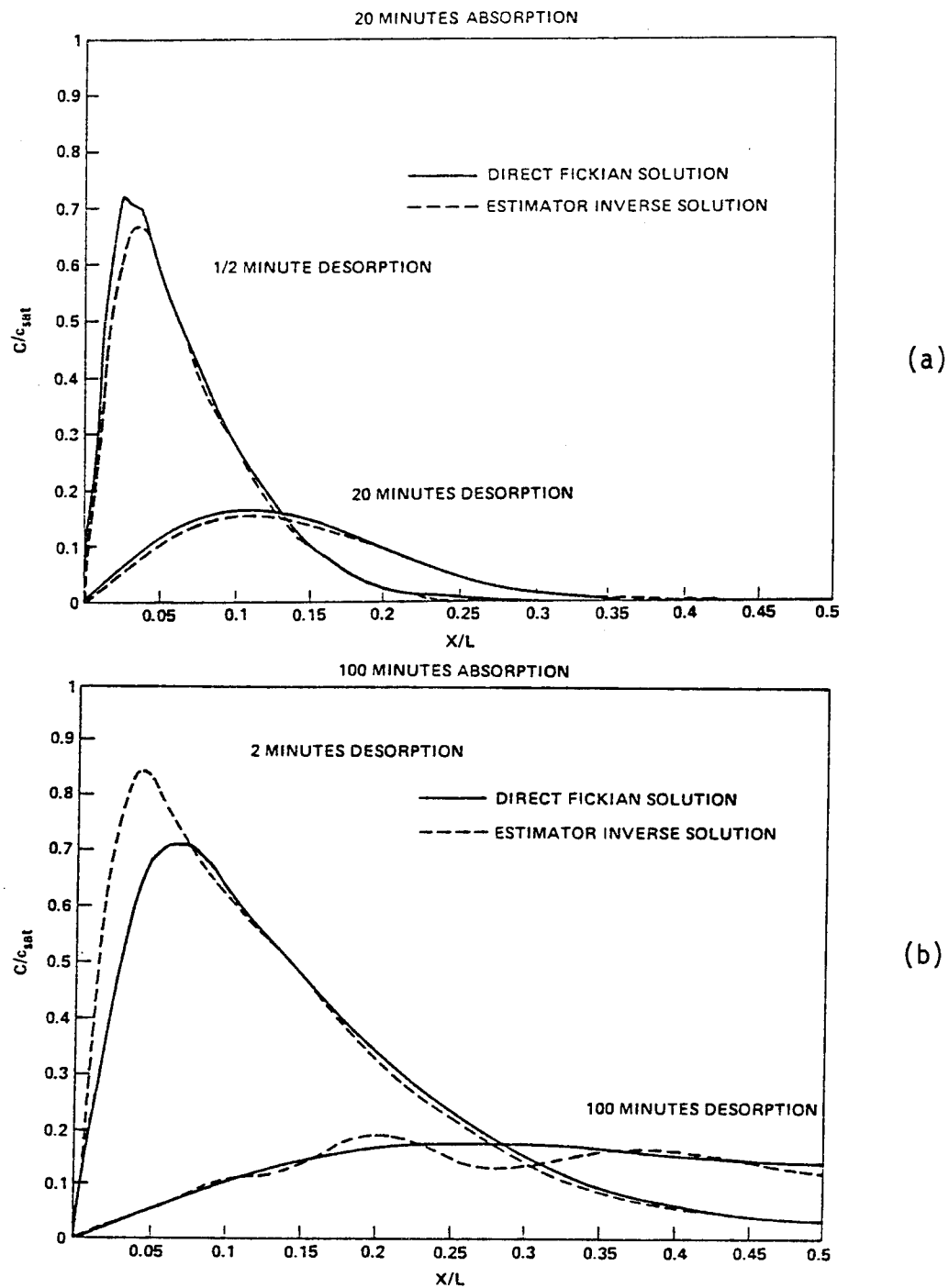


FIGURE 5
Moisture profiles via analytical modeling of partially saturated composite after (a) 20 minutes absorption and (b) 100 minutes absorption.

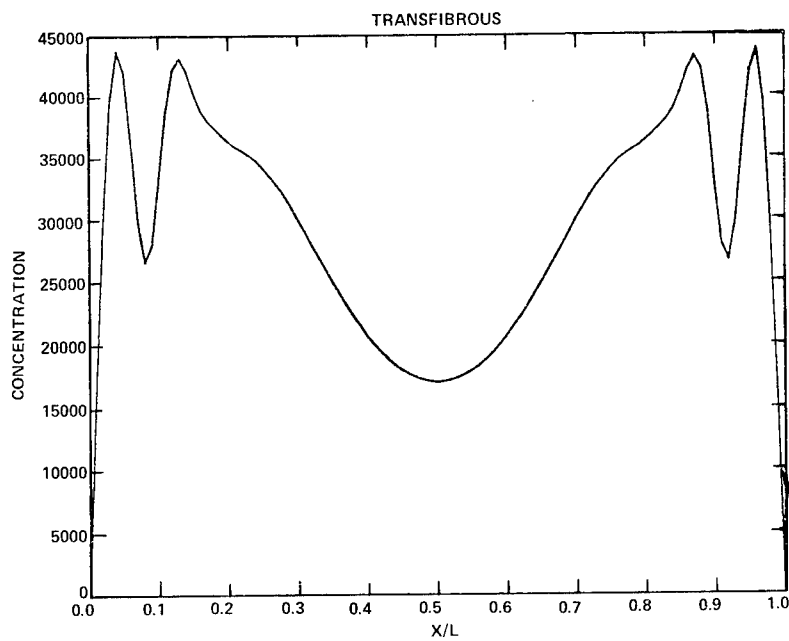


FIGURE 6
Moisture profile of composite containing air voids.

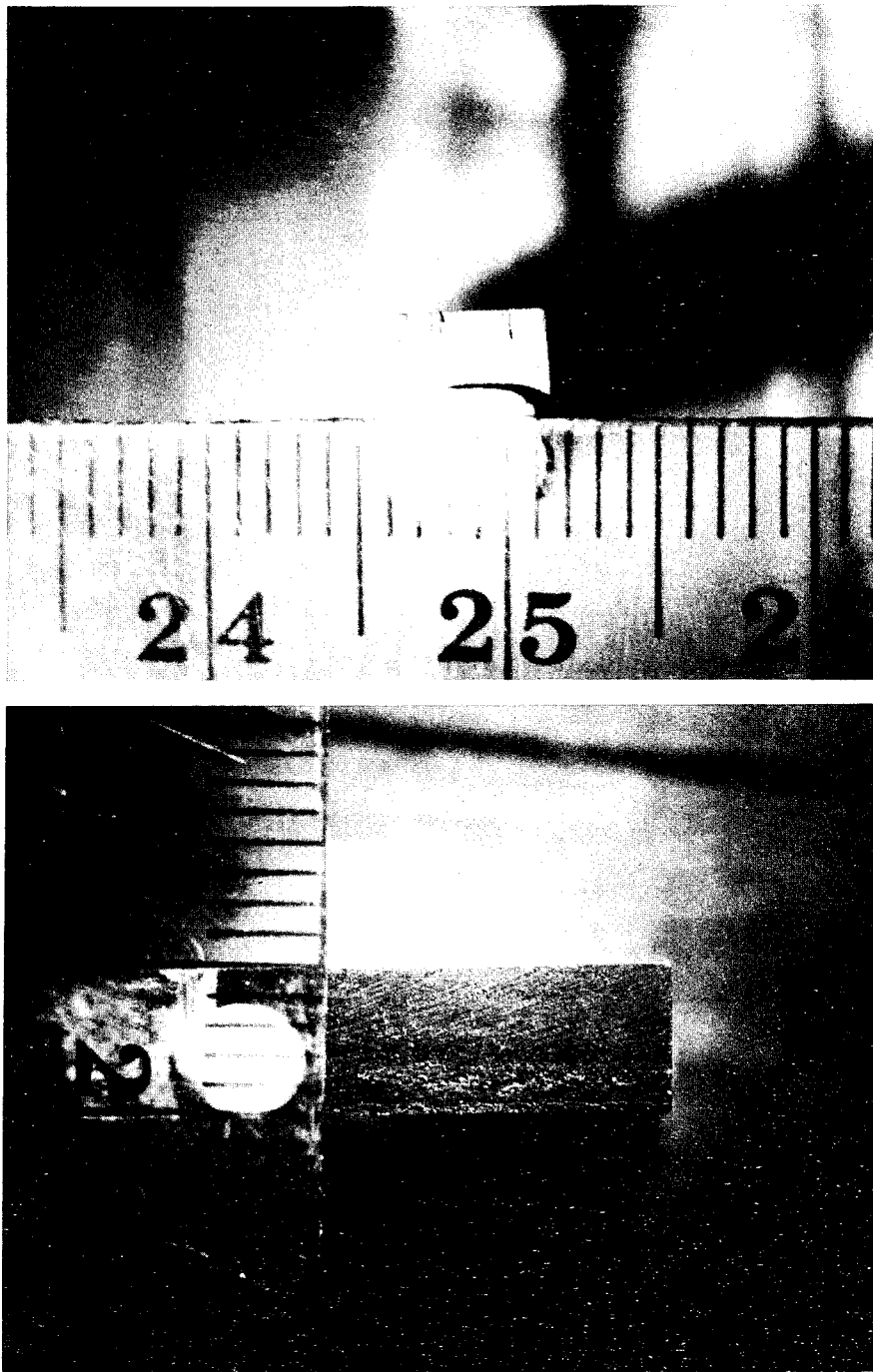


FIGURE 7

Photographs of a composite containing voids in (a) translaminar surface view (b) transfibrous surface view.

RECENT WORK ON TECHNIQUES AND APPLICATIONS OF MOISTURE BARRIERS TO GRAPHITE EPOXY COMPOSITES

James F. Haskins
General Dynamics Convair Division
P.O. Box 80847
San Diego, CA 92138

Abstract: A number of space systems such as Thematic Mapper, MAGSAT and other space optical devices require that the components be dimensionally stable during both ground and space operation. It has been found that certain graphite/epoxy composite laminates can provide extremely low coefficient of thermal expansion ($\alpha < 0.05 \times 10^{-6}$ in./in.F) and because of this are ideally suited to optical benches, telescope housings, and mirror substructures. However, the epoxy must be protected from moisture because it is hygroscopic and does change dimensions as it absorbs or desorbs moisture. Typically it may change as much as 100 microinches/inch over a period of several months when exposed to high relative humidity. This becomes a problem because most of the equipment will be manufactured, assembled, and operated in a humid environment before it is launched into space. Holding the humidity at a low level lessens this problem but does not eliminate it.

A real advance in optical equipment for use in space can be made if graphite/epoxy can be sealed from moisture without substantially changing its weight and coefficient of expansion. The objective of this work was to test the effectiveness, develop inspection procedures, and check the reliability of a moisture barrier developed previously at General Dynamics Convair Division.

This paper gives the results of a critical evaluation of the effectiveness and reproducibility of the eutectic coating. Fifteen-inch long graphite/epoxy coated specimens were used to study processing variables, inspection techniques, and dimensional changes due to moisture pickup.

Key words: graphite/epoxy; advanced composites; dimensional stability; space optics; moisture barrier; eutectic coating.

Graphite composite materials have been successfully applied to a variety of satellite structures. Weight saving resulting from excellent specific mechanical properties has been realized in addition to the attainment of stringent dimensional stability. Research and development efforts are now directed toward challenging new applications. During 1978 this effort was focused on the development of application processes for an existing moisture barrier for graphite/epoxy and the experimental verification that such a coating does indeed seal the composite from moisture.

General Dynamics discovered the moisture problem in 1970 while evaluating graphite/epoxy composites on both Air Force and NASA programs (References 1 and 2).

Graphite/epoxy composites absorb moisture from the atmosphere. This absorption causes two basic problems; i.e. (1) decrease in matrix-dominated mechanical property values and (2) changes in physical dimensions. The effects are reversible in that heat and/or vacuum will drive off the moisture and will return the composites to their dry properties and dimensions. The absorption of moisture primarily occurs in the epoxy matrix and the resulting changes in composite mechanical and physical properties are a result of this absorption by the resin. Therefore, the type of reinforcement does not greatly influence the moisture effects. Epoxy matrix composites reinforced with boron, glass, and Kevlar filaments behave similarly to graphite/epoxy composites.

This work is concerned with sealing GY-70/X-30 graphite epoxy from moisture in its isotropic layup $[(0/45/90/135)_s]_2$. This material was chosen because of its low coefficient of expansion. This makes it ideal for optical devices to be used in space. The problem with moisture absorbed by the material is that it will give up the moisture when subjected to the vacuum of its space environment. Certain optical systems will detune as the moisture is removed by the low pressure

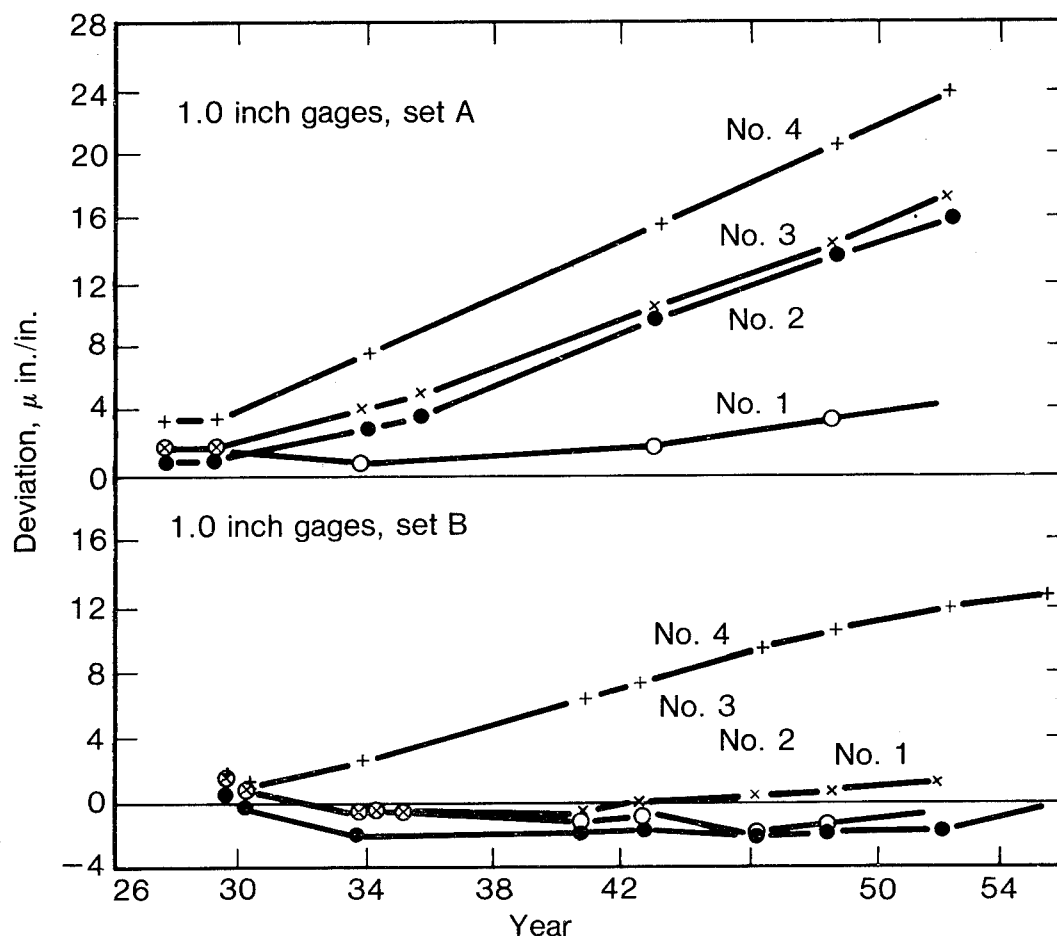


Figure 1. Example of length change with time under fixed environment for two sets of nominally similar 1-inch steel gage blocks (Emerson 1957).

of the working environment. Since ground time for many of these devices is as much as a year in 50% relative humidity, one finds that the dimensions of the optical system can change by amounts which are unacceptable. For this reason it is important to be able to provide a moisture barrier for the composite material which will seal it completely from humidities up to 100%.

Dimensional stability of materials is not generally well understood. When speaking of holding dimensions to one part in a million for long periods of time one must realize the difficulties involved when even the most stable metals are used, for example, gauge blocks, such as Johanson Blocks, made of a specially heat treated, fine grained steel which has been thermally cycled many times. Even when blocks of this type are held at constant temperature they may change in length over a period of years.

Work done by the Bureau of Standards is shown in Figure 1 for 8 blocks which were observed for 25 years. This background allows one to appreciate the extreme demands placed on a material such as graphite/epoxy. A material of this type, made up of two components of vastly different coefficients of expansion, certainly contains residual stresses because of its method of manufacture in addition to dimensional changes caused by moisture absorption. In Figure 2 both weight and length changes are shown for a typical bare laminate of the type being studied here. The barrier being studied must seal the surface of the material so that no weight or length change occurs over long periods of time.

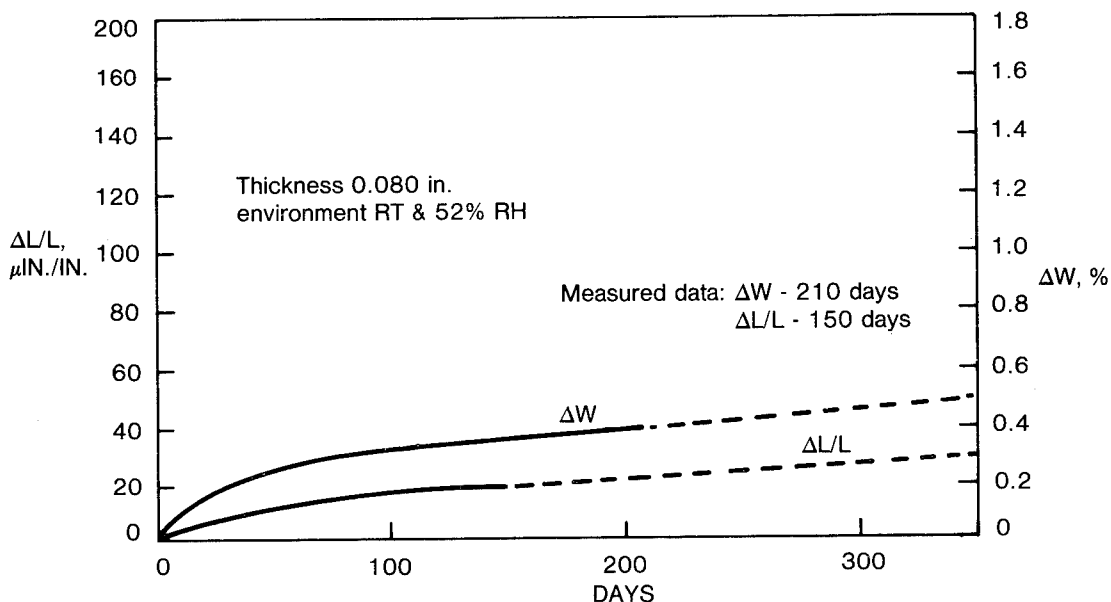


Figure 2. Environmental effects on [(0/45/90/135) s]₂ GY-70/X-30.

Objective: A real advance in optical equipment for use in space can be made if graphite/epoxy can be sealed from moisture without substantially changing its weight and coefficient of expansion. The objective of this work was to test the effectiveness, develop inspection procedures, and check the reliability of a moisture barrier developed previously at General Dynamics Convair Division. The specific objectives for 1978 were:

1. Develop a better understanding of the processing variables and their sensitivity to support the development of a production process specification.
2. Develop quality control procedures and accept/reject criteria for production hardware.
3. Demonstrate Items 1 and 2 above through fabrication and test of six 15-inch specimens using the established procedures.
4. Scale-up to approximately full-sized cylinders and demonstrate the effectiveness of the coating through test of simulated full-scale Thematic Mapper hardware.
5. Modify, if required, our specification for applying the coating to production hardware.

Approach: The effectiveness of the coating was studied by preparing samples of graphite/epoxy and coating them using the process then currently in use and measuring their dimensional stability when exposed to a humid environment.

The then current process was examined step by step and comparisons were to be made to the original process by the inventor to determine if any changes had occurred during the four years of use since its conception in 1974. Then, additional specimens were prepared using the technique representative of the original process. These specimens were carefully inspected during processing to determine if performance correlated with an exacting visual inspection.

Repeatability was studied once the process had been perfected. This was done by preparing several batches of specimens using the standardized process.

Eddy current techniques were developed to determine whether coating thickness could be evaluated by nondestructive means. Long-term evaluations were made to study the stability of the coating by observing the length of a number of specimens exposed to high humidity. Length changes were measured and recorded to the nearest microinch per inch using a special laser dilatometer. Weight gain of each of these specimens was also recorded so that any observed weight gain could be correlated with the corresponding length change. For those specimens where length and weight changes were recorded, a check of the inspection records was made to determine whether defects in the coating correlated with these changes.

A twelve-inch diameter cylinder was to be fabricated and coated. This cylinder was exposed to accelerated aging (95% relative humidity) and weight gain determined.

Progress: As part of a 1974 IRAD program, a moisture barrier coating was developed for sealing graphite/epoxy. This coating was a very special tin-indium eutectic which could be applied over the composite surface after it was copper plated. The coating was applied to a few small laboratory specimens and was checked by observing them in a humid environment. Their dimensions did not seem to change in this humid environment and the moisture barrier was considered a real breakthrough. Since its invention the requirements for dimensional stability have increased, the size of the components have increased, the plating and coating tanks have been enlarged, and the original chemicals have been replaced. As is usually the case in newly in-

vented processes, more research is needed to completely understand and document the process. The following progress was made for each of the specific objectives for 1978.

1. Processing Variables — Starting with surface preparation, it was found that the process is extremely sensitive to surface preparation and the amount of material removed by glass beading had to be carefully controlled. It was further found that contamination existed in the glass beading unit itself and a separate beading unit was recommended.

Generally speaking, standard plating practices were not being followed. Current settings were estimated rather than calculated. Bath control was poor and had to be greatly improved.

The eutectic coating is applied by spraying the eutectic in a stearic acid bath which is maintained at a temperature above the eutectic melting point. This stearic acid bath was contaminated and had to be cleaned. The spray nozzle used in applying the eutectic had been modified and had to be replaced. A brushing process used during the application of the coating had been eliminated, thus resulting in some localized bare spots; in these areas, the copper plating was visible. The excess eutectic is removed by a slinging process after the entire surface is covered. This slinging process had been changed to eliminate a bubbly appearance which later proved to affect the sealing of the composite surface.

2. Accept/Reject Criteria — To develop accept/reject criteria a number of specimens were prepared and their acceptability was measured by observing their dimensional stability.

Careful visual inspection of each specimen requires a great deal of time and the use of a low-powered microscope. A trained observer with proper light and the correct magnification was able to check the coated surface for pinholes, blisters, uncoated areas, and contaminants. A system was developed during the investigation for cataloging the imperfections and recording the data for the entire surface of each specimen. The performance of each specimen could be measured by observing changes in length during moisture exposure and comparing this to the number of imperfections found during visual inspection.

A method for measuring coating thickness was developed by using eddy current techniques. This method was able to provide a quick way of covering the entire coated surface. The instrument was adjustable and the impedance setting was varied to obtain the greatest sensitivity.

Weight gain attributable to the coating was also used as a method of measuring coating thickness. Since the moisture barrier is made up of electroless copper, copper plate, electroless tin and the eutectic, the specimens were weighed after each process step so as to measure the thickness of each layer of the coating. It was found that the copper must be thick enough for eutectic coverage. The eutectic thickness was about half as thick as the copper. These thicknesses amount to a weight change of several percent. For example, the surface area of our specimens was about 75 square inches and they weighed about 85 grams. For this case, 0.0001 inches of uniformly distributed copper would increase the weight by approximately one gram. The eutectic would increase the weight approximately 0.8 grams per 0.0001 inches of thickness. Coating thicknesses for composites can be checked very accurately by weight if the coating is uniform.

To check coating thickness and uniformity, a number of specimens of known performance in the area of moisture absorption were sectioned, mounted, and polished prior to microscopic examination. These mounts showed the uniformity of the coating and confirmed the calculated average thicknesses of each component. The variation in coating thickness was recorded and compared to previously recorded eddy current readings for the same areas. It was found that the eddy current measurements were recording the copper thickness and that variation in the tin-indium coat made little change in the eddy current readings. This provided a method of inspecting the copper thickness both before and after application of the eutectic. The eutectic thickness was checked then by weight and visual observation.

Scanning electron microscope studies were made of the coated surface. Extremely small pinholes and uncoated areas could be detected using this instrument. Such observations are not useful on large components. Studying very small pinholes and their cause did help us confirm the critical fact that the coating bath temperature must be below the temperature at which the epoxy is post cured. If this is not the case, further curing of the epoxy can cause bubbles and pinhole formation in the coating, rendering it less effective.

3. Demonstration Through Fabrication and Test — The composite material evaluated was GY-70/X-30 graphite/epoxy, 16 plies thick and laminated in what is known as the isotropic layup

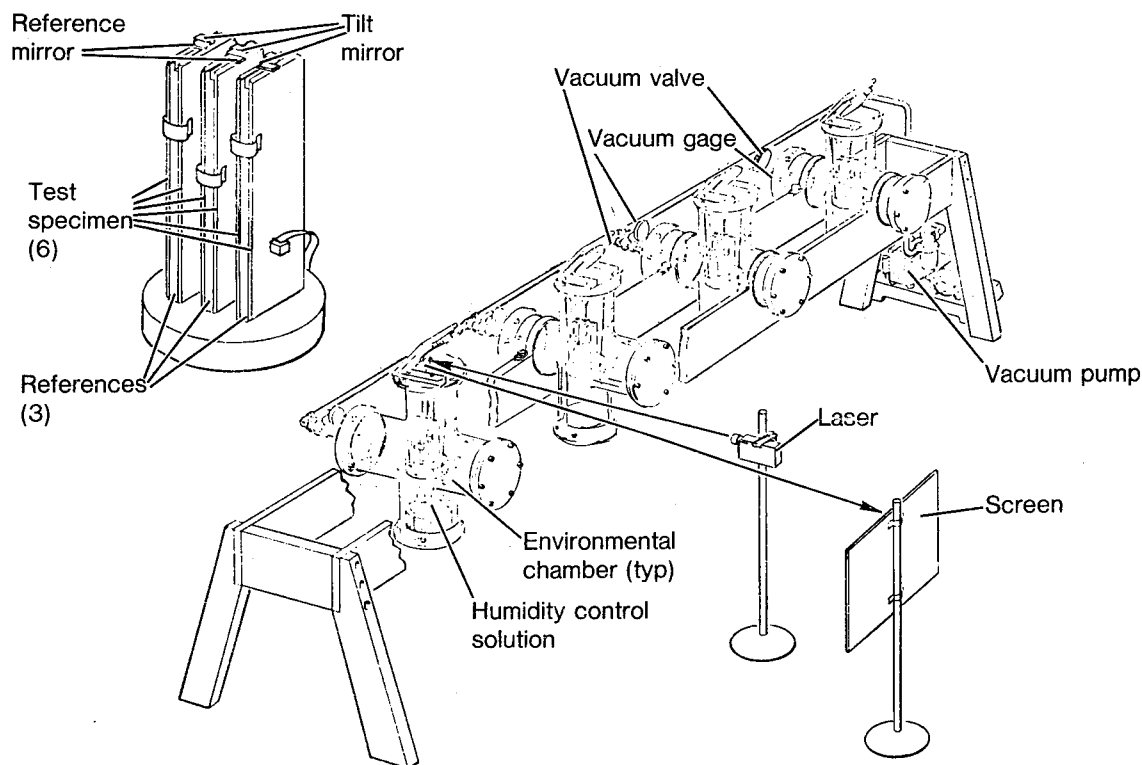


Figure 3. Hygroscopicity dimensional measurement test.

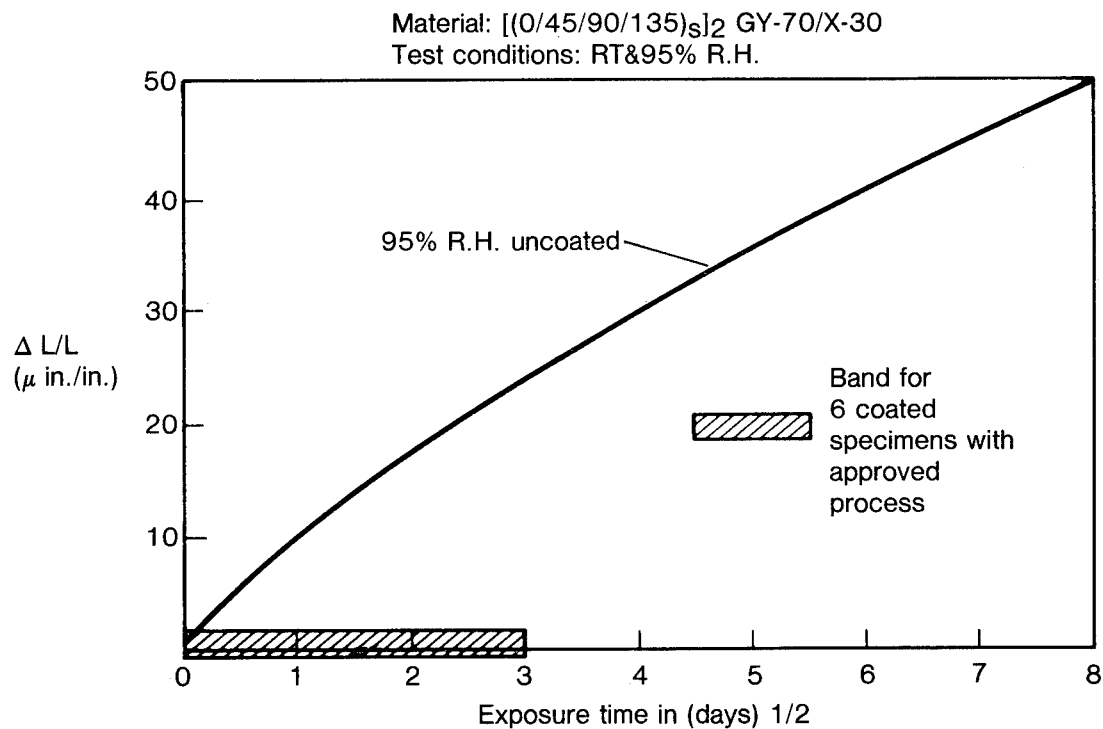


Figure 4. Dimensional stability study of six graphite/epoxy specimens (January 30 to February 8, 1978).

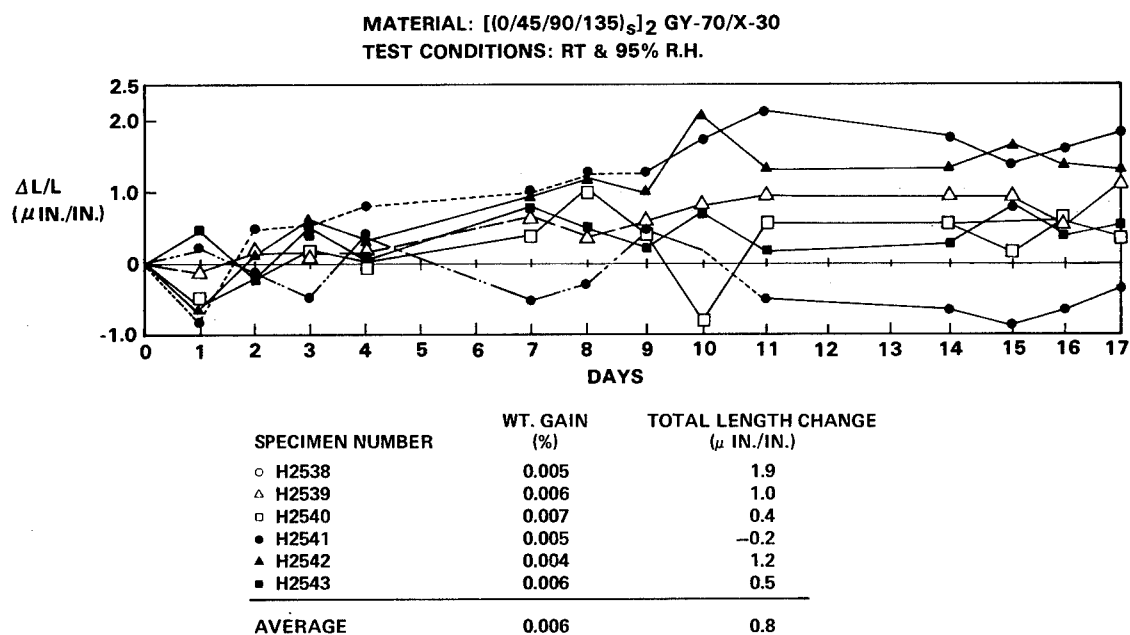


Figure 5. Dimensional stability study of six coated graphite/epoxy specimens (January 30 to February 16, 1978).

[(0/45/90/135)_s]₂. This layup gives a nominal thickness of 0.080 inches. The specimens were 15 in. long and 2¼ in. wide. This large size was chosen to increase both the accuracy of the length change measurement and the surface to be coated. The specimens used in the original work were about one third this size. The type of equipment used to make the measurements is shown in Figure 3. Length change was measured by comparing the specimen length to a calibrated piece (ULE) Ultra low expansion glass. This was done with a tilt mirror using a laser light source and an optical lever of 20 ft. This data was recorded on a stationary glass plate. The tilt mirror was supported on knife edges formed by beveling one end of both the ULE and the test specimen. The specimen was mounted against stops on the ULE and a precise spacing is established between the knife edges. This spacing and the length of the optical lever determined the magnification factor used in obtaining the length change. The length change was determined by reflecting the small laser beam from both the tilt mirror and the reference mirror and measuring the separation between these projected small spots. This difference can be measured to the nearest 1/64 of an inch so that with a knife edge spacing of one tenth inch and the reflection projected 20 ft from the mirror one can easily measure one half a microinch/inch using a 15 inch specimen.

After the process variables were brought under control by making and testing several batches of six specimens it became difficult to reduce dimensional changes much below what is shown in Figure 4. Figure 4 also shows the difference between uncoated specimens and coated specimens when exposed to 95% relative humidity for a number of days.

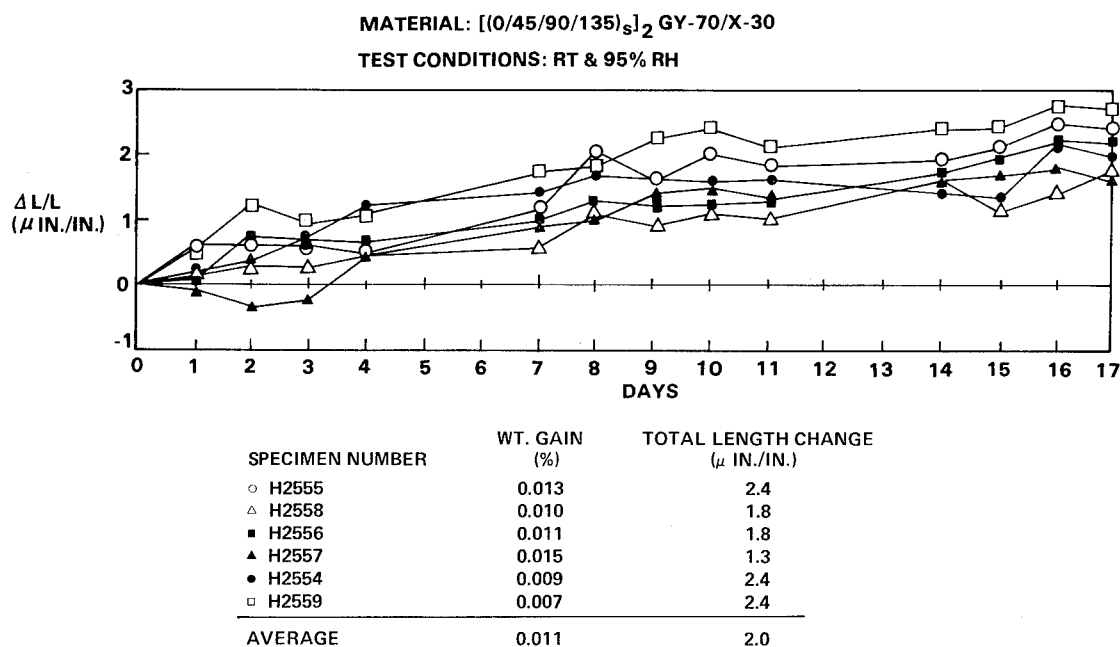


Figure 6. Dimensional stability study of six coated graphite/epoxy specimens (February 17 to March 9, 1978).

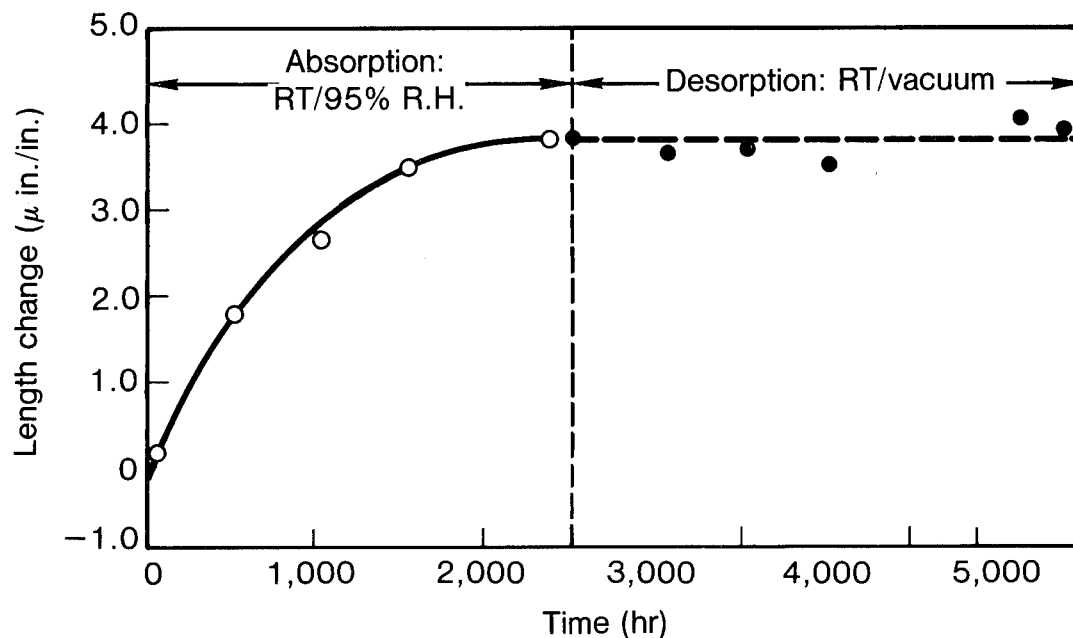


Figure 7. Exposure of eutectic coated $[(0/45/90/135)_2]_2$ GY-70/X-30 specimens (average of six specimens).

Note: Eddy Current Meter Settings

Bare GY-70/X-30:0 Meter Reading

Standard Coated Specimen: 80 Meter Reading

Reactance Setting X440 R479

	Outside			Inside			Top Baffle		Bottom Baffle	
	Top	Middle	Bottom	Top	Middle	Bottom	Top	Bottom	Top	Bottom
1	86	72	82	73	44	62	53	42	40	47
2	88	76	86	85	39	58	58	47	46	49
3	87	78	86	82	41	58	58	43	40	44
4	97	78	83	67	46	65	56	45	40	43
5	100	80	93	93	44	70	56	42	40	43
6	100	83	75	63	44	58	52	44	42	47
7	97	77	77	58	39	60	57	45	42	44
8	88	70	73	70	40	54	54	42	40	43
9	80	60	72	61	40	60	56	44	39	43
10	82	62	76	77	39	59	60	51	47	47
11	84	73	86	69	43	66	56	42	45	54
12	100	84	97	63	40	63	56	47	43	57
13	100	97	100	70	45	86	56	44	47	57
14	100	92	85	72	42	65	56	43	47	58
15	93	85	88	69	40	66	56	45	44	50
16	83	80	80	75	42	61	56	43	42	49

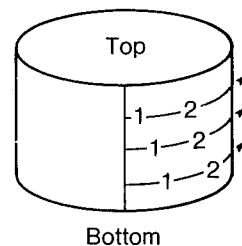


Table 1. Eddy current measurements for eutectic-coated BY-70/X-30 cylinder.

Figures 5 and 6 show studies made on two succeeding sets of six coated specimens. The moisture absorption did not correlate with the length change for the twelve specimens shown in the figures. When they were taken as two sets of six, and averaged both in weight gain and length change, Figure 5 shows a smaller weight gain and a smaller change than the set of Figure 6. However, in both cases the length change exceeded what would have been expected for an uncoated material in that environment.

The set of six specimens given in Figure 6 were kept in the 95% relative humidity environment for 2500 hours (approximately 3½ months) at which time they came to an equilibrium length. This is shown in Figure 7. At this time the moisture was removed from the chambers and the specimens were evacuated for another 3,000 hours. As can be seen in Figure 7, the lengths of the specimens remained constant. This led to the conclusion that the recorded length change was not due to moisture. The specimens had all been thermally cycled a number of times to stabilize them and relieve residual stresses, however, at this low level of length change, such changes could very well be additional stress relief. More work needs to be done in this area to determine if this is a real effect. It could be a problem if the optics were final tuned earlier than four months after the graphite/epoxy is laminated.

4. Simulated Hardware Component Test — To determine the problems associated with coating large components a 12-inch diameter cylindrical tube containing two baffles was coated using the improved process. The coated cylinder was inspected both visually and by the eddy current method. The cylinder passed the visual inspection but the eddy current readings were low on the inner wall of the cylinder and the baffles. These low readings were caused by improper anode placement during copper plating. An eddy current reading of 75 or greater was determined to be satisfactory for this coating. Table I shows the eddy current readings for various locations on the cylinder passes but the inside surface failed to meet the required 75 reading.

The eddy current method was being developed during this program and was not fully understood when the cylinder was prepared. The measurement of length change for the cylinder would be very expensive and so it was decided to measure the effectiveness of the coating by weight gain in a humid environment. The cylinder was kept at 95% relative humidity at room temperature. In 269 days its weight increased from 532.363 gms to 534.118 grams which is a weight gain of 0.33%. This is equivalent to approximately 20 microinches/inch length increase. If the entire weight gain was due to moisture this would mean the coating was about 75% effective. This cylinder is still being observed for further weight gain.

References:

1. *Advanced Composite Applications for Spacecraft and Missiles*, Phase I Final Report, AFML-TR-71-186 March 1972.
2. *Development of Design Data for Graphite Reinforced Epoxy and Polyimide Composites*, NAS 8-26198, May 1974.

SESSION 3

AEROSPACE AND AIRCRAFT APPLICATIONS AND DESIGN

Chairman: C. E. S. Ueng

Georgia Institute Of Technology

In-Service Ultrasonic Inspection System for Composites

F. H. Chang, J. R. Bell, A. H. Gardner,
C. P. Fisher and G. P. Handley
General Dynamics, Fort Worth Division
Fort Worth, Texas 76101

Abstract

Advanced composite structures are presently used on high performance U.S. Air Force aircraft to save weight and increase performance. These structures are often difficult to inspect because of their complex/multi-bondline construction and because of the general lack of experience in the inspection of composite structures in the field environment. Ultrasonic techniques have generally been employed for the detection of service induced discontinuities such as disbonds and delaminations. They are not considered cost effective for inspection of large areas for small flaws or for monitoring areas containing known small flaws for propagation during service, primarily because of the lack of flaw position locating and permanent inspection result recording devices. An ultrasonic technique was developed under an AFML contract to record the position and flaw indication in a permanent manner and minimize operator dependence to obtain a high level of inspection reliability. The technique is simple to apply in the field environment by personnel without advanced training. In the program, specimens representing typical composite structures and containing implanted flaws simulating service induced or production type defects were fabricated. Improvements were made to the state-of-the-art ultrasonic inspection techniques to detect these defects. A follow-on program is being conducted to establish the producibility of the semi-automated ultrasonic inspection system for aircraft composite structure, based on the preliminary design developed in the previous contract, to provide a complete inspection system from inception to obsolescence.

DESIGN CONSIDERATIONS FOR GRAPHITE-EPOXY LAMINATES OF LOW THERMAL EXPANSIVITY

Dennis D. Smith
Composite Design Group
Boeing Aerospace Company
Seattle, Washington 98124

Abstract: The development of graphite-epoxy laminate designs for space missions requiring structural components with near zero coefficient of thermal expansion (CTE) is examined. The selection of fiber systems and laminate designs is approached by evaluating CTE sensitivities to material and process variabilities. Uniaxial and biaxial thermal stability laminates are considered. From this design approach, material and process specification tolerances can be determined to control laminate CTE within design objectives. Design examples are presented to illustrate this laminate design approach.

Key words: Advanced composite materials; graphite-epoxy laminate design; laminate design sensitivities; thermal expansion.

INTRODUCTION

The structural efficiency of recent aerospace vehicles and vehicle components has significantly benefited from the application of advanced composite materials. In particular, graphite-epoxy has come into the mainstream of spacecraft design activities. Increased strength and stiffness, reduced weight, improved thermal stability, greater fatigue resistance, and lower cost have been exhibited as inherent characteristics of this material system. For specific applications, any one of these particular design goals may be optimized by proper consideration of the orthotropic nature of individual graphite-epoxy plies or lamina. To accomplish this, the composite designer combines several such layers to develop a multiple ply laminate with the desired mechanical and physical properties.

Designing with graphite-epoxy materials involves the weighing of various material related compromises. For example, selection of a graphite fiber and orientation of the lamina to achieve a specific property such as high stiffness may well prove to be detrimental to one or more of the other laminate properties, such as CTE. This paper considers the development of a laminate of near-zero thermal expansion and the interactive design compromises associated with its use.

MATERIALS

There are many fibers presently in use in advanced composite structures. Some of the more common of the graphite fibers fall into three main categories: 1) high strength, 2) high modulus, and 3) ultra-high modulus. Table 1 shows typical properties of these fiber systems. Most graphite filaments are made from a graphitization of the organic precursor polyacrylonitrile (PAN). A pitch precursor is still in the development stage and shows excellent cost advantages over the PAN precursor filaments.

The graphite fibers (except GY-70) are supplied to processors in tow form, (small bundles of fiber) or in woven fabric form. Tows are combined with a matrix material such as epoxy and supplied to fabricators in preimpregnated (prepreg) sheets or rolls of various widths and areal weights (weight of fiber per unit area). The fabricators, such as Boeing, combine the tapes into various laminate configurations and cure the laminates. Epoxy matrix materials are thermosetting at temperatures ranging from room temperature to 400°F. Most aerospace laminates are cured from 250°F to 350°F in a pressurized autoclave, although oven cured and press cured laminates are also made.

The combination of graphite fiber and epoxy matrix in prepreg form is the building block for the designer. Typical properties of three major graphite fiber types combined with an epoxy matrix are shown in Table 2. These are typical values which do not necessarily represent a specific graphite fiber/epoxy system and are intended to represent the material type. It can be seen from the material properties that a ply of graphite fibers and epoxy in prepreg tape form is highly orthotropic, that is, the longitudinal and transverse properties differ greatly. The material is generally considered homogeneous even though the two-phase material is obviously heterogeneous. The simple homogeneous orthotropic representation is usually necessary for designer's (macromechanical) laminate analysis. It will be seen, however, that a micromechanical analysis which recognizes the inhomogeneity of the ply but ignores the internal structure of the fiber and matrix will be required to assess specific laminate performance.

DESIGN REQUIREMENTS

When the design of a vehicle component requiring graphite epoxy is initiated, the first task is to identify the design objectives. This may be readily determined, but more likely only a higher level assembly performance is known or specified. Before the individual component performance requirements can be isolated, an investigation of component contribution to assembly or vehicle performance may be required. Such a study on a thermal stability critical 2.4-meter graphite epoxy optical support (metering) structure was performed and reported in reference 1. The metering truss structure component thermal stability

sensitivity study resolved the individual member contributions of three types of thermal deformations: despace, decenter and tilt. Figure 1 shows the truss structure and the deformation vectors. The relative distortion figure for each major component of the truss assembly is shown in Table 3. A nominal value for the coefficient of thermal expansion (CTE) is assigned to a component and all other component CTE's are made zero. For this linear system, this allows the total truss thermal performance to be a function of a singular component type. With this data, the truss tube members could be readily identified as the critical component of the metering truss structure. Successive iterations, as described in the reference, were made to ascertain the nominal CTE values and allowable CTE tolerance ranges for the individual components. The truss component thermal influence analyses were performed by utilizing a deterministic analysis approach. In deterministic analyses, the uncertainty that exists between predicted and measured performance is considered by the utilization of a safety factor. A probabilistic approach, which recognizes that performance variability is possible, is more consistent with composite materials. There are not deterministic, single-valued properties for graphite epoxy lamina and laminates. This does not mean that a probabilistic design approach incorporating a Monte Carlo random-number-generator with appropriate probability distributions functions is always required to properly assess specific laminate characteristics. However, a designer must be aware that advanced composite material characterization is statistical in nature and that certain material properties may, at times, show wide variations from nominal. The material system in lamina or laminate form has inherent variabilities which should be understood regardless of the fact that simplifying assumptions have allowed deterministic analyses to quite adequately predict these properties.

Laminate Design. The designer, once he has established the graphite-epoxy component CTE, is ready to select the fiber/epoxy system and configure the lamina plies to develop a laminate with the desired thermal stability. As discussed earlier, the laminate CTE can be determined by specification or deduced from a thermal sensitivity study. Determination of a laminate form which will result in the desired CTE, however, requires the review of potentially many candidate laminate systems. There are two basic laminate categories: isotropic laminates and anisotropic laminates. An isotropic laminate results in mechanical and physical properties which are essentially constant in any plane which passes through a point in the laminate. Such laminate properties as CTE, strength, and stiffness are essentially constant in any in-plane direction. This laminate can be more accurately described as pseudo-or quasi-isotropic since truly isotropic material behavior would be difficult to achieve. A symmetrical anisotropic (orthotropic) laminate has three perpendicular planes of material property symmetry. This laminate results in CTE, strength, and stiffness differences in the orthogonal laminate axes. The amount of difference is a function of the laminate design, but an extreme would be a unidirectional

laminate (all lamina fibers parallel). The laminate properties would be the same as the lamina properties in such a layup.

In general terms, shell structures, cylindrical assemblies and bulkheads that have structurally or thermally interactive components (rings, stiffeners, etc.) are potential applications for isotropic laminates. Tubes, rods, beams, rings, flexures and other components which do not have direct thermal stability coupling may be fabricated from orthotropic laminates. For some components, this distinction may be difficult to resolve. A general design consideration is to utilize an isotropic laminate unless there is some reason against its use. These reasons could be to increase stiffness, strength, microyield or hygroscopic stability, to name a few.

The requirement for an isotropic laminate creates a unique design condition and effectively dictates the design. Three laminate families which are commonly utilized to produce in-plane isotropy as well as out-of-plane balance are:

- 1) $(0^\circ/\pm 60^\circ)_s$ 6 ply laminate
- 2) $(0^\circ/\pm 45^\circ/90^\circ)_s$ 8 ply laminate
- 3) $(0^\circ/\pm 30^\circ/\pm 60^\circ/90^\circ)_s$ 12 ply laminate

Note: s represents symmetrical laminate

The more plies in the laminate, the closer the laminate form represents true isotropy. The 8-ply laminate is in general use as a balance between obtaining reasonable isotropy and minimizing fabrication costs. Symmetrical laminates are used to prevent in plane warpage due to unbalanced thermal or mechanical strains.

Orthotropic laminates may take many forms, such as:

$$(0_x/\theta)_s \quad (0_x/\pm\theta/90)_s \quad (0_x/\pm\theta_1/\pm\theta_2)_s$$

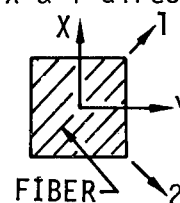
Note: θ represents crossply of undefined angle
x represents undefined number of 0° plies

Obviously, hundreds of orthotropic laminates could be designed of a graphite-epoxy material, of hybrid graphite-epoxy systems and of combinations of graphite and fiberglass, boron, or Kevlar. The designer needs to assess the design objectives and develop a thermally stable laminate design which also meets strength and stiffness requirements. In order to achieve laminate design with essentially zero coefficient of expansion (CTE) in the plane of the laminate, different design approaches must be utilized for isotropic and anisotropic laminates.

For an isotropic thermally stable laminate design, very high modulus fibers are required. Halpin and Pagano (2) developed a solution for the pseudoisotropic thermal expansion coefficient in terms of the lamina properties:

$$\alpha_x = \alpha_y = \frac{(\alpha_1 + \alpha_2)}{2} + \frac{(\alpha_1 - \alpha_2)(E_1 - E_2)}{2(E_1 + (1 + 2\mu_{12})E_2)}$$

where $\alpha_x = \alpha_y$ = laminate thermal expansion (PPM/°F) in X & Y directions
 α_1 = lamina 0° thermal expansion (PPM/°F)
 α_2 = lamina 90° thermal expansion (PPM/°F)
 E_1 = lamina 0° modulus of elasticity (PSI)
 E_2 = lamina 90° modulus of elasticity (PSI)
 μ_{12} = Poisson's ratio



In general, this equation for CTE requires that α_1 (longitudinal lamina CTE) be negative and the ratio of fiber modulus to matrix modulus be greater than 100 in order to achieve zero CTE in an isotropic laminate. As an example, laminate analyses of commercially available graphite fiber/epoxy systems allows a comparison of pseudo-isotropic laminate thermal expansion.

TABLE 4
Isotropic Laminate Thermal Expansion

<u>Fiber in Laminate</u>	<u>Isotropic Laminate CTE (PPM/°F)</u>
T300/AS	1.00 - 1.20
HMS/T-50(PAN)/MODMOR I	0.13 - 0.50
GY-70/P-75S	~ 0

Only the ultra-high modulus fibers $E_f \approx 70-75$ MSI result in an isotropic laminate of near-zero CTE. The negative fiber CTE is satisfied ($\alpha_f \approx -.7$ PPM/°F) and the fiber to matrix modulus ratio is greater than 100 ($E_f/E_m \approx 114$).

For orthotropic laminates, many different laminate configurations are capable of achieving near-zero CTE. The screening between laminates of this type generally considers laminate sensitivity to material variabilities as well as cost and secondary design requirements such as strength and stiffness.

Lamina Sensitivity. Determinate laminate analyses can establish the nominal coefficient of thermal expansion (CTE) of a graphite epoxy laminate. This type of analyses, however, will not resolve the influence of material and process variabilities of laminate CTE. In order to provide a designer some visibility into laminate CTE scatter,

lamina sensitivity studies are often needed. For critical components requiring stringent CTE control, they are essential.

All graphite fibers have variabilities associated with the predominate fiber property, which is fiber modulus. In general, as the modulus of a fiber increases, so does the statistical scatter. Therefore a designer could expect more fiber modulus variations from ultra-high modulus fibers than from AS or T300 (high strength) fibers. Increased fiber variability manifests itself as greater scatter in laminate CTE, the amount dependent upon the level of fiber dominance in any particular laminate.

For example, a lamina sensitivity study recently completed on a thermally stable pseudoisotropic GY-70/934 (fiberite 1534) laminate will be reviewed. The lamina sensitivity is determined by analyses which considers the influence of a particular variable, such as fiber modulus or fiber volume, on lamina properties. The variability of the Celanese GY-70 fiber and its influence on lamina properties is shown in Figure 2. Figure 2 shows the relationship of fiber modulus to lamina mechanical and thermal properties. The only significant lamina property changes due to fiber modulus variability is in the longitudinal (0°) lamina modulus (E_1) and in the longitudinal lamina CTE. That is, as fiber modulus increases, the 0° lamina modulus (E_1) significantly increases. The 90° lamina modulus (E_2) is not influenced by this variability, however. The shear modulus, Poisson's ratio and transverse (90°) lamina CTE as well as the transverse modulus are essentially insensitive to fiber modulus fluctuations. Actual fiber modulus test data, on material prepregged by Fiberite for Boeing shows the mean GY-70 fiber modulus to be 74.4×10^6 PSI with a standard deviation of 2.1×10^6 PSI.

Lamina properties are also influenced by the volumetric relationship of the GY-70 graphite fiber to epoxy matrix. Figure 3 shows how this relationship influences lamina properties. It can be seen that lamina properties and therefore laminate properties may be strongly influenced by the fiber to epoxy volume ratio. All lamina properties show a direct response to changes in fiber volume. Small variations in lamina fiber volume may result in significantly different lamina properties than nominal properties utilized in design.

Laminate Sensitivity. The lamina property fluctuations noted necessarily influence laminate CTE. Figure 4 shows how these changes affect the isotropic ($0/\pm 45/90$)_s GY-70 laminate CTE. From this figure, it can be seen that a ± 2 MSI lamina fiber modulus range will result in a ± 0.031 PPM/ $^\circ$ F laminate CTE variation, while a $\pm 2\%$ lamina fiber volume tolerance will vary laminate CTE over a ± 0.047 PPM/ $^\circ$ F range.

Also shown is the laminate sensitivity to the angled ply layup errors. The bottom chart of Figure 4 shows that a one degree error in layup of the $\pm 45^\circ$ ply would result in a CTE fluctuation of 0.028 PPM/ $^\circ$ F.

Figure 5 shows laminate sensitivity of an orthotropic T50 (PAN) laminate for comparison. The laminate change in CTE due to fiber modulus variation and angular errors in the cross ply lamina is less for the orthotropic laminate while the influence of fiber volume is about the same. Orthotropic laminates are generally a better laminate design selection where primary component material requirements are essentially uniaxial. When biaxial CTE control is specified, the isotropic laminate is then required.

In order to assess the performance characteristics of various orthotropic laminates, several sensitivity analyses would be required. This type of sensitivity analysis, performed either on a deterministic or a probabilistic basis, becomes, along with cost and mechanical property studies, a necessary tool for making rational design selections to meet a given set of mechanical property requirements as well as low thermal expansivity.

DESIGN VERIFICATION

From the laminate CTE sensitivity to the materials and process parameters, a designer can determine the material specification requirements as well as fabrication controls that must be imposed. Depending upon the allowable laminate CTE tolerance, the designer has a method by which to constrain only those variables which are critical and to tolerate other variables since their influence may not be significant. Material specifications and in-process controls can then be tailored toward a specific low expansion laminate.

Another consideration is the method of design verification. A trade must be made on the imposition of costly material and process controls compared to specifying design verification test requirements. If hand picked fibers, close fiber volume control and tight tolerances on ply angle are utilized, it is entirely possible that these additional program expenses could be more than offset by reduced verification testing.

SUMMARY

A composite designer has many material and laminate options when developing a low expansion component or assembly. A most important step in the development of a satisfactory design is a clear understanding of the design requirements. A vehicle or assembly sensitivity study similar to the Boeing Space Telescope truss study can be utilized to determine laminate CTE requirements at the component level.

Once the design objectives are available, a trade of candidate laminates investigating cost, weight, sensitivity to material and process variations, resultant mechanical properties, and joint or interface constraints can be made. Other considerations, not addressed here include

microyield, hygroscopic sensitivity, susceptibility to microcracking, fatigue and viscoelastic effects. Many of these parameters are difficult to determine analytically without the benefit of an existing data base of many such tests.

Of primary importance to a composite designer is the knowledge that while he is utilizing a material that is quite capable of obtaining laminates with thermal expansions in the ± 0.025 PPM/ $^{\circ}$ F range, modulus values to 30-35 MSI, strengths to well over 120 KSI, weights of 40% less than aluminum, and costs which are competitive with conventional metal structure, he must always be aware of the statistical nature of advanced composite materials. Unless a designer's "homework" is done, the same material that has such great potential may well prove that Murphy's law was right all along.

REFERENCES

- [1] Smith, D. D. and R. E. Jones, "A Statistical Evaluation of a Space Stable Optical Support Structure," SAMPE Journal, Vol. 14, No. 5 (Sept./Oct 1978), p 4.
- [2] Halpin, J. C. and N. J. Pagano, "The Laminate Approximations for Randomly Oriented Fibrous Composites," J. Comp. Mat., Vol 3 (1969), p. 720

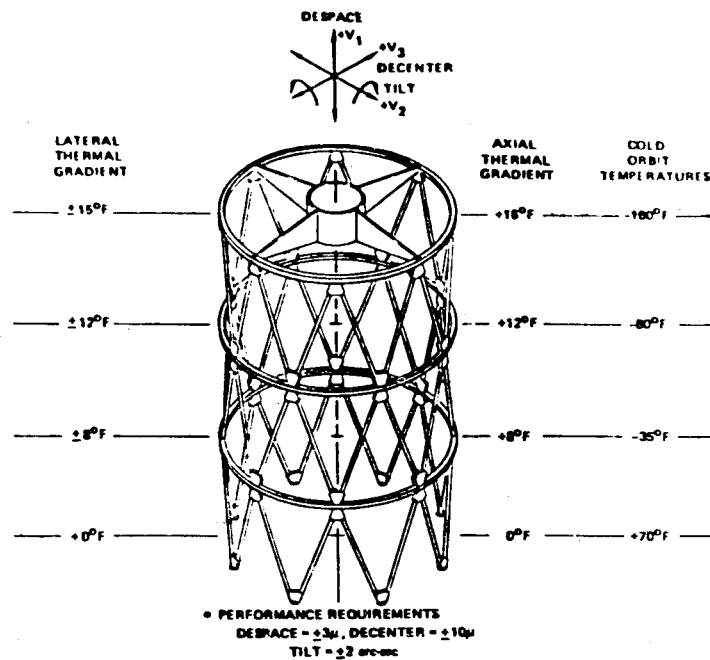


FIGURE 1 : OPTICAL SUPPORT TRUSS DESIGN

TABLE 1 : TYPICAL GRAPHITE FIBER PROPERTIES

Graphite Fiber	Type	F_{TU} (KSI)	E_T (MSI)
High Strength	AS/T300	400	32
High Modulus	HMS/T-50(PAN)	340	53
Ultra-high Modulus	GY-70	250	75

TABLE 2 : TYPICAL GRAPHITE EPOXY LAMINA PROPERTIES

Lamina Material	E_1 (MSI)	E_2 (MSI)	G_{12} (MSI)	CTE _X (PPM/°F)	CTE _Y (PPM/°F)
High Strength/epoxy	21.0	1.5	.66	-.10	14.5
High Modulus/epoxy	32.0	1.3	.60	-.30	14.8
Ultra-high Modulus/epoxy	45.0	1.2	.70	-.54	15.8

TABLE 3 : THERMAL STABILITY SENSITIVITY TO TRUSS COMPONENTS

Truss Component	Axial ΔT (axisymmetrical)			Lateral ΔT (antisymmetrical)		
	Despace (10^{-6} in.)	Decenter (10^{-6} in.)	Tilt (arc-sec)	Despace (10^{-6} in.)	Decenter (10^{-6} in.)	Tilt (arc-sec)
Trial A						
Strut .20/0	400	*	*	*	-444	-1.60
Ring .20/0	-40	*	*	*	264	0.15
Spider Beam .20/0	11	*	*	*	-102	0.04
Hub .20/0	7	*	*	*	2	0.01
Total	+378 > 118				-280 < 394	-1.40 < 2

*Negligible

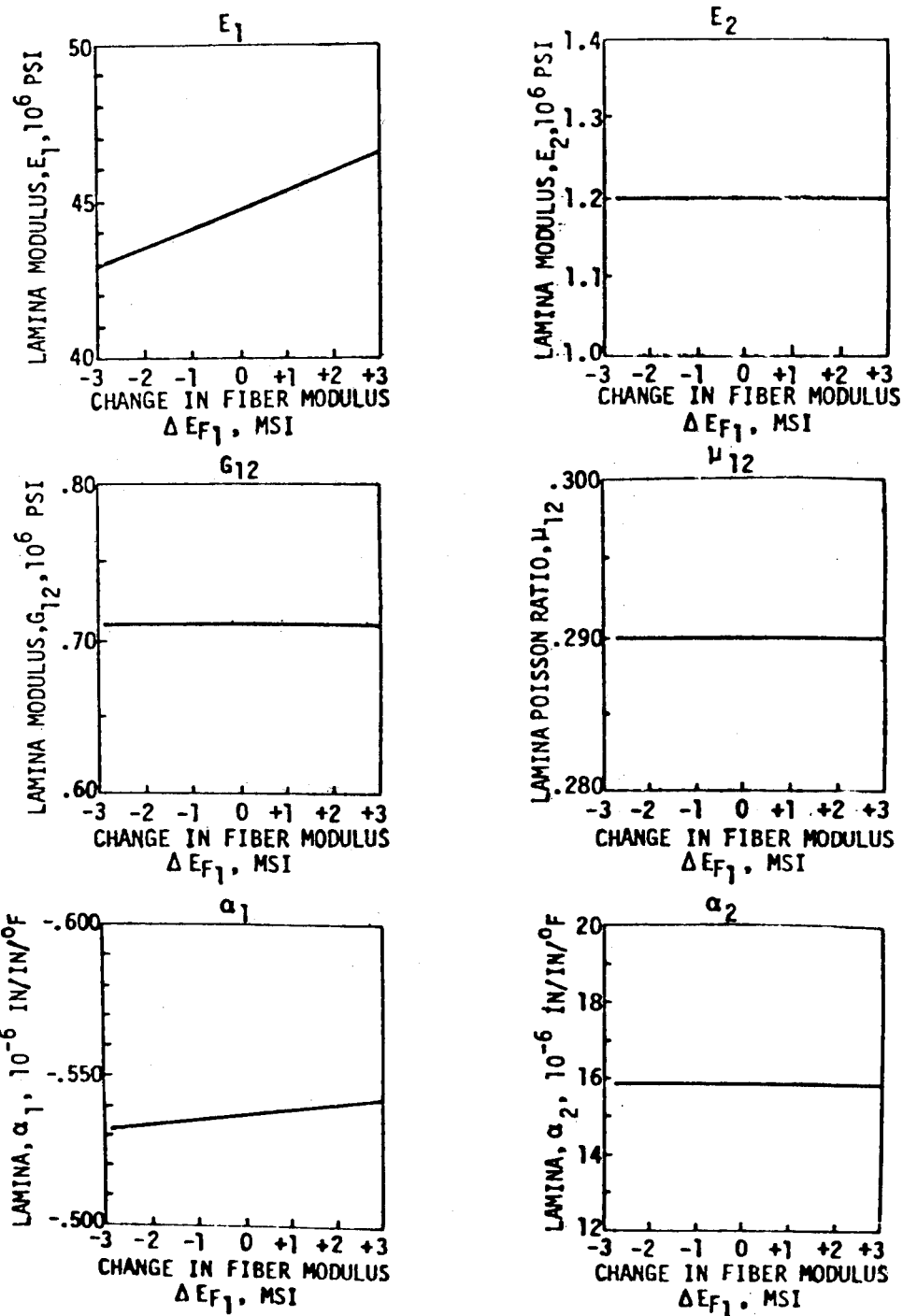


FIGURE 2 : LAMINA PROPERTIES VS GY-70 FIBER MODULUS

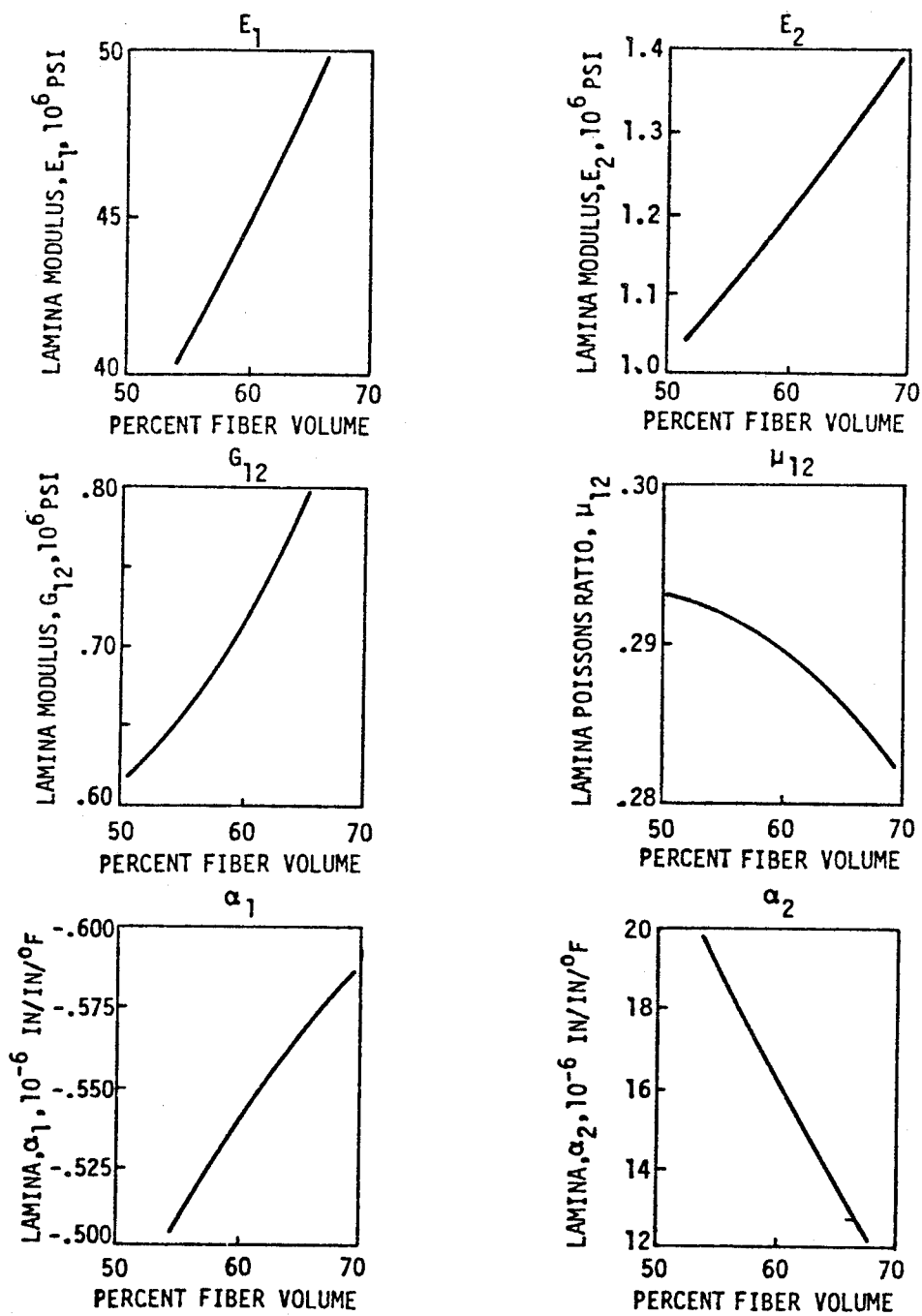


FIGURE 3 : LAMINA PROPERTIES VS GY-70 FIBER VOLUME

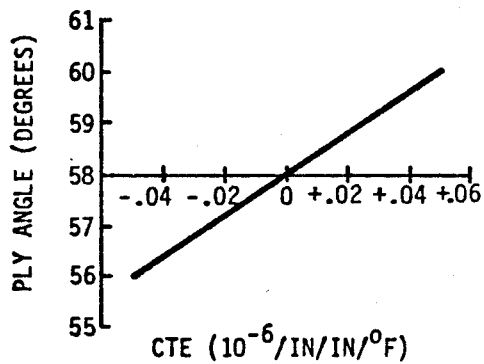
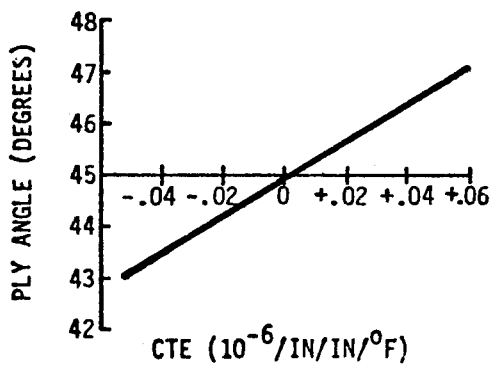
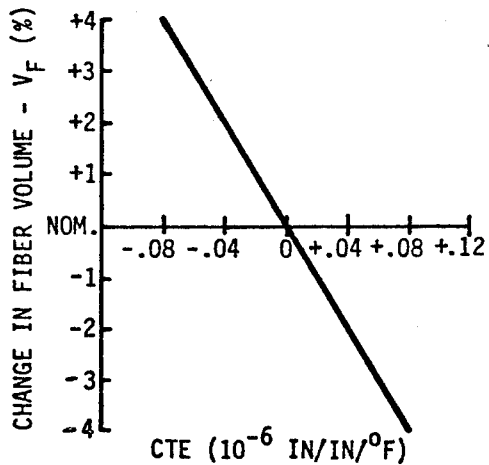
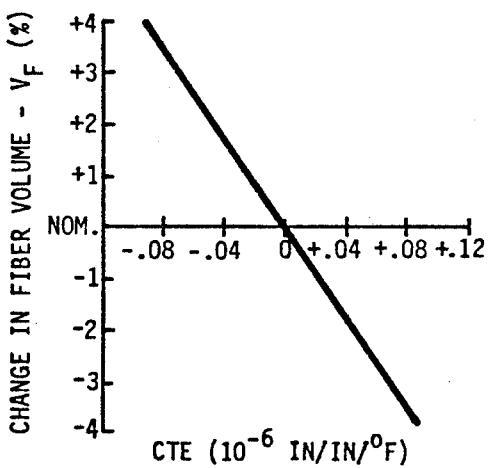
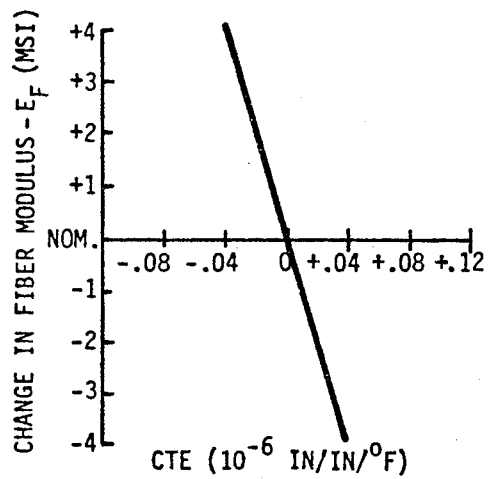
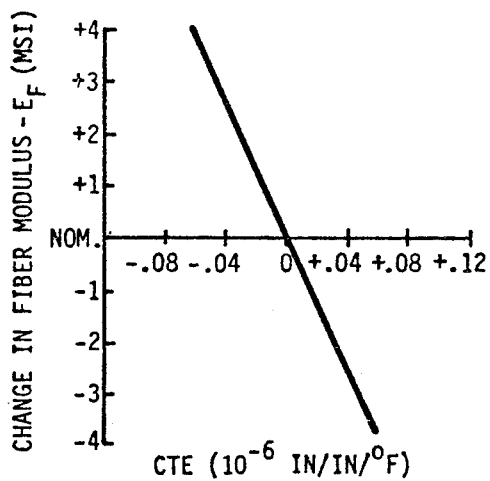


FIGURE 4 : GY-70 ISOTROPIC LAMINATE CTE SENSITIVITY

FIGURE 5 : T50(PAN)/T300 ORTHOTROPIC LAMINATE CTE SENSITIVITY

AIRCRAFT COMPOSITE MATERIALS SELECTION AND APPLICATION

V. L. Reneau
The Cessna Company
Wichita, Kansas 67277

Abstract: Composite aircraft structure requires proof of safety and durability similarly to metallic structure. The proofs of structural analysis methods, reliable material properties, and of assembly methods are similar to those required for metal structure. The effects of environment, time and fatigue damage are different than for metal and must be compensated for when design properties (allowables) are developed. Design allowables are not as readily available for composites as for metals and frequently must be obtained by testing.

Key words: Composites; design allowables; aircraft.

The Citation III airplane is the aircraft on which Cessna has chosen to introduce load carrying graphite and Kevlar fiber reinforced composite structure. It is a 10 to 15 place jet aircraft capable of operating at an altitude of 51,000 ft. Its flaps, spoilers, wing tips, engine nacelles, radome and most of the fairings are made from composite materials. Graphite and/or Kevlar are used in the flaps, nacelles and spoilers. The environmental exposures anticipated for the airplane were used in the tests conducted to develop design allowables for the composites.

The analysis of composite parts has one more phase than that of a metal part in that the internal structure of the parts is designed and analyzed along with their external shape and size. Fiber reinforced materials have directional properties. In some cases, it is advantageous to design the internal structure of parts so that most of the fibers are parallel to the load directions to maximize stiffness and strength where they are needed.

The rigorous analysis of crossplied fibrous composite materials is not simple and requires either a computer or a lot of someone's time. In general, tedious matrix calculations are required to obtain crossply properties from fiber direction design allowables. Several computer programs are available which will handle either simple or sandwich panel structure. If a few numbers only are required the calculations can be approximated on a programmable desk calculator.

These calculations must necessarily interact with the design calculations for overall part stress and deflection. Once calculated or

measured property values have been obtained for a given crossplied composite structure they can be used in normal analysis of the part.

There are some precautions necessary to prevent twisting of laminated parts from temperature changes or loading. For example, a crossplied part should be assembled so that its internal structure is mirror imaged across its center plane. If the part is a sandwich, each skin should be balanced across its center plane and each skin should be a mirror image of the other.

Structural composite materials are glass, Kevlar, graphite or boron fiber reinforced resins. For some unknown reason they have been divided into glass fiber reinforced materials and "advanced composites" which includes the rest.

They are selected in theory for a combination of cost, strength, stiffness, density and environmental suitability that will give a functional part at the least weight and cost. Actually, the availability of certifiable property data may select the material and will certainly limit use to a few well characterized materials.

Design allowables are reduced mechanical properties. They are obtained from the means of the test data by subtracting a multiple of the standard deviations from them. The multiplier is usually three or four depending on the number of specimens tested and the degree of reliability required.

This value is further reduced by factors for temperature extremes, moisture and other anticipated environments, aging and fatigue damage. The final design allowables are noticeably smaller than the corresponding test averages. The method is taken from MIL-HBK-5 "Metallic Materials and Elements for Aerospace Vehicles" Section 1.4, or from "The U.S.A.F. Design Guide for Advanced Composites Materials".

The multiplier for the standard deviation is a function of the number of specimens tested and the degree of assurance required. Ultimately, it derives from the standard non-skewed "bell" distribution curve. For example a "B" basis design allowable is an allowable above which the strength, etc., of 90% of the specimens can be expected to fall 95% of the time. An "A" basis allowable is one above which the strength of the specimens will fall 95% of the time. An "A" allowable is the set of properties required for primary structure. A "B" allowable is the set of properties required for secondary load carrying structure or experimental structure.

The factors for calculating these reduced values can be obtained from standard tolerance factor plots. For example if 6 specimens are tested and a "B" allowable is required, the standard deviation of the 6 data points is multiplied by about 3 and subtracted from the mean of the 6 data points. If 10 specimens had been measured, the multiplier is about 2.3. For "A" allowables, the multiplier is higher.

The effects of moisture, temperature, fatigue, and exposure to fuel, cleaning solutions, lubricating oils and hydraulic fluids were obtained by testing several groups of coupons for each exposure. The difference between the means of the "unexposed" coupons and those of the "exposed" coupons was subtracted from the reduced properties obtained from the standard deviation reductions. When all the anticipated effects of aging and environmental damage had been subtracted the residual mechanical properties were used for design allowables.

A graphite fiber composite was selected for the aircraft spoilers and the flap substructure because of its high strength, stiffness and long fatigue life. The specific material was Narmco 5208 epoxy resin reinforced with Union Carbide T-300 graphite fiber. It was selected because Kenneth Hofer at the Illinois Institute of Technology Research did a thorough characterization of it for the Air Force ① and because the Air Force, Boeing, Lockheed and McDonnell-Douglas were using it in major flight test articles under NASA contract. It was sufficiently characterized that design allowables could be calculated from available data. We would have preferred a 250°F cure rather than the 350°F required for 5208, but, the desired moisture resistance and data were not available.

The Kevlar composite used in the Citation III nacelles and in the skin panels on the flaps was selected because of its low density, high stiffness and good impact resistance. Kevlar itself is less dense than either glass or graphite and has very high tensile strength. Its compressive strength is low, especially in warm humid conditions. In stiffness and impact strength controlled designs, such as the Citation III nacelles, a Kevlar composite is an advantageous choice.

The specific Kevlar fabrics (Hexcel F-155 & F-161 - Kevlar) and resin combinations were selected partly because they were being used on the Lockheed L-1011 and on a Sikorsky helicopter. The full gamut of test data for calculating design allowables was not available and Cessna did the coupon testing required.

① AFML TR-74-266 "Development of Engineering Data on the Mechanical and Physical Properties of Advanced Composite Materials" Hofer, K.E. et. al.

After components are designed and the first units are built of composite materials with reliable design allowables, it is necessary to assure that the parts are acceptable by component testing. This testing determines if they were cured properly, if the joining and assembly methods are adequate and if the assembly has adequate fatigue life and damage tolerance to operate safely over the anticipated life of the airplane.

For example: a Citation III prototype flap was loaded to 150% of the expected design load both before and after environmental exposures simulating the service environment expected. Sixty thousand design limit load fatigue cycles were imposed on a second unit after saturation exposure to hot water. It also survived 150% of design limit load. The ability of the flap to carry such a load after environmental exposure indicates that mechanical property reductions for design allowables were reasonable. Finally a third unit was damaged by successively cutting the front and rear spar caps, making a 14" saw cut through a skin panel and finally cutting a spar loose from the load fitting at one end. It survived a limit load test after each injury and survived 15,000 limit load fatigue cycles with spar cap and a 2.5" length, skin panel cut at the same place. (Each cut was repaired after the test and before the next damage and test cycle).

All this work is part of the certification procedure. The Federal Aviation Administration (FAA) requires that a manufacturer show by test or analogy with a similar design that an airplane will be safe to fly over its expected life

The details of FAA requirements peculiar to composite structure are contained in FAA Advisory Circular #20-107, "Composite Aircraft Structure" and in FAR 25 sections 613 & 853. In general it requires proof of design allowables, static strength and safe life.

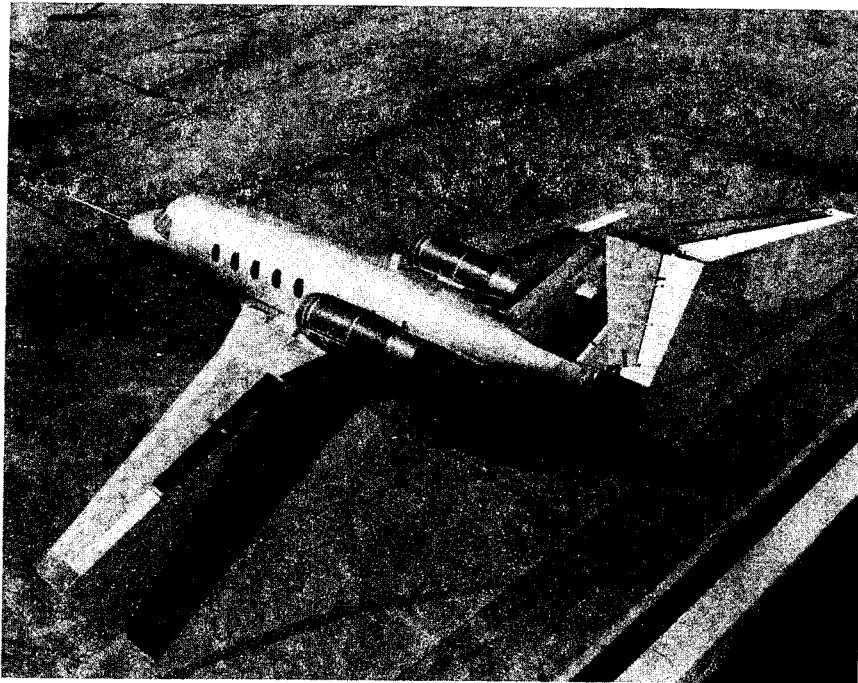


FIGURE 1
THE CITATION III AIRPLANE

-65°F TO + 160°F
 WATER
 OILS AND FUELS
 CLEANING SOLVENTS

FIGURE 2
 ENVIRONMENTAL EXPOSURE

$$\frac{E_0}{E_a} = \cos^4 a + \frac{E_0}{E_{90}} \sin^4 a + \frac{\sin^2 a}{4} \frac{2a (E_0 - 2 a_0)}{(E_{90})}$$

FIGURE 3 ELASTICITY
 EQUATION

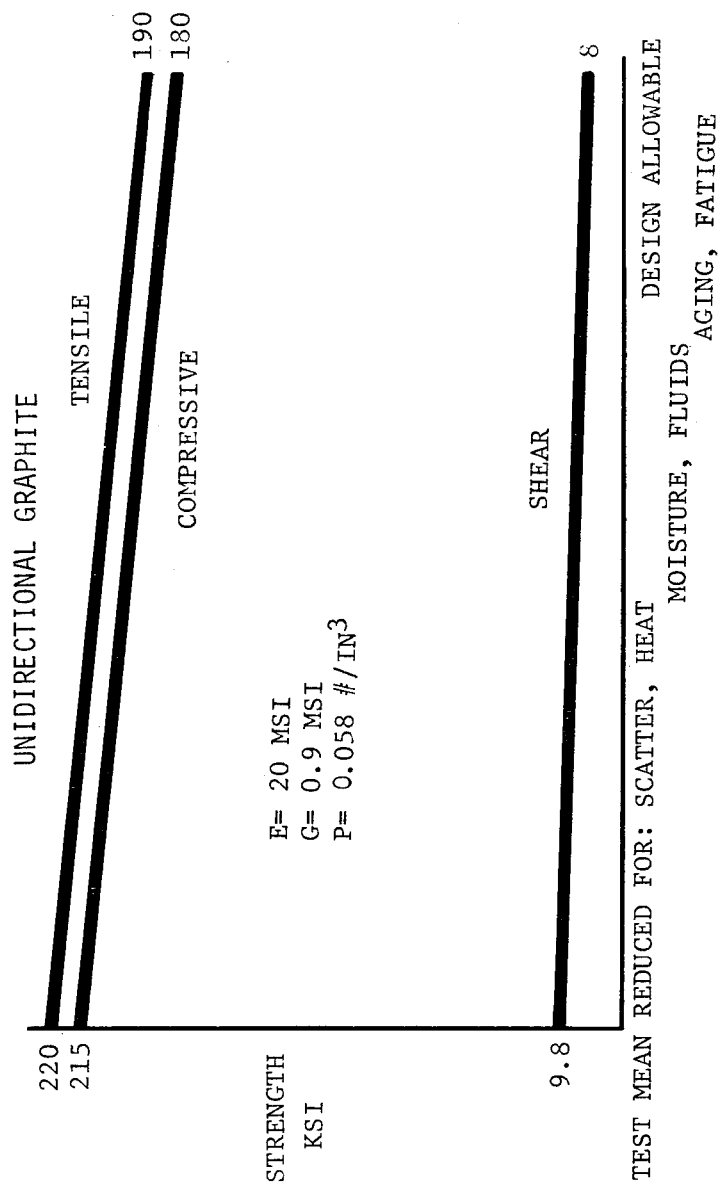


FIGURE 4

GRAPHITE DESIGN ALLOWABLES

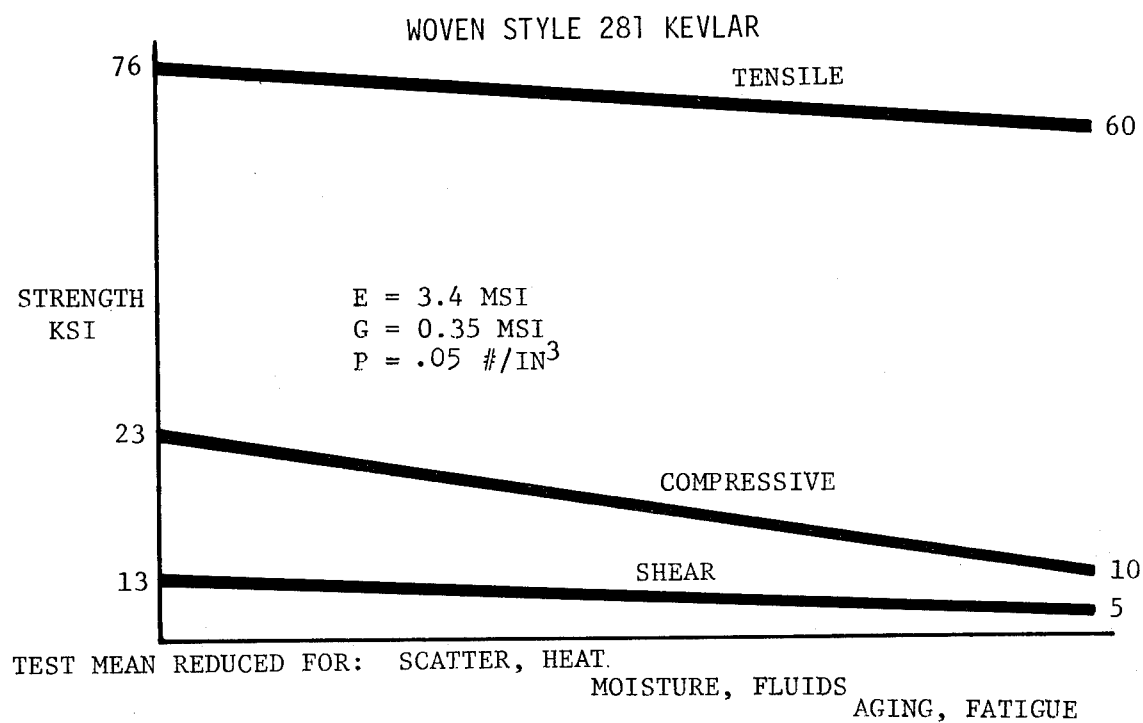


FIGURE 5
KEVLAR DESIGN ALLOWABLES

COMPOSITE STRUCTURES IN ROTORS AND PROPELLERS

David F. Thompson, President
T M Development, Inc.
Chester, Pa. 19013

ABSTRACT

A variety of composite rotor blade and propeller designs are reviewed. Desirable blade composite material qualities are enumerated. Various failsafe design features are shown for propeller blades. Multiple load path design features are discussed. Some manufacturing and quality control aspects of composite blade construction are discussed. Composite material properties versus cost factors are discussed.

Key words: Composite propellers and rotors; propeller materials requirements; blade aeroelastic behaviour; propeller fatigue behaviour; failsafe blade design; blade manufacture and quality control.

INTRODUCTION

This paper includes a partial review of composite propeller and rotor blade work of D. F. Thompson and John A. McAfee and their company, T M Development, Inc. of Chester, Pa.

EXAMPLES OF COMPOSITE BLADE DESIGNS

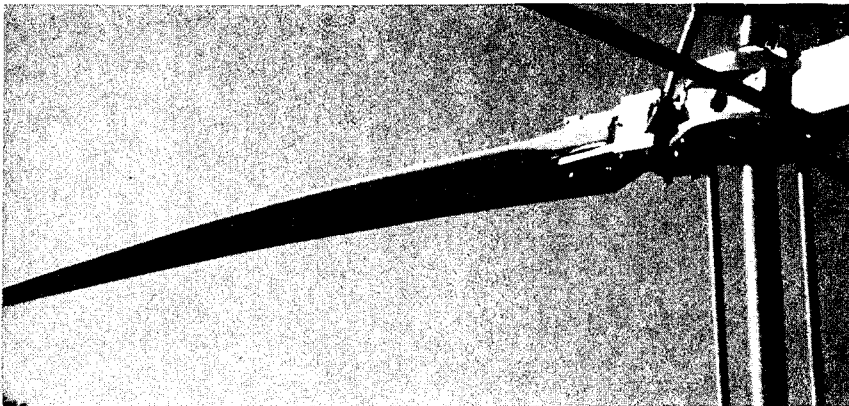


Fig. 1 Fiberglass Main Rotor Blade

This was an early parallel-filament glass-epoxy prepreg blade design flown on two experimental small helicopter designs in the early 1960's. The metal rootend fitting was bonded to, and also captured by continuous filament-tape wraparounds, step-tapered outboard. A rigid foam core stabilized the structural shell. A taper ratio of two and a nine degree, non-linear twist distribution provided excellent hovering efficiency. Airfoil is symmetrical 63₂-015 section.

A set of these blades survived, undamaged, when a sudden transmission seizure stopped the coaxial rotor from 400 rpm in 1½ revolutions! Films revealed that large whipping deflections of the blades stored energy, preventing destructive peak loads.

Fig. 2 Tail Rotor Blade

This linear filament glass/epoxy tail rotor blade weighs only 1.2 lb. per blade. Airfoils are 23 series cambered sections. Root-end connection is similar to Fig. 1 main rotor blade using a wrapped fitting. Rotor diameter is 4 feet.



Fig. 3 Fiberglass Propellers, One Piece

A series of propellers was developed in the early 70's for

small, homebuilt aircraft. Diameters of 48 to 60 inches were built for engines of 60 - 70 hp (VW, etc.) turning at up to 4000 rpm. These propellers were of a one-piece, twisted-plate design format (similar to early aluminum propellers). Material was solid parallel-filament E-glass/epoxy prepreg and the process was single-stage compression molding in matched, closed dies. An .018 stainless steel leading edge wrap was cobonded during the molding cycle. These achieved considerable technical success in terms of aerodynamic performance, structural toughness and reliability.

Fig. 4 Stacked Four-blade Propeller

This illustrates how four (and six blade) propellers may be assembled by stacking two-blade units. This was an air-boat propeller design to absorb 130 hp at 3500 rpm with a 54 inch diameter.

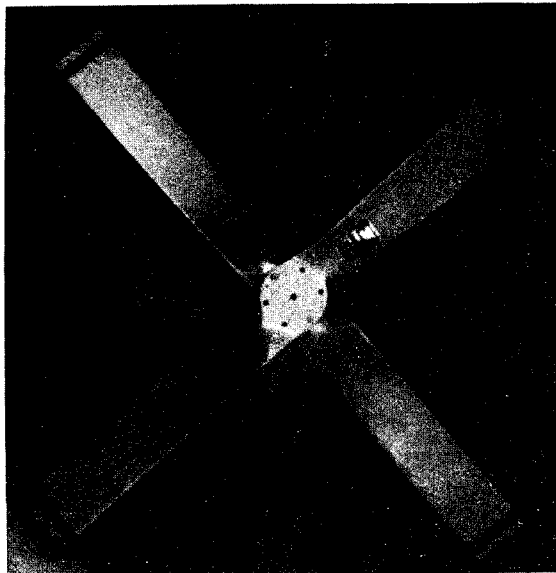


Fig. 5 Variable Pitch Propeller Blades

These fiberglass/epoxy blades were designed with an internal "coke bottle" metal fitting molded into the rootend which mates with a pitch-change retention bearing. A foam core filler stabilized the composite structural shell. A formed stainless steel leading edge abrasion cap was molded-in and cobonded to the blade.



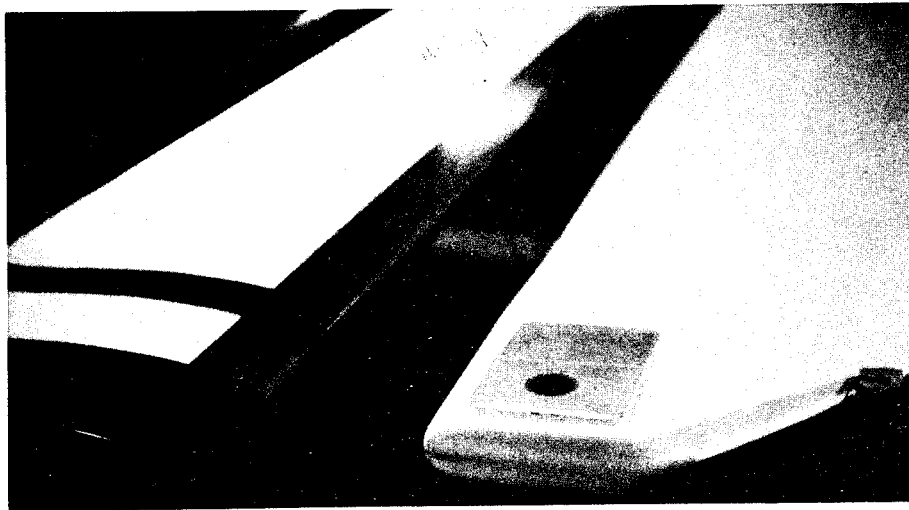
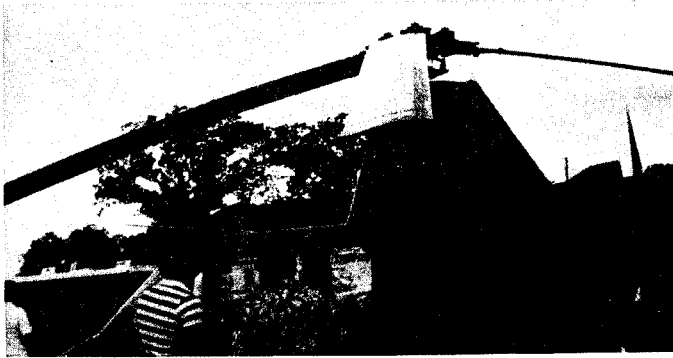


Fig. 6a and b Main Rotor Blades-Glass/Epoxy

These straight, eleven inch chord rotorcraft blades feature a bonded-plus-wraparound filament root retention and a molded-in trailing-edge strut attach fitting. Airfoil is symmetrical 13% thick section. Replacing 35 foot diameter wood blades on a two place rotorcraft, these have demonstrated excellent dimensional stability, consistent tracking and smooth flight behaviour with little maintenance required. These FRP blades were designed to closely duplicate the mass and stiffness distributions of the original wood blades so as to avoid introducing new undesired dynamic effects.



Fig. 7 Turbo-Propeller Blades

Developed for, and in cooperation with, Hartzell Propeller, Inc. are these composite, wide-chord "paddle-blades". They are designed for efficiency at greatly reduced tip speeds to provide quiet operation. Propeller diameters to 9 feet have been developed, for turbo-prop engines in the 1000 hp class, fitting standard Hartzell constant-speed hubs. Both fiberglass/epoxy and Kevlar/epoxy designs have been built. The Kevlar blades have been designed to very thin tip airfoil sections (t/c of 1.5%). The first Kevlar bladed propeller design has now received FAA certification and production go-ahead.

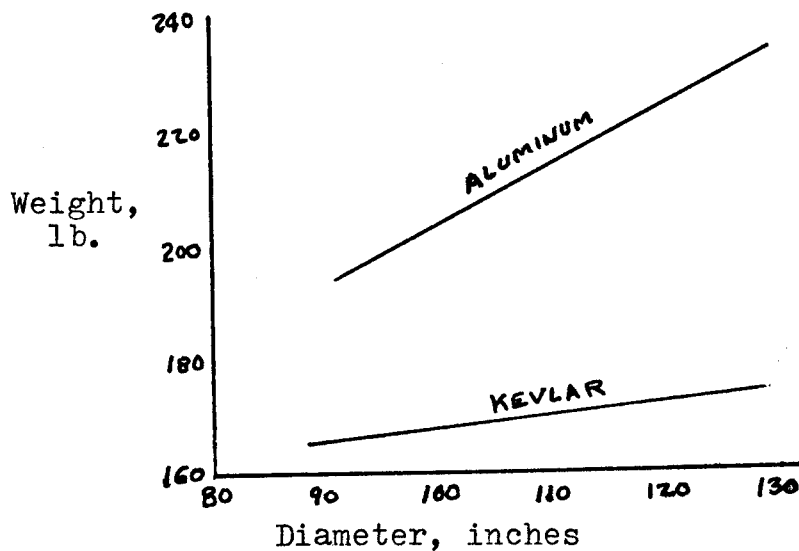


Fig. 8 Propeller Weight Trends for Metal and Composite Blades

The above chart illustrates the substantial weight savings achievable with Kevlar blades in turboprop propellers.

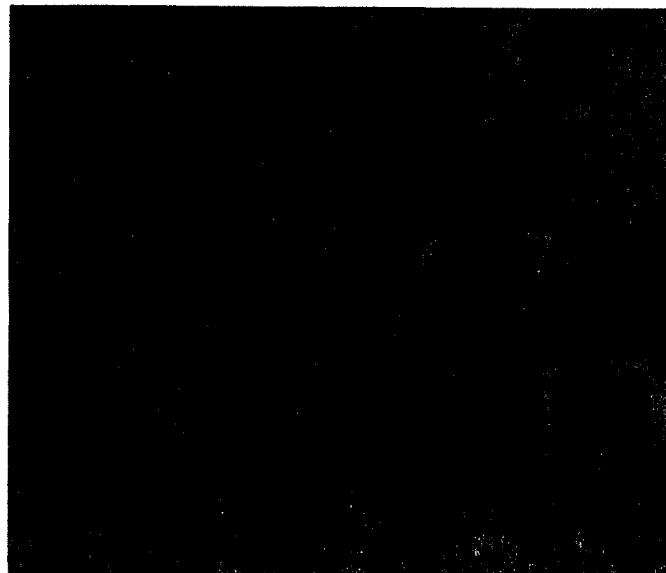


Fig. 9 Mini-RPV Propellers - Kevlar/Epoxy

This is a 30 inch diameter ground adjustable-pitch propeller designed by T M Development, Inc. for an RPV 2-stroke engine test program, absorbing 25 hp at 7500 rpm. Hub is aluminum

alloy and blades are of Kevlar/epoxy, oriented filament construction.

BLADE MATERIAL REQUIREMENTS

Aerodynamic shape factors include planform, airfoil section progression along the blade, twist distribution and tip shape. Ideally these factors should be selected by the aerodynamicist and designer without undue limitations imposed by the materials and processes of manufacture. Modern composites do, in fact, allow the propeller and rotor designer extensive freedom to configure for performance without sacrificing practical structural and manufacturing features. This occurs partly due to the unique ability with composites to create a considerable variety of structural density and stiffness qualities within a selected aerodynamic envelope. Their high specific strength and stiffness qualities are advantageous in this. Considerable latitude is available, even after the tooling is built, to modify the propeller structural and vibrational characteristics. This sort of modification is possible by several means. First, by changes of type of filament and resin system (prepreg system) for greater or less stiffness, including possible hybrid combinations of reinforcements, with glass, graphite and Kevlar as obvious candidates. Secondly, by changing the fiber orientation, structural behaviour may be changed. For example, it might be desired to soften the blade bending stiffness while increasing the torsional stiffness. This could readily be done by increasing the proportion of biasply filaments to spanwise filaments. Third, if the propeller design embodies a low-density foam, honeycomb core, or a hollow cavity within the composite structural shell, the design thickness of the shell may be readily changed without disturbing the blade aerodynamic envelope design. By the methods described, a basic composite rotor blade or propeller design, within a fixed external envelope, can be adapted to have a variety of structural, aeroelastic and/or mass characteristics.

FATIGUE PROPERTIES OF COMPOSITE BLADES

Starting in the 1950's, laboratory tests began to reveal the remarkably favorable fatigue properties of properly designed glass filament/epoxy reinforced plastic blade structures. These favorable fatigue properties are even more strongly evident in today's composite blade structures, notably in Kevlar/epoxy applications. These properties include: (1) Non-notch sensitivity due to multiple filament load paths, with related zero or slow propagation of structural damage,

(2) Appreciable internal damping which tends to limit peak values of resonant vibration stress levels when they occur, (3) Absence of the stress-corrosion-fatigue destructive sequence sometimes experienced by lightweight metal structures, (4) Visual evidence of fatigue damage which eases inspection techniques and permits "failsafe" operational characteristics, (5) Generally high fatigue-strength to weight ratios as compared with traditional blade materials.

MANUFACTURING & QUALITY CONTROL CONSIDERATIONS

The primary manufacturing method selected for these products was compression molding to positive stops. In this molding approach, the molding pressure is, in part, a function of the layup thickness, hence carefully designed and accurately performed layups are required.

An air conditioned clean assembly room is necessary to provide controlled conditions for blade layup.

Individual blade logs are kept by blade serial numbers and include element weights, material batch numbers, recorded cure cycle charts and test results from co-molded test coupons.

FAA process and facility approvals must be obtained in order to manufacture production run blades under an Approved Type Certificate. Process and quality control manuals are required to be prepared and observed. All materials are purchased under strict control specifications.

FAILSAFE BLADE DESIGN FEATURES

As described above, certain inherent "failsafe" tendencies exist in some composite filament reinforced-plastic structures. Additional failsafe benefits are achieved by designing the blade with alternate load paths. This is accomplished in the blade rootend retention area by allowing for: (1) High quality adhesive bonding of the composite blade shell to a metal rootend fitting, plus, (2) Mechanical "capture" gripping action of blade shell onto the root fitting by means of a flared "coke bottle" effect in a round type (propeller) fitting, or by wraparound of a flat block type (rotor blade) fitting by the spar filament tapes, (3) Reinforcement of fitting mechanical capture by filament overwraps locally.

Outboard of the critical rootend connection, failsafe behaviour is obtained by designing the basic blade to moderate

stress levels with a spread-out distribution of the primary tensile filaments. Thus, even a substantial sized damage tends to leave enough material to prevent catastrophic failure. Then, the tendency for slow damage propagation allows the blade structure to survive until inspection and maintenance procedures correct the problem.

COMPOSITE MATERIAL PROPERTIES VERSUS COST FACTORS

Generally, the blade designer must attempt to fulfill rotor or propeller blade performance and safety requirements at minimum cost. This would dictate the use of the least costly composite material system for any specific blade design program.

As the structural and/or aeroelastic rigorousness of the blade specification increase, so the composite material selection may be forced into the more expensive materials. In some propeller designs, reduced blade weight with the more exotic fibers will partly alleviate the higher cost per pound of material. Helicopter rotor blades, however, more usually demand discrete mass properties to control coning angle and blade dynamics.

If an E-glass/epoxy prepreg meets the technical requirements of a particular blade design it is the obvious choice at, perhaps, \$ 5.00/lb. However, in a higher performance application, an appreciably greater material stiffness/weight ratio might prove desirable to avoid flutter and divergence tendencies in an unusually thin blade configuration. In such a case the appropriate selection might be a Kevlar/epoxy prepreg at, perhaps, \$ 25.00/lb., or some ingenuously engineered hybrid combination of E-glass with graphite fibers at \$ 50/lb. to give an "optimum" product performance/cost factor.

Also, the straight material performance/cost factors must be biased by the influences of material selection on blade process costs. Handling and layup manhours will differ for the various materials. Probable scrap and spoilage rates may differ. Potential differences in product development and certification costs due to the perceived risk level of material "unknowns" must also be taken into account when planning an advanced blade program.

SESSION 4

AEROSPACE AND AIRCRAFT APPLICATIONS AND DESIGN

**Chairman: J. J. Scialdone
Goddard Space Flight Center**

DEVELOPMENT OF A LIBRARY MODULE FOR THE
ANALYSIS OF ADVANCED COMPOSITE MATERIALS

Karyn T. Knoll
Non-metallic Materials Division
Air Force Materials Laboratory
Wright-Patterson AFB, Ohio 45433

Abstract: Because of their orthotropic nature, advanced composite materials present some special problems to the engineer. The relation between the elastic constants of an orthotropic material is more complex than that of an isotropic material. In addition, composites exhibit coupling between normal and shear deformations as well as between bending and stretching load responses. The more complicated behavior of advanced composites is usually handled using techniques of matrix mathematics, but the required bookkeeping often overwhelms the isotropic-trained engineer who is used to working with fewer terms and less complicated equations. This paper discusses the development of a module, designed to be used with the Texas Instruments TI-58 and TI-59 desktop calculators which can be used to handle much of the required "bookkeeping". Given such input as the elastic constants of a single ply of composite material, the stacking sequence of a laminate, and the applied loads (or strains), the module will output desired information such as the physical properties of a laminate, the strains (or loads) in both the whole laminate and the individual plies, and the values of the laminate properties as the laminate is rotated. The module will also provide "strength ratios" for a particular laminate and load vector to indicate how close the material is to failure. It is hoped that this module will make the analysis and use of advanced composites seem less formidable to both research and developmental engineers.

Key words: Advanced composite materials; composite materials analysis; orthotropic materials; programmable calculators; solid state software.

The orthotropic behavior of advanced composite materials can be described using techniques of matrix mathematics. However, the bookkeeping required by such techniques can soon become overwhelming. The Air Force Materials Laboratory at Wright-Patterson Air Force Base has recently completed a set of calculator programs capable of handling much of the

required bookkeeping. These programs are presently being fabricated into a library module which can interface with a standard TI-58 or TI-59 calculator. (A library module is a solid state, plug-in set of prewritten, read-only programs.) See Figure 1. This paper discusses the structuring and potential applications of the composite materials module.

The module consists of nine user-accessible programs which calculate material properties, initial stresses and strains, mechanical properties, strength ratios, and translated moduli for both single plies and laminates of a composite material. Because the calculator's data storage registers are unaffected by the call for a program, the results of one program can easily be used as input for another. Several of the programs in the composite materials module are designed to be used in conjunction with one another.

Program 1 of the composite materials module provides data which is essential to all remaining programs. This program partitions the calculator to insure the proper number of data storage registers, clears the calculator memory, and performs a test to determine whether or not the calculator is connected to the PC-100A printer (since all programs have been designed to work on or off the printer). It then allows the user to input the engineering constants - the longitudinal, transverse, and shear moduli and the major Poisson's ratio - and the thickness of a single ply for the desired material. Program 1 also allows the user to convert his input data into English or SI units. This conversion can be performed on an individual entry or on the entire list as desired. Upon completion of input data entry, Program 1 calculates the reduced stiffness moduli (Q's), the compliances (S's), and the invariants required to calculate rotated values of moduli for a single ply. These results are then used by the remaining eight programs in the module.

Programs 2 and 3 deal with initial stresses and strains induced by changes in temperature and moisture concentration. Program 2 is concerned with stresses and strains in a single ply of composite material. The user inputs four environmental coefficients - one each in the longitudinal and transverse directions for thermal and for moisture effects. Again, these values can be converted into English or SI units either singly or as a list. Next, the user must input temperature change, moisture concentration, and curing strains. The program will then calculate initial stresses and strains for the ply. Program 2 can provide the user with single-ply initial stresses and strains in both the ply-axis system and in a coordinate system rotated thru any angle from the ply

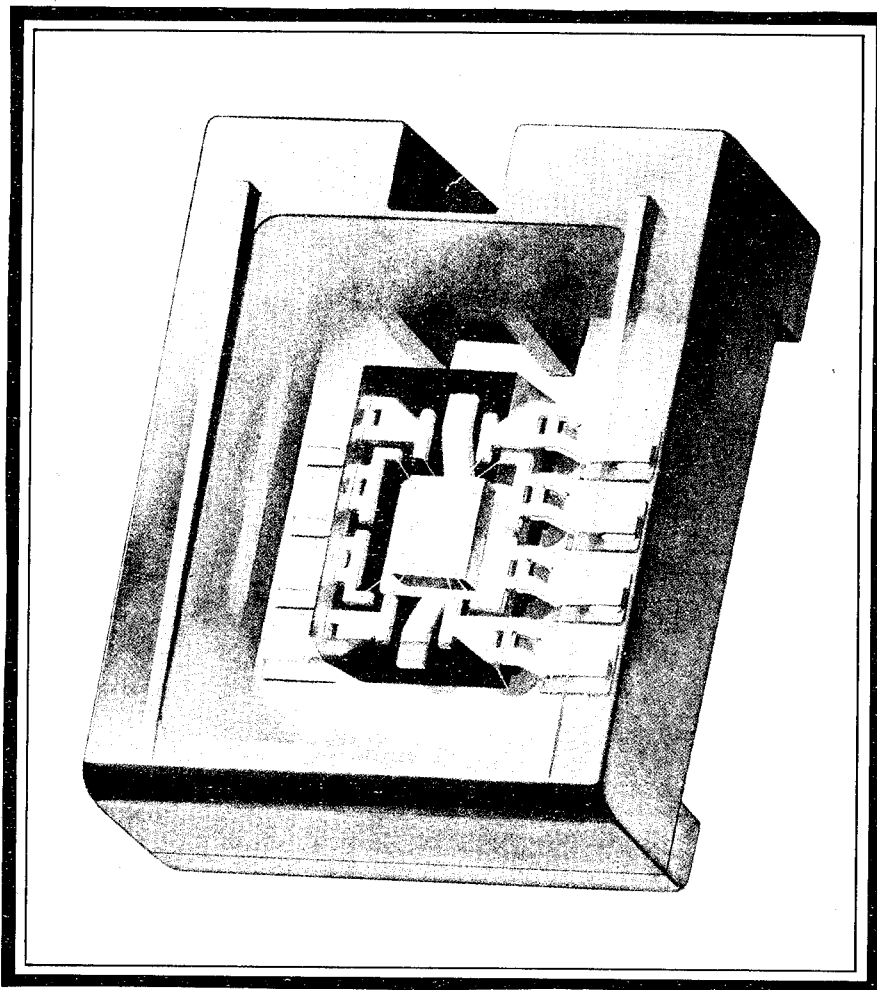
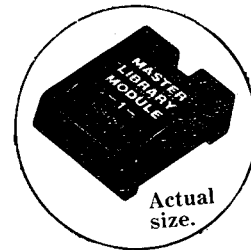


FIGURE 1: ENLARGED VIEW OF A LIBRARY MODULE

axes. Program 3 is used to calculate non-mechanical stresses and strains in a laminate. Non-mechanical stresses and strains are caused by the fact that plies at different orientations want to expand different amounts but are prevented from doing so by their presence in the laminate. See Figure 2. After the user inputs the stacking sequence of the laminate of interest, the program calculates the non-mechanical loads and strains for the given laminate. Program 3 is also capable of providing the stresses and strains in each ply of the laminate in both the ply- and laminate-axis systems. The initial strains from Program 2 as well as the non-mechanical strains from Program 3 are retained thruout the execution of Programs 5 and 6 so that they are available for use in the calculation of the strength ratios.

Program 4 calculates the mechanical properties of a single ply of composite material. This program calculates both the on- and off-axis values of the stiffness moduli and compliances. Rotation of stresses and strains is also accomplished by Program 4. In addition, multiplication of stiffness moduli and strains or compliances and stresses can be performed for both the on- and off-axis cases.

Program 5 is used to handle in-plane properties of laminates. Elements of the in-plane moduli (A-matrix) and their inverses can be calculated for any given laminate (symmetric or unsymmetric). Program 5 also provides values of the A- and inverse A-matrices rotated from the original laminate axes thru any desired angle. For symmetric laminates, this program can be used to multiply the A-matrix and the in-plane strains or the inverse A-matrix and the applied loads. Program 5 can also provide the stresses and strains in each ply of the laminate in both the ply- and laminate-axis systems.

Program 6 is similar to Program 5 except that it deals with the flexural rather than the in-plane case. This program can be used to calculate elements of the flexural moduli (D-matrix) and their inverses for any given laminate (symmetric or unsymmetric). Values of the D- and inverse D-matrices rotated thru any desired angle from the original laminate axes can also be calculated. For symmetric laminates, Program 6 can be used to multiply the D-matrix and laminate curvatures or the inverse D-matrix and the applied moments. Stresses and strains in each ply of the laminate in both the ply- and laminate-axes systems at any given distance from the laminate midplane can be calculated by Program 6.



Uncured ply - no environmental effects

When heat or moisture is applied, the ply expands. The amount of expansion is related to the ply orientation. For example:



Zero-degree ply wants to expand an amount equal to e_L



90-degree ply wants to expand an amount equal to e_T



However, when the two are placed together in a laminate, each acts on the other and they "compromise" so that both expand an amount equal to the non-mechanical strain e^N

FIGURE 2: Non-mechanical strains in a laminate

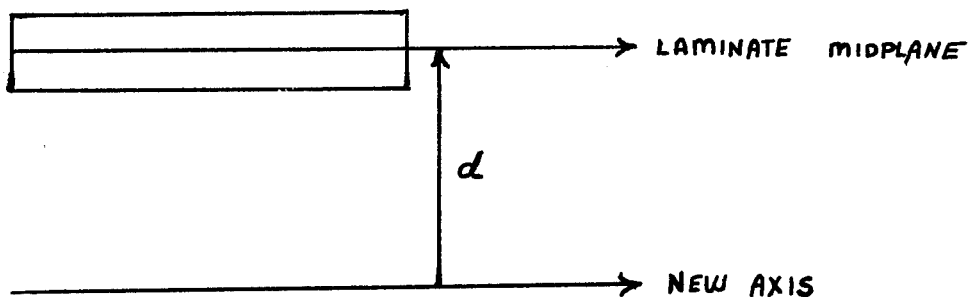


FIGURE 3: Translation of moduli by a distance "d"

Program 7 calculates values for the coupling moduli (B-matrix) and their inverses for unsymmetric laminates. This program can also rotate the values of the B- and inverse B-matrices thru any desired angle from the original laminate axes. Although Program 7 does not perform any multiplication, its output can be used as input for programs (written by the module user) dealing with unsymmetric laminates.

Program 8 uses the strains generated in previous programs (both mechanical and non-mechanical) to calculate values for the strength ratios of each ply in a given laminate. The user should use Program 1 to provide the necessary material properties, Programs 2 and 3 to calculate non-mechanical strains, and Program 5 for in-plane mechanical loads or Program 6 for bending. It is then necessary to input ultimate strengths for the material of interest. Program 8 allows the user to convert the input ultimate strengths into English or SI units either singly or as a complete list. After all of the ultimate strengths for the material have been input, the values of the F's and G's - coefficients for the strength ratio equation - are calculated and output. Program 8 then calculates the strength ratio for any ply of the given laminate when supplied with the ply orientation (for the in-plane case) or the ply orientation and distance of the ply from the laminate midplane (for the bending case). When the non-mechanical strains are negligible, the user may skip their calculation and proceed directly from Program 1 to Program 5 or 6.

Program 9 calculates the values of the A-, B-, and D-matrices and their inverses when translated a distance, d , from the midplane of the laminate. See Figure 3. After using Program 1 to calculate the needed material properties, the user inputs the stacking sequence and the distance from the midplane of the laminate. Program 9 then calculates the translated values of the A-, B-, and D-matrices using the following relationships:

$$\begin{aligned} A'_{ij} &= A_{ij} \\ B'_{ij} &= dA_{ij} + B_{ij} \\ D'_{ij} &= d^2A_{ij} + 2dB_{ij} + D_{ij} \end{aligned}$$

where the primed variables are translated values and

unprimed variables are those which have been calculated from the laminate midplane. Program 9 will also invert the translated matrices. This program can be used to calculate moduli for stiffeners or sandwich beams.

To demonstrate the use of the module, I'll describe a sample problem done with the programs used in the development of the module. Figure 4 illustrates the keyboard of a standard TI-59 calculator. (A TI-58 is the same except that there is no "write" command). Figure 5 shows the output produced by the PC-100A printer. (The symbols typed next to the printed output have been added for this explanation. They are not produced by the PC-100A printer). If this problem were run off the printer the numerical answers would appear in the display of the calculator and the user would be able to step thru them using the Run/Stop (R/S) key.

The problem solved in Figure 5 is to find the mechanical stresses in the center of each ply (in both the ply- and laminate-axes systems) in a $[0/\pm 45]_s$ laminate of AS/3501 when a bending moment of 1000 Nm is applied in the 1-direction. After inserting the composite materials module and turning the calculator on, the user should press 2nd ENG to put the calculator in engineering notation. If another type of output (e.g. FIX 3) is desired, the user may set the calculator in the desired notation and the numerical output will be printed (or displayed) in the desired notation. However, some of the labels may be incorrectly printed if the calculator is in other than engineering notation.

To solve the sample problem, the user must first press 2nd PGM 01 to call the first program. This program allows him to input the engineering constants and ply thickness for AS/3501 and to calculate the material properties which will be required by the moment/curvature program. After calling Program 1, the user presses E which partitions and clears the calculator memory, tests for the printer connection, prints "ENT" (to tell the user to enter his data), and places a "1" in the display to inform the user that the calculator is ready for the first engineering constant (E_L). The user must then key in the value of E_L for AS/3501 and press R/S to enter this value. The calculator then prints the value of E_L and places a "2" in the display indicating that it now requires the value of the second engineering constant (E_T). The user continues entering the engineering constants and the ply thickness for AS/3501. Following entry of the fifth value, the calculator advances the paper

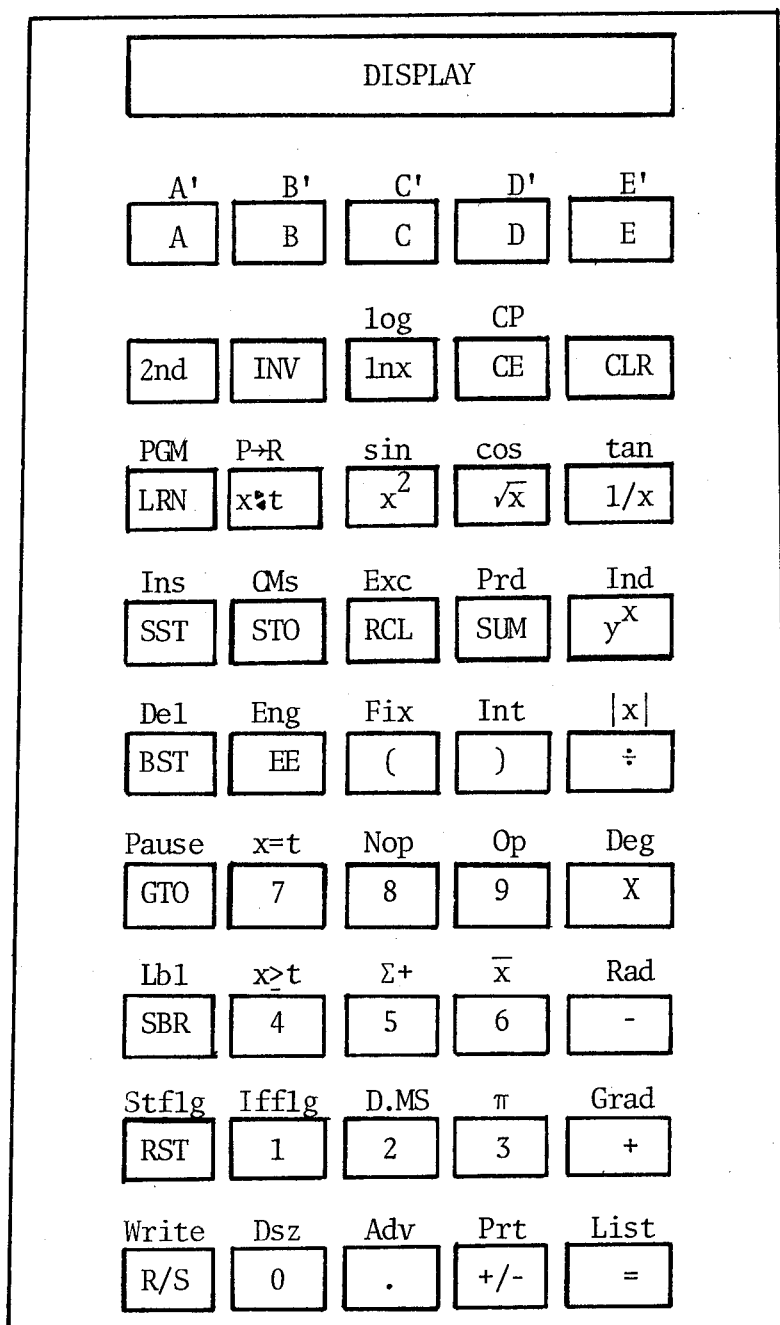


FIGURE 4: Keyboard of TI-59 calculator

PROGRAM 1

ENT

127.55 09 E(L)
11.032 09 E(T)
4.4816 09 G(LT)
250. -03 V(LT)
133.35-06 h_o

Q

128.24325 09 Q(11)
11.09196 09 Q(22)
2.77299 09 Q(12)
4.4816 09 Q(66)
0. 00 Q(16)
0. 00 Q(26)

S

7.8400627-12 S(11)
90.645395-12 S(22)
-1.9600157-12 S(12)
223.13459-12 S(66)
0. 00 S(16)
0. 00 S(26)

U

55.18475 09 U(1)
58.575644 09 U(2)
14.482853 09 U(3)
17.255843 09 U(4)
18.964453 09 U(5)

I

36.220297 09 I(1)
18.964453 09 I(2)
58.575644 09 R(1)
14.482853 09 R(2)

FIGURE 5A: SAMPLE PROBLEM

PROGRAM 6

```

        6. 00 N

        0. 00
      -45. 00
        45. 00
        45. 00
      -45. 00
        0. 00

      L
        1. 03 M(1)
        0. 00 M(2)
        0. 00 M(6)

      DI
    246.35097-03 d(11)
    1.4681115 00 d(22)
   -120.23466-03 d(12)
    2.1592145 00 d(66)
    62.830219-03 d(16)
    671.50235-03 d(26)

      L
        1. 03 M(1)
        0. 00 M(2)
        0. 00 M(6)

      E
    246.35097 00 K(1)
   -120.23466 00 K(2)
    62.830219 00 K(6)
  
```

PROGRAM 6

```

        0. 00  $\theta$ 
        2.5 00 z

      E'
    82.127254-03  $\epsilon(1)'$ 
   -40.083231-03  $\epsilon(2)'$ 
    20.946024-03  $\epsilon(6)'$ 

      E
    82.127254-03  $\epsilon(1)$ 
   -40.083231-03  $\epsilon(2)$ 
    20.946024-03  $\epsilon(6)$ 

      Q
    128.24325 09 Q(11)
     11.09196 09 Q(22)
      2.77299 09 Q(12)
      4.4816 09 Q(66)
          0. 00 Q(16)
          0. 00 Q(26)

      E'
    82.127254-03  $\epsilon(1)'$ 
   -40.083231-03  $\epsilon(2)'$ 
    20.946024-03  $\epsilon(6)'$ 

      L'
    10.421115 09  $\sigma(1)'$ 
   -216.86354 06  $\sigma(2)'$ 
    93.871702 06  $\sigma(6)'$ 

      L
    10.421115 09  $\sigma(1)$ 
   -216.86354 06  $\sigma(2)$ 
    93.871702 06  $\sigma(6)$ 
  
```

FIGURE 5B:
SAMPLE PROBLEM

PROGRAM 6

-45. 00 0
1.5 00 z

E'

6.3293996-03 $\epsilon(1)'$
18.897014-03 $\epsilon(2)'$
73.326291-03 $\epsilon(6)'$

E

49.276352-03 $\epsilon(1)$
-24.049939-03 $\epsilon(2)$
12.567615-03 $\epsilon(6)$

Q

128.24325 09 Q(11)
11.09196 09 Q(22)
2.77299 09 Q(12)
4.4816 09 Q(66)
0. 00 Q(16)
0. 00 Q(26)

E'

6.3293996-03 $\epsilon(1)'$
18.897014-03 $\epsilon(2)'$
73.326291-03 $\epsilon(6)'$

L'

864.104 06 $\sigma(1)'$
227.15629 06 $\sigma(2)'$
328.61911 06 $\sigma(6)'$

L

874.24925 06 $\sigma(1)$
217.01104 06 $\sigma(2)$
-318.47385 06 $\sigma(6)$

PROGRAM 6

45. 00 0
500. -03 z

E'

6.2990047-03 $\epsilon(1)'$
2.1097999-03 $\epsilon(2)'$
-24.442097-03 $\epsilon(6)'$

E

16.425451-03 $\epsilon(1)$
-8.0166462-03 $\epsilon(2)$
4.1892048-03 $\epsilon(6)$

Q

128.24325 09 Q(11)
11.09196 09 Q(22)
2.77299 09 Q(12)
4.4816 09 Q(66)
0. 00 Q(16)
0. 00 Q(26)

E'

6.2990047-03 $\epsilon(1)'$
2.1097999-03 $\epsilon(2)'$
-24.442097-03 $\epsilon(6)'$

L'

813.65527 06 $\sigma(1)'$
40.868893 06 $\sigma(2)'$
-109.5397 06 $\sigma(6)'$

L

536.80179 06 $\sigma(1)$
317.72238 06 $\sigma(2)$
386.39319 06 $\sigma(6)$

FIGURE 5C: SAMPLE PROBLEM

and awaits further instruction. If the user wishes to convert the units of any entry, he must key in the entry and press C (to convert from English to SI) or 2nd C (to convert from SI to English) before he presses the R/S key; to convert all five entries, the user should press C or 2nd C after entering the fifth value. The calculator will then print out the converted values for all five input values. Upon completion of data entry for AS/3501, the user presses key A and the calculator calculates and prints out the reduced stiffness moduli (Q), compliances (S), the U's (constants required for the calculation of off-axis values of Q), and the invariants (I).

After using Program 1 to calculate the required values of the material properties for AS/3501, the user presses 2nd PGM 06 to call Program 6 which deals with mechanical bending of a laminate. To enter the laminate's stacking sequence, the user presses A and a zero is displayed. The user keys in the total number of plies in the laminate (in this case, 6) and presses R/S. The total number of plies is printed, the paper is advanced, and a "6" is displayed to indicate that the ply orientation of the sixth (top) ply is required. The user keys in a "0" and presses R/S to enter this value. The zero is printed and a "5" is displayed indicating that the fifth ply orientation is now needed. The user continues entering all ply orientations in the laminate (as the display counts down). Upon entry of the last angle, the calculator advances the paper and awaits instruction.

To enter the applied bending moments, the user presses SBR STO D and a "1" is displayed. The user keys in 1000 and presses R/S to enter the value of M_1 . A "2" is then displayed to indicate that the value of M_2 should now be entered. Following entry of all three bending moments (M_1 , M_2 , and M_6), the user may press SBR RCL D to output the stored values thereby allowing him to check his input data.

Once the stacking sequence and bending moments have been entered, the laminate curvatures can be calculated by pressing SBR RCL SBR INV B SBR X SBR RCL D. SBR RCL SBR INV B calculates and outputs the values of d_{ij} (the inverse of the D-matrix). SBR X tells the calculator it will be performing a matrix multiplication. SBR RCL D outputs the stored bending moments. Upon completion of this sequence, the matrix multiplication $d_{ij}M_j$, which results in the values of κ_j , is automatically performed. The user then presses SBR RCL E to output κ_i . If the user

wishes to simply perform the matrix multiplication $d_{ij}M_j$ without outputting the values of d_{ij} and M_j , he can omit the SBR RCL before SBR INV B and before D.

Once the laminate curvatures have been calculated, the stresses and strains in each ply of the laminate (in both the ply- and laminate-axis systems) can be found. Since all ply stresses and strains are calculated in the same manner, only the -45 degree calculations (Figure 5C) will be explained here. To describe a desired ply the user presses 2nd C and a zero is displayed indicating that the ply's orientation is required. The ply angle should be entered using the R/S key and a "1" will be displayed to tell the user that a value of Z (distance from the laminate midplane to the point of interest) is needed. Since we are interested in the stresses and strains in the center of the upper -45 degree ply, a 1.5 (the value of Z in units of ply thickness) is keyed in and R/S is pressed. Now that the ply of interest has been identified, the ply strains may be recalled by pressing SBR RCL E for ply strains in the laminate axes and SBR RCL 2nd E for ply strains in the ply axes. Ply stresses can be calculated by multiplying the on-axis values of Q and the ply strains in the ply-axes system. This multiplication is performed by pressing SBR RCL C SBR X SBR RCL 2nd E. The resulting ply stresses can be output by pressing SBR RCL D for ply stresses in the laminate axes and SBR RCL 2nd D for ply stresses in the ply axes. Once the stresses and strains in the -45 degree ply have been output, the user may calculate the ply stresses and strains in any other ply by pressing 2nd C, identifying the new ply, and repeating the sequence. The results of all three ply orientations of our sample laminate are shown in Figures 5B and 5C. Once again, if the user did not want to output the values of Q_{ij} and ϵ_j when he performed the matrix multiplication to calculate the stresses, he could have omitted the SBR RCL before C and before 2nd E.

As can be seen in Figures 5B and 5C, the symbol "L" is used to identify force-related parameters (stress, loads, and moments) and "E" is used for displacement-related parameters (strains and curvatures). This symbology is used in all programs in the module. Also, in programs dealing with laminates, primed values indicate "ply axes" and unprimed values mean "laminate axes" where stresses and strains are concerned.

Though calculation of the ply stresses in the sample problem may seem complicated the first time thru, Figure 6

KEYSNOTES

2nd PGM 01	Calls Program 1
E	Enter E_L , E_T , G_{LT} , ν_{LT} , h_o (Use keys C and 2nd C for unit conversion)
A	Calculates Q, S, U, I
2nd PGM 06	Calls Program 6
A	Enter laminate stacking sequence
SBR STO D	Enter M_1 , M_2 , M_6
SBR INV B SBR X D	Multiplies $d_{ij}M_j$ (Result: k_i)
SBR RCL E	Recalls curvatures (k_i)
2nd C	Enter ply orientation and z
SBR RCL 2nd E	Recalls ply strains (ply axes)
SBR RCL E	Recalls ply strains (laminate axes)
C SBR X 2nd E	Multiplies $Q_{ij}\epsilon_j'$ (Result: σ_i')
SBR RCL 2nd D	Recalls ply stresses (ply axes)
SBR RCL D	Recalls ply stresses (laminate axes)

FIGURE 6: Summary of solution to sample problem to find stresses in the center of each ply of a $[0/\pm 45]_s$ laminate to which a moment ($M_1=1000$ Nm) is applied^s

illustrates that the problem solution is actually quite straightforward. To simplify program use, labels identifying the user-defined keys will be provided for each program. A user who has become familiar with the composite materials module can calculate ply stresses in each ply in less than fifteen minutes. When I solved the same program using a non-programmable calculator, the solution required several hours and much more paper. In addition, the possibilities for error were limitless.

As mentioned earlier, the programs for the composite materials module have been turned over to Texas Instruments Incorporated for fabrication of the module. The library modules are scheduled for delivery sometime in September of 1979.

The Air Force Materials Laboratory foresees several potential applications for the composite materials module. Though computers will still be needed for detailed analyses, the calculator/module combination can provide the engineer with a fast, economical way to perform preliminary calculations which can give him a "feel" for various trends. Armed with this information, he can then make more efficient use of his computer resources.

By relieving the user of the necessity of having to set up all of the necessary calculations on his own, the module enlarges the group of personnel able to perform composite material calculations. Calculations which were once performable only by a small number of highly paid engineers or consultants can be done by junior engineers or technicians. Figure 7 lists some of the calculations carried out by the composite materials module.

Once the number of people able to do composite material analyses has increased, the need for many of the expensive tests being done today in order to obtain empirical results for use in design specifications may decrease. The module may also provide a quick and easy means for technicians to check test results as testing is being done. In addition, engineers will have a readily available method for obtaining information concerning proposed designs during the course of their planning sessions.

Finally, the module can be an aid to a short-course in composite materials. By relieving students of the need to laboriously perform all of the long and somewhat tedious

$$\begin{aligned}
m &= 1/(1-(v_{LT})^2 E_L/E_T) & U_1 &= (1/8)(3Q_{11}+3Q_{22}+2Q_{12}+4Q_{66}) \\
Q_{11} &= mE_L & Q_{22} &= mE_T & U_2 &= (1/2)(Q_{11}-Q_{22}) \\
Q_{12} &= v_{LT}Q_{22} & U_3 &= (1/8)(Q_{11}+Q_{22}-2Q_{12}-4Q_{66}) \\
Q_{16} &= 0 & U_4 &= (1/8)(Q_{11}+Q_{22}+6Q_{12}-4Q_{66}) \\
Q_{26} &= 0 & U_5 &= (1/2)(U_1-U_4)
\end{aligned}$$

$$\begin{aligned}
I_1 &= U_1 - U_5 & e_L &= \alpha_L^T \Delta T + \alpha_L^H c + e_L^c & N_1^N &= p_{\sigma}^N V_{0A} + q_{\sigma}^N V_{1A} \\
I_2 &= U_5 & e_T &= \alpha_T^T \Delta T + \alpha_T^H c + e_T^c & N_2^N &= N_1^N - 2q_{\sigma}^N V_{1A} \\
R_1 &= |U_2| & \sigma_L &= Q_{11}e_L + Q_{12}e_T & N_6^N &= -q_{\sigma}^N V_{2A} \\
R_2 &= |U_3| & \sigma_T &= Q_{12}e_L + Q_{22}e_T
\end{aligned}$$

$$\begin{aligned}
F_{11} &= 1/(X_L X_L') & G_{11} &= F_{11}Q_{11}^2 + 2F_{12}Q_{11}Q_{12} + F_{22}Q_{12}^2 \\
F_{22} &= 1/(X_T X_T') & G_{22} &= F_{11}Q_{12}^2 + 2F_{12}Q_{12}Q_{22} + F_{22}Q_{22}^2 \\
F_{12} &= F_{12}^* \sqrt{F_{11}F_{22}} & G_{12} &= F_{11}Q_{11}Q_{12} + F_{12}Q_{11}Q_{22} + F_{12}Q_{12}Q_{22} + F_{22}Q_{12}Q_{22} \\
F_{66} &= 1/(X_{LT})^2 & G_{66} &= F_{66}Q_{66}^2 \\
F_1 &= 1/X_L - 1/X_L' & G_1 &= F_1Q_{11} + F_2Q_{12} \\
F_2 &= 1/X_T - 1/X_T' & G_2 &= F_1Q_{12} + F_2Q_{22}
\end{aligned}$$

$$\begin{aligned}
a &= G_{66}(\epsilon_6^M)^2 + G_{11}(\epsilon_1^M)^2 + 2G_{12}(\epsilon_1^M)(\epsilon_2^M) + G_{22}(\epsilon_2^M)^2 \\
b &= G_1(\epsilon_1^M) + G_2(\epsilon_2^M) + 2G_{11}(\epsilon_1^M)(\epsilon_1^N - e_L) + 2G_{12}((\epsilon_1^M)(\epsilon_2^N - e_T) + (\epsilon_2^M)(\epsilon_1^N - e_L)) \\
&\quad + 2G_{22}(\epsilon_2^M)(\epsilon_2^N - e_T) + 2G_{66}(\epsilon_6^M)(\epsilon_6^N) \\
c &= 1 - G_{11}(\epsilon_1^N - e_L)^2 - 2G_{12}(\epsilon_1^N - e_L)(\epsilon_2^N - e_T) - G_{22}(\epsilon_2^N - e_T)^2 - G_{66}(\epsilon_6^N)^2 - G_1(\epsilon_1^N - e_L) \\
&\quad - G_2(\epsilon_2^N - e_T) \\
S^M &= (b/2a) - \sqrt{(b/2a)^2 - (c/a)} \\
S^M &= (b/2a) + \sqrt{(b/2a)^2 - (c/a)}
\end{aligned}$$

$$\begin{aligned}
X'_{11} &= U_1V_0 + U_2V_1\cos 2\phi + U_2V_2\sin 2\phi + U_3V_3\cos 4\phi + U_3V_4\sin 4\phi & Q_{11} &= U_1 + U_2 + U_3 \\
X'_{22} &= U_1V_0 - U_2V_1\cos 2\phi - U_2V_2\sin 2\phi + U_3V_3\cos 4\phi + U_3V_4\sin 4\phi & Q_{22} &= U_1 - U_2 + U_3 \\
X'_{12} &= U_4V_0 - U_3V_3\cos 4\phi - U_3V_4\sin 4\phi & Q_{12} &= U_4 - U_3 \\
X'_{66} &= U_5V_0 - U_3V_3\cos 4\phi - U_3V_4\sin 4\phi & Q_{66} &= U_5 - U_3 \\
X'_{16} &= -\frac{1}{2}U_2V_2\cos 2\phi + \frac{1}{2}U_2V_1\sin 2\phi - U_3V_4\cos 4\phi + U_3V_3\sin 4\phi & Q_{16} &= 0 \quad Q_{26} = 0 \\
X'_{26} &= -\frac{1}{2}U_2V_2\cos 2\phi + \frac{1}{2}U_2V_1\sin 2\phi + U_3V_4\cos 4\phi - U_3V_3\sin 4\phi
\end{aligned}$$

$$A'_{ij} = A_{ij} \quad B'_{ij} = dA_{ij} + B_{ij} \quad D'_{ij} = d^2A_{ij} + 2dB_{ij} + D_{ij}$$

FIGURE 7

matrix mathematics required to solve composites problems, more time can be devoted to grasping concepts without sacrificing the valuable experience of obtaining numerical solutions. The possibility of arithmetic error in the calculation of results is also greatly reduced.

It is hoped that with the aid of the composite materials module, the orthotropic material calculations which right now seem so formidable to many will eventually become as familiar and straightforward as those for isotropic materials.

ACKNOWLEDGEMENTS

The author gratefully acknowledges Stephen W. Tsai, Frank Huber, and Marvin Knight of AFML, Roy Chardon of Kirtland AFB, and the personnel of Texas Instruments in Lubbock, Texas for their aid and advice in the development of the composite materials module.

REFERENCES

1. "Personal Programming", Texas Instruments Incorporated (1977).
2. S. W. Tsai and H. T. Hahn, "Composite Materials Workbook", Technical Report AFML-TR-78-33 (1978).
3. S. W. Tsai and H. T. Hahn, "Introduction to Composite Materials, Volume 1: Deformation of Unidirectional and Laminated Composites", Technical Report AFML-TR-78-201, Volume 1 (1978).
4. S. W. Tsai and H. T. Hahn, "TI-59 Magnetic Card Calculator Solution to Composite Materials", Unpublished (1979).

STRUCTURAL SMC -- MATERIAL, PROCESS AND PERFORMANCE REVIEW

Ralph B. Jutte
Owens-Corning Fiberglas
Technical Center
Granville, Ohio 43023

Abstract: Sheet molding compound (SMC) has been used for functional or fascia automotive parts such as front and rear panels for several years. When properly formulated, processed, and molded, SMC has a potentially substantial role in the manufacture of more structurally demanding automotive parts. *(2) A versatile family of high strength SMC's can be used for automotive parts where design is*

Through variations in the materials, equipment and processing techniques, different types of SMC can be produced. These are random fiber SMC (SMC-R); continuous fiber SMC (SMC-C); and directional fiber SMC (SMC-D).

Representative formulations show how static mechanical properties are dependent upon glass content, glass orientation, and on the test temperature. *with modified*

Based on equivalent performance, these systems are lighter in weight than steel and are generally less costly, on a material basis, than aluminum.

Key Words: Glass fiber reinforcement; polyester resin, structural sheet molding compound.

The increasing costs of energy and the drive to conserve energy from conventional resources have caused major changes in materials technology. Attention is now being given to materials, processes, and products which combine low energy for manufacturing and reduced energy of operation.

This attention has caused design engineers and FRP materials suppliers to extend the use of FRP from typical applications in which appearance is the prime requirement to so-called "structural" applications, where parts are required to carry loads in addition to those imposed by fasteners and their own weight. Coupled with this extension of FRP use is the added requirement that designs in FRP be of maximum efficiency; that is, that the parts most efficiently utilize the properties of the material.

Owens-Corning Fiberglas has undertaken a program to address these issues. We have developed an easy-to-manufacture, versatile family of structural sheet molding compound materials, denoted SMC-R, SMC-C/R, SMC-D, and SMC-D/R, and have committed significant effort to characterizing these materials relative to their engineering mechanical properties. Additional work is underway to develop constitutive relationships among composition, process parameters, molding conditions, and engineering properties.

This report will define the OCF structural SMC materials, identify the advantages of each, and report on static mechanical properties as well as process methods.

SMC-R

SMC-R (Figures 1 and 2) is defined as RANDOM FIBER SMC. It contains reinforcements with a fiber length of three inches or less in a random pattern in two dimensions. Nominal glass content is denoted by the number after the letter R, e.g., SMC-R50 would contain 50 percent glass fiber by weight. Most SMC used today is SMC-R. The usual reinforcement is chopped roving, although chopped strand mat also is suitable. The reinforcement can be cut to the uniform lengths, or a combination of lengths can be used. The usual length used in industry today is one inch. Although nominal glass content for structural applications ranges from 30 to 70 percent by weight, the majority of interest is at 50 percent or higher glass content.

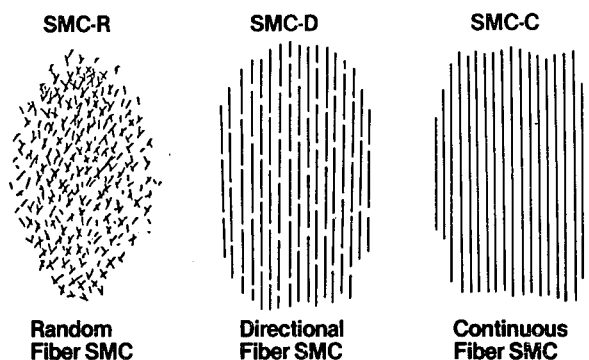


Fig. 1 - SMC type designates reinforcement configuration used

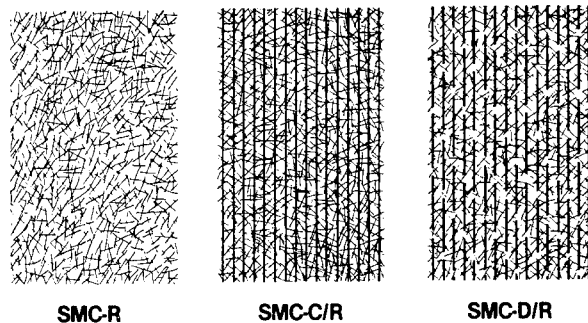


Fig. 2 - Combination of fibers can be used to expand basic systems.

- **Materials** - a variety of resins such as polyesters, vinyl esters and epoxies have been evaluated and used during prototyping. This report covers data based on the Owens-Corning Fiberglas (OCF) E980 polyester resin, a high-reactivity isophthalic polyester resin specifically selected for use in structural SMC. Low shrink additives can be incorporated into the resin for such applications as wheels where superior dimensional and warpage control is desired. In the majority of structural applications, surface appearance characteristics and dimensional control are adequate without the use of low shrink additives.

Glass roving at glass concentrations below 45 percent can be either OCF 951 or OCF 433. Above 45 percent, OCF 433 glass is recommended because its more soluble size system allows it to be processed into a denser, more uniform sheet. The greater filamentation associated with this product allows better glass distribution and carrying characteristics during molding at higher glass contents. Usually, the more highly soluble systems also give better strength but lower impact resistance.

All the above fibers are E glass. Other candidate reinforcements include high-strength S-2 Glass®, graphite, and aramid.

The wide variety of SMC catalysts, promoters, and mold releases used in present SMC production parts are applicable for use in structural SMC.

Fillers, used as extenders to reduce costs, normally are added at levels as high as tolerable. The highest loading ratios can be achieved with ground limestone (CaCO_3) and it is commonly used for applications that do not require flame retardancy. Specific resin to filler ratios depend largely on the glass content and process

considerations; glass wet-out on the SMC equipment being of greatest importance. Typical filler to resin ratios are 1.5 to 1 at 30 percent glass content and 0.5 to 1 at 50 percent glass content. No filler is recommended for the 65 percent glass formulation.

A variety of alkaline earth metal oxides and hydroxides can be used to thicken SMC paste. Selection of a specific thickener depends on the resin type, filler content, and desired matured viscosities. As filler content decreases, thickening rates become slower and viscosities plateau at a lower level. At lower filler levels, magnesium oxide (MgO) thickener works well. It should be carefully stored prior to use or used in slurry form to prevent hydrolysis.

Specific formulations for SMC-R50 and SMC-R65 are shown in Table A.

SMC-R50

Resin Paste

Resin	OCF-E980	100 Parts
Inhibitor	Benzoquinone	.0005 phr
Catalyst	T-Butyl Perbenzoate	1 phr
Mold Release	Zinc Stearate	2.5 phr
Filler	Calcium Carbonate	50 phr
Thickener	Magnesium Oxide	1.5 phr

Compound

Resin Paste – 50 Parts
Glass – OCF 433AB – 50 Parts

SMC-R65

Resin Paste

Resin	OCF-E980	100 Parts
Inhibitor	Benzoquinone	.0005 phr
Catalyst	T-Butyl Perbenzoate	1 phr
Mold Release	Zinc Stearate	2.5 phr
Thickener	Magnesium Oxide	1.5 phr

Compound

Resin Paste – 35 Parts
Glass – OCF433AB – 65 Parts

Table A

- Processing - conventional SMC machines are used to make SMC-R. A paste containing the resins, fillers, catalyst, mold release and thickening agents are uniformly metered onto the carrier films (Figure 3).

Care must be taken to produce an SMC product which thoroughly wets out at the higher glass contents. This may require a slower line speed and a reduced weight per square foot sheet than used at the lower glass contents. At the 60 to 70 percent glass range, sheet weights up to 20 ounces per square foot have been produced at line speeds to 10 to 20 feet per minute.

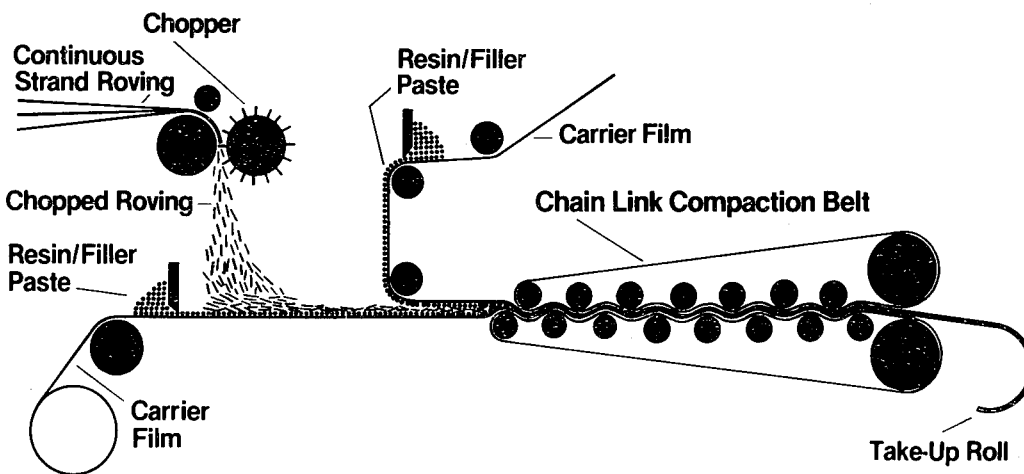


Fig. 3 - SMC-R production process

Molding conditions vary with part complexity. In general, 800 to 1500 pounds per square inch (psi) molding pressures are used. Mold temperatures are typically 290 to 310°F. The higher glass content materials mold quite satisfactorily under the same conditions, commonly used to mold SMC-R30 compounds.

The matured paste viscosity of SMC-R30 polyester compounds is commonly 40 to 60 million centipoise as measured by a Brookfield HBT Viscometer. SMC-R50 and R65 compounds (Table A) are generally molded at a lower viscosity. A paste viscosity of five to twenty-five million centipoise appears satisfactory. Lower viscosities result in a tacky sheet and separation of the resin and glass during molding. Higher viscosities require proportionally higher molding pressures.

- **Advantages and Limitations** - SMC-R has the greatest molding versatility. Parts of varying cross sections including ribs and bosses are moldable even at the high glass content. However, presence of deep ribs and bosses may require shorter fibers and lower glass contents to maintain good glass distribution and fill out.

SMC-R has application in parts where strength uniformity is important. It is considered isotropic in an unmolded state, but becomes anisotropic upon flowing in the mold. To minimize its anisotropic properties, a charge with the maximum mold coverage should be used. This will minimize flow and resultant knit lines. The presence of fiber orientation and knit lines can be measured, to some degree, by molding multi-color compounds, by burnoff of molded parts and X-ray techniques. These techniques are valuable for determining a proper charge pattern.

- Mechanical Properties - Strength Properties at Various Glass Contents - SMC-R has no inherent directional characteristics. However, this isotropy is sacrificed if extensive flow occurs.

Figures 4 through 6 present tensile, flexural, and impact strength properties from a variety of compounds at varying glass contents for polyester resin based systems. These figures are based on data from flat laminates made with a variety of polyester matrix formulations that contained 20 to 65 percent glass by weight and tested at 23°C. These properties generally vary linearly with glass content.

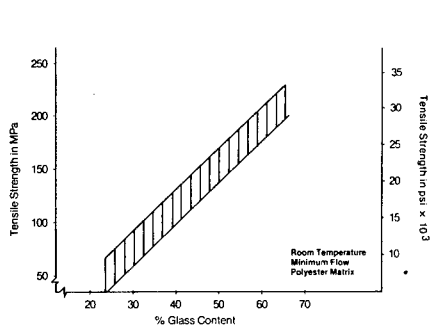


Fig. 4 - General range of average tensile strengths at various glass contents for SMC-R systems

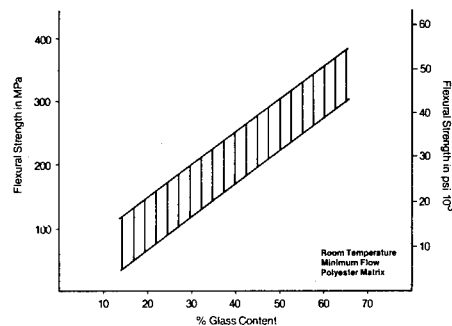


Fig. 5 - Dependence of flexural strength on glass content for SMC-R systems

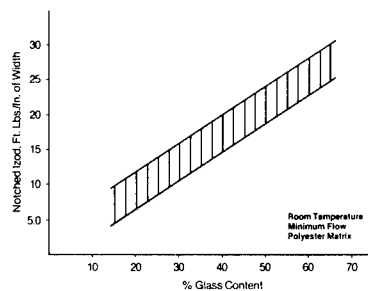


Fig. 6 - Effect of glass content on notched izod impact for SMC-R systems

Properties at Elevated Temperatures - it is necessary to consider performance data at, or near, the operating temperatures encountered in a specific application.

Static tensile and flexural properties of laminates were measured at elevated temperatures after short term exposure conditioning -- 30 minutes as specified by ASTM test methods D790 and D638. Figures 7 through 14 show these properties for SMC-R50 and SMC-R65 systems. The graphs include the mean of the data and the predicted 95 percent confidence limits of the mean based on ten specimens, five taken normal and five parallel to the major axis of the molded plaque. These specific limits may vary if different molding parameters are used.

The properties presented are for systems formulated as shown in Table A. Test plaques were 30.5 centimeter (12 inch) by 45.7 centimeter (18 inch) by 2.5 ± 0.25 millimeter (0.1 ± 0.01 inch) thick and molded at $149^{\circ}\text{C} \pm 5.5^{\circ}\text{C}$ ($300 \pm 10^{\circ}\text{F}$) for two minutes under 5.5 MPa (800 psi). The SMC charge was dimensioned to cover 80 percent of the mold for the SMC-R65 and 45 percent for the SMC-R50. To minimize random flow effects, laminates were molded with all plies of the same dimension and to a nominal thickness of 2.5 millimeter (0.1 inch). To include data variation from other sources, such as change in raw materials, process set-up and operation, laminate testing samples were prepared and tested over a six month period. The number of specimens per test condition ranged from 40 to 70.

The increased variation in the SMC-R50 data as compared to the SMC-R65 data can be largely contributed to the material molding charge used, 45% and 80% coverage respectively. This resulted in additional flow induced fiber orientation in the SMC-R50 system, thus increased mechanical property variability.

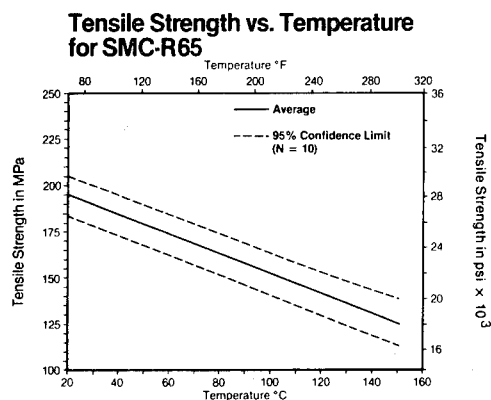


Fig. 7 - Tensile strength versus temperature for SMC-R65

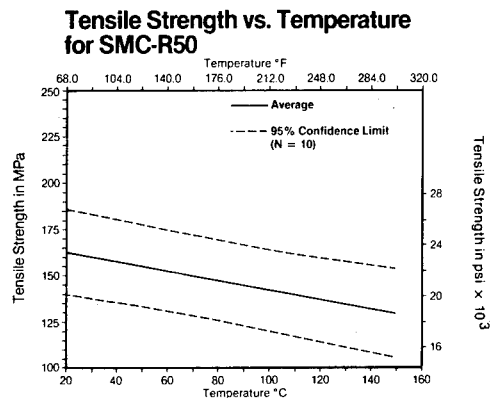


Fig. 8 - Tensile strength versus temperature for SMC-R50

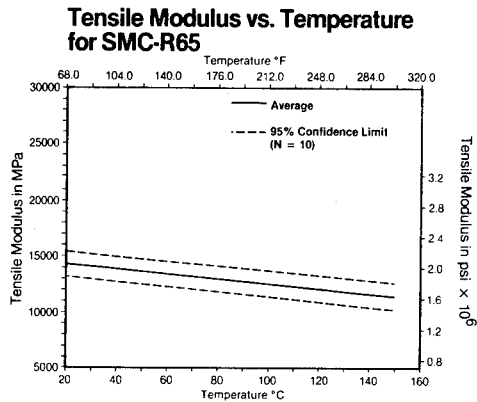


Fig. 9 - Tensile modulus versus temperature for SMC-R65

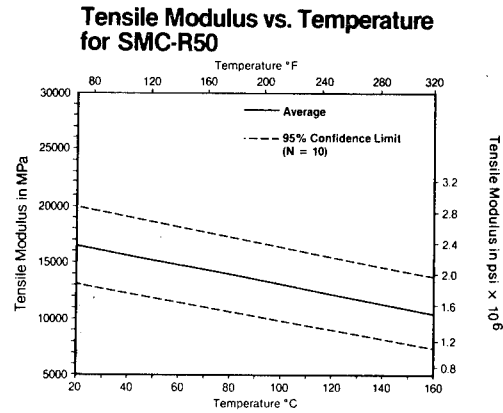


Fig. 10 - Tensile modulus versus temperature for SMC-R50

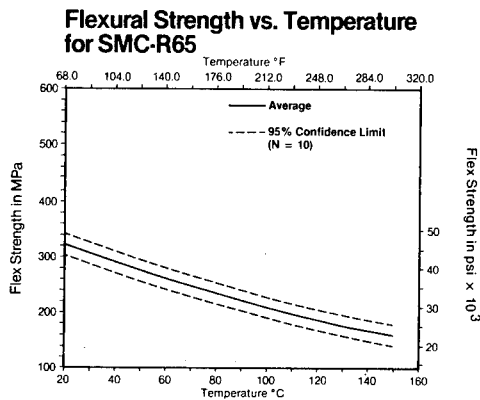


Fig. 11 - Flexural strength versus temperature for SMC-R65

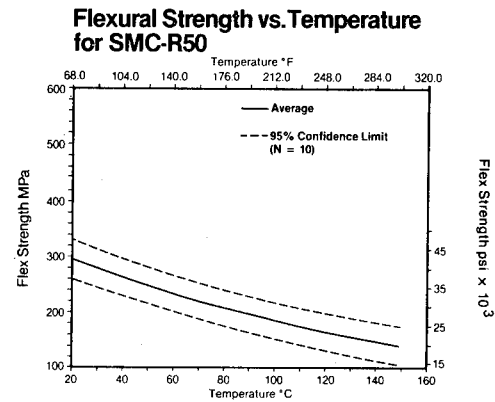


Fig. 12 - Flexural strength versus temperature for SMC-R50

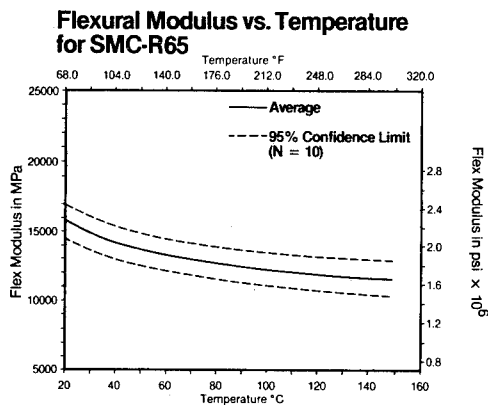


Fig. 13 - Flexural modulus versus temperature for SMC-R65

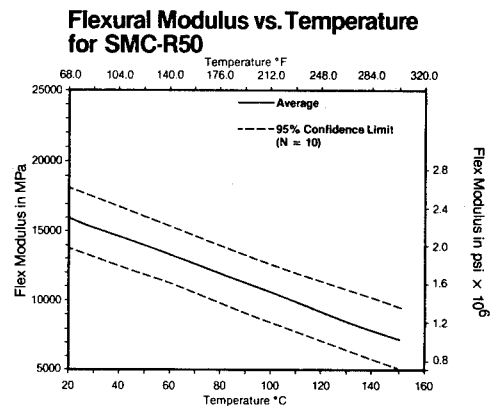


Fig. 14 - Flexural modulus versus temperature for SMC-R50

SMC-C and SMC-C/R

SMC-C (Figure 1) is defined as CONTINUOUS FIBER SMC. It contains continuous reinforcing fiber deposited in a unidirectional fashion. Continuous Fiber SMC often is produced in combination with random fibers as SMC-C/R (Figure 2).

In these two systems, the reinforcement content can be adjusted up to 70 percent by weight to produce compounds tailored to specific applications.

Examples of specific types would be SMC-C60, e.g., 60 percent unidirectional fibers; and SMC-C30/R20, e.g., 30 percent unidirectional fibers combined with 20 percent random chopped fibers.

- Materials - continuous reinforcement input used could be from numerous ends of roving or possibly a unidirectional mat, sometimes called a "beam". When continuous reinforcement is used with chopped random fibers (SMC-C/R), one might consider hybrid combinations of various types of fibers, for example, S-2 Glass and E glass, graphite and E glass, and aramid with E glass. The majority of our work has been directed toward using glass roving input, generally E glass.

Other material considerations for SMC-C are similar to those discussed previously for SMC-R.

- Processing - a belt type SMC machine (Figure 15) can be used to produce SMC-C or SMC-C/R, although some additions and modifications are necessary. When continuous roving is used as the input reinforcement, a twist will occur if the roving is pulled from inside the package. This can be minimized by using a low-yield roving pulled from the outside. Yield is defined as yards/pound of reinforcement.

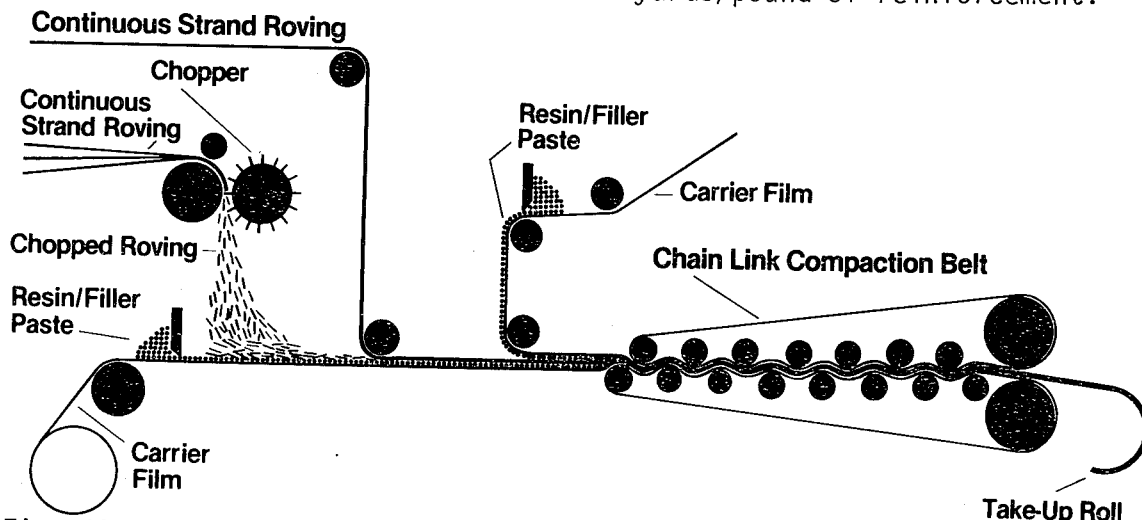


Fig. 15 - Schematic of SMC-C/R production process showing introduction of continuous and chopped reinforcement

Provisions must be made for additional creel space and equipment to pull from the outside of the roving package. A creel for this purpose is shown in Figure 16. A roving spacing device must also be added to the SMC machine to evenly distribute the rovings across the sheet width. One technique using a hinged center point tube holder allows this bank width to be varied (Figure 17).

To enhance the wet-out without strand pattern disturbance, a single flexible chain link belt was added to the compaction section (Figures 18 and 19). This prevents the roving strands from falling into and following the serrations found in typical compaction rollers. A further refinement to the Owens-Corning development machine is a double chain link belt compaction section for even better wet-out (Figures 20 and 21).

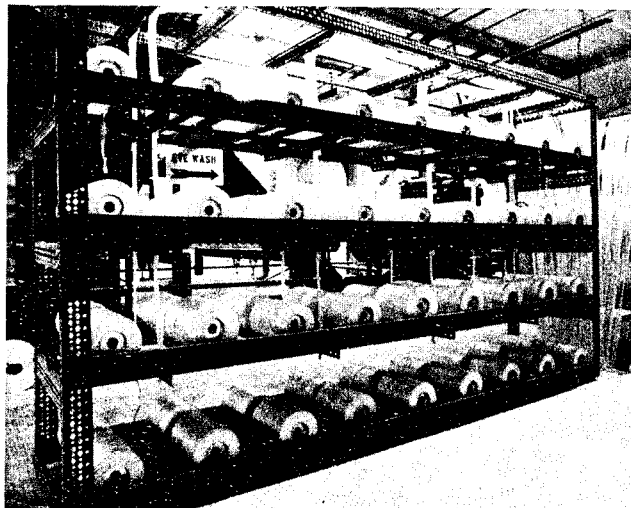


Fig. 16 - Creel for SMC-C set up for outside pull of roving

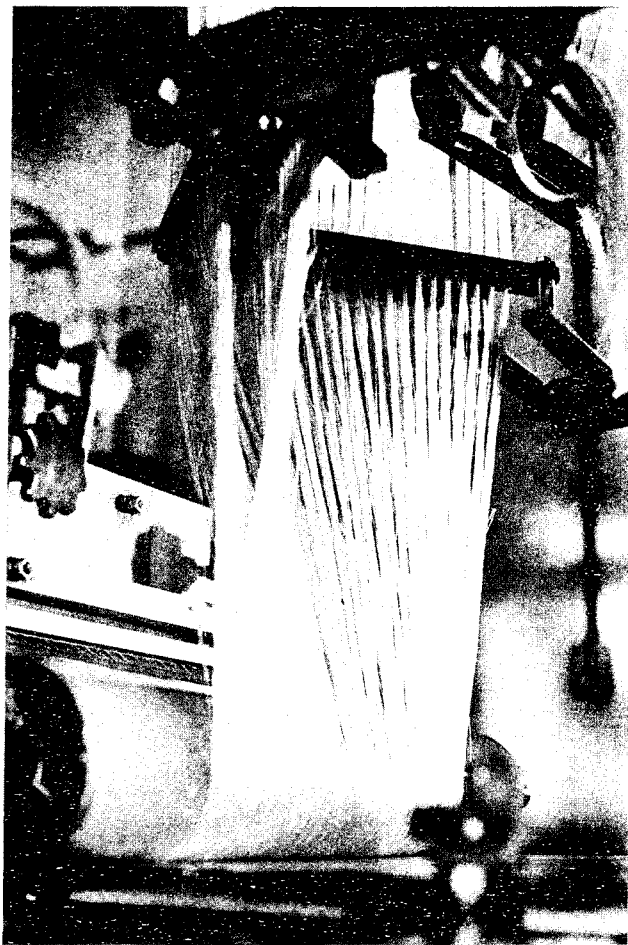


Fig. 17 - View of the adjustable roving spacing device and the continuous roving entering the SMC compaction section



Fig. 18 - SMC compaction section showing a single steel mesh belt that has been added to an existing unit

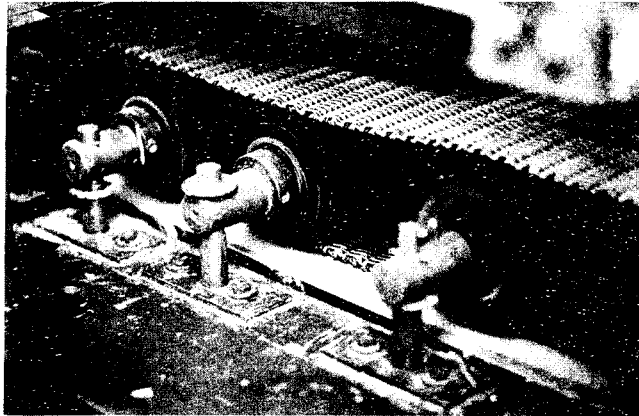


Fig. 19 - Side view of an SMC compaction section showing single mesh belt around existing serrated compaction rollers

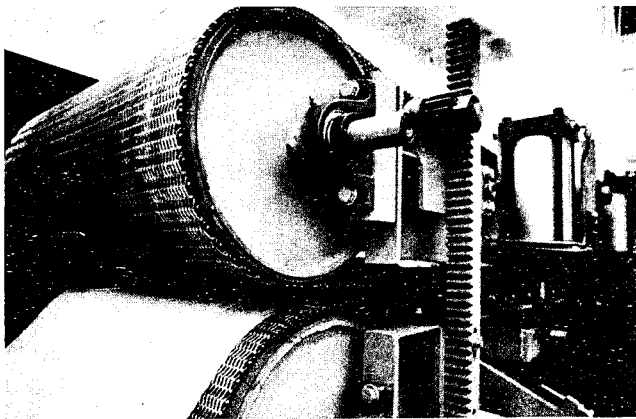


Fig. 20 - End view of double mesh belt SMC compaction unit

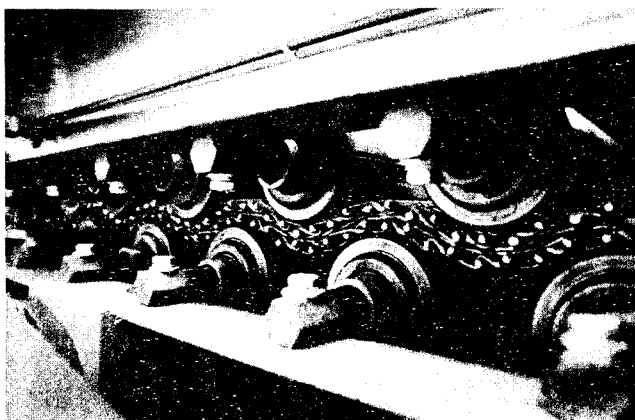


Fig. 21 - Side view of double mesh belt unit showing "working" action taking place on both sides of SMC sheet

- Advantages and Limitations - SMC-C - this system is capable of producing the maximum mechanical properties in the direction of the fibers, but with low values when tested perpendicular to the fiber direction.

Combining plies at various angles to one another could be done to minimize the severe anisotropy of mechanical properties, and to "build" specific property performance characteristics as needed particularly modulus and impact (Figure 22).

Strategic placement in parts of SMC-R can be used to strengthen specific areas.

Creel and machine modifications are necessary to produce the product.

Sheet weight may be somewhat restricted compared to SMC-R.

Because of unidirectionality of reinforcement, the handling integrity of SMC-C sheet is not as good as SMC-R.

Flow limitations would require practically 100 percent mold coverage in the fiber direction. Some degree of flow in the lateral direction is possible depending on part shape and resin system used.

Incorporation of bosses, ribs or any three-dimensional design feature in the part is not desirable.

SMC-C/R - the incorporation of random chopped fiber into the SMC-C system improves its processing and charge handling prior to molding.

There is an improvement in the transverse mechanical properties as the ratio of chopped to continuous fibers is increased.

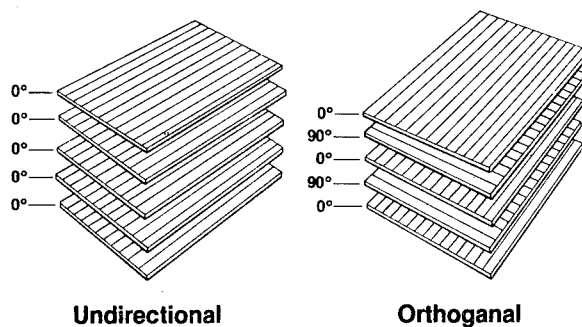
Higher sheet weight products can be more easily produced for the same total glass content than with unidirectional fiber above.

The same charge pattern and flow limitations mentioned in SMC-C system will prevail but to a lesser degree. The feasibility of incorporating minor bosses and ribs will be somewhat improved, particularly when the proportion of the chopped fiber is increased.

Parts may be molded with either the continuous or chopped random fibers at the surface. Random fibers produce a more uniform appearance, while the continuous fibers on the surface produce somewhat better flexural properties.

The process considerations for 100 percent continuous unidirectional fiber also apply here.

● Mechanical Properties - limited mechanical properties have been generated to-date on SMC-C and SMC-C/R systems (Figures 23 through 26). The data clearly shows excellent ultimate strength properties as well as the high directionality associated with materials systems employing continuous fibers. Use of continuous fibers significantly increases the modulus values, above those achievable with SMC-R systems at comparable glass contents.



Examples of laminate ply construction
when using SMC-C

Continuous		1 ply
Random		
Random		1 ply
Continuous		
or		
Random		1 ply
Continuous		
Continuous		1 ply
Random		

For laminates requiring more than two plies, balance of ply construction is recommended. The flatter the laminate requirements, the more critical this balance ply construction becomes to prevent warpage.

Fig. 22 - Examples of laminate ply construction when using SMC-C

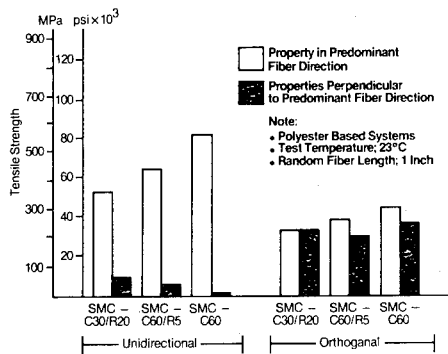


Fig. 23 - Tensile strengths as effected by different types of SMCs, laminate construction, and fiber orientation

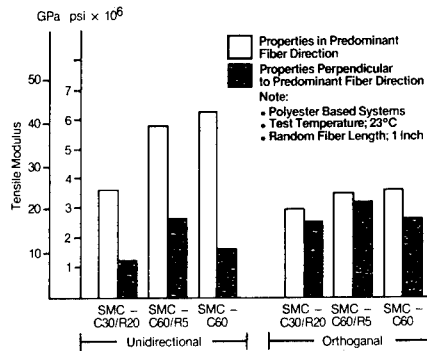


Fig. 24 - Tensile modulus values as effected by different types of SMCs, laminate construction, and fiber orientation

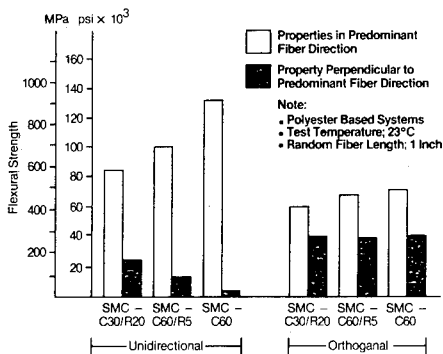


Fig. 25 - Flexural strengths as influenced by different types of SMCs, laminate construction, and fiber orientation

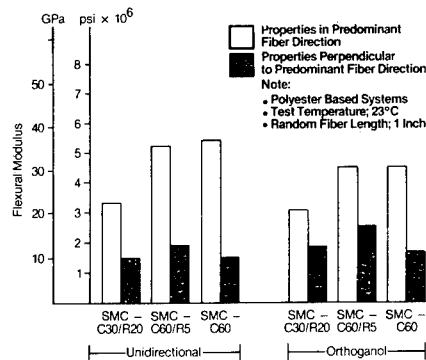


Fig. 26 - Flexural modulus values as influenced by different types of SMCs, laminate construction and fiber orientation

SMC-D and SMC-D/R

SMC-D (Figure 1) is defined as DIRECTIONAL FIBER SMC. It contains fibers of four inches or longer in length in a discontinuous unidirectional pattern. Handling and performance considerations, however, generally require the Directional Fiber SMC to be made in combination with some random fibers as an SMC-D/R system (Figure 2).

- Materials - the resin, filler, reinforcement, and other material considerations for SMC-D are the same as those discussed in the previous SMC-R and SMC-C sections.

- Processing - there are two SMC manufacturing approaches in use to produce the SMC-D and SMC-D/R material systems; on-line and off-line. Both use a similar long fiber cutting arbor to cut the roving into the long, unidirectional pattern. The blades in this arbor are set-up to cut fibers into long lengths on a random cut pattern (Figure 1).

Using the on-line approach, introduced by OCF-Europe in support of the FRP bumper programs, the long glass fiber cutter is placed on the SMC machine. By synchronizing the peripheral speed of this long cutter with the belt speed, long fibers are cut onto the moving SMC web so that the roving ends butt against one another (Figures 27 and 28).

The alternate approach to producing the SMC-D/R material is an off-line operation using an SMC-C/R material matrix as described previously. Figure 29 shows the off line making of SMC-D/R charge pattern, and molding results. The sheet is allowed to thicken to three million centipoise (as measured by the Brookfield HBT Viscometer) or above in paste viscosity before being processed through the long cutter.

The blades pierce the carrier film and cut the continuous rovings into predetermined lengths. Thus, SMC-C/R is converted into SMC-D/R. This operation could be incorporated into the conventional SMC cutter/slitter machines.

- Advantages and Limitations - the major reason for considering the SMC-D approach is its improved molding characteristics relative to SMC-C. Cutting the continuous fibers allows the material to flow in the fiber direction as well as in the transverse direction. Thus, this system provides a compromise between the good flow characteristics of SMC-R and the superior mechanical properties of SMC-C.

Two process approaches are available. An additional cutter must be utilized for either approach. The use of a secondary piercing operation may provide the most versatility since all three SMC materials can then be produced on one machine.

SMC-D has a definite direction bias relative to mechanical properties; therefore, it should be used where this characteristic contributes to part performance. Specific material selection is based on part requirements and molding limitations.

Random windows occur in the molded laminate. Their size and effect are controlled by the degree of flow occurring, the length of the fibers used, ratio of long and short fiber contents, and the overall glass content.

Similar to SMC-C requirements, additional roving creel space is necessary.

As in SMC-C, a balanced ply construction is recommended in the molded part to minimize residual stresses and warpage.

- Mechanical Properties - Owens-Corning is currently reviewing test procedures to permit representative measurements of SMC-D properties at high glass contents. The concern is that since some localized discontinuities exist (windows) the relatively small test specimens currently specified in standard ASTM test methods may not provide a true definition of composite properties.

Mechanical properties of SMC-D systems are expected to fall between those of SMC-R and SMC-C systems of comparable glass content with values approaching those of SMC-C as the length of the long unidirectional fibers increase.

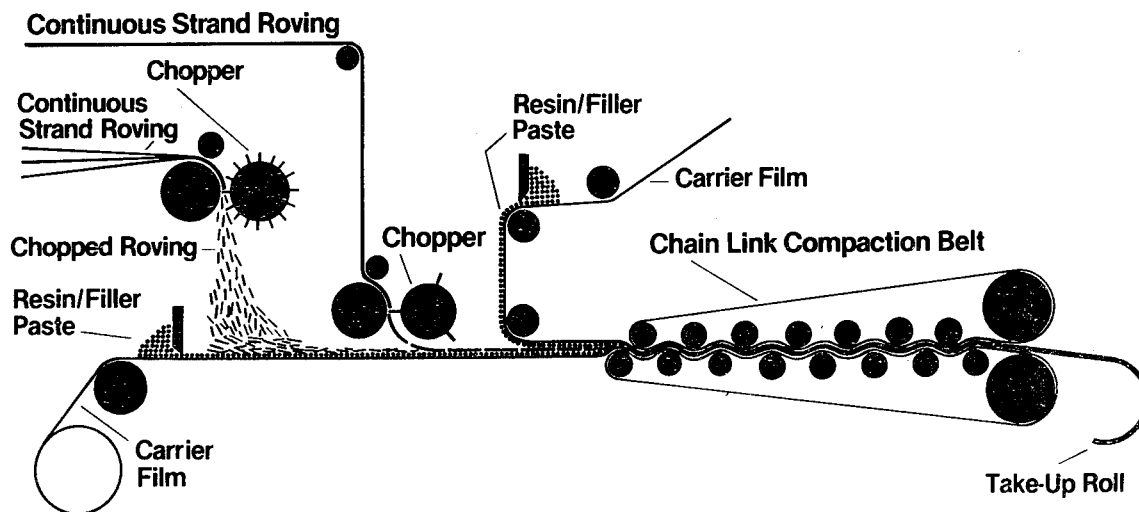


Fig. 27 - Schematic of SMC-D/R on-line production process utilizing two roving choppers

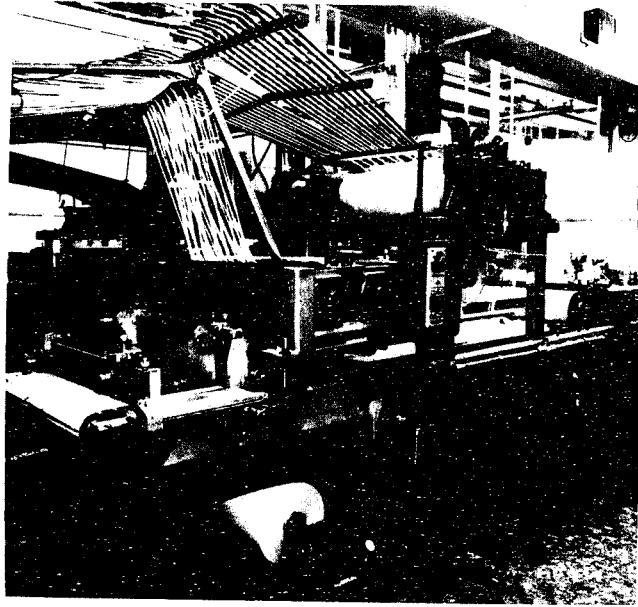


Fig. 28 - On-line SMC-D/R process showing long and random fiber cutters on an SMC machine

Off-Line Production Process

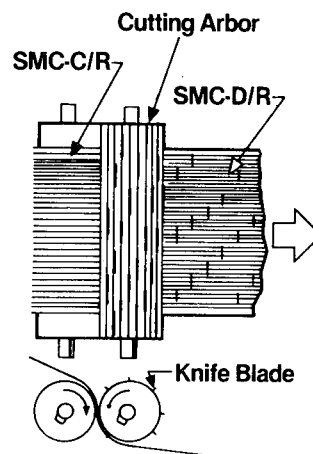


Fig. 29 - Schematic of SMC-D/R off-line production process showing secondary piercing operation used to convert SMC-C/R and SMC-D/R

Cost and Performance Comparisons

- **Raw Material Cost** - SMC formulations for use with 30 percent to 65 percent glass content by weight were established and composite raw material cost per pound calculated (Table B). These formulations were based on the use of polyester resin, calcium carbonate filler and other commonly used components. Raw material cost varied from \$0.38 per pound for 30 percent glass content to \$0.56 per pound for 65 percent glass contact composition.
- **Process Cost** - Processing costs to make the sheet product are expected to vary depending on the type of SMC produced and glass content desired. As indicated in previous processing discussion, some equipment modifications are necessary to produce the SMC-D and SMC-C materials. Generally, higher glass contents mean a lower weight per square foot product at a slower line speed. This reduces productivity thus increasing costs. Additional experience is needed before process cost variables can be accurately assessed.
- **Performance Comparisons** - the performance data previously shown indicates the relatively broad range of properties that can be obtained by varying the SMC composition and type. A multitude of different compositions and additional comparisons can be made in each category. In Tables C and D, representative SMC systems were selected and equivalent performance calculations and comparisons made. For comparative purposes, representative values for high strength low alloy steel (HSLA 950) and aluminum (7021-T6) currently being used for bumpers have been included.

Volume Costs - cost per cubic inch takes into consideration both the material cost per pound and the material density. Since the densities of SMCs we have presented are nearly constant at 0.066 pounds per cubic inch, volume costs are directly proportional to the material's cost per pound. The higher density of steel and aluminum make them significantly more costly than SMC on simple volumetric basis.

Flexural Strength - when comparing the different SMC-R systems, an increase in the glass content provides a weight savings but no appreciable cost savings for equivalent flexural strength performance.

The thinner laminates at the higher glass contents can provide weight savings but the increased material costs negates any cost saving.

When the SMC-D and SMC-C systems are used effectively with the stress applied in the direction of the predominant fiber direction, additional weight and cost savings over the SMC-R systems can be expected.

Stiffness - comparing the SMC systems, it is apparent that the much higher modulus values of SMC-C systems allow for decreased laminate

thickness, thus weights, over the SMC-R systems.

When compared with the HSLA steel, the SMC systems are lighter in weight, but more costly. When compared with the aluminum, the SMC systems are less costly and for SMC-C the weight is also less (Table D). These values for SMCs, however, are conservative since the comparisons are based on flat plate theory and do not take into account the ease of molding SMC into complex shapes, addition of ribs and changing cross sectional geometry, and the commonly used techniques for adding stiffness.

Tensile Strength - when comparing the SMC systems to steel and aluminum the same general trend in cost and weight as noted in stiffness apply.

Comparing the various SMC systems, the value of increased glass loading and fiber orientation is evident. The higher tensile strengths occurring from use of higher glass contents allow a reduction in thickness that more than offsets higher material costs. As a result, there is a significant weight and cost savings potentially available where higher glass type SMCs are applicable.

SMC Raw Material Costs (Cost Calculations based on prices in effect March 1, 1979)									
Glass Content		Resin	Filler	Reinforcement	Catalyst	Mold Release	Thickener	Total	
		Polyester	Calcium Carbonate	Fiberglass Roving	T-Butyl Perbenzoate	Zinc Stearate	Magnesium Oxide		
	\$/lb.	.49	0.05	0.58	\$2.16	0.94	0.88		\$/lb.
30%	Parts lbs.	35	35	30	0.35	0.98	0.53	101.8	
	Cost \$	17.15	1.75	17.40	0.76	0.83	0.47	38.36	0.377
40%	Parts lbs.	35	25	40	0.35	0.88	0.53	101.8	
	Cost \$	17.15	1.25	23.20	0.76	0.83	0.47	43.66	0.429
50%	Parts lbs.	35	15	50	0.35	0.88	0.53	101.8	
	Cost \$	17.15	0.75	29.00	0.76	0.83	0.47	48.96	0.481
60%	Parts lbs.	35	5	60	0.35	0.88	0.53	101.8	
	Cost \$	17.15	0.25	34.80	0.76	0.83	0.47	54.26	0.533
65%	Parts lbs.	35	0	65	0.35	0.88	0.53	101.8	
	Cost \$	17.15	0.0	37.70	0.76	0.83	0.47	56.91	0.559

Table B

Cost-Performance Comparisons for Raw Materials (Cost Calculations based on prices in effect March 1, 1979)												
Materials	Cost \$/lb.	Density lb./in. ³	Volume Costs ¢/in. ³	Flexural Strength (1)			Stiffness (1)			Tensile Strength (1)		
				Strength 10 ³ psi	Thickness Inches (2)	Cost \$/sq. ft.	Flexural Modulus 10 ⁶ psi	Thickness Inches (3)	Cost \$/sq. ft.	Strength 10 ³ psi	Thickness Inches (4)	Cost \$/sq. ft.
SMC-R30	0.377	0.066	2.49	23	0.114	0.41	1.9	0.219	0.79	11	0.091	0.33
SMC-R40	0.429	0.066	2.83	30	0.100	0.41	2.0	0.215	0.88	17	0.059	0.24
SMC-R50	0.481	0.066	3.17	37	0.090	0.41	2.2	0.209	0.95	23	0.043	0.20
SMC-R65	0.559	0.066	3.69	48	0.079	0.42	2.3	0.206	1.09	30	0.033	0.18
SMC-C30/R20 unidirectional	0.481	0.066	3.17	85	0.059	0.27	3.3	0.182	0.83	55	0.018	0.08
SMC-C60/R5 orthogonal	0.559	0.066	3.69	68	0.066	0.35	4.5	0.164	0.87	40	0.025	0.13
SMC-C60/R5 unidirectional	0.558	0.066	3.69	100	0.055	0.29	5.3	0.156	0.83	64	0.016	0.09
SMC-C60 unidirectional	0.533	0.066	3.52	130	0.048	0.24	5.4	0.154	0.78	81	0.012	0.06
Steel (HSLA 950)	0.192	0.271	5.20	50	0.078	0.58	30	0.087	0.65	50	0.020	0.15
Aluminum 7021-T6	0.87	0.090	7.83	50	0.078	0.88	10	0.126	1.42	50	0.020	0.23

Notes: 1. Properties from predominant fiber direction in laminate.
2. Thickness to support 100 pounds on a 1 inch wide sample on a 2 inch span at indicated stress.
3. Thickness to support 100 pounds on a 1 inch wide sample on a 2 inch span with 0.01 inch deflection.
4. Thickness to support 1000 pounds on a 1 inch wide sample at indicated stress.

Table C

Material Systems	Pounds for Equivalent Performance Basis - 10 Pounds Steel				Dollars for Equivalent Performance Basis - \$1.00 Steel			
	Volume Filling	Flexural Strength	Stiffness	Tensile Strength	Volume Filling	Flexural Strength	Stiffness	Tensile Strength
SMC-R30	2.4	4.5	6.1	11.1	0.47	0.72	1.23	2.21
SMC-R40	2.4	3.1	6.0	7.2	0.52	0.72	1.36	1.64
SMC-R50	2.4	2.8	5.9	5.2	0.58	0.72	1.48	1.36
SMC-R65	2.4	2.5	5.8	4.0	0.67	0.74	1.69	1.21
SMC-C30/R20 unidirectional	2.4	1.8	5.1	2.2	0.58	0.48	1.30	0.57
SMC-C30/R20 orthogonal	2.4	2.1	4.6	3.0	0.67	0.61	1.34	0.93
SMC-C60/R5 unidirectional	2.4	1.7	4.4	2.0	0.67	0.50	1.28	0.57
SMC-C60 unidirectional	2.4	1.5	4.3	1.5	0.64	0.43	1.21	0.43
Steel (HSLA 950)	10.0	10.0	10.0	10.0	1.00	1.00	1.00	1.00
Aluminum (7021-T6)	3.3	3.3	4.8	3.3	1.40	1.41	2.03	1.43

Table D

Summary

A versatile family of high-strength SMC materials has been developed. The basic systems are designated SMC-R, SMC-C, and SMC-D, where R, C, and D stand for "Ramdon", "Continuous", and "Directional", and indicate the configuration of the reinforcement used. Combination of fibers allow other systems to be considered also, such as: SMC-C/R and SMC-D/R. These materials are processable on conventional SMC machines with minor modifications, and thus provide the compound with the ability to produce structural grade SMC with a minimum capital investment.

The molder is provided a materials system with which he can deliver mechanical properties and selective directional reinforcement in order to comply with special part requirements. This flexibility in reinforcement will lead to improved efficiency of design, which will result in minimum part cost and weight for any given application.

Data reported in this paper have been for conventional static mechanical properties. Although such data are necessary for any design and are sufficient for those applications where cyclic loading is not significant, in order for the use of these materials to be extended to the broad range of parts for which they are suitable, fatigue information as well as data on shear properties and Poisson's ratio is necessary. At this time, Owens-Corning is well underway with a program to develop these properties for SMC-R, SMC-C, and SMC-D, which will lead to an even wider range of applications than those presently considered.

Development of a Graphite-Epoxy Spacecraft Precision Mounting Platform

Kathleen S. Budlong and Alvin W. Sheffler
RCA Astro-Electronics Division
Princeton, New Jersey 08540

Abstract

A wide variety of spacecraft applications require structure which is ultra-light in weight while satisfying tight stiffness (resonant frequency) criteria, along with critical pointing accuracy and thermal distortion requirements. This paper presents the design, analysis, and test of a graphite-epoxy precision mounting platform intended to replace the current aluminum platform being flown on an Air Force satellite program.

The Precision Mounting Platform (PMP) provides an instrument mounting surface which is defined and controlled for each instrument to within 0.01 degree. It maintains a mutual alignment of the instruments to within 0.003 degree through the full range of thermal gradients occurring on orbit. While the aluminum PMP uses active thermal controls to minimize thermal gradients and maintain alignment, the composite design takes full advantage of the near zero coefficient of thermal expansion of the GY70/X-30 graphite-epoxy, thus eliminating active control. The ultra-high stiffness of the composite is also critical in maintaining the resonant frequency range defined by overall spacecraft dynamics for the aluminum PMP. The graphite-epoxy PMP provides in addition a weight savings of 32 percent while fulfilling all the requirements of a direct replacement for the current aluminum version.

SESSION 5

AUTOMOTIVE APPLICATIONS AND DESIGN

Chairman: W. W. Gunkel

General Motors Technical Center

Design Analysis of Automotive Composite Structures

M. F. Kowalski, D. S. Fine, and R. K. Herrman
Chevrolet Engineering Center
Warren, Michigan 48090

Abstract

Advanced composite materials offer potential for structural mass reduction in automotive structures due to their high strength-to-weight ratios. In addition, they provide styling freedom to reduce aerodynamic drag forces and part consolidation advantages for vehicle system design. Consequently, they may play an increasing role in the reduction of fuel consumption in the next generation of automobiles.

Traditionally, prevention of mechanical failure has been a key automotive design goal. This is necessitated because our products are often subjected to abuse for lack of required periodic inspections and maintenance. Failures lead to product liability claims, high warranty repair costs, and dissatisfied customers. Failure prevention is difficult because of the wide variety of operating conditions and environments our product experiences, and because the product must be produced by a mass production technology at a cost our customers can afford. Considering the fact that there are over 15,000 parts in an average automobile, our components must be designed for very high reliability.

Because of the nature of advanced composite materials, particularly their anisotropy and their multiple failure modes, the design and analysis procedures currently employed to minimize failure on metal structures are not adequate for composite structures. In anticipation of the need to address the automotive design possibilities of composite materials, a study has been conducted to determine what modifications are needed in the existing finite element structural analysis procedures. It has been found that a composite material analysis program, SQ5, now widely used in the aerospace industry, offers potential for automotive structural analysis.

SQ5 is based on classical laminate plate theory and can be used in two modes. The first is an input pre-processor to compute equivalent orthotropic properties from a laminate description. The second is an output post-processor to predict first ply failure and safety margins from laminate strength data. The program has been modified to employ the interactive Tsai-Wu tensor polynomial lamina strength failure criterion. Limited comparisons have been performed with theoretical solutions, based on classical laminate plate theory, and with test data for static and dynamic response of composite panels. Predicted failure loads have also been compared with measurements.

Fiberglass Reinforced Plastics Use in Transportation Vehicles

R. D. Pistole
GTR Reinforced Plastics Company
South Field, Michigan 48037

Abstract

The use of Fiberglass Reinforced Plastics (F.R.P.) in ground vehicles has steadily increased in recent years.

In 1975 one of F.R.P.'s largest penetrations into exterior passenger car panels was grille opening panels or front headers. This use was cost effective due to the consolidation of many metal parts by one F.R.P. molded panels.

Today, with the need for lighter weight automobiles to improve fuel economy, F.R.P. is again the answer with its additional advantages.

One piece truck hoods are becoming more popular as they too turn to fiberglass composites. Many new truck designs utilizing F.R.P. are appearing on our highways.

The manufacturing of F.R.P. car and truck components will be discussed in this presentation.

DESIGNING AUTOMOTIVE COMPONENTS WITH CONTINUOUS FIBER COMPOSITES

H. T. Kulkarni and P. Beardmore

Research Staff - Ford Motor Company, Dearborn, Michigan 48121

ABSTRACT:

The primary characteristics of continuous graphite fiber reinforced plastics as structural materials are high specific strength and modulus and exceptional fatigue strength. All these properties are a function of fiber orientation in the individual layers and the lay up sequence. The advantages of continuous fiber reinforced composites relative to the conventional chopped fiber systems currently utilized in automobiles lies in the ability to apply these composites in major load/stiffness critical components. The application of a composite materials design methodology to prototype automotive components is described. Examples of different types of components are given, specifically wheel and body structures. Both the design and the fabrication of these structures in composite materials are described and any specific problems are outlined.

Key words: Automotive component design; continuous fiber composite materials; fabrication; finite element stress analysis; front end; graphite; part integration; wheel.

I. INTRODUCTION:

Current automotive usage of fiber reinforced plastics is limited primarily to the application of chopped fiber reinforced materials which can at best be applied in semi-structural applications. The application of fiber reinforced composites to structural, safety related components requires the introduction of continuous fibers into these systems in order to withstand the structural loads imposed on the components. Continuous graphite fiber reinforced composites exhibit high specific strength and modulus in combination with excellent fatigue strength, making these materials excellent candidates for load bearing and stiffness critical applications. These materials offer the incentive of large potential weight savings over conventional materials and thus are attractive from the viewpoint of minimizing overall vehicle weight with the associated increase in fuel efficiency. The application of GrFRP materials in the aerospace industry has developed a background of baseline data and design procedures which might be utilized in the design

of automotive components in these materials.

Drawing on the recent Ford experience in the design and fabrication of a full size GrFRP 1979 Ford experimental vehicle, the present paper attempts to illustrate the differences in approach for the design of composite components relative to conventional steel components. As part of this vehicle program a composite component design methodology was established for automotive components by drawing together all the best parts of design systems available through the aerospace industry into one integrated design program specifically tailored for automotive applications. This design methodology was used for all GrFRP components and a short summary of the procedure is given in Section 2. The design methodology is described in detail elsewhere (1) and the current description of the methodology is only intended as a summation. Illustrations of the usage of the methodology are given in Sections 3 and 4. The design of a strength critical component, namely the GrFRP wheel is detailed in Section 3, whereas by way of contrast a stiffness critical design, namely the GrFRP front-end structure, is outlined in Section 4. This procedure is followed in order to provide a comparison for the basic design philosophy used based on the differing critical requirements of the component under consideration. Again, neither of these illustrations is intended to be completely detailed since the complete integrated design cycle for both of these components has been the subject of separate papers (2) and (3). The overall intent of this presentation is to provide a capsule summary of design techniques with illustrations which can be used in understanding the application of continuous fiber reinforced composites in automotive or other types of ground transportation. For extensive details on the procedures the references quoted above should be studied.

2: DESIGN METHODOLOGY FOR COMPOSITE COMPONENTS

A typical automotive component design cycle is shown in Figure 1. There are three distinct phases involved and the overall design cycle is independent of the materials used. Phases 1 and 3 are independent of material and therefore are common to both composite components and conventional isotropic material components. However, the details of the design Phase 2 are dependent on the material and it is in this aspect of the design cycle that special consideration must be given when designing with composite materials. Phases 1 and 3 are self explanatory and reference 1 should be used to obtain further details of these aspects of the design cycle.

Phase 2 of the design cycle consists of five basic elements as shown in Figure 1. These are (a) laminate design, (b) stress analysis, (c) fabrication methods, (d) cost analysis and (e) failure analysis. Of course, the impact of the last three of these factors on the design of composite components is similar to the effect on conventional components.

There are significant differences between composite materials and conventional materials in the specific details of these latter three factors but the overall methodology of consideration in the design phase is very similar. As a distinct example of the differences in these factors, consider the influence of fabrication methods. The utilization of plastic based composite materials allows the opportunity for integration of several parts into a single fabricated piece. This technique of component integration is one of the key factors in application of all plastics into automotive components and represents an area where fabrication cost savings and advantages in overall stiffness can be obtained based on the unique nature of the material relative to steel. The cost advantage, of course, accrues from the elimination of assembly costs at later stages and the increased stiffness developed by the elimination of joints. This example of the differences in fabrication techniques between composite materials and conventional materials illustrates the interplay of the five factors listed above in arriving at the best overall design for given functional requirements. The two areas of Phase 2 which require a unique approach for the application of composites are laminate design and stress analysis and these will be discussed separately below.

(a) Laminate Design

The stacking of individual composite layers to form a part involves the selection of the individual layers to yield the required laminate properties. Consequently, the basic design parameters going into the design of the laminate are the layer properties and the laminate parameters. These are as follows:

- . Layer parameters - type and orientation of fibers, type of matrix, form of the layer (cloth or tape).
- . Laminate parameters - stacking sequence of the layers.

The design of the initial laminate must be based on a selective predominant design criterion. The criterion might be one of the following:

- . Match the stiffness and/or strength of the steel component or some given percentage thereof.
- . A specified strength and/or stiffness criterion with no reference to a steel component.

Once the choice of the predominant design criterion is made, an initial laminate is developed by following the iterative technique as shown in Figure 2. Based on simple hand calculations a reasonable initial laminate design is developed by this iterative procedure prior to the full stress analysis.

(b) Stress Analysis

Except for very simple components, all laminate designs are verified in detail by the application of a finite element stress analysis procedure.

In this technique a composite finite element model is developed for the component. The stress analysis differs from such analysis for conventional materials in that it involves lamination theory, that is the ability to examine the stresses in the individual layers which make up the laminate. The normal criterion for failure is over stressing relative to the design allowables in any layer in the structure. Obviously, failure could occur in a subsurface layer which is not visible on external examination and thus the failure criterion must be applied to every layer to insure integrity of the total structure. This is in distinct contrast to isotropic materials where failure normally initiates on the surface and is, therefore, evident by visual examination.

The final laminate design is fine tuned by iteration involving changes in the stacking sequence and orientation until all layers are judged to be satisfactory under the imposed load conditions. In addition, weight minimization can be achieved by eliminating excessive overdesign. With experience, the number of iterations involved in the final stress analysis will be limited, yielding an efficient and flexible design system.

In the following two sections, examples are given of the application of the design methodology to a GrFRP wheel and a GrFRP front end structure. The basic material properties used in the design of these components are listed in Table 1. The components are currently installed on the experimental GrFRP Ford and have to date successfully operated through all vehicle evaluations.

3: STRENGTH CRITICAL COMPONENT - GrFRP WHEEL

(a) Design Requirements

There are two basic requirements which dictate the design of the composite wheel. Firstly, there are specific load carrying capabilities which are evaluated by the following critical tests;

- . Rim roll fatigue - an examination of the fatigue strength of the wheel rim.
- . Rotary fatigue - a test of the fatigue life of the wheel spider under a bending load.
- . Impact - a test of the integrity of the wheel rim under severe impact load simulating curb impact vehicle operation.

The second critical requirement for the wheel is based on the axisymmetric nature of this component. This geometric constraint involves a design such that the load input points will change as the wheel rotates. The wheel must therefore have equal strength and stiffness along any radial direction from the center of the wheel.

(b) Laminate Design

Consideration of the three loading conditions noted above indicated that the dominant critical load requirements were those required to pass the impact tests. The basic design philosophy adopted was to design the composite wheel to pass the impact tests, evaluate such design analytically and ensure that the design would also pass both the fatigue tests. Based on the impact loads, the number of composite layers required for satisfactory wheel performance were computed. Details of the impact loads are given in reference 2. Laminates were designed with alternate layers of GrFRP cloth at orientations of $0^{\circ}/90^{\circ}$ and $\pm 45^{\circ}$ to give approximately equal strength and stiffness along the radial directions.

(c) Stress Analysis

The finite element model generated for the GrFRP wheel is shown in Figure 3. The laminate properties for various elements in the model were defined and the model was analyzed for the various critical load cases discussed previously. The layer stresses computed for both the spider bending and the rim roll fatigue loads were far below the design allowables for the individual GrFRP cloth layers. However, the laminate design as shown in Figure 4 was rejected since the induced layer stresses under the impact loads were much higher than the design allowables. The localized high stress areas in this design are shown in Figure 4. Modification of the laminate and subsequent stress analysis reduced the high stress areas adjacent to the bolt holes to within safe limits. The final laminate design and stress distribution is shown in Figure 5.

(d) Fabrication and Testing

The wheels were fabricated by conventional aerospace techniques resulting in a final component as shown in Figure 6. Note the stainless steel trim ring on the GrFRP wheel which was both a styling feature and a functional feature. This ring helped to distribute the loads both in the impact test and also in tire changing procedures. This GrFRP wheel design (Figure 5 and Figure 6) was subjected to all the critical tests mentioned above. As predicted by the stress analysis, the wheel successfully passed all of the tests. It should be noted that a prototype wheel of the initial laminate design as shown in Figure 4 was also built and tested and the wheel failed in the impact test. Since the stress analysis for this particular design had indicated that failure would occur in the impact test, the excellent correlation between the stress analysis for both the initial and the final design and the testing results gave great confidence in the composite design methodology procedure which had been utilized for all the other components.

The GrFRP wheels represent a 42.7 pound weight saving for the vehicle (8.55 pounds per wheel) for approximately 45% weight savings. It should be noted that the wheels represent one of the most difficult design fabrication tasks in the vehicle. Thus, the weight saving of approximately 45% relative to steel is not as high as can be achieved in many of the components with less stringent requirements. Typically in those types of components weight savings up to 65% can be successfully obtained. The severe loading conditions and critical safety requirements for the wheel impose greater restrictions on the design flexibility for composites than in most other vehicle components and thus do not represent the kind of weight savings that might be expected from these materials. On the other hand, the successful design and fabrication of wheels represents a major achievement in the ability of the materials to withstand very complex and severe loading environments.

4: STIFFNESS CRITICAL COMPONENT - GrFRP FRONT END STRUCTURE

(a) Design Requirements.

The dominant design factor for the front end structure was selected as stiffness based on the paramount need to meet critical NVH ride quality requirements. Thus, the overall design philosophy was based on deflection requirements with the modification that the deflection could be adjusted to allow for the lower input loads since the overall weight of the vehicle was reduced by about one-third.⁽³⁾ Based on this philosophy, the individual components of the front end structure were divided into two different groups, namely bending critical components and torsion critical components. In addition, local areas such as the bolt attachment points were separately analyzed for strength critical requirements to insure the integrity of the joints.

(b) Laminate Design.

The mechanical properties of the individual layers used in the design of the front end structure are given in Table 1. For a component which is considered to be primarily bending stiffness critical, the GrFRP laminate design was matched to the bending stiffness of the steel part. Likewise, for torsional stiffness critical components, the torsional stiffness of the GrFRP components was matched to the torsional stiffness of the corresponding steel part. As a consequence of choosing a critical stiffness parameter, the GrFRP components only matched the steel in either torsional or bending stiffness and differed in the second stiffness area. This follows the basic design philosophy of composites in that the maximum weight reduction is obtained by using the directionality of these materials to match the critical requirements, and having lesser properties in other less critical directions.

The stiffness of the individual components of the front end structure was matched by using the following equations:

Bending Stiffness.

$$\frac{E_s t_s^3}{12} = \sum_{i=1}^n E_{ig} \left(\frac{t_{ig}^3}{12} + t_{ig} \cdot Y_i^2 \right) \text{-----(1)}$$

Torsional Stiffness.

$$G_s K_s = G_g K_g \times \frac{(W_s)}{W_g} \text{-----(2)}$$

Where E = Young's Modulus, G = Shear Modulus
t = thickness, i = ith layer
n = total number of layers
Y = distance from neutral axis
W = Weight of the car
K = torsional constant

Subscript. g = GrFRP, s = steel

Based on these calculations, the thickness of each individual composite part was computed and the parts are compared with the steel parts in Table 2. One difference between the GrFRP front end structure and the steel front end structure lies in the fender inner apron. In the steel assembly, the fender inner apron is non-structural and is made of polypropylene. In the GrFRP structure, the inner apron was made structurally effective by fabricating this fender in GrFRP.

It is clear from comparison of the data in Table 2 that only one of the two critical stiffnesses are matched in the composite material relative to the steel component. It should also be pointed out that whichever of the design criteria are used, i.e. bending or torsional stiffness, the GrFRP component only had to be 67% of the steel stiffness to match the same deflection criteria. As mentioned previously all the bolted joints between the radiator and fender and between the fender and the body were examined for failure modes such as shear out, net tension and bearing strength. A major integration of components was achieved in the GrFRP front end. In each fender assembly parts in steel were integrated into parts in GrFRP. Likewise, in the radiator support assembly, parts in steel became parts in GrFRP. Such part integration supports the point made earlier about fabrication advantages of GrFRP.

(c) Stress Analysis

Finite element models for both the steel front end and the composite front end were generated as shown in Figures 7 and 8. To test the adequacy of the structure, loads were applied to the assemblies at two frame mount locations on the radiator support lower extension. Models were analyzed for both bending and torsional load cases. The static analyses were carried out using finite element codes which have the capability of both isotropic and anisotropic material analysis. The results of the analysis are summarized in Table 3. Note that based on the weight of the steel vehicle, namely 3750 pounds, the GrFRP front end structure is only 80% as stiff in both bending and torsion as the steel structure. However, based on the 2500 pound weight of the composite vehicle, the relative stiffness of the GrFRP front end structure is 20% greater than that of the steel structure in both bending and torsion. Thus, the analysis would predict that the composite front end structure in the composite vehicle would act as a structure of increased stiffness relative to vehicle performance when compared to the steel vehicle, i.e., the analysis predicted that no problem should result in the NVH characteristics of the front end from a stiffness viewpoint.

(d) Fabrication and Testing

The individual components of the composite frontend assembly were fabricated by conventional aerospace hand layup techniques as discussed before. The individual components were assembled into the complete front end structure and installed on the experimental GrFRP vehicle, Figure 9. The complete vehicle is currently undergoing vehicle evaluation tests and has successfully demonstrated that the design of the front end based on stiffness critical criteria has not reduced the NVH characteristics of the structure. The overall GrFRP front end assembly weighed 30 pounds versus 95 pounds in steel. This represents a weight savings of 68.4% and demonstrates the potential of these materials in reducing the weight of conventional structures.

5: CONCLUSIONS

Current aerospace design techniques can be adapted for the application of continuous fiber composite materials to conventional automotive structures. Such a procedure has been used to design various parts of an experimental GrFRP vehicle and the influence of different design constraints on the successful functionality of the components has been demonstrated. This demonstrates that highly anisotropic materials can be successfully utilized for the design of complex geometric components with highly complicated stress environments. Also, the potential of these materials for successful weight saving applications in these types of structures is illustrated. Provided no other constraining factors, particularly, cost and high yield manufacturing techniques, can be

successfully resolved, the potential for widespread usage of continuous fiber reinforcement composites in the transportation industry has been shown to be technically feasible.

REFERENCES

1. H. T. Kulkarni and P. Beardmore, "Design Methodology for Automotive Components Using Continuous Fiber Reinforced Composite Materials". FORD TECH. REPORT NO. SR-79-04, To Be Published.
2. M. B. Motwani and H. T. Kulkarni, "Experimental Graphite Reinforced Plastic Wheel for '79 GrFRP Ford Concept Vehicle". SAMPE Meeting, May 8, 1979.
3. H. T. Kulkarni, G. Lim, R. C. Knight, P. Beardmore "Design and Fabrication of Automotive Components in Graphite Fiber Reinforced Composites, Part II Front-End", SAE Paper No. 790031, Feb. 26, 1979.

TABLE 1
GrFRP LAYER MECHANICAL PROPERTIES

<u>Stiffness</u> <u>Property</u>	<u>GrFRP Tape</u>	<u>GrFRP Cloth</u>
$E_{11} \times 10^6$ psi	21.0	10.3
$E_{22} \times 10^6$ psi	1.2	10.3
$G_{12} \times 10^6$ psi	0.65	1.0
Poisson's Ratio ν	0.25	0.09
Thickness 't' inches	0.005	0.011
 <u>Strength</u>		
T_{11} Ksi	190.0	76.0
T_{22} Ksi	5.0	74.0
C_{11} Ksi	160.0	64.8
C_{22} Ksi	20.00	61.0

T = Tension, C = Compression, E = Young's Modulus, G = Shear Modulus.
1,2 = Along and perpendicular to the fiber axis.

TABLE 2
COMPARISON OF THICKNESS, BENDING AND TORSIONAL STIFFNESS
OF THE GrFRP PARTS WITH STEEL PARTS

COMPONENT	ASSEMBLY	t_{gr}/t_{st}	STIFFNESS RATIO $\frac{(Gr)}{(St)}$	
			BENDING	TORSION
Fender Outer Panel	Fender	1.42	0.9	0.58
Front Reinforcement		1.26	0.628	0.51
Top Front Reinforcement		1.63	1.177	0.66
Side Front Reinforcement		2.31	3.39	0.94
Rear Side Reinforcement		1.79	1.49	0.80
Wheel Opening Reinforcement		1.57	1.067	0.72
Upper Support	Radiator support	1.05	0.44	0.15
Upper Reinforcement		2.57	5.5	0.72
Lower Supports		1.43	0.945	0.41
Gussetts		1.43	0.945	0.41
Lower Extensions		1.48	1.04	0.34
Side Supports		3.09	6.40	1.17

Gr = GrFRP
St = Steel

TABLE 3
RELATIVE STIFFNESS OF THE FRONT END ASSEMBLIES IN PERCENTAGE BASED
ON THE FINITE ELEMENT ANALYSIS

Total weight of the car in lbs.	Front End fabricated with	Stiffness in Percentage	
		Bending	Torsion
3750	steel	100	100
3750	GrFRP	80	81
2500*	GrFRP	121	121

* Input loads to the GrFRP front end assembly will be $\frac{2}{3}$
(i.e. $\frac{2500}{3750}$) of the input loads to the steel front end assembly.

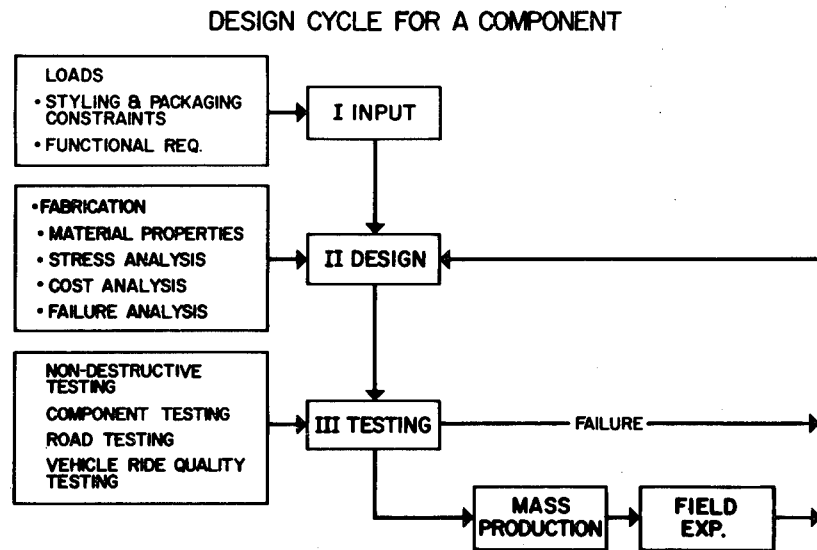


Fig. 1. Design cycle for a component showing the progressive development of the design.

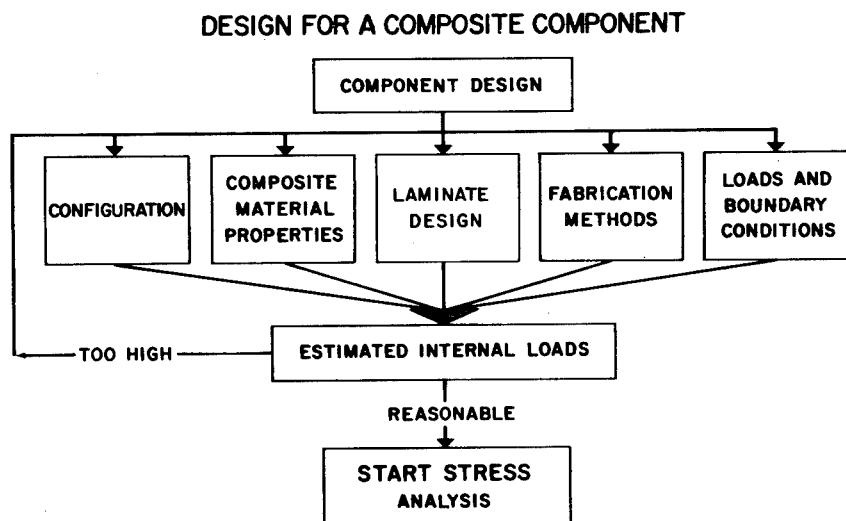


Fig. 2. Flow chart of the development of efficient laminate design.

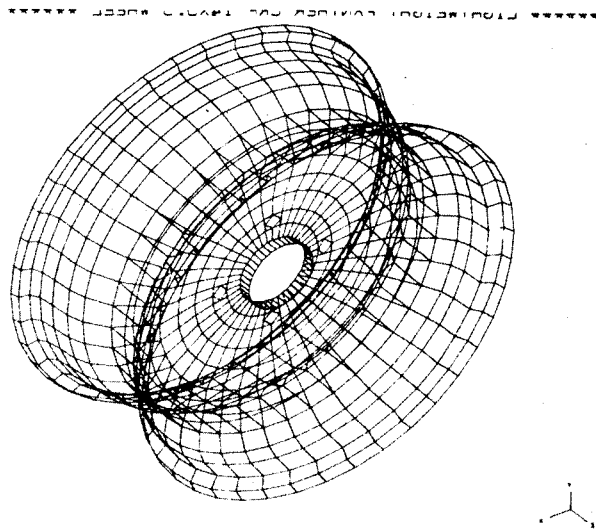


Fig. 3. Finite element model of the wheel.

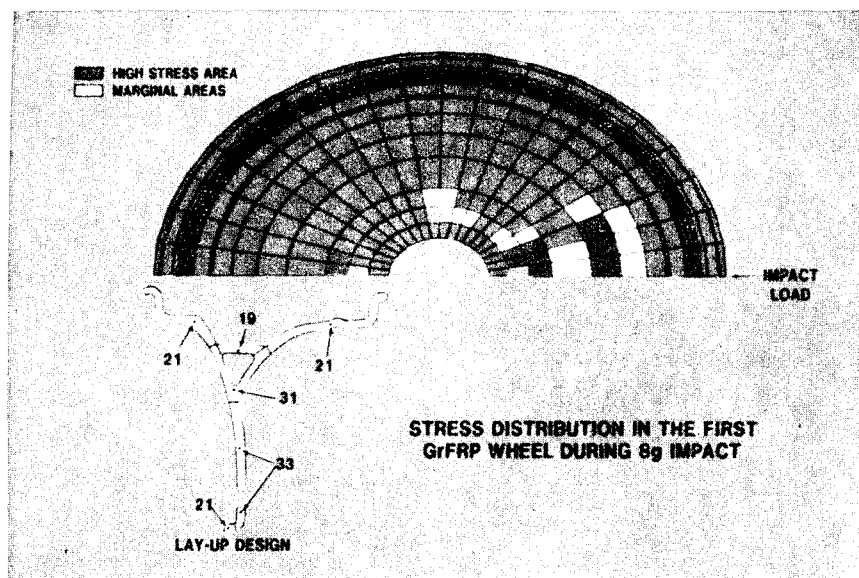


Fig. 4. Initial lay-up and stress-distribution in the first GrFRP wheel design due to 8g impact load.

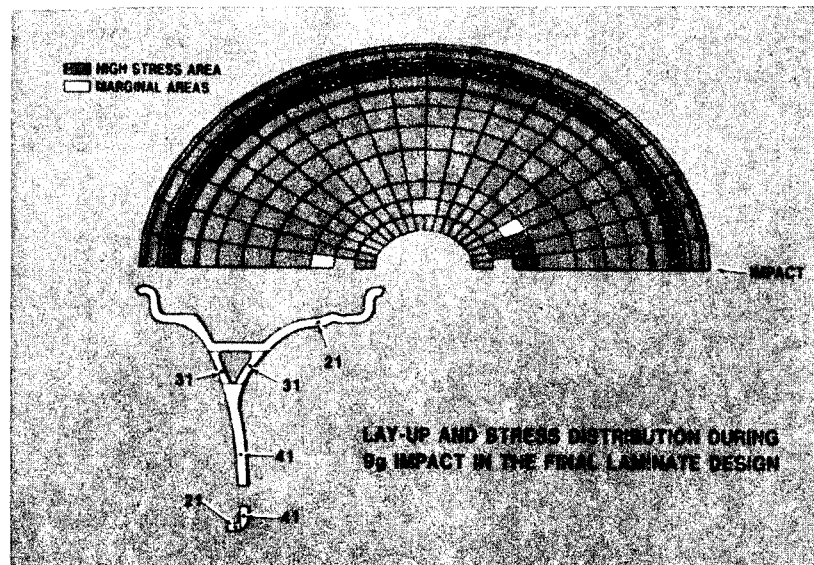


Fig. 5. Final lay-up and stress-distribution in the GrFRP wheel design due to 9g impact load.

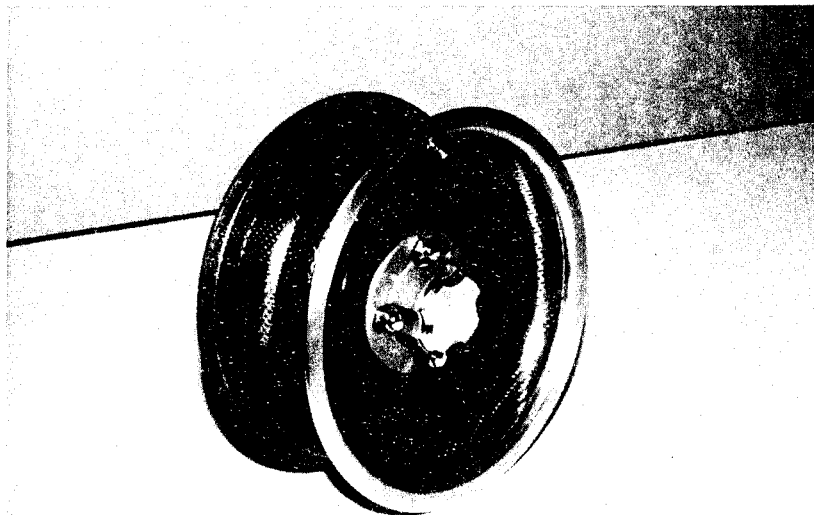


Fig. 6. GrFRP wheel and trim rim ring.

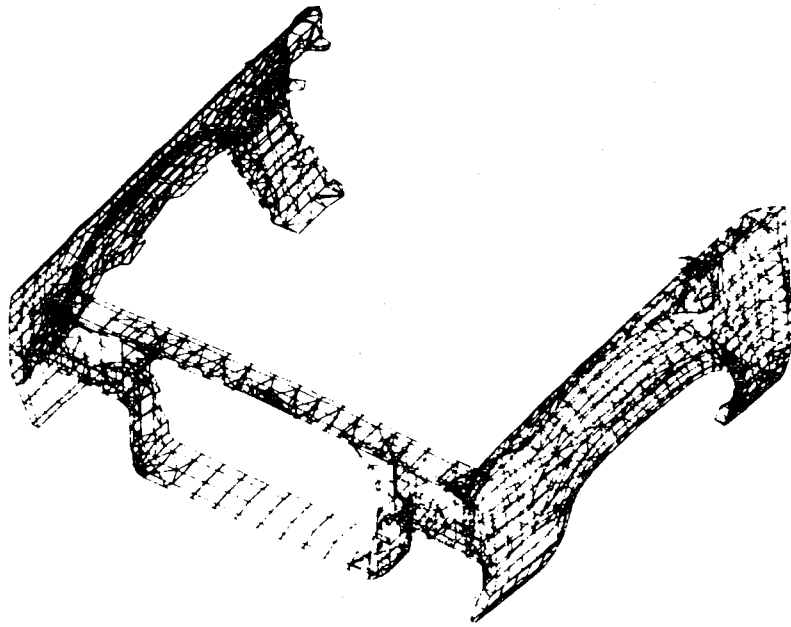


Fig. 7. Finite element model for the steel Front End assembly.

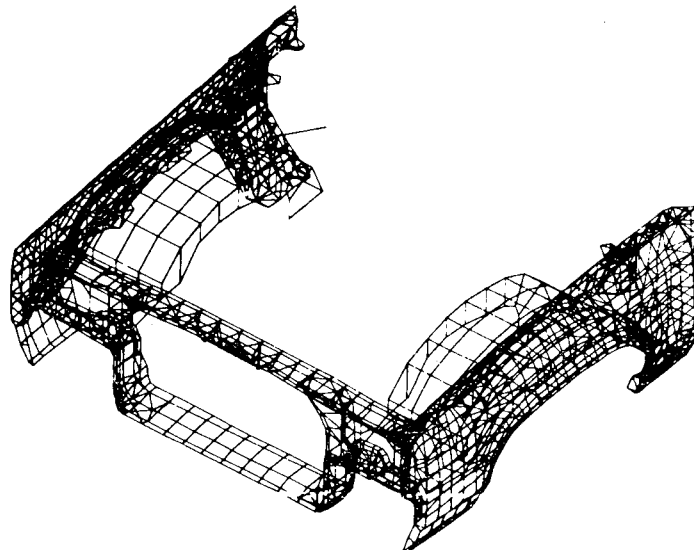


Fig. 8. Finite element model for the composite Front End assembly.



Fig. 9. GrFRP Ford experimental vehicle.

SESSION 6

INDUSTRIAL APPLICATIONS AND DESIGN

Chairman: J. E. Stern

(substituting for Anton Hehn)

Goddard Space Flight Center

FABRICATION OF LARGE COMPOSITE SPARS AND BLADES

By

O. Weingart
Structural Composites Industries, Inc.
6344 North Irwindale Avenue
Azusa, California 91702

Abstract: A national wind energy program has been established to develop the technology necessary to enable wind energy systems to be cost-competitive with conventional power generation systems and capable of rapid commercial expansion for producing significant quantities of electrical power. Wind Turbine Generators being developed under this program will require rotor diameters of up to 300 ft.

Because of the considerable extension in the technology required to design and construct blades of this size, it was highly desirable to establish an early technology base. To that end, the Department of Energy, through NASA-Lewis Research Center has awarded several contracts for the design, fabrication and test of large low-cost wind turbine blades built of composite materials.

This paper describes SCI's fabrication of a 20,000 lb. one piece, composite spar for a 150 ft. long developmental blade. Also discussed are a recent SCI design study of a composite blade for the 300 ft. diameter Mod-2 Wind Turbine, and a new SCI contract from DOE/NASA for design and possible fabrication of low cost composite blades for the 125 ft. diameter Mod-OA Wind Turbine.

Key Words: Wind turbine; composite materials; filament winding; large composite structures; rotor blades.

The Department of Energy, through NASA-Lewis Research Center, awarded a contract to a team composed of Kaman Aerospace Corporation and SCI to design, fabricate, test and evaluate a potentially low cost blade for a 300-foot diameter rotor.

Kaman has considerable experience in the design and construction of composite rotor blades for helicopters. SCI has 20 years of background in the design and fabrication of large, low cost composite structures, especially those produced by automated filament winding. Kaman and SCI pooled their talents to propose a low cost blade of unique composite construction. The primary structural element of

the blade is the one piece 20,000 pound spar. For fabrication of this structure, SCI developed a new, patent pending, filament winding process called the TFT* process. This process allows rapid spar production, with low cost materials, and minimum labor. This low cost spar - comprising 85% of the composite blade weight - is the key to the low cost of the composite blades.

Blade and Spar Description: The 150 ft. composite wind turbine blade consists of a filament-wound E-glass/epoxy leading edge D-spar, afterbody panels of paper honeycomb with E-glass cloth skins and a pultruded trailing edge spline. The afterbody panels are joined to the spar and spline by bonding. The blade is attached to the hub by a steel adapter which is bolted to the composite spar. A steel truss carries trailing edge spline loads to the adapter. The general arrangement is shown in Figures 1 and 2.

The SCI spar is 135 ft. long (141 ft. as-wound prior to trimming) with a 'D' shaped cross-section, (Figure 3) which tapers from approximately 7 ft. chord by 4 ft. height at the root to 2 ft. chord by 7 inches high at the tip. Minimum wall thickness tapers from three inches at the reinforced root joint area to 1 inch at the tip. There is a 15° linear twist from root to tip. This spar is one of the longest one-piece filament wound structures ever attempted.

The spar material is an E-glass/epoxy composite in which ninety percent of the structural fibers are oriented nearly parallel with the longitudinal axis of the blade. Local reinforcement is provided at the root by interleaving $\pm 45^\circ$ and 90° plies between the plies of essentially 0° unidirectional material to achieve an isotropic structure for attachment of the root end adapter.

Manufacturing Considerations: Fabrication of such large monolithic composite spars presents some interesting challenges:

Size: The most obvious challenge is the gross size of the structure. Fortunately the filament winding process is not limited to any particular size. It is merely necessary to provide a sufficiently large mandrel, winding machine and oven for the part in question. SCI had previous experience with rocket motor cases and transportation containers up to 22-1/2 ft. diameter by 60 ft. long, so the spar represented an increase in length, but not in diameter, over our in-house state-of-the-art.

Mandrel Deflection: The very long length and slenderness of the spar was itself a problem, as mandrel deflection could be quite large, and the rotation during winding could rapidly accumulate a large number of reverse bending stress cycles. Furthermore the airfoil shaped cross section of the mandrel caused a change in effective stiffness

* TFT stands for transverse filament tape

of roughly 5 to 1 as the chord line rotated from horizontal to vertical. (This was christened the "flip flop" effect.) The solution used in this project was careful mandrel design, combined with an adjustable center support or 'steady rest' to reduce the unsupported span. Linear finite element analysis, by the 'SAP' Program, was used to predict the mandrel deflections and stresses, for various stiffness distributions and support conditions, during the mandrel design iterations (Figure 4).

Mandrel Extraction: Another problem area associated with the long slender shape of the spar was that of mandrel extraction. Although we felt that the natural taper of the spar would allow easy extraction in production, in spite of the length and the twist of the mandrel, we proposed a low-risk extraction method for the prototype, which is described below under 'spar fabrication'. As a further precaution, a multiple layer release system was used, consisting of alternate coats of PVA film and fluorocarbon dispersion release agents. A beneficial effect of the highly axially oriented composite is its ability to accept high extraction forces.

Winding Pattern: The winding pattern had to produce a low-cost composite, with high axial strength and stiffness, in a structure where both wall thickness and circumference taper from root to tip. The usual approach to this problem would be to use low angle helical winding. However, this type of pattern requires that all filaments passing any plane near the large circumference root must also pass any plane near the small circumference tip. Thus the wall thickness naturally tends to increase from root to tip, just the opposite to the desired direction of taper, when helical winding is used. Also some angle of winding must be used in helical winding, so truly axial filament orientation is not achieved.

A tapered wall can be approximated by helical winding of layers of gradually diminishing length. This technique requires movable dummy head or disc for pattern turnaround part way down the mandrel. The dummy is moved for each new layer length. The end of each layer must be tied down and trimmed prior to proceeding with the next layer. This slows the winding process and increases labor hours and material waste.

The patent-pending process developed by SCI for the 150 ft. spar allows high speed continuous winding of 0° filaments to produce tapered wall on a tapered mandrel, without any trimming or dummy heads. 90° or $\pm 45^\circ$ filaments can also be applied as required. This process minimizes the labor and material waste during spar winding.

Tooling and Equipment: The prototype spar was wound on a 150 ft. long, 30,000 lb. low-cost steel mandrel, which is a stressed-skin/stringer design similar to aircraft wing structures. An adjustable steady rest was used to support the mandrel near its center. The

mandrel has accumulated approximately 10,000 cycles of rotation to date with no sign of fatigue failure.

The spar filament winding machine has a 150 ft. carriage stroke and is capable of rotating the 50,000 lb. fully wound mandrel up to 10 RPM. It is one of the largest known filament winding machines.

An 80 ft. long hot air oven was built for curing the spar in two stages. The oven is 10 ft. high by 10 ft. wide and is capable of 250°F temperatures. The spar mandrel, winding machine, and oven, shown in Figure 5, and associated equipment were designed and built by SCI during the latter half of 1977.

Spar Fabrication: The spar was wound during February 1978 at the SCI plant in Mira Loma, California (Figure 6).

A half-inch thick shell was first wound on the mandrel, and cured. The aft web was cut longitudinally and wedged open to free the mandrel. The cut shell was repaired with a spanwise hand-layup doubler of glass cloth. The spar wall was then wound to full thickness and again cured. Because of the mandrel steady rest, each of the two basic winding steps described above had to be done in two stages, with a long scarfed area joining them together so that the total winding process consisted of four steps as shown in Figure 7.

Mandrel Extraction Procedure: The mandrel tailstock was removed and the spar was supported on heavy machinery dollies. Large screw jacks, built into the root end of the mandrel and bearing on a metal plate at the heavy root end spar buildup, were used to push the spar off the mandrel until it was sliding freely. A truck mounted winch was then used to pull the spar completely free of the mandrel and out of the building. The mandrel was blocked to prevent it from sagging as the spar pulled clear (Figure 8). During the final stages of extraction, a large forklift and a mobile crane were used to support the spar.

Spar Handling and Shipping: The spar was lifted by the mobile crane using a spreader bar and sling centered over the C. G. It was loaded on a 60 ft. flatbed truck for a short trip to a nearby rail siding (Figure 9), where it was loaded onto an 89 ft. flat car (Figure 10). Two 60 ft. flat cars were used as idlers to protect the overhang at each end of the 89 ft. flat car, but the spar was supported by the center 89 ft. car only.

During its cross-country train trip from Southern California to Connecticut, the spar was accompanied by the Kaman Program Manager, who rode in the caboose. Figure 11 shows the 150 ft. blade nearing completion at Kaman. The finished 150 ft. blade withstood static flatwise bending loads equivalent to a 165 MPH wind.

Future Production: Future production spars will be wound in one continuous process, using a smooth "hard tooling" production mandrel, which should eliminate the preliminary mandrel freeing step. The final production process will not require the mandrel steady rest, thus allowing full-length winding passes without interruption.

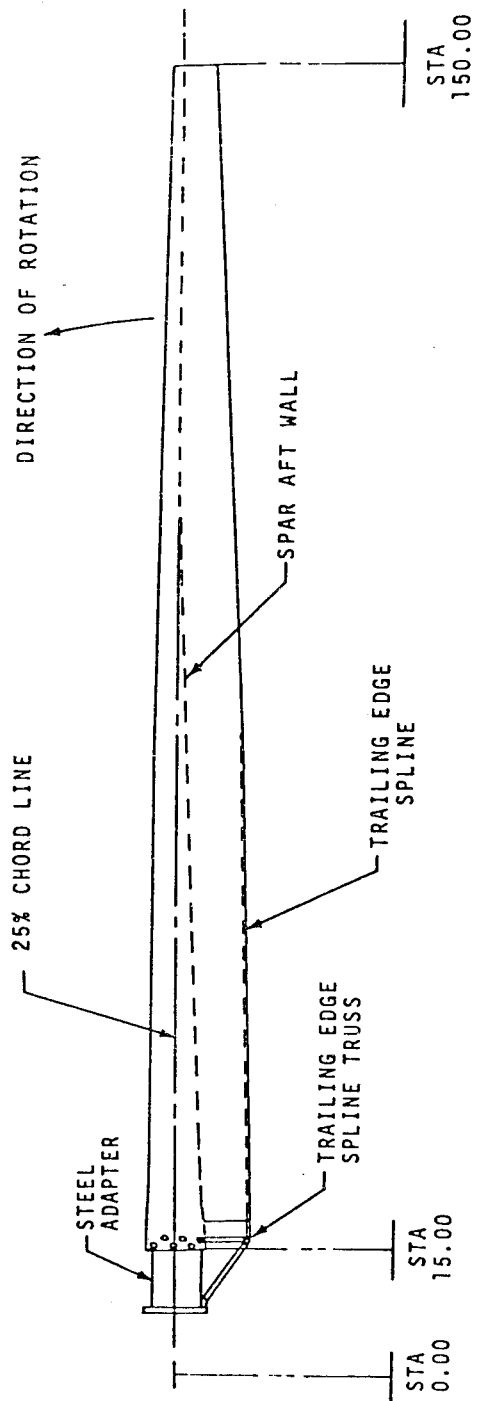
In order to achieve the lowest possible production cost, SCI feels that the entire rotor blade, including the afterbody, must eventually be built by filament winding. This approach was used by SCI in a preliminary design study we recently conducted for Boeing Engineering and Construction Division, the prime contractor for the Mod-2 Program.

The SCI design approach differs from the previous 150 ft. blade design described here in that all major composite structural elements are filament wound. In addition, the final Boeing design for the Mod-2 Wind Turbine requires a substantially different rotor configuration than was anticipated at the start of the 150 ft. Blade Program 2-1/2 years ago. The basic TFT winding process developed by SCI is employed in the new composite rotor design, but the orientation of reinforcement in the composite is different, based on data gained from the structural tests of the 150 ft. blade. Figures 12 and 13 show construction and a typical cross section of the Mod-2 composite rotor.

In April 1979 SCI was awarded a NASA contract to design and fabricate low cost composite rotor blades for the 125-foot-diameter wind turbine.

The program's emphasis will be on developing the engineering and manufacturing technology necessary to build such large windmill rotors at low cost. NASA will install the low-cost composite blades on a 200 kW Mod-OA Wind Turbine for operational tests.

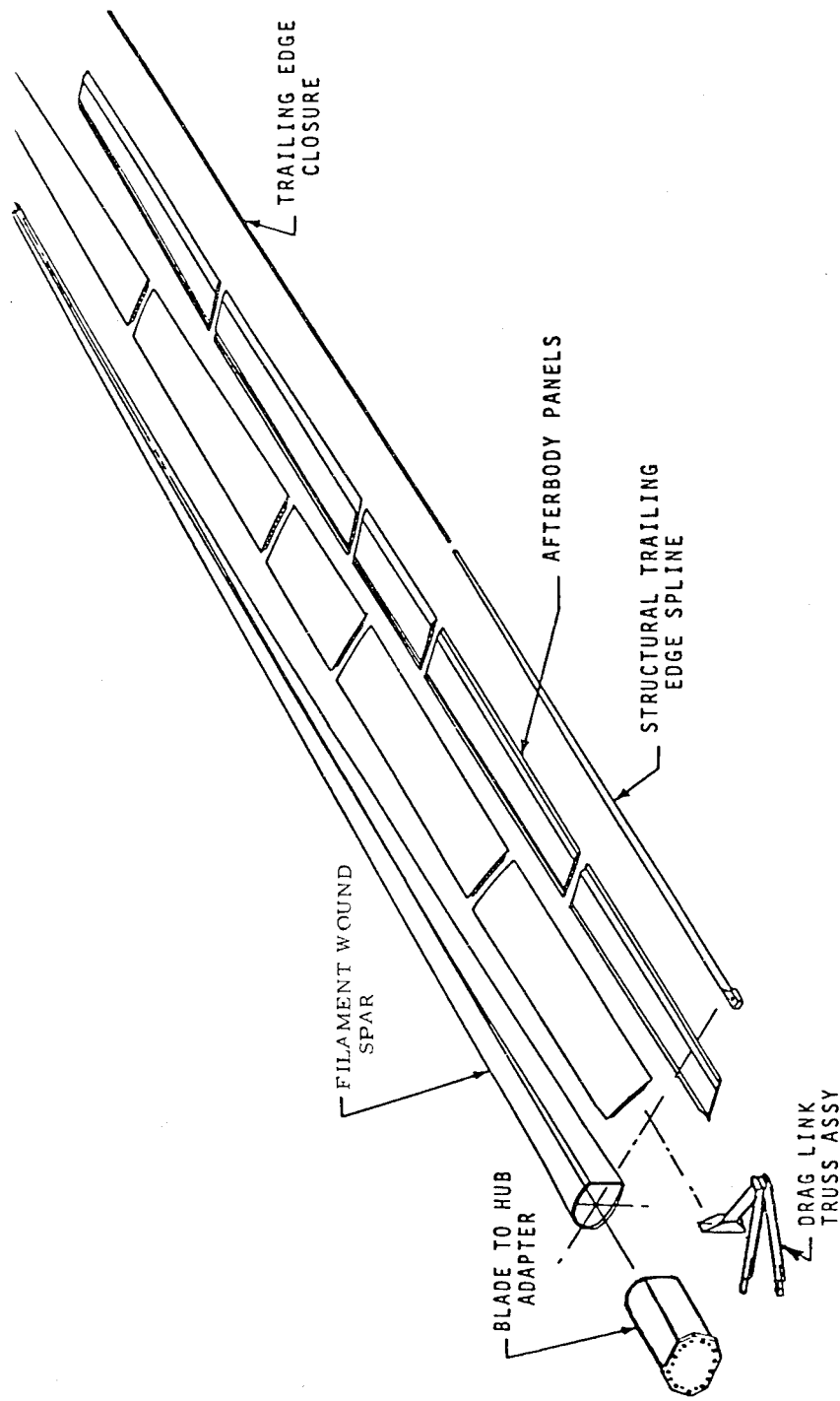
SCI received the low cost blade contract from NASA's Lewis Research Center in Cleveland, Ohio, which is the developing agency for DOE on large-scale windmills. This prime contract is expected to lead to a major extension of rotor design and manufacturing technology. The first phase consists of blade design and evaluation and the optional second phase involves fabrication of two blades. The SCI low cost composite rotor blades will have an all-filament-wound structure and will weigh approximately 2500 pounds each. They will be built by the SCI TFT process, which is also being used, under license from SCI, to fabricate rotor blades for the DOE/NASA Mod-1 200 Foot diameter Wind Turbine Generator and for the DOE/Rockwell International 40kW Small Wind Energy Conversion System.



150 FT WIND TURBINE BLADE

Figure 1

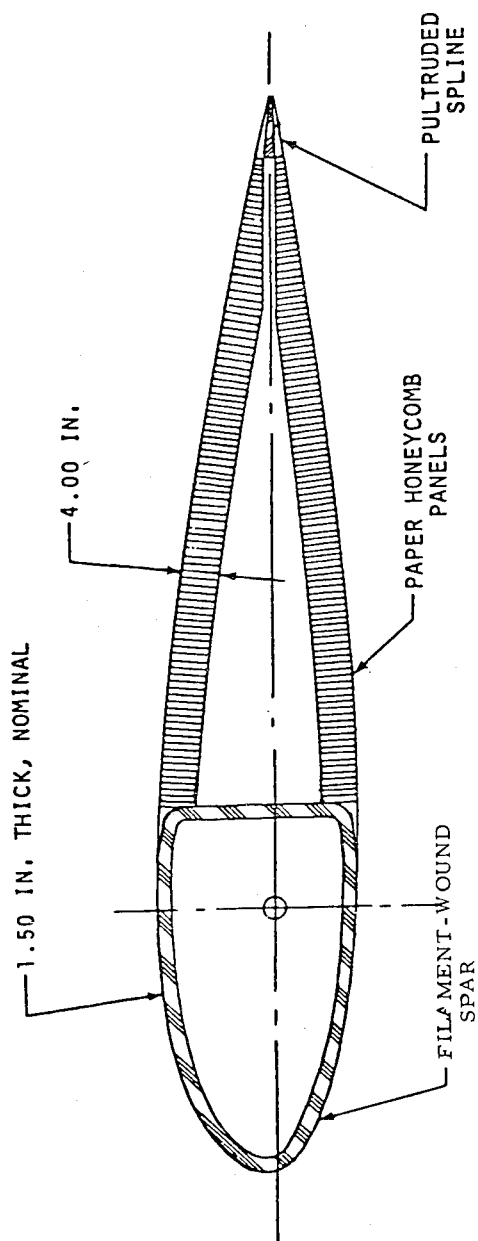




ASSEMBLY DETAILS
150 FT WIND TURBINE BLADE

Figure 2



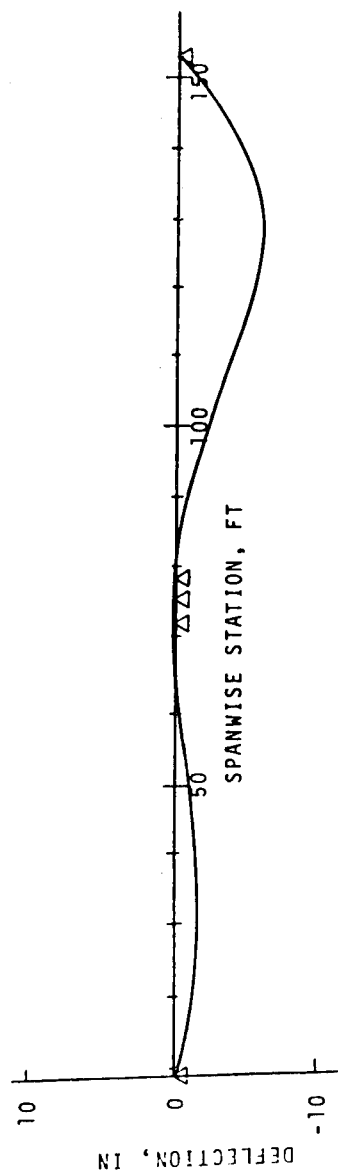


BLADE SECTION AT MID-SPAN

23018 AIRFOIL

Figure 3





MAX DEFLECTION = 5.8 IN
ALLOWABLE = 6 IN

Figure 4

MANDREL DEFLECTION
(CHORD HORIZONTAL)
(FULLY WOUND)



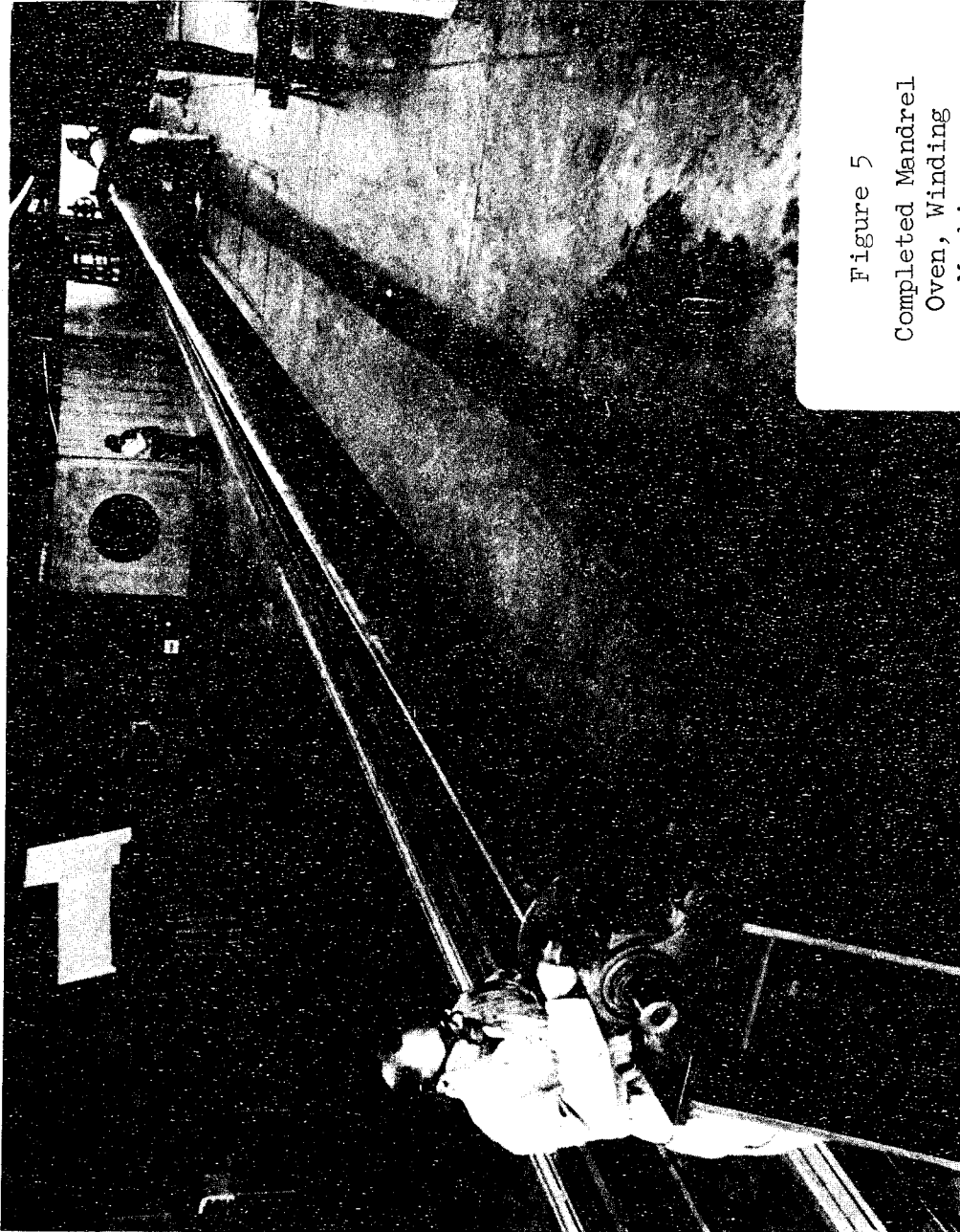


Figure 5
Completed Mandrel
Oven, Winding
Machine

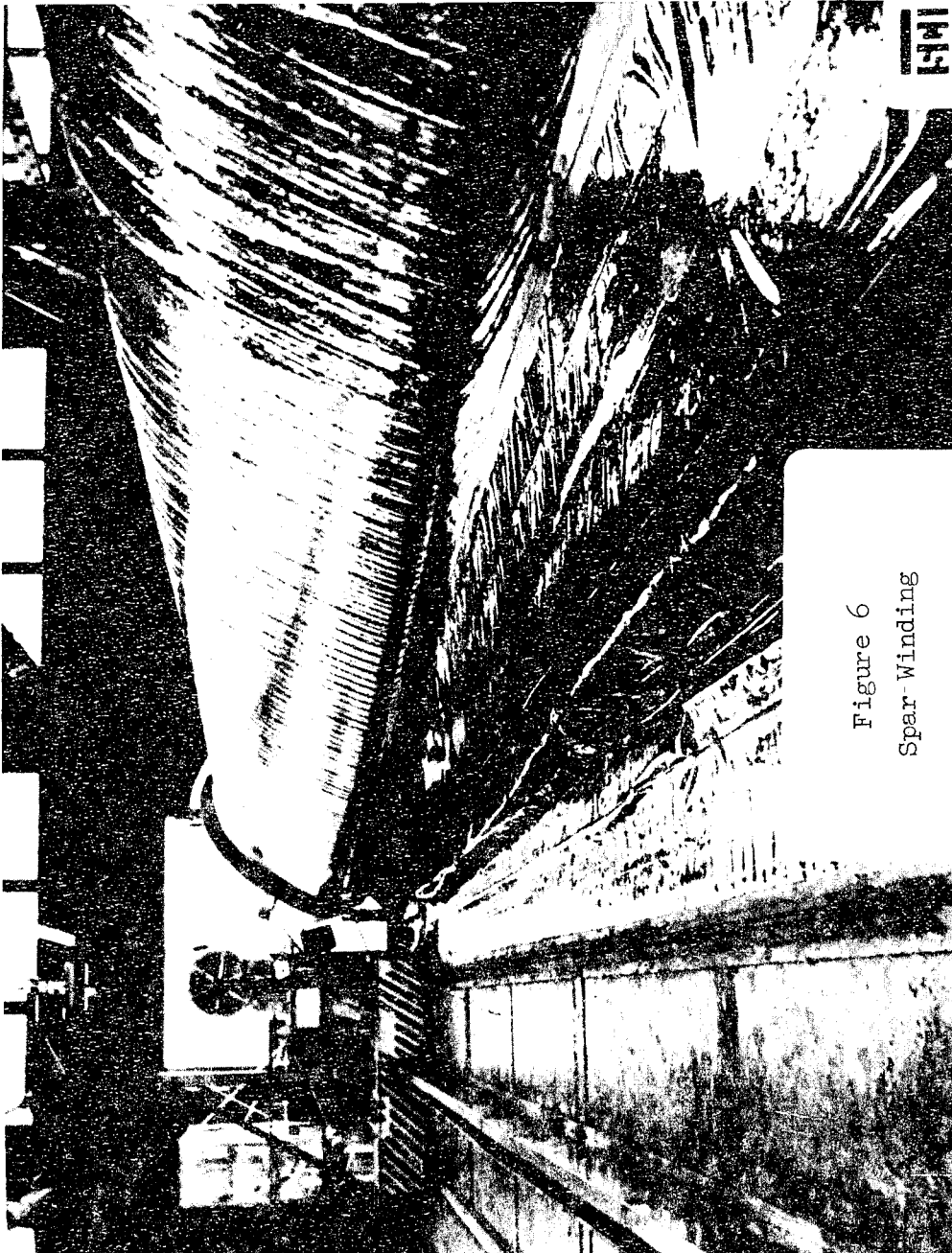


Figure 6
Spar-Winding

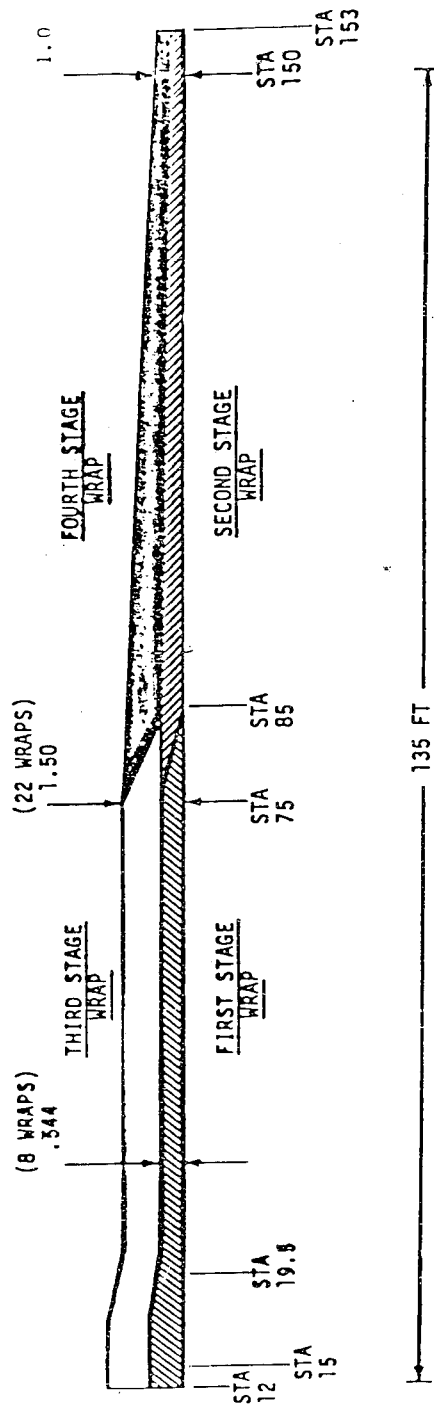


Figure 7

SCI 150' WTG SPAR
FOUR STAGE WINDING SCHEDULE



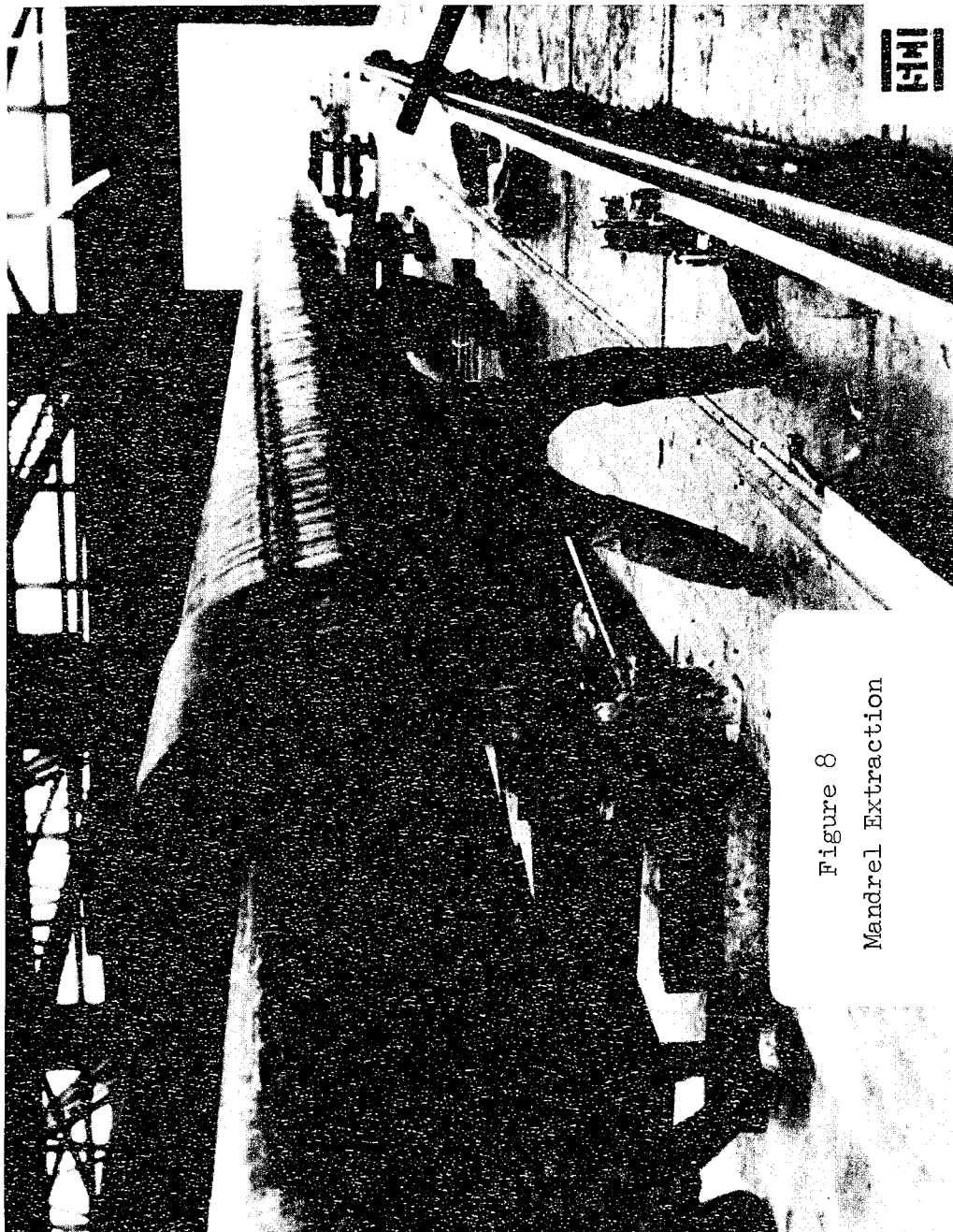


Figure 8
Mandrel Extraction

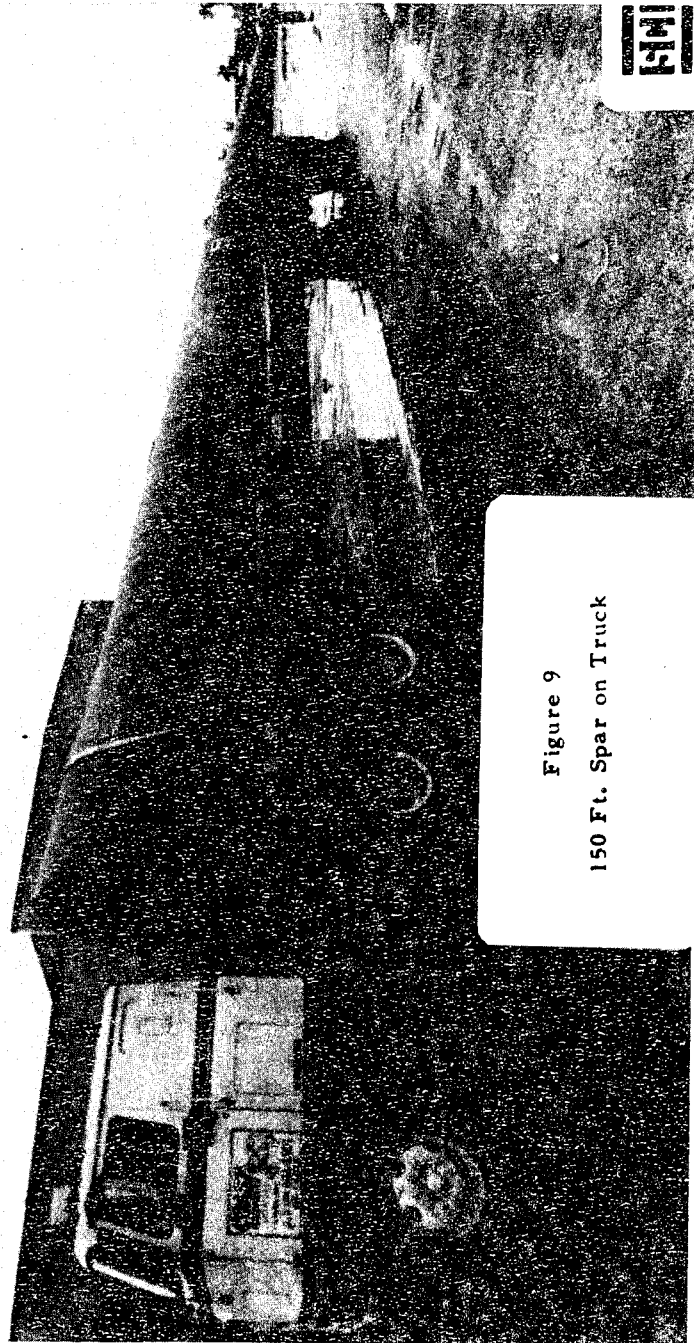


Figure 9
150 Ft. Spar on Truck

150

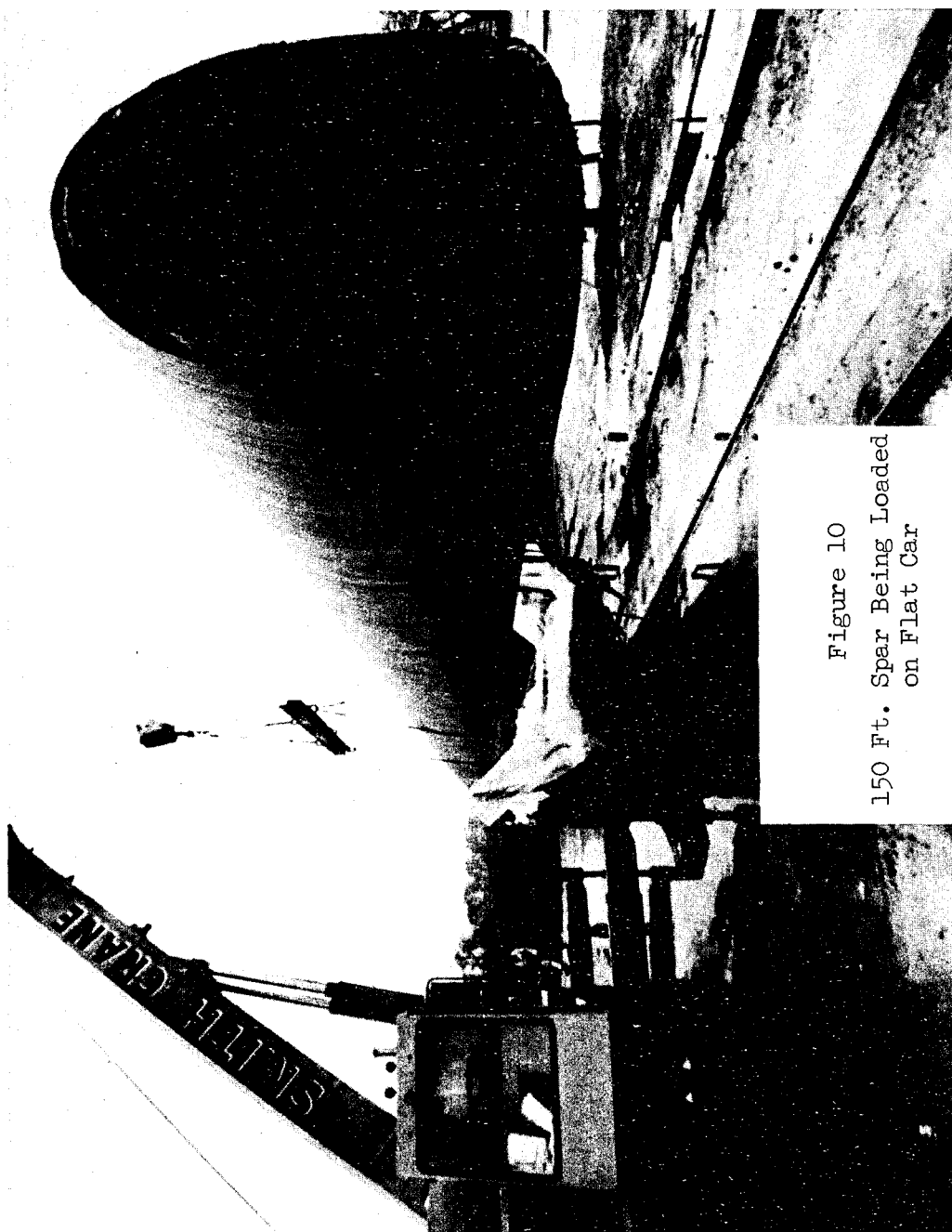


Figure 10
150 Ft. Spar Being Loaded
on Flat Car

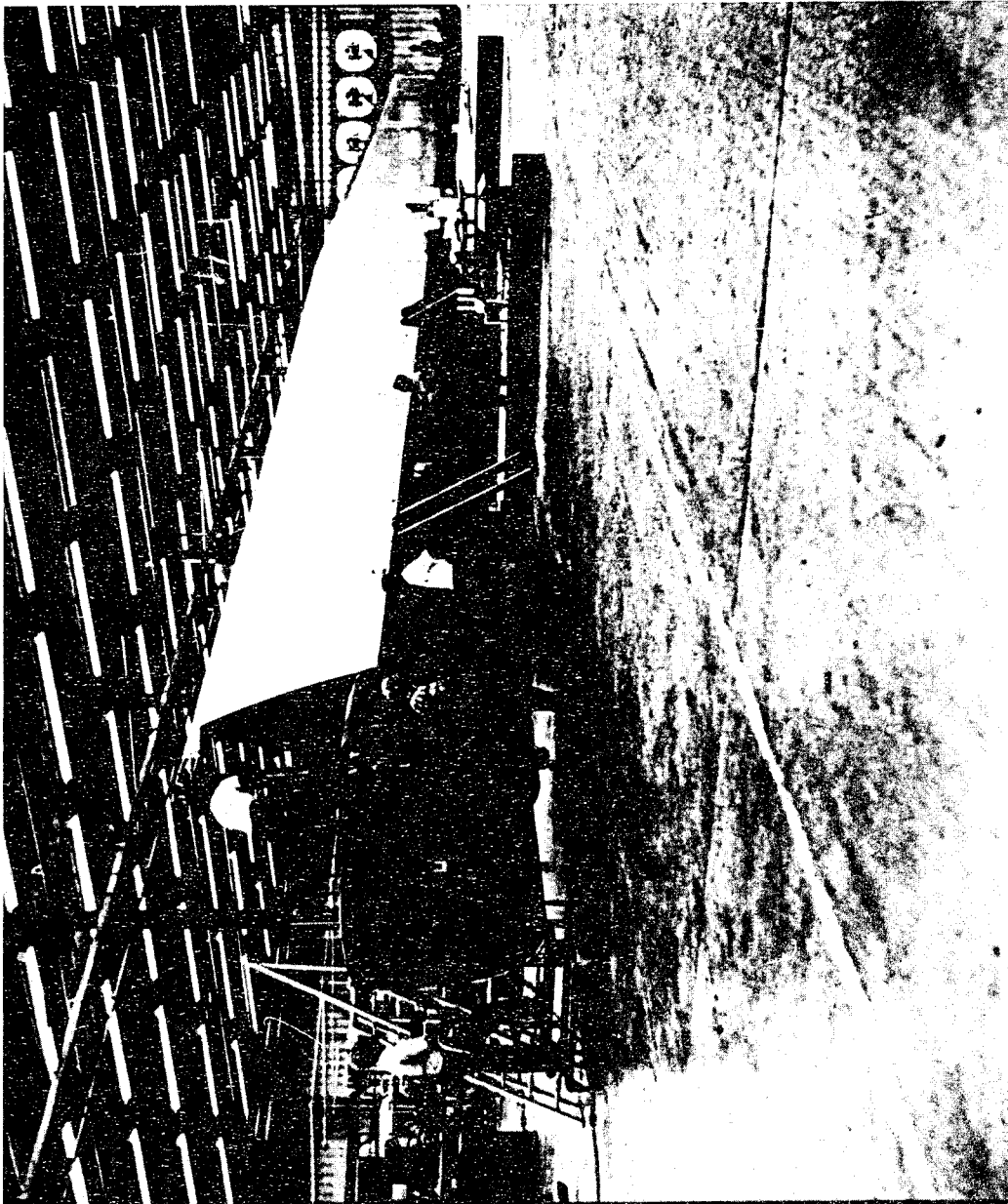


Figure 11
150-Foot Wind Turbine Blade

171

Figure 12
**COMPOSITE ROTOR
ROTOR ASSEMBLY**

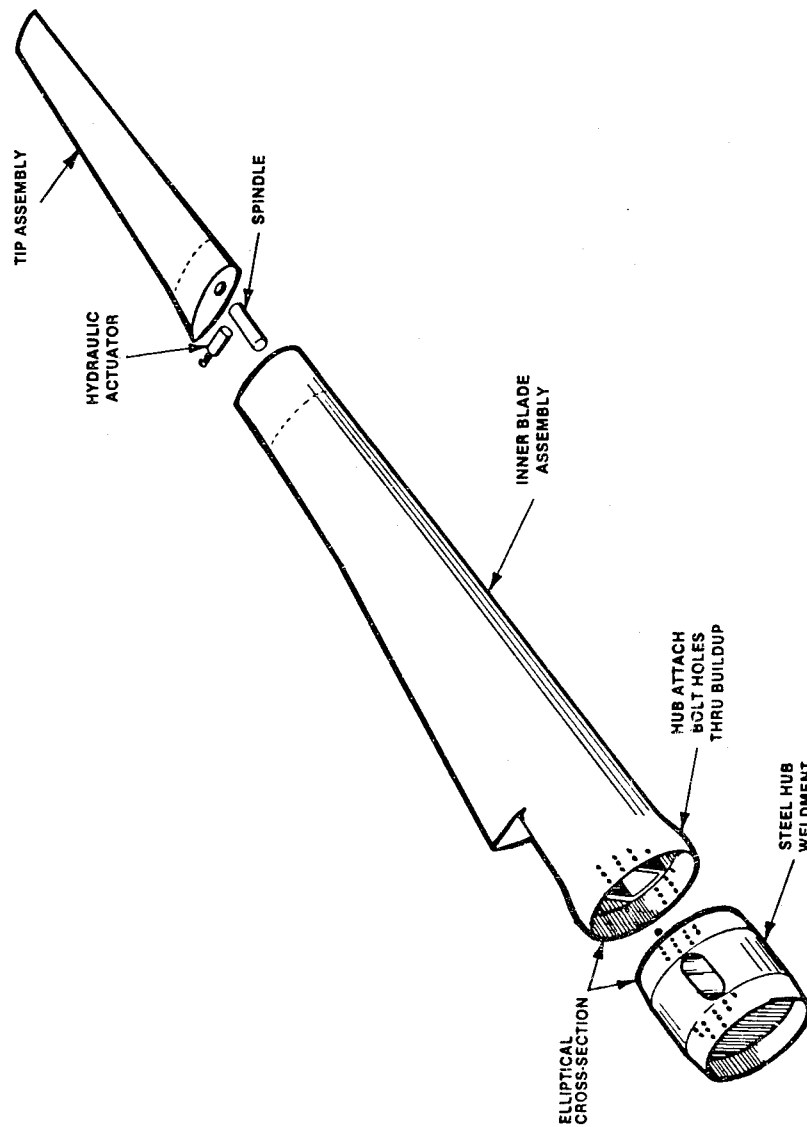
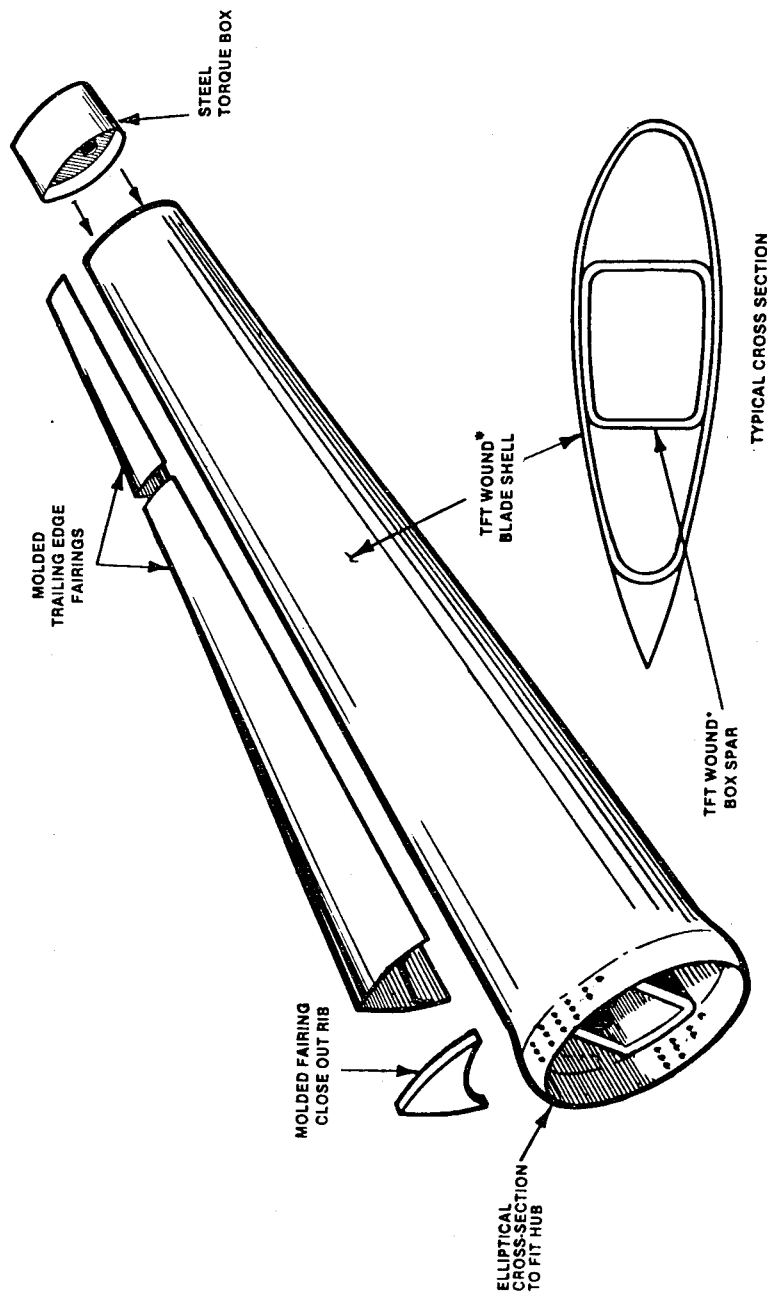


Figure 13

COMPOSITE ROTOR INNER BLADE ASSEMBLY



[®]BCI PATENT PENDING

The Effect of Fiber Orientation on the Design Parameters of Reinforced and Filled Thermoplastic Compounds

Peter J. Cloud and Robert T. Alvord
LNP Corporation
Malvern, Pennsylvania 19355

Abstract

Objective: To determine the limiting design stress and modulus value which can be substituted into Hookeian stress-strain equations to enable the engineer to safely design with discontinuous fiber reinforced injection moldable thermoplastics.

Compounds Investigated

- I. Resins: A. 6/6 Nylon
B. Polycarbonate
- II. Additives: A. Glass Fibers - .0004" diameter x .050" long
electrical grade reinforcing fiber
B. Carbon Fiber - .0003" diameter x .035" long, high
modulus (30MM psi) highly graphitized re-
inforcing fiber
C. Glass Beads - .0015" - .0005" diameter solid glass
bead
- III. Compounds: A. Nylon 6/6
1. RF-1006 - 30% Glass Reinforced
2. RB-1008 - 40% Glass Bead
3. RF-1006MG - 15% Glass Bead, 15% Glass Fiber
4. RC-1008 - 40% Carbon Fiber Reinforced
B. Polycarbonate
1. DF-1006 - 30% Glass Reinforced

Quality Assurance of Manufactured Components

R. D. Margolis

Rockwell International, Plastics Division
Thousand Oaks, California 91360

Abstract

This paper describes progress to date on a joint effort of Rockwell Plastics and Ford Motor Company to apply non-destructive testing techniques in the quality control testing of adhesive bonded plastic truck hood assemblies. The program involves selection of a suitable sonic testing device to measure adhesive bond integrity along with laboratory trials to establish procedures and measure the instrument's flaw detection capabilities. In addition, several plant trials are underway to test the instrument's viability in an industrial environment and provide a data base for establishing quality control specifications.

SESSION 7

INDUSTRIAL APPLICATIONS AND DESIGN

**Chairman: C. O. Smith
University Of Nebraska**

DEGRADATION DATA OF KEVLAR PRESSURE VESSELS

W.D. Humphrey
Brunswick Corporation/Technical Division
Lincoln, Nebraska 68504

Abstract: Recent hydroburst tests of Kevlar/epoxy composite pressure vessels showed losses in strength when subjected to extended periods of high temperature and high humidity. These pressure vessels had served to monitor the aging characteristics of Rocket Motor Cases during Engineering Development tests. Since Kevlar was a relatively new material replacing fiberglass in this application, it was considered important that these results be verified in a controlled experiment utilizing accelerated aging methods.

To measure these effects, two series of tenth-scale models of Rocket Motor Cases were fabricated, which included two different resin systems and two very different design concepts. The accelerated degradation of Kevlar composites from high temperature and humidity was evaluated by means of water boil tests for periods of up to ten days.

Hydroburst tests of these aged vessels showed Kevlar to have much less degradation than fiberglass. Actual values were determined to be dependent on the resin system used and also dependent upon the dryness of the composite at the time of test. Wet composites acted as if a plasticizer was added to the resin system and in the configuration tested actually regains virgin strength.

Key words: degradation; moisture; Kevlar 49; One-Tenth Scale Motor Case; water boil; temperature effects; epoxy resins; S-glass.

Introduction: The impact of degradation from long term environmental storage became a factor at the end of the MX Advanced Technology Program¹ when two full-scale Kevlar 49² units were burst tested at hoop fiber stress values of 388 and 391 ksi. These units were tested after approximately one year of uncontrolled warehouse storage. A 10 percent

¹This work was supported by SAMSO under Contract F04701-73-C-0423 through the office of J.N. Mason, Major USAF, Propulsion Division, Directorate of Engineering. Aerojet Solid Propulsion Company, Sacramento, California, served as prime contractor and Brunswick Corporation, Lincoln, Nebraska, served as the subcontractor of case development.

²duPont Kevlar[®] Aramid Fiber, Type 969.

reduction of strength compared to a baseline hoop fiber stress of 430 ksi. This latter unit had been tested within three months of fabrication. In addition to these full-scale case results, significant degradation was noted with a series of tenth-scale MX pressure vessels stored for periods of up to two years at temperatures of 100°F and 150°F at 95 percent relative humidity.

This data was contradictory with data reported by other Rocket Motor Case manufacturers, which showed 6 inch pressure vessels actually getting stronger after one year of exposure to high temperature and humidity. At the same time, duPont reported that moisture degradation was strictly resin dependent. DuPont's 72 hour water boil data of flex and shear strengths indicated degradation to be no worse than for fiberglass and that with "better" resin systems, degradation leveled off at 10 percent.

In order to understand this data, Brunswick initiated an IR & D study of the effect of accelerated aging of Kevlar pressure vessels. This study provided new insight and understanding of the degradation mechanisms of Kevlar composites.

Literature Review: The in-house testing program included a brief literature review of existing data, which hopefully would assist in explaining the nature of the failure mechanism. Some of the more meaningful data are discussed in the following sections.

DuPont Design Manual (Reference 1): The duPont Design Manual documented several important characteristics of Kevlar 49, which are important to this study. The manual reported that the effect of tap water on Kevlar roving or yarn is zero after 24 hours at room temperature. The same unimpregnated roving loses approximately 2 percent of its residual strength after 100 hours of water boil.

The moisture gain of Kevlar is reported to be 3.5 to 4 percent at equilibrium. The time to reach equilibrium is 22 hours at 55 percent relative humidity and 72°F. The long term use temperature in air is 320°F and decomposition of Kevlar occurs at 930°F.

The loss in tensile strength in air at 100°C (212°F) is 12.5 percent (460/525 ksi) and at 200°C (392°F) is 25 percent (395/525 ksi). Similarly, the loss in elastic modulus at 100°C is 8 percent and at 200°C is 12 percent. These data are plotted in Figure 1 showing tensile strength and modulus at temperatures for both air and nitrogen environments.

The adverse effect of ultraviolet radiation is well documented and is becoming better understood. This ultraviolet degradation effect initiates at the exposed surface and progresses inward. An unprotected woven fabric loses half of its strength in only five weeks of Florida sun; whereas, a three-strand rope (1/2 inch diameter) has lost 19 percent of its strength after one year in the same sun conditions. See Table I.

Note that the effect stabilizes at 69 percent strength retention after 18 to 24 months.

MX Aging Vessels (Reference 2): As a portion of the MX Advanced Technology Program, a series of one-tenth scale vessels were fabricated concurrent with the full-scale rocket motor cases and served as witness vessels. A long term aging program was conducted, which indicated an excessive loss of residual strength with one of the resin systems tested.

The test vehicle used was a pressure vessel modeled as a scale version of the full-scale baseline design and is discussed in detail later. Three different design/material combinations were studied as follows:

1. All released Kevlar/LRF-209³
2. All bonded Kevlar/LRF-216
3. Noninterspersed bonded polar and released hoops Kevlar/LRF-216

Where LRF-209 resin is a highly crosslinked epoxy aromatic amine resin system with high heat distortion temperature (HDT) properties, LRF-216 resin is a low crosslinked epoxy anhydride using a proprietary catalyst with a relatively low HDT property. The bonded versus release system referred to a special coating utilized to limit the adhesive properties of the Kevlar fiber in order to enhance its strength in biaxial strain fields.

The vessels were proof tested to 3,320 psig and then exposed to 95 percent relative humidity at either 100°F or 150°F and stored for various lengths of time until ready for burst. Prior to burst test, the vessels were dried for 96 hours at 150°F.

A complete tabulation of these data are shown in Table II and plotted in Figure 2. A summary of degradation as measured follows:

1. All Released, Interspersed, LRF-209

150°F	One Year	7.8 percent
	Two Years	10.4 percent
100°F	One Year	3.5 percent
	Two Years	6.0 percent

2. Bonded, Interspersed, LRF-216

150°F	One Year	13.2 percent
	Two Years	28.3 percent
100°F	One Year	9.2 percent
	Two Years	9.2 percent

³LRF denotes Lincoln Resin Formula (Brunswick Corporation).

3. Hybrid, Noninterspersed, LRF-216

150°F

16 months

22.5 percent

Moisture Effects on Structural Resins: Many studies (References 3-5) have shown that absorbed moisture results in significant degradation of the matrix sensitive mechanical properties, particularly at higher temperatures; whereas, fiber controlled composite properties are relatively unaffected. Most investigations agree that this degradation property is attributed to the plasticizing effect of moisture on the resin modulus and lowers the glass transition temperature. Water behaving as a plasticizing agent disrupts the strong hydrogen bond present in highly polarized epoxy resin systems. This is reversible to some extent and can promote a change in failure mode between wet and dry specimens. High heat distortion resin systems are not as significantly affected at high temperature moisture exposure as are the lower heat distortion resins. It is interesting to note that one investigator (Reference 5) attributed the increased strength in wet laminates to swelling of the resin matrix, which (in certain configurations) relieves the residual interlaminar shear stresses.

IR & D Test Program--Test Vessel: The use of pressure vessels, which contain a biaxial stress field, has proven to be the most reliable means of establishing valid design allowable data. Brunswick has developed extensive burst strength data for Kevlar 49/epoxy composites using the tenth-scale second stage MX vessel. The vessel is designed to fail at mid-cylinder in a controlled manner. Design verification and reliability testing indicate that the mode of failure and achieved level of burst pressure are very repeatable. This vessel has been used on many programs, which accounts for the large data base. Subtle processing parameters, such as hoop winding terminations and dome reinforcement locations, have been studied and their influence on performance is controlled. This makes it possible to isolate effects of the variable under study with a minimum number of replicate specimens. A design summary is shown in Figure 3.

Test Plans (LRF-092 Resin System): The initial program consisted of 21 vessels all wound with LRF-092 resin. The LRF-092 resin is a highly crosslinked epoxy anhydride/tertiary amine resin system with a good heat distortion temperature. The resin is widely used on many of Brunswick's pressure vessels and, thus, dictated a strong need for degradation data for in-service applications.

Nine of these first 21 vessels were selected by random numbers for long term storage tests, where six vessels were of the released configuration and three of the bonded configurations. The remaining vessels were proof tested and assigned for testing as follows.

Bonded

(2) virgin burst
(2) 72 hour water boil and burst
(2) 240 hour water boil and burst

Released

(2) virgin burst
(2) 72 hour water boil and burst
(2) 240 hour water boil and burst

Test Results (LRF-092 Resin System)--Bonded Vessels: The burst results of all LRF-092 vessels are summarized in Table III. The virgin strength of bonded vessels was established from two vessels which demonstrated identical strengths (4,490 psig and 346 ksi hoop stress); this was also in excellent agreement with the hoop stresses 340 to 345 ksi established by bonded vessels during the MX program.

The 72 hour water boil vessels tested at 4,490 and 4,590 psig, indicating zero degradation in these two vessels, while the 240 hour water boil vessel burst at 4,120 and 4,400 psig indicating 92 and 98 percent strength retention. As the results show, the degradation of Kevlar/LRF-092 vessels was much less than expected based on the MX witness vessel tests at Aerojet.

Released Vessels: The burst test results of these vessels are also summarized in Table III. Virgin strength was assigned at 5,600 psig (431 ksi), based on the results of S/N 762 and based on the mean value of the MX statistical series (Reference 2).

The 72 hour water boil vessels burst at 5,690 and 5,630 psig, indicating a net improvement in performance which parallels the results of the three day water boil tests of bonded vessels.

An unexpected phenomenon occurred during cool-down from water boil with S/N 747 and 748 released hoop vessels. A partial vacuum was created inside as the vessels were cooled (the ports had been sealed for protection during boiling). This caused one dome on each vessel to buckle away from the released fiber cylinder. It was elected to test these vessels and to evaluate the effects of buckled domes. Both vessels failed prematurely in areas where the buckling had occurred (see Figures 4 and 5). Consequently, two vessels which had been selected for environmental storage, were shifted to the boil tests as replacements. Following ten days of water boil, with a modified vent plug installed, vessels S/N 758 and 764 were burst tested. The vessels failed at 5,580 and 4,600 psig, indicating residual strengths of 100 and 82 percent respectively (the dome/knuckle failure of S/N 764 is not a normal failure mode and generally indicates nontypical failure levels). In any case, the test results for released fiber vessels substantiate the results of bonded vessels. That is, both showed degradation of Kevlar/LRF-092 vessels to be much less than expected.

Environmental Studies: Long term aging studies are currently underway at Brunswick in an environmental chamber at 150°F and 95 percent relative humidity. The vessel assignment was altered to provide two

replacement vessels for the 240 hour water boil matrix. The dates of installation and S/N of these vessels are as follows:

<u>S/N</u>	<u>Configuration</u>	<u>Date Installed</u>
753	Bonded - proofed & coated	1/10/78
755	Bonded - proofed	1/10/78
757	Bonded - not proofed	1/10/78
761 - 763	Released - proofed & coated	1/10/78
759 - 560	Released - proofed	1/10/78

In addition, one spool of bare Kevlar roving from the same lot used to wind the above vessels was placed in storage January 18, 1978. An additional spool of bare Kevlar roving was placed in storage September 18, 1978, and additional spools are planned for six month intervals.

It is planned to store these vessels and spools continuously for 18 and 24 months and then hydroburst and perform strand tensile tests to establish degradation correlation with accelerated aging tests.

Test Plans (LRF-216 Resin System): The accelerated aging tests of Kevlar/LRF-092 vessels showed only minor degradation occurring after 240 hours of water boil and no effect at all was noted for 72 hour water boil. These results were surprising and indicated that the LRF-092 resin system provided excellent moisture resistance for the pressure vessels. The MX witness vessels with LRF-216 resin indicated excessive degradation (up to 28 percent) after exposure to an environment of 150°F and 95 percent relative humidity; it was important to determine if this resin system was alone responsible for these poor results. Therefore, twelve additional vessels (six released and six bonded) were added to the program.

Test Results: A variable not previously considered was incorporated into the study. This variable was the condition of the composite (wet or dry) at the time of burst test. It was suspected that the drying operation of 96 hours at 150°F performed on the MX witness vessels may have altered the performance of those vessels. This tendency was established by the initial LRF-216 tests. S/N 774 and S/N 765 were tested shortly after cooling to room temperature and achieved 95 and 96.5 percent of virgin strength, while S/N 772 and 769 (tested following three days drying at room temperature) achieved only 90 and 92.5 percent of virgin strength. See Table IV summary.

Upon reviewing the significance of these results, it was elected to deviate from the original test plan and delete the 72 hour water boil tests and utilize the remaining vessels to screen the effect of the wet or dried laminates. Hence, the next four vessels were subjected to ten day water boil. Two of these vessels were tested wet and two tested after three days of drying at 150°F. The dried vessels, S/N's 773 and 770, burst at 87 percent and 91 percent of ultimate, while the "wet" vessels, S/N 771 and 776, burst at 102 and 98 percent of ultimate. The

relationship continued to hold true, indicating that "dried" laminates tested lower than "wet" laminates.

The four remaining vessels were subjected to the same wet/dry screening test, except the drying time was extended to match the four days actually used by Aerojet. The dried vessels S/N 776 and 768 tested at 90 and 97 percent of virgin strength, while the "wet" vessels S/N 775 and 767 tested at 100 percent and 87 percent of virgin values. The lower burst value, 4,870 psig, of S/N 767 was uncharacteristic, but the mode of failure (dome/knuckle/cylinder) was nontypical indicating that the vessel was suspect.

Summary data for all vessels fabricated and tested during the program are shown in Table V. Apparent thicknesses at three stations in the cylinder using pi tape measurements, total assembly weights prior to environmental exposure, date of winding, and test results are all summarized in this table.

Discussion: The results of this program showed, first, that Kevlar does not degrade appreciably in pressure vessels following ten days of water boil. Our literature search had prepared us somewhat for these results. As mentioned, duPont measured only 2 percent degradation of bare Kevlar fibers after 100 hours of water boil. Greater degradation had been noted as a surface effect from ultraviolet radiation. This surface effect could destroy thin laminates, but in thicker sections (ropes or cables), equilibrium was reached at about 70 percent strength retention. Composite vessels are protected from sunlight by the resin matrix, and the effect of ultraviolet exposure is expected to be low. Further, the vessels tested by Aerojet were conditioned in a protected environment.

Returning to our original conclusion that Kevlar in pressure vessels does not appreciably degrade, we found similar performances in both LRF-092 and LRF-216 resins. If one low value, 82 percent, can be excused from the LRF-092 results, and 87 percent excused from the LRF-216 results (both nontypical failures), we have good correlation with less than ten percent degradation. The vessels fabricated using LRF-216 resin indicated that performance was affected by the test method. Dried vessels tested at an average of 92 percent of virgin strength and "wet" vessels tested at 99.5 percent of virgin strength. See Figure 6. The nontypical failures are unique to water boil tests and did not occur in the virgin tests of Browning and Whitney (Reference 3). The dome failures appear to be caused by water propagating between layers, perhaps originating at the fitting interface. Pending tests with the high temperature/humidity exposed vessels could resolve this question.

Our literature search also sheds light on the wet versus dry Kevlar composites. Brunswick MX work (Reference 2) concluded that water acted as a plasticizing agent, disrupting the bonding in high polar epoxy resin systems. The reversibility of the water absorption effect and the resulting change in failure modes from wet to dry were explained. The higher heat

distortion resins were shown to be less affected by moisture than were the lower heat distortion resins where water boil affected weight gains.

It has been noted that LRF-209 vessels degraded 10 percent after two years of 150°F and 95 percent relative humidity; but LRF-216 vessels degraded over 28 percent for the same tests. It follows that the heat distortion temperature for the resins, as cured in these vessels, was 310°F for LRF-209 and only 150°F for LRF-216. The higher heat distortion resins actually are more densely crosslinked and, thus, have fewer reactive sites where plasticizing can occur. This difference in heat distortion temperatures helps explain the performance differences in vessels fabricated from these two resins.

The 1/10 scale MX vessel was designed specifically to fail in the mid-cylinder section by over-reinforcing the dome areas. By isolating the Kevlar fibers using the released fiber mechanism, pure tensile loads were achieved in the fiber while strained in a biaxial strain field. Without this releasing mechanism, the Kevlar fibers would be subjected to biaxial loads which could transversely pull the fibers apart. This is the primary reason for the 25 percent performance gain in released fiber vessels. It was demonstrated during the MX program that a very flexible, high-elongation resin, acted very much like released fibers by allowing deformation within the matrix rather than at the fiber/resin interface.

In fact, no additional improvement was measured by combining the above "chicken fat" resin with released fibers. It is believed that the differences measured in this study between wet and dry resins parallel that observation and that "wet" vessels in fact represent a plasticized resin system.

For comparison purposes, the results of this study are plotted in Figure 7 (previous Brunswick data, Reference 6) showing the improved performance of Kevlar 49 over two types of S-glass. Note that the strength loss in Kevlar vessels, regardless of the resin system used, is much less than with fiberglass when utilizing the same test vessels and test procedures.

Conclusions:

1. Degradation in Kevlar pressure vessels is much less than in fiberglass pressure vessels and is a function of the resin system used. High heat distortion resins, such as LRF-092 and LRF-209, retain 95 percent of virgin strengths after water boil; Kevlar with a lower heat distortion resin (LRF-216) still performed well, retaining 90 percent of virgin strength.
2. It was demonstrated by this study that for a Kevlar vessel designed for membrane critical loading (i.e., mid-cylinder in the MX 1/10 scale) the dryness of the composite at the time of test can influence performance. This is particularly true when the resin has a low heat distortion temperature such as LRF-216, where water boil alters

the characteristic of the resin. Original strengths were retained in bonded LRF-216 vessels when testing, while the composite was still wet (plasticized).

3. The literature search and a review of previous Brunswick data point out several characteristics of Kevlar that should be considered in establishing performance standards.
 - a. Water boil of bare fiber has little effect on performance (2 percent after 100 hours).
 - b. Appreciable loss in strength occurs at the fiber surface from ultraviolet radiation and/or oxidation. This is primarily a surface effect and its extent is thickness dependent.
 - c. The degradation of Kevlar from temperature alone is significant, limiting the time of exposure and preventing high temperature (+200°C) usages of this fiber.
 - d. The effect of moisture on a resin system is reversible and can be utilized in certain applications to enhance performance.

REFERENCES

1. Kevlar 49 Data Manual, E.I. duPont and Company, Wilmington, Delaware, revised October, 1977.
2. MX Program Chamber Development, Final Report - Phase II, Brunswick Corporation to Aerojet Solid Propulsion Company, Contract S-117039.
3. Browning, C.E. and Whitney, J.M., "The Effects of Moisture on the Properties of High Performance Structural Resins and Composites," Fillers and Reinforcements for Plastics, Advances in Chemistry Series 134, 1974, pp. 137-148.
4. Tompkins, S.S., "Analysis of Moisture Absorption and Diffusion in Fiber Reinforced Polymeric Resin - Matrix Composite Materials," Ph.D. dissertation, University of Virginia, May, 1978.
5. Lee, B.L., Lewis, R.W., and Sacher, R.E., "Environmental Effects on the Mechanical Properties of Glass Fiber/Epoxy Resin Composites," Army Materials and Mechanics Research Center, June, 1978.
6. Reiners, A.E., "Characterize Type 449 Roving," Design and Development Memo #289, Brunswick Corporation, Lincoln, Nebraska, September, 1978.

THE EFFECT OF TEMPERATURE ON THE
TENSILE PROPERTIES OF YARN OF
KEVLAR® 49 ARAMID

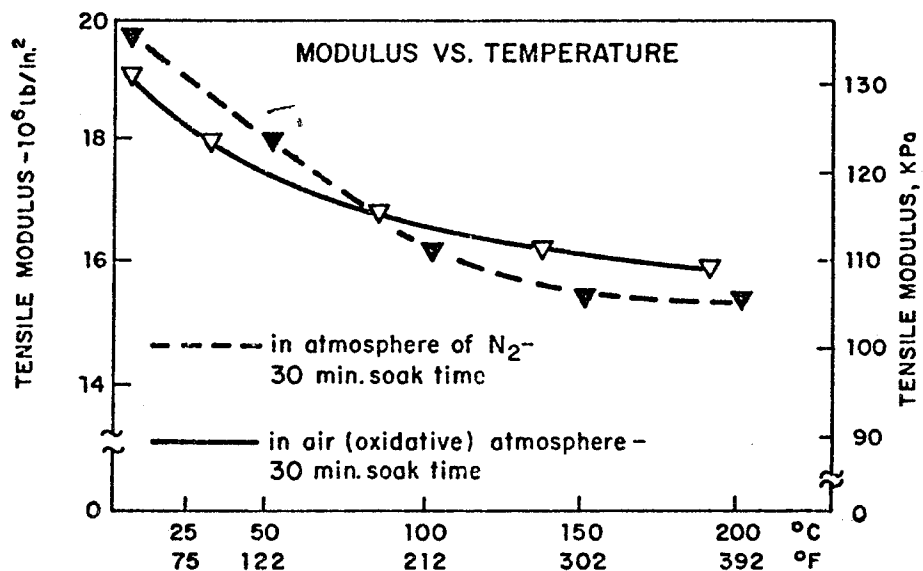
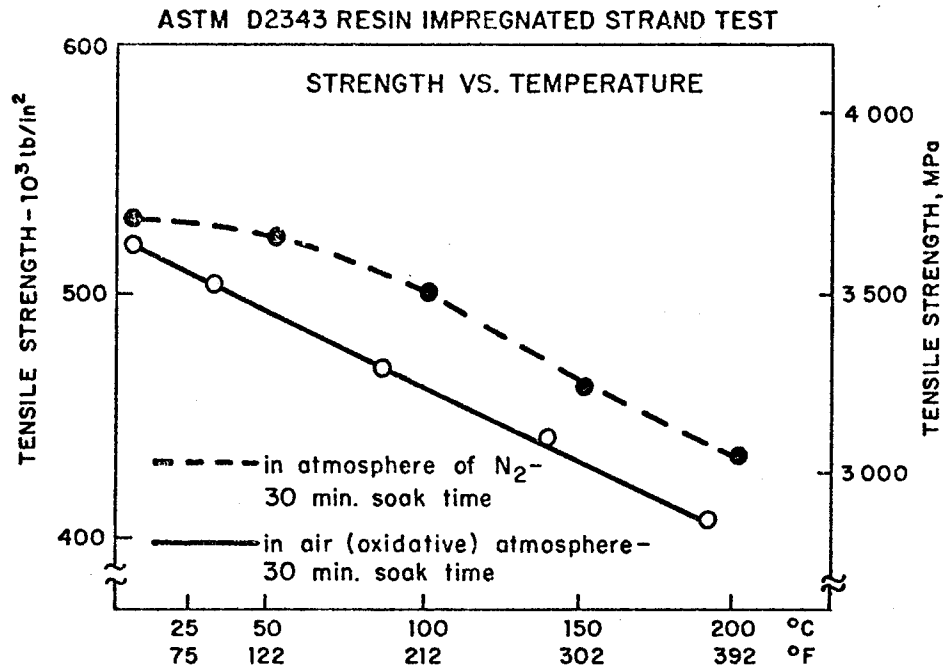


FIGURE 1

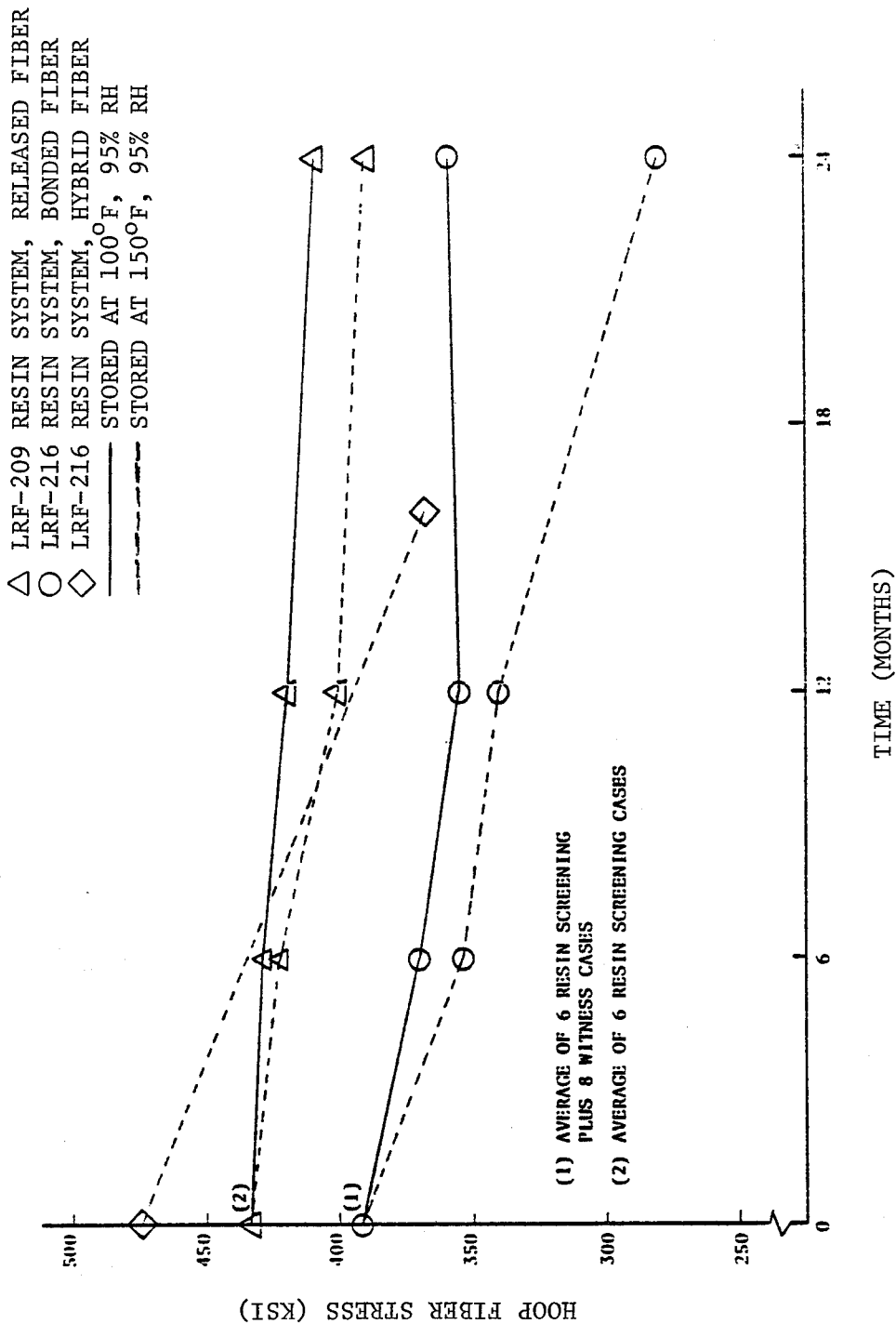


Figure 2. Hoop Fiber Stress of One-tenth Scale Cases after Exposure to Long-term Aging Environments

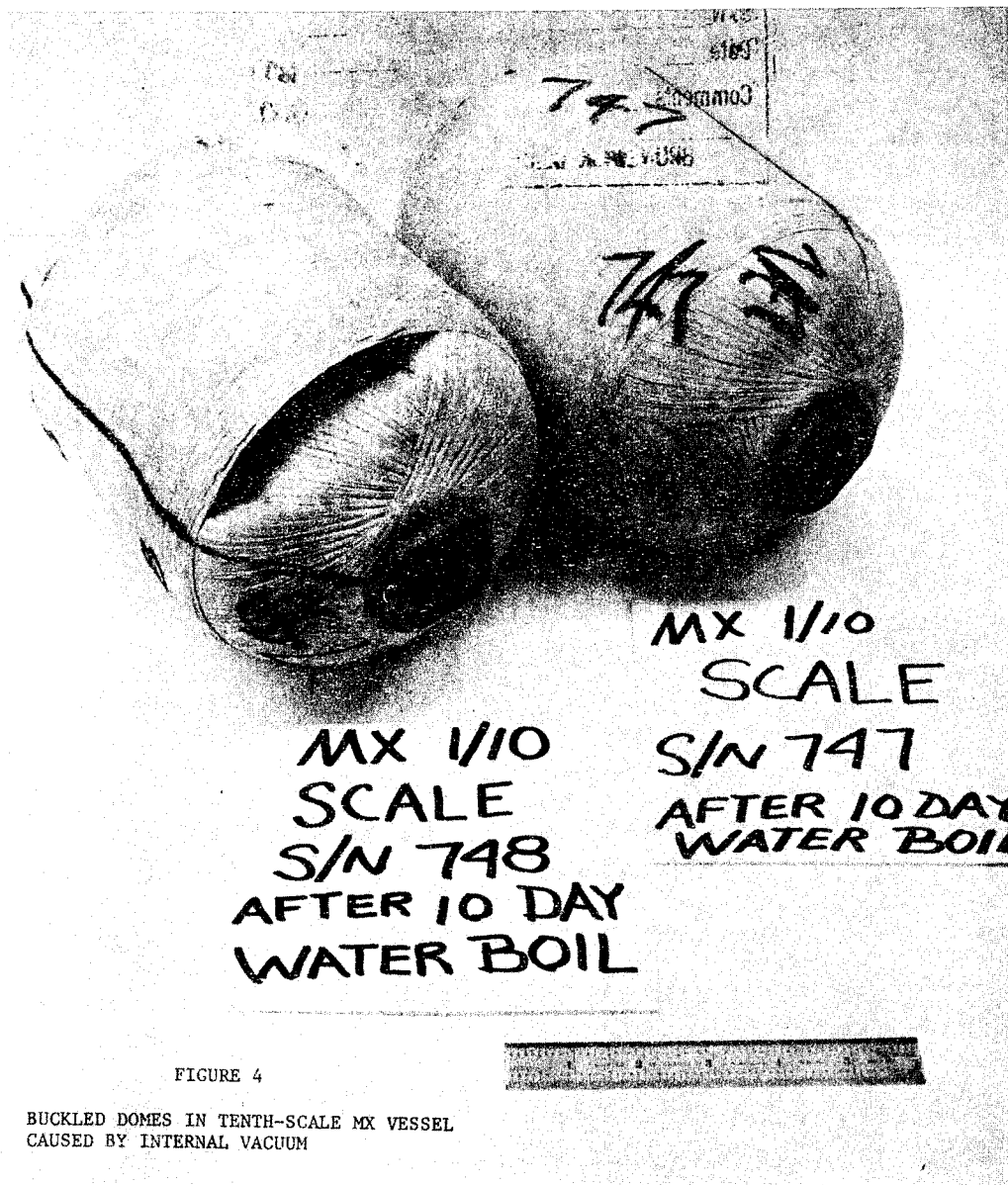


FIGURE 4

BUCKLED DOMES IN TENTH-SCALE MX VESSEL
CAUSED BY INTERNAL VACUUM

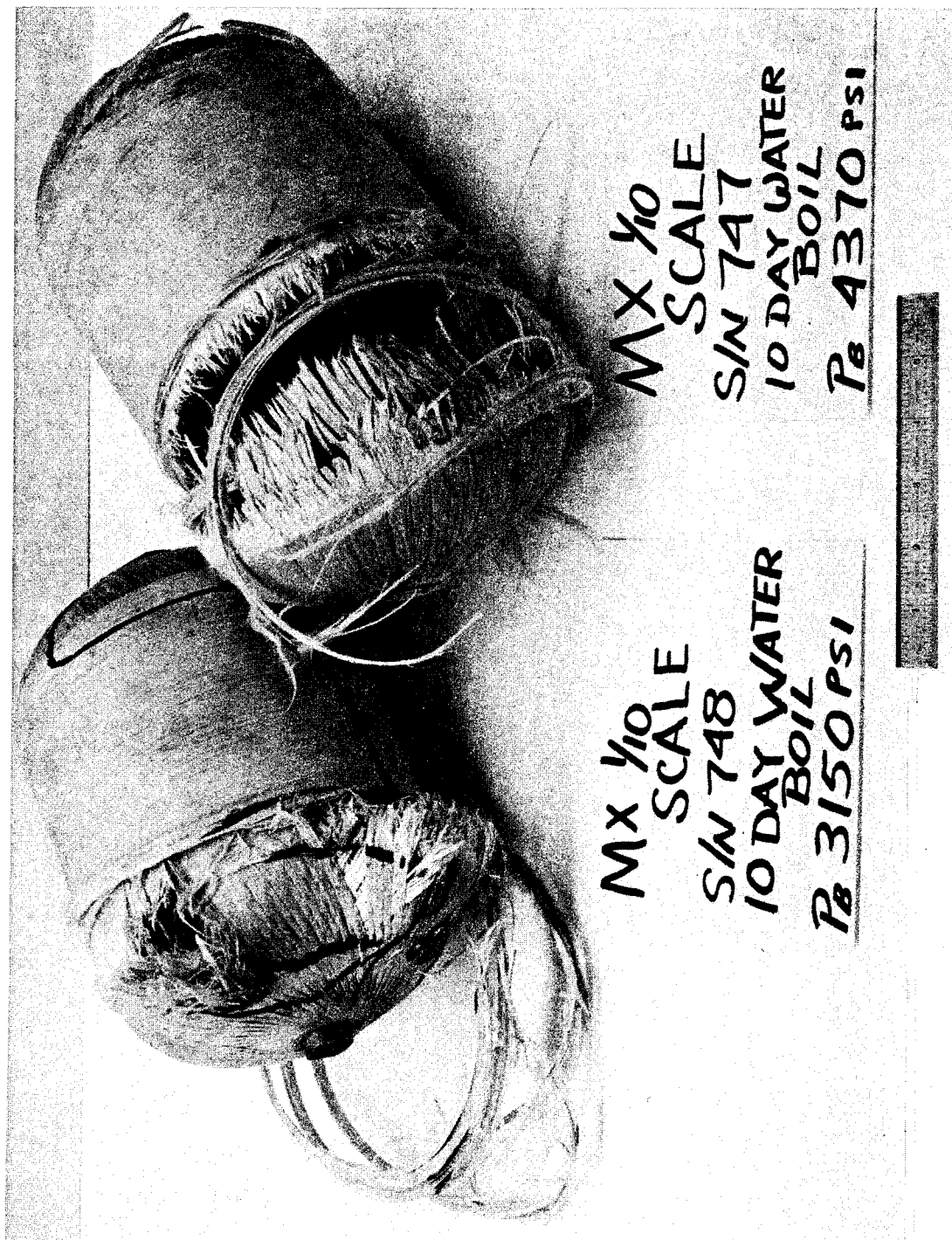


FIGURE 5. FOLLOWING HYDROBURST OF BUCKLED DOME VESSELS

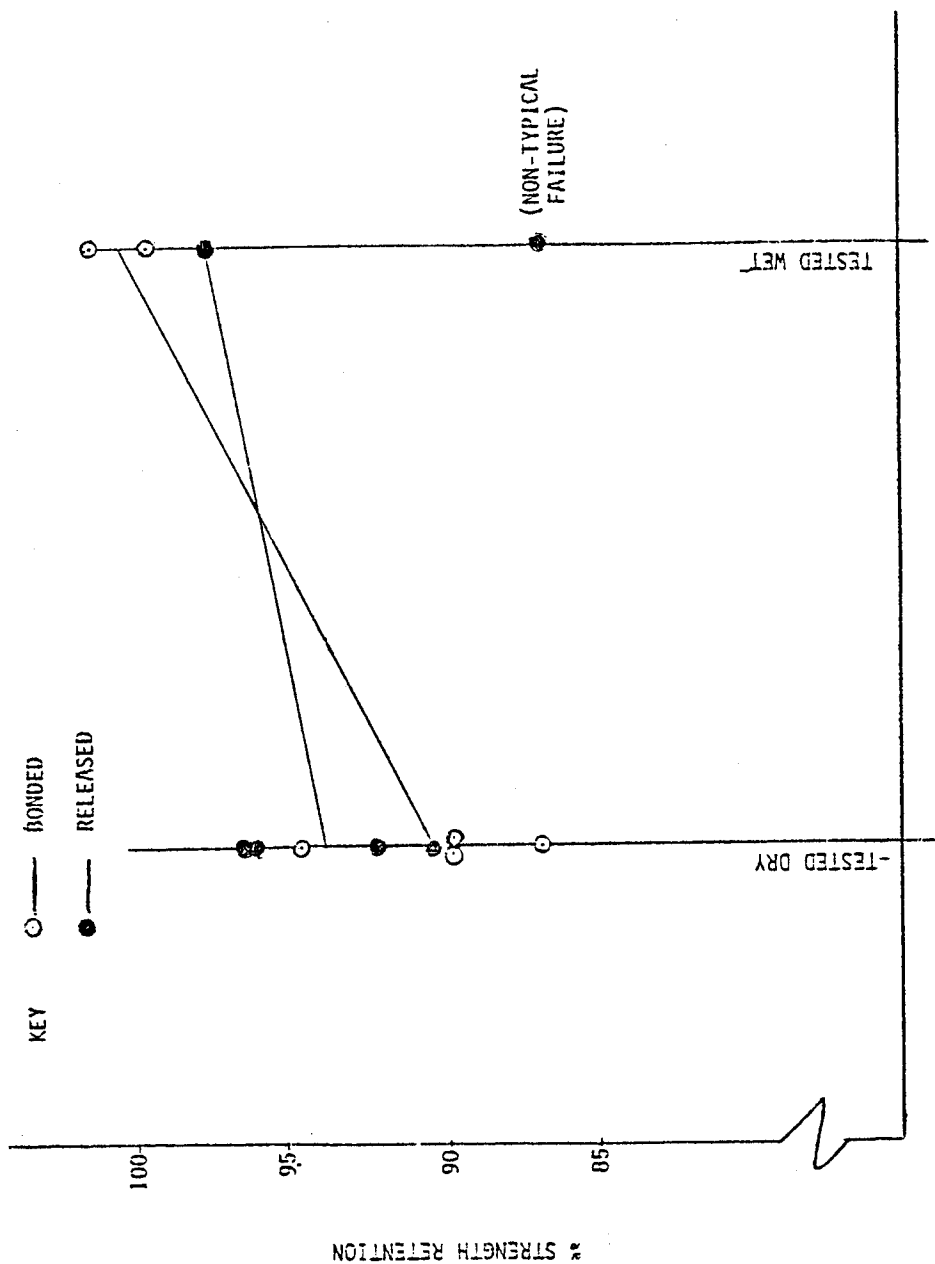


Figure 6
TEST RESULTS FROM COMPOSITE
CONDITIONING AFTER BOIL
(LRF-216)

FIBERGLASS DEGRADATION

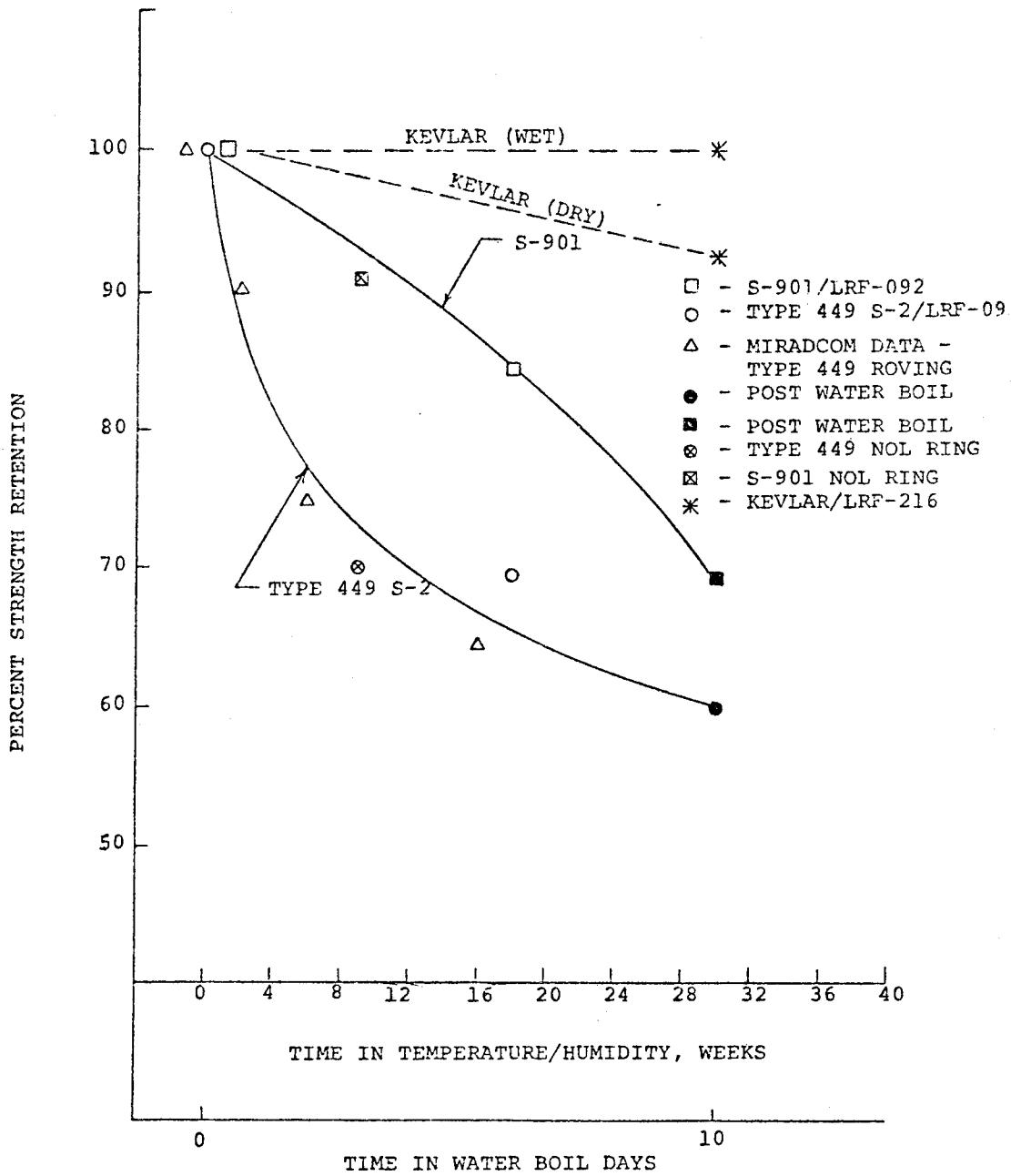


FIGURE 7

TABLE I
(FROM REFERENCE 1)

ULTRAVIOLET STABILITY OF KEVLAR 49 ARAMID FIBER

KEVLAR 49 PRODUCT FORM	BREAK LOAD		STRENGTH RETAINED %
	LBS/IN	(kN/m)	
FABRIC WOVEN FROM 380 DENIER (420 DTEX) YARN 4.5 MIL (0.11 mm) THICK			
UNEXPOSED	300	52	----
FLORIDA* SUN, 5 WEEKS	154	27	51
	LB.	(N)	
3-STRAND ROPE, 1/2 IN. (13 mm) DIAMETER			
UNEXPOSED	14,400	64,050	--
FLORIDA SUN, 6 MONTHS	13,000	57,830	90
12 MONTHS	11,600	51,600	81
18 MONTHS	9,950	44,260	69
24 MONTHS	9,940	44,220	69

*HIALEAH

TABLE II

DATA SUMMARY - ONE-TENTH SCALE CASE
LONG-TERM AGING PROGRAM
(B. Hope - 11/1/77)

SERIAL NUMBER	RESIN SYSTEM(1)	TYPE FIBER	STORAGE CONDITIONS		STORAGE TIME (MONTHS)	BURST PRESSURE (PSIG)	HOOP FIBER STRESS (KSI)	BURST LOCATION
			TEMP. (°F)	R.H. (%)				
(3)	209PP	Released	---	--	0	5,638	434	Mid Cylinder
404	209PP	Released	100	95	6	5,550	428	Mid Cylinder
402	209PP	Released	100	95	12	5,440	419	Mid Cylinder
401	209PP	Released	100	95	24	5,300	408	Mid Cylinder
405	209PP	Released	150	95	6	5,510	424	Mid Cylinder
403	209PP	Released	150	95	12	5,190	400	Mid Cylinder
406	209PP	Released	150	95	24	5,050	389	Mid Cylinder
(3)	216PP	Bonded	---	--	0	5,083	392	Mid Cylinder
194	216PP	Bonded	100	95	6	4,800	370	Mid Cylinder
193	216PP	Bonded	100	95	12	4,620	356	Mid Cylinder
199	216PP	Bonded	100	95	24	4,650	358	Mid Cylinder
400	216PP	Bonded	150	95	6	4,590	354	Mid Cylinder
195	216PP	Bonded	150	95	12	4,420	340	Mid Cylinder
196	216PP	Bonded	150	95	24	3,650	281	Cylinder-Axial
(4)	216PP	Hybrid(2)	---	--	0	6,165	475	Mid Cylinder
663	216PP	Hybrid(2)	150	95	16	4,600	354	Mid Cylinder
664	216PP	Hybrid(2)	150	95	16	4,950	381	Mid Cylinder

- (1) PP = Preimpregnated Roving
(2) Hybrid Case: Bonded Polar Fiber, Released Hoop Fiber
(3) Average of Six (6) Resin Screening Cases
(4) Average of Four (4) Control Cases

TABLE III
KEVLAR AGING WITH LRF-092 IN 1/10 SCALE MX VESSELS

<u>BONDED</u>	<u>S/N</u>	<u>BURST PRES. (PSI)</u>	<u>$\sigma_{\theta\theta}$ (KSI)</u>	<u>STR. RETENT (%)</u>
240 HR. WATER BOIL	745-746	4120-4400	317-339	95
72 HR. WATER BOIL	749-750	4490-4590	346-354	101
VIRGIN BURST	754-756	4490-4490	346-346	100
STORED (W. PROOF & COATED)	753	***		
STORED (W. PROOF)	755			
STORED (NO PROOF)	757			
 <u>RELEASED CIRCS</u>				
240 HR. WATER BOIL (1ST)	747-748	4370**-3150*	337-243	N/A
240 HR. WATER BOIL (2ND)	758-764	5580-4600	430-354	100-82
72 HR. WATER BOIL	751-752	5690-5630	438-433	101
VIRGIN BURST	762	5600-	431	100
STORED (W. PROOF & COATED)	761-763	***		
STORED (W. PROOF)	759-760			

*BUCKLED DOME FROM VACUUM PRESSURE

**BUCKLED LINER FROM VACUUM PRESSURE

***TO STORAGE (1/10/78) AT 150°F and 95° R.H.

TABLE IV

LRF-216/KEVLAR

DEGRADATION FROM 240 HR. WATER BOIL

S/N	BONDED-240 HOUR WATER BOIL	ΔWT** (GRAMS)	BURST PRESSURE (PSI)	STRENGTH RETENTION (%)	FAILURE MODE
776	DRIED 4 DAYS @ 150°F		4020	90	MID-CYL
773	DRIED 3 DAYS @ 150°F	24	3920	87	MID-CYL
774	DRIED 1 DAY @ R.T.	51	4250	95	MID-CYL
772	DRIED 3 DAYS @ ROOM TEMP.	47	4050	90	MID-CYL
775	TESTED WET!!	49	4520	100	MID-CYL
771	TESTED WET!!	19	4580	102	MID-CYL
			4223	94%	
			AVG WET---101%		
			AVG DRY--- 90.5%		
<u>RELEASED HOOPS-240 HOUR WATER BOIL</u>					
768	DRIED 4 DAYS @ 150°F	42	5430	97	MID-CYL
770	DRIED 3 DAYS @ 150°F	48	5110	91	MID-CYL
765	DRIED 1 DAY @ R.T.	48	5400	96.5	MID-CYL
769	DRIED 3 DAYS @ ROOM TEMP.	54	5180	92.5	MID-CYL
767	TESTED WET!!	57	4870*	87*	KNUCKLE!! (PORT TAN)
766	TESTED WET!!	20	5510	98	MID-CYL
			5326	95%	
			AVG WET---98%		
			AVG DRY---94%		

*NON-TYPICAL FAILURE DATA NOT INCLUDED IN ANALYSIS

**NET WEIGHT GAIN FROM WATER BOIL TESTS. DOES NOT INCLUDE DRYING OPERATION.

TABLE V

SUMMARY TABLE OF TENTH-SCALE DATA

S/N	COMPOSITE THICKNESS			AVG. THICK (IN.)	RESIN SYSTEM	BOILED	RELEASED	DATE WOUND	WEIGHT (GRAMS)	BURST (PSI)	REMARKS
	TWO (IN.)	MID (IN.)	AFT (IN.)								
745	.113	.109	.111	.111	LRF-092	X		11/9/77	1273	4120	
746	.115	.107	.109	.110		X		11/10/77	1280	4400	
747	.122	.124	.129	.125			X	11/14/77	1420	4370	
748	.122	.122	.131	.125			X	11/14/77	1498	3150	
749	.100	.109	.141	.130		X		11/18/77	1280	4490	
750	.133	.109	.129	.124		X		11/18/77	1279	4590	
751	.125	.123	.129	.125			X	12/1/77	1290	5690	
752	.125	.120	.130	.127			X	12/2/77	1295	5630	
753	.107	.109	.110	.109				12/5/77	1260		STORED
754	.114	.109	.110	.111		X		12/6/77	1259	4490	
755	.110	.106	.115	.116		X		12/6/77	1238		STORED
756	.116	.111	.124	.110		X		12/6/77	1257	4490	
757	.116	.105	.114	.110		X		12/6/77	1230		STORED
758	.125	.126	.118	.123			X	12/7/77	1277	5580	
759	.116	.118	.131	.122			X	12/7/77	1297		STORED
760	.141	.128	.133	.134			X	12/8/77	1284		STORED
761	.131	.118	.120	.123			X	12/8/77	1277	5600	
762	.120	.120	.124	.121			X	12/8/77	1324		STORED
763	.150	.127	.147	.141			X	12/9/77	1305	4600	
764	.125	.123	.123	.123	LRF-092 LRF-216		X	12/9/77	1263	5400	
765	.115	.115	.117	.115			X	1/26/78	1254	5510	
766	.113	.117	.121	.117			X	1/26/78	1242	4670	
767	.111	.110	.110	.110			X	1/26/78	1261	5430	
768	.122	.118	.120	.120			X	1/27/78	1248	5180	
769	.115	.114	.114	.114			X	1/27/78	1238	5110	
770	.113	.109	.105	.109			X	1/27/78	1240	4580	
771	.139	.110	.140	.130		X		2/2/78	1231	4050	
772	.141	.114	.132	.129		X		2/3/78	1243	3920	
773	.137	.113	.147	.132		X		2/3/78	1264	4250	
774	.144	.114	.145	.134	LRF-216	X		2/3/78	1249	4520	
775	.137	.108	.145	.129		X		2/3/78	1242		
776	.146	.112	.148	.135		X		2/3/78		4020	

DESIGN ASSURANCE OF A LEAK FAILURE MODE
FOR COMPOSITE OVERWRAPPED METAL TANKAGE

W.W. Schmidt
Brunswick Corporation/Defense Division
Lincoln, Nebraska 68504

Abstract: Assuring a leakage failure mode requires that the outer composite shell be designed such that its minimum cyclic fatigue life is approximately an order of magnitude greater than that of the metal liner. This requires making an accurate fatigue life prediction for both the composite shell and metal liner. It is further possible to determine the critical flaw size for unstable crack growth within the metal liner by application of fracture mechanics principles. A semi-empirical formula has been developed for this purpose since the stresses induced in the metal liner upon initial pressurization exceed the yield strength of the liner material in all cases, which violates a basic assumption of linear elastic fracture mechanics. It is often found that the critical flaw depth is greater than the thickness dimension of the metal liner. In these instances, leakage will occur prior to unstable crack growth. For designs in which unstable crack growth can occur, a dynamic analysis has been developed. This analysis provides a means of assessing the magnitude of shock induced stresses in the composite shell due to the sudden loss of the liner's load carrying capability. Details of these design procedures are provided.

Key words: composite materials; filament wound tankage; leakage failure mode; linear elastic fracture mechanics; critical flaw size; cyclic fatigue life; metal liner.

Filament wound tankage often requires the use of a metal liner, i.e., permeation barrier, due to a requirement for a low allowable leakage rate, fluid compatibility considerations, or exposure to extreme temperatures. A desirable feature of metal-lined composite tankage, in addition to light weight and improved damage tolerance, is an inherent benign failure mode under normal conditions which consists of leakage of the contents without catastrophic rupture. Design procedures to ensure that a new or existing design will possess this feature have been developed.

The principal means of assuring a leakage failure mode is to design the outer composite shell so that its minimum cyclic fatigue life is at least approximately an order of magnitude greater than that of the metal liner. This is facilitated by the fact that fiber reinforced composites do naturally possess much greater fatigue lives than metals in the range of strain amplitudes common to this class of structures. For example,

cycle lives of over 100,000 pressurization cycles have been demonstrated for Kevlar* 49 reinforced elastomeric-lined pressure vessels which cycled from zero percent to 55 percent of the rupture pressure. This corresponds to a strain amplitude which is close to one percent.

Once a designer has performed a complete stress analysis of the tank under study, assessment of its fatigue lives for both the composite and metal liner are straightforward. Graphical data presentations for commonly used composite overwrap materials are available in references [1] and [2]. These empirically derived relationships require only that the designer know the percentage of available strength which is being utilized at the operating condition which is being evaluated. Low cycle fatigue as it pertains to metals is a broad field for which an abundance of theory and data presentations are readily available. Two comprehensive texts, references [3] and [4], will provide a designer seeking knowledge of fundamentals a clear understanding of cyclic fatigue phenomenon.

At the stage of the design effort at which the fatigue lives are known to exhibit the desired ratio of composite life to liner life, the designer may still not possess sufficient information to assure that a liner fatigue crack will not initiate a "premature" composite failure. In order to achieve confidence, the designer must either ensure that any fatigue crack will propagate through the thickness without attaining critical size, or ensure that the composite shell possesses sufficient strength to contain pressure and shock loading released due to a sudden complete liner failure.

All metal-lined composite tankage is subjected to a proof test as a final operation in the normal manufacturing sequence. In addition to demonstrating structural integrity, the proof test develops a permanent compressive stress in the metal liner (and a usually quite small tensile stress in the composite overwrap) which permits more efficient structural utilization of the metal than in a monolithic tank. Because the proof test plastically deforms the metal liners, the analysis of crack behavior at the proof stress level is beyond the realm of linear elastic fracture mechanics, thus requiring a semi-empirical approach, references [5] and [6], to assess this regime from a fracture perspective. It is also quite common to utilize aluminum alloy liners which plastically deform at the maximum expected operating pressure, MEOP, which necessitates the use of the approach described.

* duPont Kevlar[®] Aramid Fiber, Type 969.

In the plastic regime near TUS, the fracture behavior of part-through cracks can be represented by:

$$S_f = TUS (1 - Hc^2) \quad (1)$$

where,

S_f = liner stress
 TUS = tensile ultimate strength
 $H = .112 (TUS/K_f)^4$
 c = half-crack length
 and K_f = fracture toughness.

The above can be rewritten as:

$$c = \left[\frac{1}{H} \left(1 - \frac{S_f}{TUS} \right) \right]^{1/2} \quad (1A)$$

Application of the stated relationship can be used to estimate the critical half-crack length associated with an inelastic liner stress state.

If the liner stress at the pressurization condition being evaluated is less than the tensile yield strength, an estimate of the critical flaw size can be made by applying the following equation which defines plane strain fracture toughness:

$$K_{IC} = S_f \sqrt{\pi c} \quad (2)$$

where,

K_{IC} = plane strain fracture toughness

and S_f and c are as previously defined.

Usually, the liner thickness will not be sufficient to satisfy the criteria for plane strain conditions to exist. In these instances when the sample is thin and the degree of plastic constraint acting at the crack tip is minimal, plane stress conditions prevail and the metal liner will exhibit greater toughness. Therefore, the actual value of c which is calculated is not valid; however, a conservative value is quickly determined. This check is simplified since values of plane strain fracture toughness, K_{IC} , are generally available for most commonly used metal liner materials since this is a material constant which is not dependent on specimen geometry. The plane stress fracture toughness, K_C , is dependent on both the material and specimen geometry; and, therefore, a single value of this parameter for a given material does not exist.

The designer will usually determine as a result of the approximation of the half-crack length, c , which is approximately equal to the crack depth, a , that the dimension is greater than the metal liner thickness. This implies that the critical crack size is relatively large in comparison to the thickness and that any crack which is experiencing growth due to repeated loading will attain a breakthrough condition, i.e., leakage, prior to unstable crack growth. If the designer suspects unstable crack growth could occur prior to breakthrough and subsequent slow leakage, a dynamic analysis of the composite shell should be performed.

The approach described requires that the period of natural vibration for the composite shell be calculated. Next, the time required for the pressure induced liner loading to be relieved is estimated. A comparison of the time of energy release and the period of natural vibration for the composite shell will allow determination of the magnitude of the shock induced stress increase. Finally, the adequacy of the structure to withstand the potential occurrence of sudden liner failure is assessed.

The period of natural vibration for a complete spherical membrane shell can be found by applying the following equation:

$$\tau = 2\pi R \sqrt{\frac{(1-\nu)}{2E} \frac{\rho}{g}} \quad (3)$$

where,

τ = period of natural vibration
 R = radius
 E = tensile modulus of elasticity of composite
 ν = Poisson's ratio of composite
 ρ = density of composite
 and, g = acceleration of gravity

Relationships for cylindrical shell geometries as well as shells with bending resistance are contained in reference [7].

The crack tip velocity approaches the speed of sound in the material which is:

$$c = \sqrt{\frac{Eg}{\rho}} \quad (4)$$

where, c = speed of sound
 and, E , g , and ρ are as defined above

It is necessary for the designer to assume an approximate distance at which the crack propagation would terminate. This will depend largely on the amount of available strain energy which is stored in the metal

liner. It is usually discovered that the time of energy release is substantially less than the period of natural vibration for the composite shell. Therefore, the effect of this sudden shock is to induce a dynamic load into the composite which is up to two times the amount of contained pressure loading which is carried by the metal liner prior to failure. The shock spectrum for a step-ramp function as a function of time, t_1 , divided by the period of natural vibration, τ , is presented graphically in reference [8]. Once the amount of additional load is determined, the designer can easily calculate the corresponding maximum stress in the shell and demonstrate design adequacy.

The sequence of design events which have been described is shown in Figure 1. Both possible redesign phases would undoubtedly require consideration of the addition of composite overwrap material, since in each instance, lowered stresses within the composite shell would be needed to permit confirmation of the desired leakage failure mode.

Finally, the application of the above described procedure will be illustrated by considering a possible design. Representative performance requirements and a physical description of the selected design are contained in Table I. Also contained in Table I are the liner and composite stresses at proof pressure and at maximum operating pressure. Cycle lives for both the composite and liner have been calculated and these are also contained in Table I.

A comparison of the cyclic fatigue lives indicates that the structure's life is limited by the metal liner.

$$\frac{\text{Fatigue life composite}}{\text{Fatigue life liner}} = \frac{20,000}{550} = 36$$

The values of liner stress contained in Table I are not the principal stresses, but are rather the values of stress intensity which are determined by applying the following equation:

$$S_f = \frac{1}{\sqrt{2}} \left[(\sigma_m - \sigma_\theta)^2 + (\sigma_\theta - \sigma_z)^2 + (\sigma_z - \sigma_m)^2 \right]^{1/2} \quad (5)$$

where,

σ_m , σ_θ , and σ_z are stresses in the meridional, circumferential and radial directions, respectively

The use of an effective stress is warranted due to the presence of a biaxial stress field. It will be noted that at the proof pressure level, the liner stress exceeds the yield strength of the liner material. This requires that equation (1A) be used to assess the ability of the proof test to screen critical flaws. Application of equation (1A) yields:

$$H = .112 \left[44 \text{ ksi} / 26.6 \text{ ksi} - \sqrt{\text{in.}} \right]^4$$

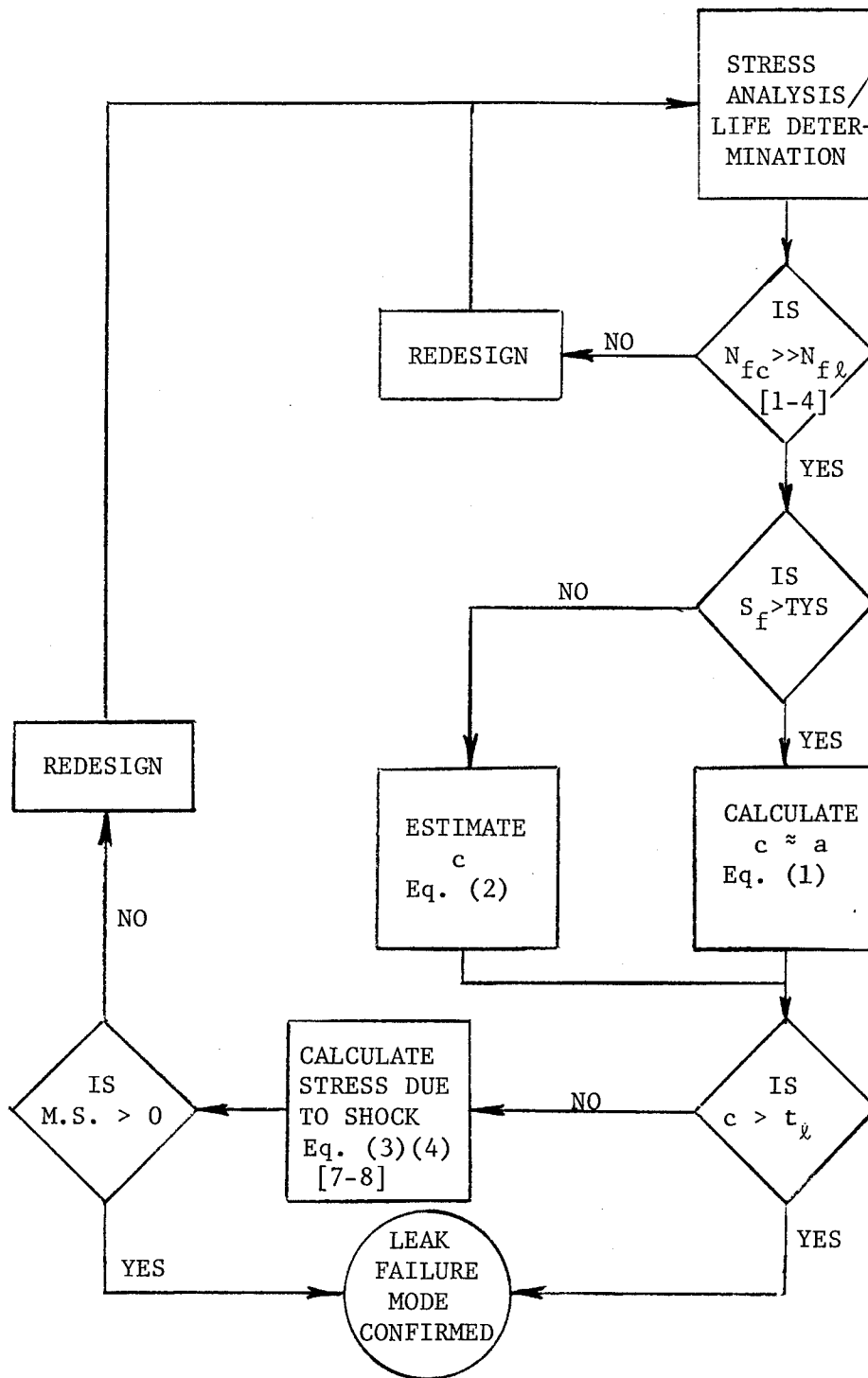


Figure 1. Design Flow Diagram

TABLE I
DESIGN PARAMETERS

Example Tank

<u>Physical Description</u>	
Shape	Spherical
Composite material	S-glass/epoxy
Liner material	6061-T6 aluminum alloy
Radius (mean), R	5.14 inches (130 mm)
Composite thickness, t_c	.460 inches (11.7 mm)
Liner thickness, t_l	.050 inches (1.27 mm)
Proof pressure, P'_{fl}	9,000 psig (62.05 MPa)
Operating pressure, P	6,000 psig (41.34 MPa)
<u>Liner Material Properties (typical)</u>	
Tensile yield strength, TYS	38 ksi (262 MPa)
Tensile ultimate strength, TUS	44 ksi (303 MPa)
Fracture toughness, K_{fI}	26.6 ksi $\sqrt{\text{in.}}$ (29.2 MPa $\sqrt{\text{m}}$)
Modulus of elasticity, E	10,000 ksi (68.9 GPa)
Poisson's ratio, ν	.33
Density, ρ	.10 lb./in. ³ (2.77 gm/cc)
<u>Performance Characteristics</u>	
Liner stress { at proof, S_f' { at oper., S_f	41.6 ksi (286.8 MPa) 32.1 ksi (221.3 MPa)
Composite stress { at proof { at oper.	46.7 ksi (322.0 MPa) 30.7 ksi (211.7 MPa)
Percent load carried { at proof by liner { at oper.	7.0 percent 8.5 percent
Liner cycle life, 0-oper.-0, N_{fll}	550 cycles
Composite cycle life, 0-oper.-0, N_{fc}	20,000 cycles

$$= .838 \text{ in.}^{-2} (.0013 \text{ mm}^{-2})$$

and

$$c = \left[\frac{1}{.838 \text{ in.}^{-2}} \left(1 - \frac{41.6 \text{ ksi}}{44 \text{ ksi}} \right) \right]^{1/2} = .255 \text{ in. (6.48 mm)}$$

From the approximate flaw size calculated, it is evident that the proof test will not screen defects with dimensions less than the wall thickness. Consequently, the assurance of safe life during subsequent cycling is dependent on a realistic evaluation of crack growth. It is also evident that for the operational cycles after a proof test, the critical failure condition is crack breakthrough and subsequent liner leakage.

If the previous design were altered according to the tabulation below, a new assessment would be necessary.

	<u>Design per Table I</u>	<u>New Design</u>
Composite Material	S-glass/epoxy	Kevlar 49/epoxy
Composite Thickness	.46 in. (11.7 mm)	.20 in. (5.08 mm)
Liner Thickness	.05 in. (1.27 mm)	.25 in. (6.35 mm)

The new performance characteristics are as follows:

Liner stress { at proof, S_f'	42.0 ksi (289.6 MPa)
{ at oper., S_f	18.8 ksi (129.6 MPa)
Composite stress { at proof	74.3 ksi (512.3 MPa)
{ at oper.	61.0 ksi (420.6 MPa)
Percent load carried { at proof	35.7
by liner { at oper.	20.8
Liner cycle life, 0-oper.-0	2,000
Composite cycle life, 0-oper.-0	40,000

Again, a comparison of the cyclic fatigue lives indicates that the structure's life is limited by the metal liner.

$$\frac{\text{Fatigue life composite}}{\text{Fatigue life liner}} = \frac{40,000}{2,000} = 20$$

Application of equation (1A) for this design yields:

$$c = \left[\frac{1}{.838 \text{ in.}^{-2}} \left(1 - \frac{42 \text{ ksi}}{44 \text{ ksi}} \right) \right]^{1/2} = .233 \text{ in. (5.92 mm)}$$

In this instance, the critical flaw depth (assumed equal to the half-crack length) is seen to be approximately equal to the liner thickness.

To determine the condition in which a liner failure could cause rupture of the composite, a dynamic analysis of the composite shell will be performed by applying equations (3) and (4). The period of natural vibration of the composite shell is:

$$\tau = 2\pi(5.14 \text{ in.}) \left[\frac{(1 - .27)}{2(5.14 \times 10^6 \text{ psi})} \frac{.050 \text{ lb./in.}^3}{(32.2 \text{ ft./sec.}^2)(12 \text{ in./ft.})} \right]^{1/2}$$

$$= .98 \times 10^{-4} \text{ sec.}$$

The crack tip velocity approaches the speed of sound in the liner material which is

$$c = \left[\frac{(10 \times 10^6 \text{ psi})(32.2 \text{ ft./sec.}^2)(12 \text{ in./ft.})}{(.10 \text{ lb./in.}^3)} \right]^{1/2}$$

$$= .197 \times 10^6 \text{ in./sec. } (5.00 \times 10^6 \text{ mm/sec.})$$

It is assumed that the pressure is released when the crack has traveled one-fourth of the circumference from the site of failure initiation. The time required is:

$$\text{time, } t_1 = \frac{\pi R}{c} = \frac{\pi(5.14 \text{ in.})}{2(.197 \times 10^6 \text{ in./sec.})}$$

$$= .41 \times 10^{-4} \text{ sec.}$$

Because the time of energy release is substantially less than the period of natural vibration for the composite shell, the effect of this shock is to induce a dynamic load into the composite which is up to two times the amount which is carried by the liner prior to failure. The shock spectrum for a step-ramp function for $t_1/\tau = .41/.98$ would indicate a load factor of 1.8. Composite stresses at the proof pressure are tabulated below:

Nominal Composite Stresses at 9,000 psig (62.05 MPa)

Prior to liner failure	74.3 ksi (512.3 MPa)
At failure, no shock	115.6 ksi (797.0 MPa)
At failure, maximum shock	148.6 ksi (1,024.6 MPa)

Design allowable stress 104.0 ksi (717.1 MPa)

$$\text{M.S.} = \frac{104}{148.6} - 1 = -.30$$

Based on the above values of nominal composite stress, it is concluded that composite rupture would be possible at a pressure less than the stated proof pressure if the liner were to suddenly fail. Since this design provides a low overall margin of safety, this tank would not be considered safe and complete redesign would be deemed appropriate.

The above calculations have been included to familiarize the reader with the stated design techniques. It has been the author's experience, that all metal-lined composite tankage which has been designed and manufactured by the Brunswick Corporation for which similar analyses have been performed, have clearly satisfied the design requirements which provide assurance that the desired feature is present. These findings have been confirmed in all cases by destructive testing of replicate test articles. The described design approach is deemed highly valuable as a means of providing quantitative substantiation of a design claim and a means of predicting actual composite behavior at elevated stress levels at which time a composite failure could be influenced by the presence of a metal liner.

REFERENCES

1. Humphrey, W.D., and Foral, R.F., "Fatigue and Residual Strength Tests of Fiberglass Composite Pressure Vessels," ASME paper 74-PVP-47, presented at the Pressure Vessels and Piping Conference, Miami Beach, Florida, June 24-28, 1974.
2. Kevlar* 49 DP-01** Data Manual, E.I. duPont de Nemours and Company, Incorporated, Textile Fibers Department, Wilmington, Delaware, and updates.
3. Manson, S.S., Thermal Stress and Low-Cycle Fatigue, McGraw-Hill, New York, 1966.
4. Sandor, B.I., Fundamentals of Cyclic Stress and Strain, The University of Wisconsin Press, Madison, Wisconsin, 1972.
5. Bockrath, G.E., and Glasco, J.B., "A Theory of Ductile Fracture," MDC-G-2895, McDonnell Douglas Astronautics Company, August 1972.
6. Feddersen, C.E., "Fracture Behavior of Surface-Cracked Tension Elements," AIAA Journal, Volume 9, No. 12, December 1971, pp. 2309-2313.
7. Kraus, H., Thin Elastic Shells, John Wiley and Sons, New York, 1967.
8. Thomson, W.T., Vibration Theory and Applications, Prentice Hall, Incorporated, Englewood Cliffs, New Jersey, 1965.

* duPont trademark.

** Temporary designation for generic assigned by FTC.

Composite Materials in Recreational Equipment

David Ratchford
Marshall Vega Corporation
Marshall, Arkansas 72650

Abstract

The general requirements of materials for recreational equipment are discussed, these being high strength-to-weight ratio, fatigue resistance, the ability to store and release energy, durability, aesthetic acceptability, and manufacturing capability.

It is developed, by engineering analysis, that composites of glass fibers, graphite fibers, or their combination, bonded into a resinous matrix of thermo-setting polyester or epoxy are uniquely suited to these purposes. These composites have extremely high strength-to-weight ratio, excellent durability and excellent fatigue characteristics, all unaltered through wide environmental extremes. Additional advantages are that the flexural characteristics of the material can be designed, through stress-directed fibers, to suit the purpose; and that glass fibers are non-yielding, i.e., yield and ultimate strength are the same, meaning that lower safety factors can be used. Such composites are ideally suited for handling, for the storage and release of energy and for the durability required of rough treatment.

An important and large scale application is limbs for bows used in archery. Design parameters would be light weight, high strength, fatigue resistance and quick energy release.

The limbs may be solid FRP composites, or FRP composites in the form of "backing" which is laminated to wood cores. In either case the limb is formed to a taper in order to minimize weight and to reduce inertia and present a low profile to wind resistance upon release. Load requirements are almost purely flexural, therefore fiber orientation is 100% parallel to the longitudinal axis of the limb. Glass or graphite fiber content is usually in the order of 70%. The limb has a flexural strength of approximately 150,000 psi, and a flexural modulus of 5.5×10^6 psi. High heat-distortion resins are used so that the bow can be stored in automobile trunks where temperatures can go above 150°F. An aesthetically attractive, abrasive-resistant finish is usually applied to the limb.

Additional applications in archery are bows molded entirely in one piece, and arrow shafts.

SESSION 8

INDUSTRIAL APPLICATIONS AND DESIGN

Chairman: R. E. Maringer

Battelle Columbus Laboratories

HOLOGRAPHIC NONDESTRUCTIVE EVALUATION OF SPHERICAL KEVLAR/EPOXY PRESSURE VESSELS

D. M. Boyd and B. W. Maxfield
Lawrence Livermore Laboratory, University of California
Livermore, California 94550

Abstract: Three spherical kevlar/epoxy pressure vessels were evaluated using holographic interferometry. The holographic interferograms provide information on the failure modes, displacement profile, and possible fiber damage. The holograms show a symmetric anisotropic displacement pattern even though the vessels failed due to a leak in the aluminum mandrels. The presence of a biconvex fringe pattern found during the testing of vessel three is believed to indicate matrix crazing. This information would be useful for burst-type failure analysis. Holographic interferometry has been shown to supply information on the characteristics of kevlar/epoxy pressure vessels under stress.

Key words: composites; holography; interferometers; matrix crazing; nondestructive testing; pressure vessels.

Introduction

Although the properties of individual fibers and fiber bundles provide the basic information needed to design fiber reinforced pressure vessels, it is only through a combination of destructive and non-destructive evaluations of completely fabricated units that true vessel performance can be assessed. Holographic interferometry is one of the nondestructive testing techniques which has been used successfully in evaluating composite pressure vessels (1,2). The anisotropic expansion of these vessels is easily measured using the wide field of view surface displacement information available from holographic interferograms.

This paper reports on the use of holographic interferometry to examine three thin walled kevlar/epoxy pressure vessels. The information so obtained was evaluated both quantitatively and qualitatively; only minor differences in surface displacement patterns were evident. It is, however, demonstrated that both local matrix crazing and the anisotropic expansion of the vessels are easily measured by holographic interferometry. These results solidify the potential of holographic nondestructive testing for evaluating the strength and overall quality of kevlar/epoxy pressure vessels.

Pressure Vessel Design Information and Test Procedure

The three thin walled pressure vessels that we examined were fabricated from the organic fiber Kevlar 49 using the epoxy system DER 322 (Dow Chemical)/Jeffamine T-403 (Jefferson Chemical) in a 100/44.7 ratio. The 114 mm outer diameter pressure vessels were wound over 1 mm thick 1100 aluminum (hydroformed) spherical mandrels. Each mandrel has electron beam welds at the waist, the fill tube and the opposite pole plug. Further details on the construction of these NASA experimental gas storage vessels are contained in Ref. 3.

Holographic testing of the pressure vessels was performed in a high pressure cell having a fully equipped holography system with remotely operated laser shutter, multiple exposure plate holder, and gas and hydro pressure supply equipment. The optical configuration used in making the holograms is shown in Fig. 1. With this configuration, two holograms are made simultaneously such that nearly 360 degrees of the vessel can be examined. The multiple exposure plate holder allows for up to twelve double exposure holograms to be made remotely without changing the photographic plate (4).

All measurements described here were made using a double exposure holographic technique; each exposure was made at a constant pressure, P , with a small pressure increment, ΔP , between exposures. This procedure was repeated as the vessel was pressurized. The reconstruction of each double exposure hologram consists of an interference pattern superimposed upon an image of the object; we call this the fringe pattern.

All three vessels evaluated in this experiment have a design burst pressure of 34 MPa. In order to ensure that the fringe density in each reconstruction is not too high, the incremental change is limited to 170 kPa. Pressure vessels A and B had been pressurized previously to 20 MPa and 31 MPa respectively for acoustic emission testing prior to the holographic examination. Three different test cycles to 4.8, 22 and 31 MPa maximum pressure were run on these two vessels with several holograms being made during each pressurization cycle. The resulting measurements were then compared and evaluated seeking evidence for possible damage caused by the initial acoustic emission pressure test. The third vessel, previously unpressurized, began leaking at 13.8 MPa.

Results

The first series of tests on vessels A and B, which went to only a maximum pressure of 4.8 MPa, showed no significant differences between the vessels. As shown in Fig. 2a, the fringe pattern obtained for these vessels is nonsymmetric around the fill tube. Figure 2b is the fringe pattern of the same vessel after rotating 180 degrees

about the fill tube axis. The similarity between these two patterns shows that the displacement profile is symmetric about the two poles. The nonsymmetric fringe pattern is a simple consequence of vessel positioning during testing and is not due to the presence of a flaw. Figure 3 (a,b,c,d) gives typical fringe patterns for the second pressure test series on vessels A and B up to a maximum pressure of 22 MPa with the vessel arranged to view the waist region. The location of the waist weld in the aluminum liner is evident in Figs. 3a and 3c. As the pressure increases, the aluminum bladder yields and the effect of the bladder on the surface displacement is no longer seen, as shown in Figs. 3b and 3d. Previous examination of several aluminum bladders showed fringe patterns similar to Figs. 3a and 3c. Thus, the stronger waist weld region is displacing less than the remainder of the bladder prior to the onset of yield.

During this second test series, an LVDT displacement transducer was positioned to measure the radial expansion of the pressure vessels. Figure 4 is a plot of the relative displacement of the fill tube and waist regions versus pressure for vessels A and B. In these displacement plots, the change in slope occurring at 5.1 MPa is due to yielding of the aluminum liner. Vessel A registers a smaller displacement than vessel B because of plastic deformation following the higher prepressurization test (31 MPa versus 20 MPa for vessel B).

Figure 5 (a,b,c,d) shows the fringe pattern obtained during the second pressure cycle to 22 MPa for vessels A and B with vessel arranged so that the poles regions could be examined. The displacements are symmetric about the fill tube. The higher fringe density at the higher pressures for the same pressure increment is entirely consistent with the LVDT displacement measurements.

Converting the fringe pattern to a surface displacement vector is possible for a single view hologram only when the part geometry and the direction of displacement are known. Under the assumptions of radial expansion and collimated illumination, the surface displacement of a spherical pressure vessel is given by:

$$\Delta r = \frac{n\lambda}{2 \cos(\arcsin X_n/R)}$$

where n is the fringe number, λ is the wavelength of light, R is the radius of vessel and X_n is the distance from center of vessel to fringe n . These assumptions are reasonable for our vessel and optical configuration; in particular, illumination by a diverging beam produces less than a 3% error in Δr . Figure 6 shows the waist and pole-equator displacement profiles calculated for pressure vessel B. Note particularly that the fill tube region displaces twice as much as the waist region and that the displacement field is symmetric

about the fill tube.

In order to test the vessels at pressures closer to where burst is expected, a containment box with Lexan windows was placed over the vessel during the next pressure series. All vessels were repressurized in an attempt to produce limited damage to the kevlar fiber. Vessel A was pressurized to 31 MPa, held at pressure for 50 minutes and then depressurized. The fringe patterns resulting from subsequent pressurization to 7.0 and 27.7 MPa are shown in Fig. 7 (a,b,c,d). Leaking of hydraulic fluid (which obliterates the fringe pattern) from the pole opposite the fill tube is evident in Figs. 7c and 7d. The vessel does, however, appear to be maintaining its strength as indicated by the symmetric displacement.

Leaking occurred at 28.9 MPa during the testing of vessel B. Typical fringe patterns shown in Fig. 8 are strong evidence that this vessel is also maintaining its strength at these pressures. The location of the leaks in vessels A and B was found by gamma radiography after pressurizing the vessels with a radiographically opaque barium solution. Cracks in the aluminum liner at the plug weld opposite the fill tube was found to be the cause of leakage.

Pressure vessel C, which was also to have been tested to 31 MPa, began leaking at 13.8 MPa and the test was stopped. We interpret the fringe patterns obtained on a subsequent pressurization to indicate possible matrix damage. For example, Fig. 9a shows a discontinuity in the fringe pattern near the pole. At higher pressures, a biconvex fringe pattern develops, as shown in Fig. 9b. The discontinuity obvious in Fig. 9a turns out to be the starting site of the biconvex fringe pattern shown in Fig. 9b. The long axis of the biconvex pattern is aligned with the direction of the kevlar fiber winding pattern. Thus it appears that the low pressure (7 MPa) discontinuity may be due to matrix crazing. This is the subject of continuing investigation.

Discussion

This holographic evaluation of spherical kevlar/epoxy pressure vessels has provided information on three significant aspects of the pressure vessel design. First, the fringe patterns show that symmetric displacement patterns occur about the two poles. This symmetry is related to the fiber winding pattern and at the lower pressures is affected by the aluminum bladder (see Figs. 3 and 5). Although there is displacement symmetry, the fringe patterns are distinctly not symmetric. Displacement contours have been quantified as shown in Fig. 6. All three vessels show the pole region to have greater radial displacement than the weld region. Previous work shows a direct correlation between the higher displacement (stress) at the poles and the site of failure during burst tests (3). This indicates

that the fringe pattern around the poles might be a useful measure of either composite vessel performance or strength.

The second aspect of design confirmed by these tests is that failure of vessels may occur in two ways. Bursting, which was not studied in this sequence of measurements, is the result of failure of the kevlar/epoxy matrix under stress. In these tests, failure was due to cracks in the aluminum liner which resulted in fluid leakage. Although the vessels leaked during pressurization, the location of the crack in the liner is not readily identifiable from the fringe patterns. The visible portions of the fringe patterns indicate that these vessels were maintaining strength (see in Figs. 7 and 8) even though the liners were leaking.

Thirdly, we wish to point out the significance of the biconvex fringe pattern found during the testing of vessel C. This biconvex pattern is occurring at lower pressures where delamination and fiber breakage do not normally occur. In addition, the pattern is aligned with the winding direction. Thus, the biconvex pattern may be associated with matrix crazing produced by the initial pressurization (in this case, to 13.8 MPa). The quantity and location of these patterns might prove useful in predicting the stress resistance of vessels. A combined test program of acoustic emission and holographic interferometry on parts having no previous stress (pressure) history should now be made in order to have a more controlled and easily interpretable set of measurements.

Conclusion

A comparison of fringe patterns showed only minor variation in the displacement profiles of three spherical, kevlar/epoxy pressure vessels. Three characteristics of the kevlar/epoxy pressure vessels were obtained from the holographic tests. The failure of all vessels was due to a leak in the aluminum liner and not by bursting. The fringe patterns provide displacement profiles showing areas of high stress and show that vessels expand with axial symmetry during pressurization. The presence of a biconvex fringe pattern is believed to be a result of matrix crazing. Further testing will be performed using combined holographic interferometry and acoustic emission to better characterize spherical kevlar/epoxy pressure vessels. The results of further testing may find a means of nondestructively evaluating composite pressure vessels during a proof test pressure cycle.

Acknowledgment

This work was performed under the auspices of the U.S. Department of Energy by the Lawrence Livermore Laboratory under Contract No.

W-7405-Eng-78. We thank Bill Billings, Ken Harrison, and W. W. Wilcox, Lawrence Livermore Laboratories, for their assistance in performing the experimental work.

References

- 1) Meyer, M.D. and Katayanagi, T.E. "Holographic Examination of a Composite Pressure Vessel," Journal of Testing and Evaluation, Vol. 5, No. 1, Jan. 1977, pp 47-52.
- 2) Erf, R.K. "Solid Propellant Rocket Inspection", Holographic Nondestructive Testing, edited by Robert K. Erf, Academic Press, New York, 1974, pp 365-372.
- 3) Hamstad, M.A. "Variabilities Detected by Acoustic Emission from Filament Wound Aromid Fiber/Epoxy Composite Pressure Vessels," UCRL-86268, Lawrence Livermore Laboratory, Livermore, California, Nov. 30, 1977.
- 4) Multiple exposure plate holder designed by W. Jorgenson of Sandia Corporation, Livermore, California.

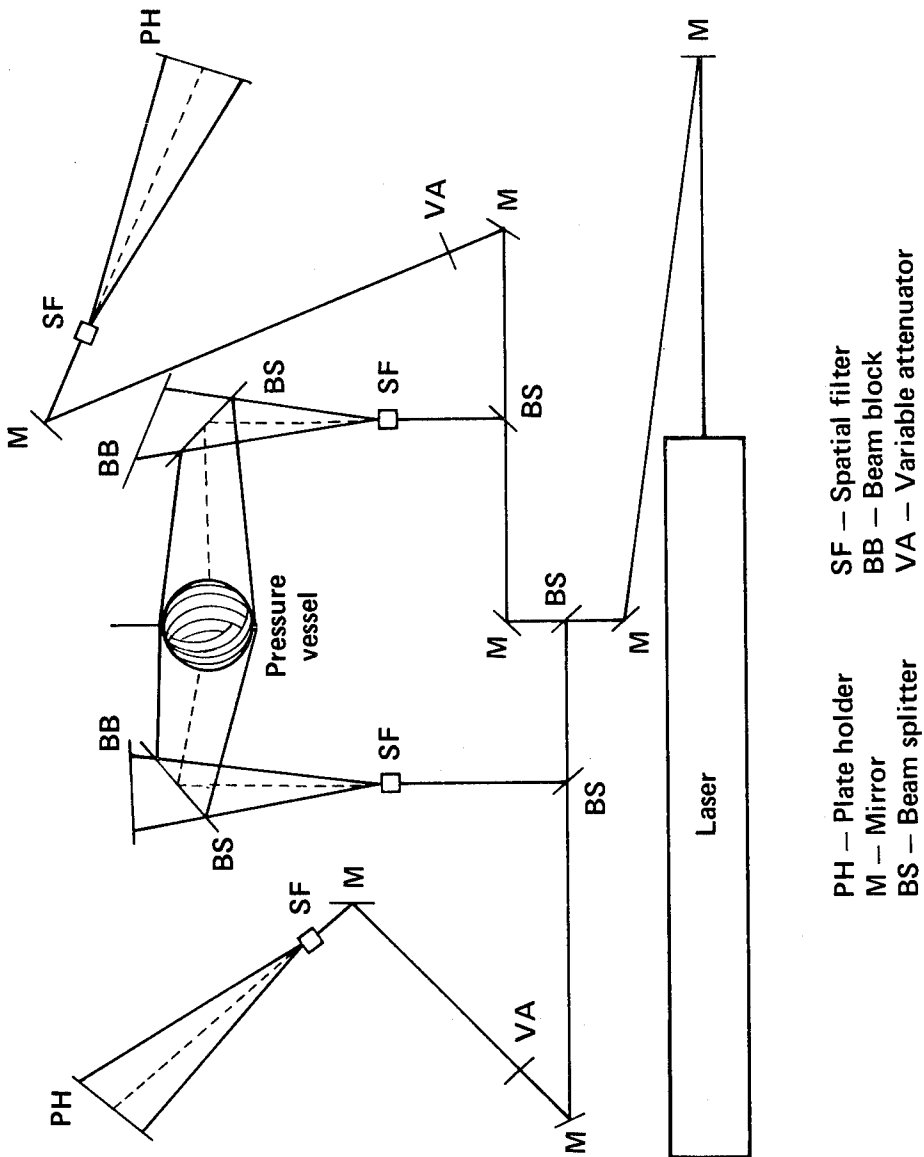
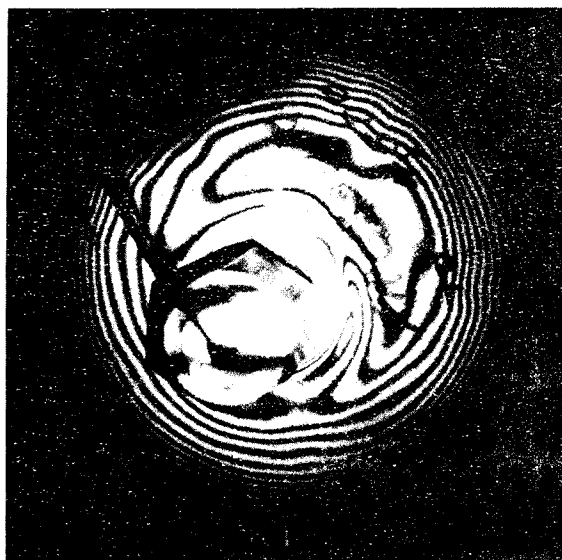
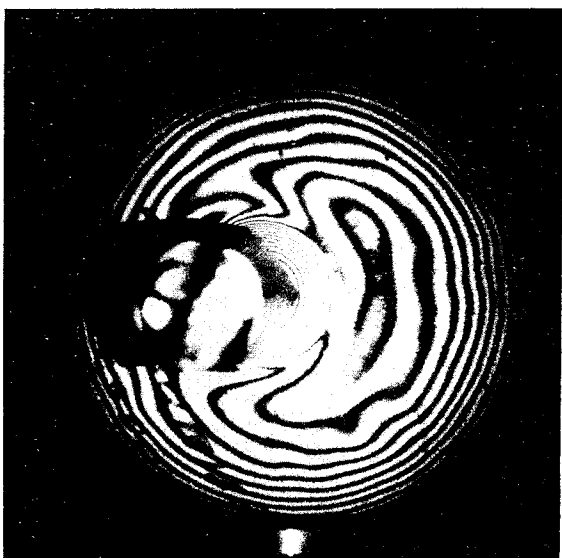


Fig. 1 Holographic interferometer optical configuration; the illumination beam half angle is about 8 degrees.

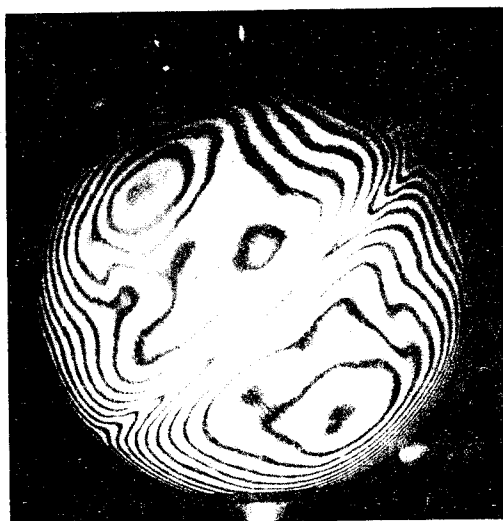


a)

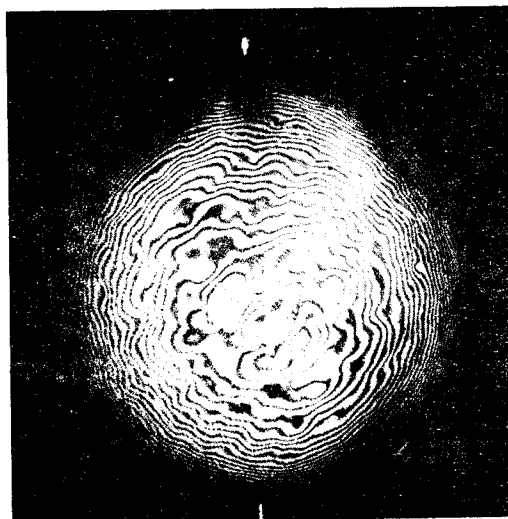


b)

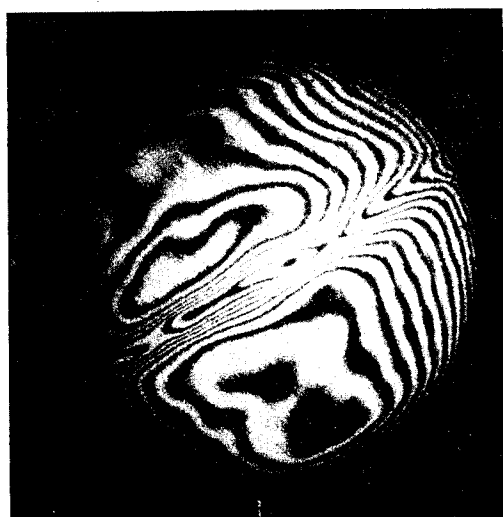
Fig. 2 Low pressure fringe pattern for Vessel A; $P = 4.5$ MPa, $\Delta P = 0.3$ MPa: (a) viewed from the fill tube end and (b) after rotation of vessel by 180 degrees about the fill tube.



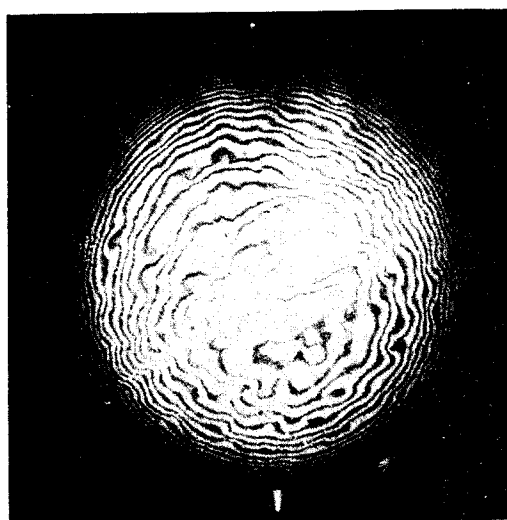
(a)



(b)



(c)



(d)

Fig. 3 Fringe patterns showing the effect of the welded waist for Vessels A and B: (a) Vessel A; $P = 3.9$ MPa, $\Delta P = 0.2$ MPa, (b) Vessel A; $P = 20.7$ MPa, $\Delta P = 0.2$ MPa, (c) Vessel B; $P = 3.9$ MPa, $\Delta P = 0.2$ MPa (d) Vessel B; $P = 20.7$ MPa, $\Delta P = 0.2$ MPa.

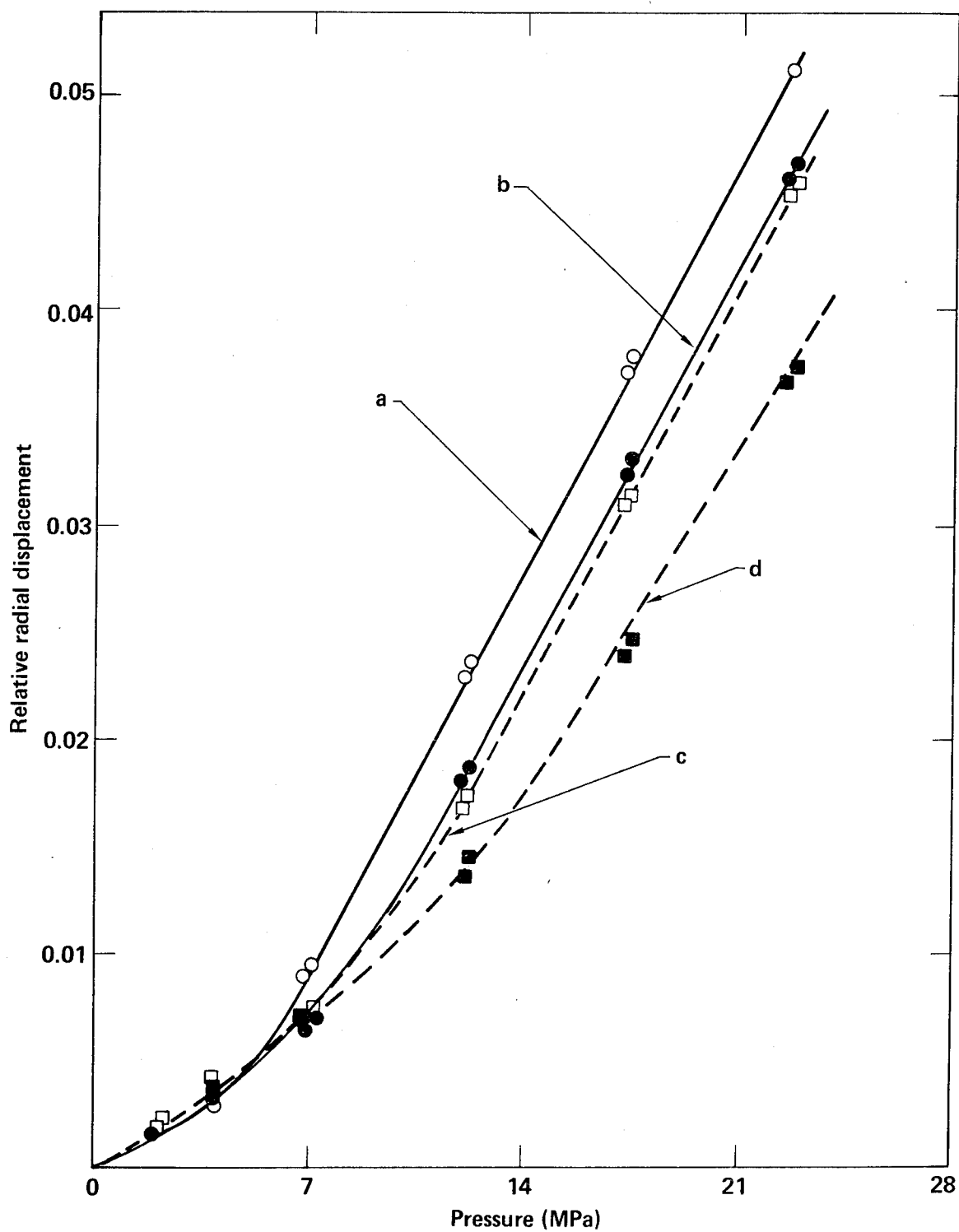
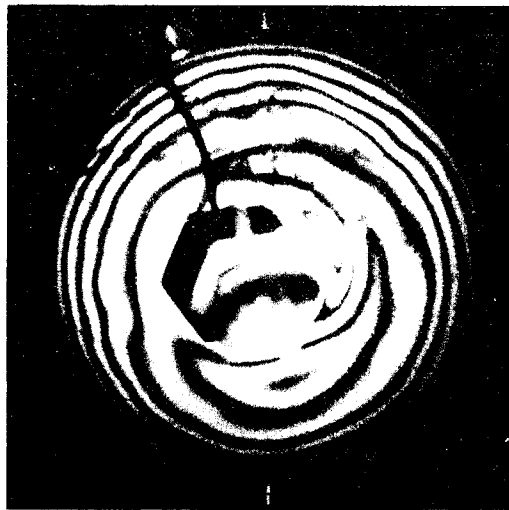
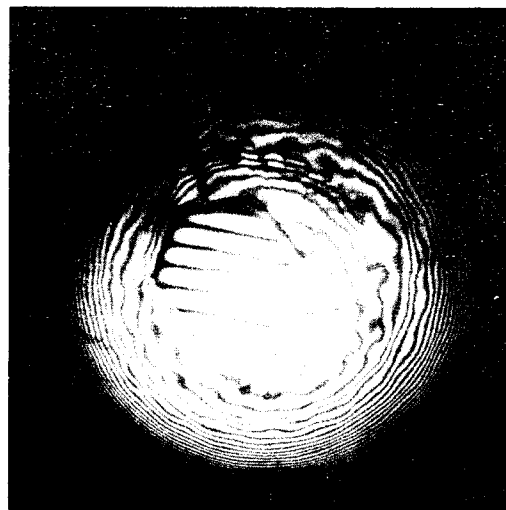


Fig. 4 Relative radial displacement versus pressure for vessels A and B: (a) pole of Vessel B, (b) pole of Vessel A, (c) waist of Vessel B, (d) waist of Vessel A.



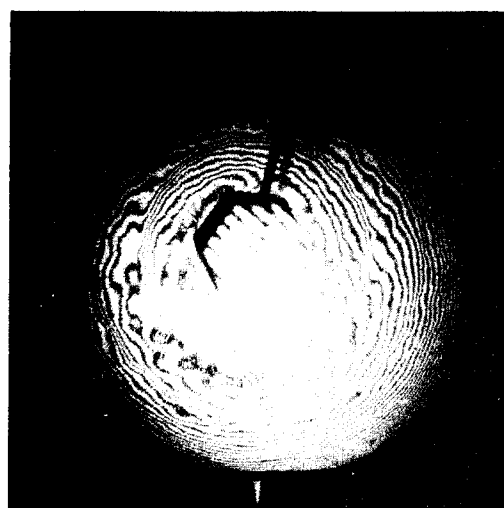
(a)



(b)

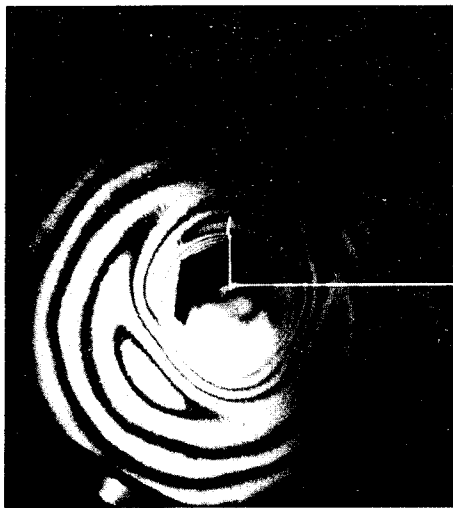


(c)

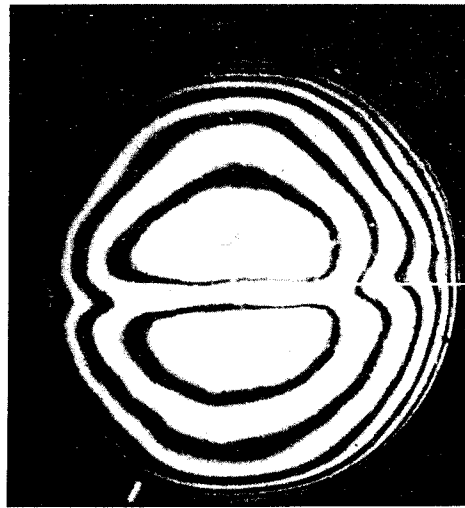


(d)

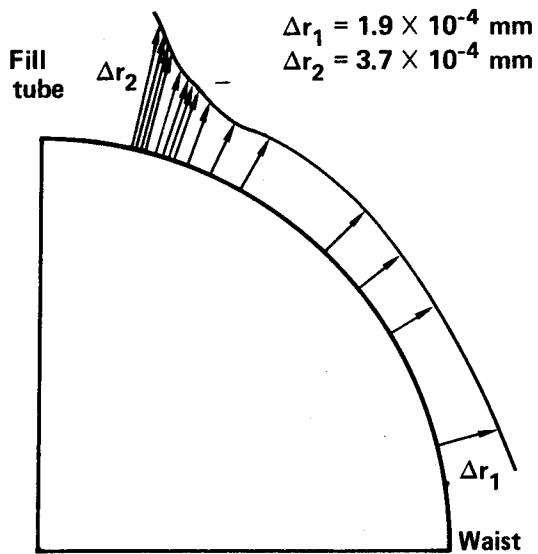
Fig. 5 Fringe patterns showing the increase in fringe density at low and high pressures for the same pressure increment of 0.2 MPa: (a) Vessel A; $P = 3.9$ MPa, (b) Vessel A; $P = 20.7$ MPa, (c) Vessel B; $P = 3.9$ MPa, (d) Vessel B; $P = 20.7$ MPa.



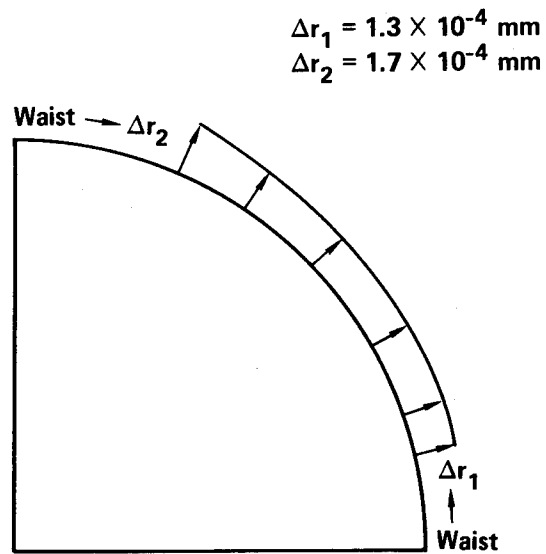
(a)



(c)

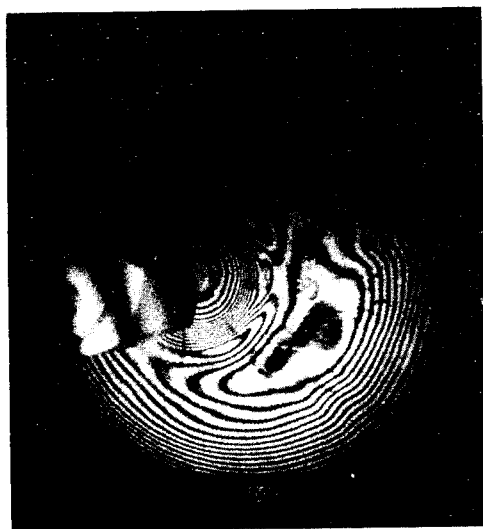


(b)

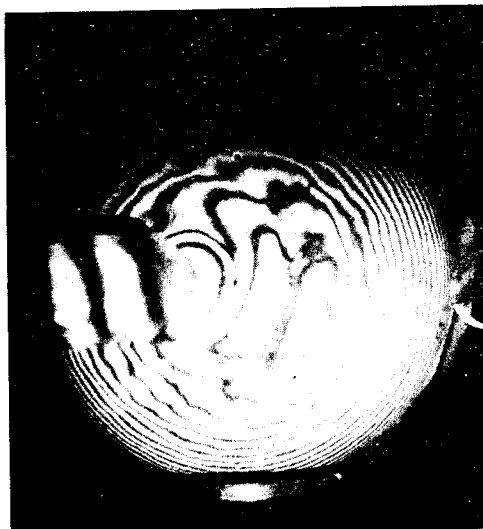


(d)

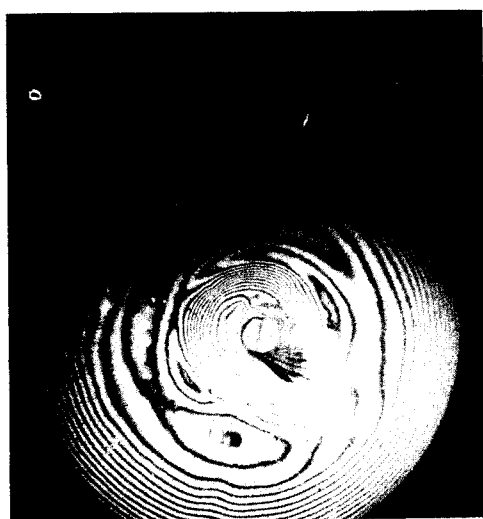
Fig. 6 Fringe patterns and the resulting radial displacement contours for Vessel B; $P = 3.9 \text{ MPa}$, $\Delta P = 0.2 \text{ MPa}$, (a) fill tube to waist along indicated contour, (b) around waist weld equator along indicated contour.



(a)



(b)

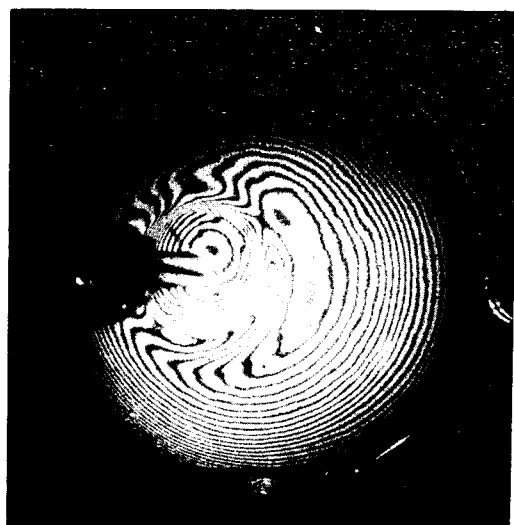


(c)

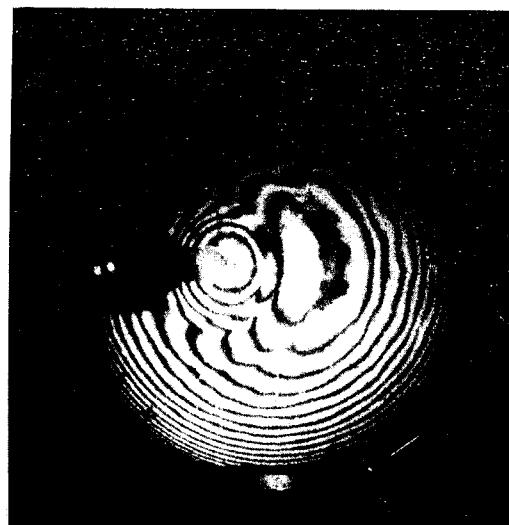


(d)

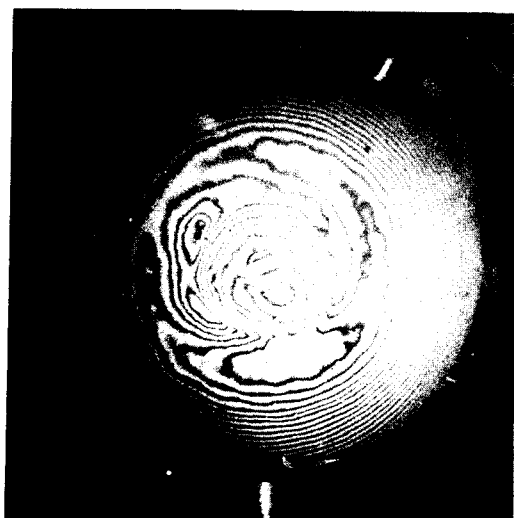
Fig. 7 Fringe patterns from Vessel A after pressurization to 31 MPa showing evidence of leak near the pole opposite the fill tube: (a) fill tube pole; $P = 6.9$ MPa, $\Delta P = 0.2$ MPa, (b) fill tube pole; $P = 27.6$ MPa, $\Delta P = 0.2$ MPa, (c) opposite pole; $P = 6.9$ MPa, $\Delta P = 0.2$ MPa (note leakage) (d) opposite pole; $P = 27.6$ MPa, $\Delta P = 0.2$ MPa (note leakage).



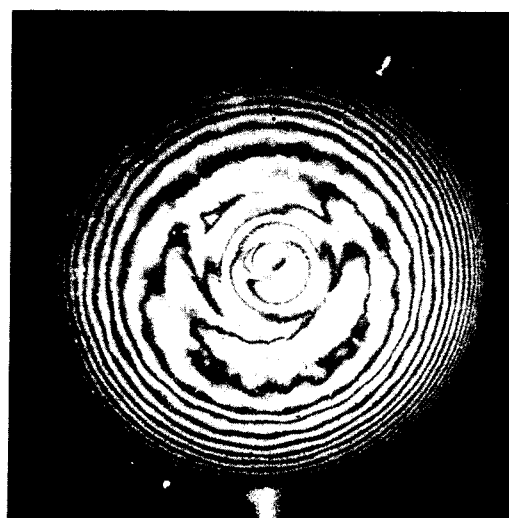
(a)



(b)

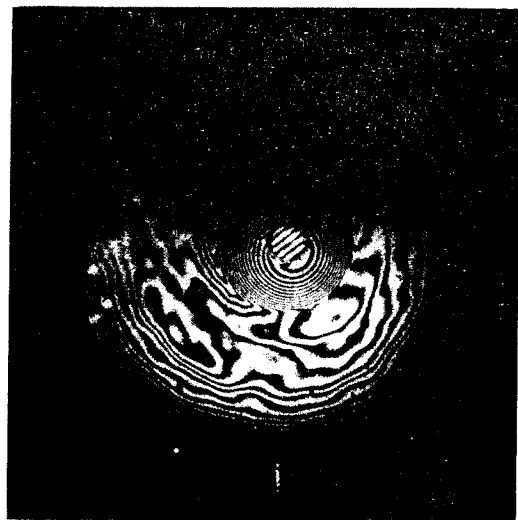


(c)

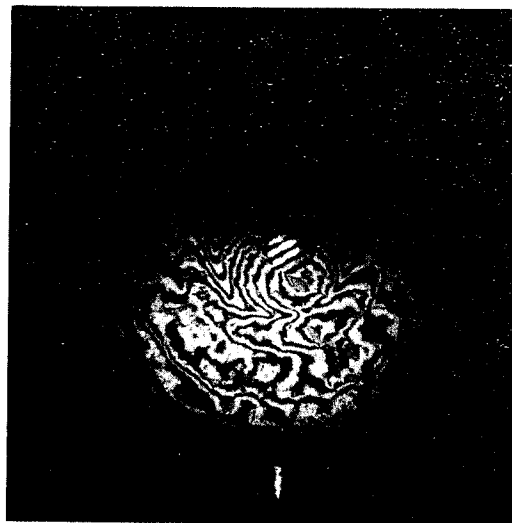


(d)

Fig. 8 Fringe patterns of Vessel B after pressurization to 31 MPa showing both poles prior to onset of leakage at 28.9 MPa: (a) fill tube pole; $P = 10.3$ MPa, $\Delta P = 0.2$ MPa, (b) fill tube pole; $P = 27.6$ MPa, $\Delta P = 0.2$ MPa (c) opposite pole; $P = 10.3$ MPa, $\Delta P = 0.2$ MPa.



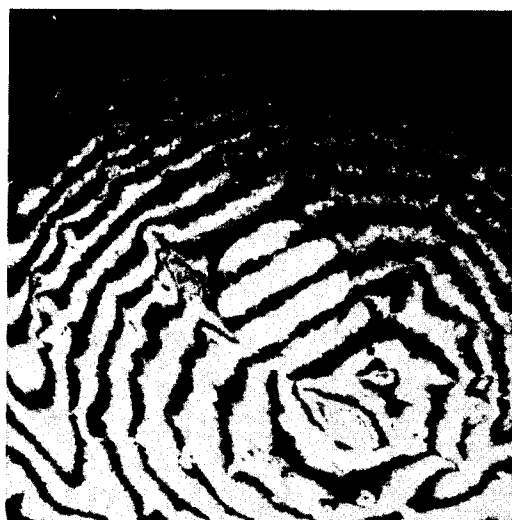
(a)



(b)



(c)



(d)

Fig. 9 Fringe patterns showing locations of possible matrix crazing after pressurization of Vessel C to 13.8 MPa: (a) opposite pole; $P = 6.9$ MPa, $\Delta P = 0.2$ MPa with $4\times$ magnification of the central region with discontinuity in the fringe pattern and (b) opposite pole; $P = 10.3$ MPa, $\Delta P = 0.2$ MPa with $4\times$ magnification of central region showing the typical biconvex fringe pattern which starts at the discontinuity described in (a) above.

The Air Force "Manufacturing Cost/Design Guide (MC/DG)"

Bryan R. Noton
Battelle Columbus Laboratories
Columbus, Ohio 43201

Captain Dan L. Shunk
Wright Patterson Air Force Base
Wright Patterson Air Force Base, Ohio 45433

Abstract

The purpose of the MC/DG is to enable designers at all levels to conduct, firstly, urgently needed, quick, simple, cost-trade comparisons of manufacturing processes, and, secondly, structural performance/cost trade-offs on both components and subassemblies. The MC/DG will consist of two volumes--"Airframe Structure" and "Manufacturing Technologies". The MC/DG is being developed for the Air Force by a team consisting of Battelle's Columbus Laboratories (BCL) and the following aerospace companies:

General Dynamics Corporation, Fort Worth Division
Grumman Aerospace Corporation
Lockheed-California Company
Northrop Corporation, Aircraft Group
Rockwell International Corporation, Los Angeles Division

The Boeing Commercial Airplane Company is participating in a critique mode.

Two contracts have been awarded on the MC/DG. The first program (Contract No. F33615-75-C-5194) was completed in July, 1976, and is reported in AFML-TR-76-227. The objectives were to:

- Identify the data requirements for both conventional and emerging manufacturing methods
- Identify the basic format design criteria and the formats for each MC/DG manufacturing technology section
- Prepare a detailed model of the complete MC/DG for industry examination
- Prepare an MC/DG implementation plan to collect and develop data in the identified formats.

The objectives of the second contract, a 15-month program, awarded in September, 1977, are to develop certain sections of the MC/DG for demonstration. These sections are:

- Phase I: "Sheet-Metal Aerospace Discrete Parts"
- Phase II(a): "First-Level Mechanically-Fastened Assemblies"
- Phase II(b): "Advanced Composite Fabrication"
- Phase III: "Trade-Off Study on Fuselage Shear Panel".

This paper will present the results from each of the above phases and the utilization of the MC/DG sections in design studies involving metallic and non-metallic structures.

TENSILE STRENGTH AND FAILURE MODES
OF BORON-EPOXY COMPOSITE WITH A NOTCH

Charles E. S. Ueng
Georgia Institute of Technology
Atlanta, Georgia 30332

Abstract: The purpose of this paper is to study the tensile strength and failure modes of boron-epoxy composites with an edged notch. Through the use of finite element crack program, both heterogeneity and orthotropy of material properties are brought into consideration in this paper. For comparison purposes, tension tests of actual composite samples with notches are also performed. Notch insensitivity and the failure modes are discussed. The fracture toughness of the test material is also determined. The results obtained here are important for further understanding of the failure of unidirectional boron-epoxy advanced composites.

Key words: Boron-epoxy; edge cracks; failure modes; finite element method; tensile strength.

1. Introduction:

Due to the increased use of modern composite materials in structural applications, there has been a growing interest in the study of fracture of composites. Three basic approaches are generally available: (1) a statistical theory to predict the number of cut fibers in a simple composite structure and to investigate what effects these broken fibers have on structural strength; (2) extension of linear-elastic fracture mechanics theory to orthotropic or anisotropic materials and then to fibrous composites; and (3) study of cracks in a heterogeneous material or at an interface and the extension of that theory to the case of a fibrous composite. Rosen and Dow [1] and Zweben [2] have researched a statistical approach to investigate the fracture of composites. It was noted in [2] that a drastic reduction in composite strength would take place when only a few fibers are cut in a theoretical and hypothetical model. In some early research on the fracture of orthotropic materials, Sih, Paris and Irwin [3] noted that "for problems involving self-equilibrating loads, the stress intensity factors are the same for both isotropic and anisotropic materials". But this has been shown [4,5,6] not to be always the case. The investigation of a crack at or near an interface between dissimilar materials has been reported in [4,7,8]. Erdogan [7] found that for cracks at or near a bi-material interface, mostly aluminum-epoxy, the power of the singularity at the crack tip ranged between zero and one, depending on

the crack direction and loading condition. In the case of an isotropic material, there is always a square root singularity regardless of loading condition as noted in one of the earliest investigation on cracks by Williams [9]. Olster and Jones [8] reported that for cracks perpendicular to the fibers in a composite, the toughness increased in proportion to the debonding, implying that a weak interface is desirable for increased toughness. They also found that in a multidirectionally reinforced composite, the toughness is primarily controlled by those filaments most nearly perpendicular to the crack. Cooper and Kelly [10] experimentally investigated the conditions under which a notch-insensitive composite could be produced and attempted to predict the values of the work of fracture for a notch-sensitive material. They noted that an important function of the matrix lies in increasing the work of fracture by plastic flow, or other means, rather than by acting as a physical barrier to crack growth. They discovered that notch-insensitivity could be accomplished if splitting parallel to the fibers at the notch is complete. Hoover and Allred [11] observed that changes in crack length do not significantly alter the delamination process and the consequent notch insensitivity in single edge notch specimens of Borsic-Al composites with weak fiber-matrix bonds. Mandell, Wang and McGarry [12] investigated the size and character of the damage zone at the tip of sharp notches in fiber reinforced laminates. The damage zone was found to increase in extent approximately in proportion to K_I^2 up to fracture for notch-sensitive laminates. But for notch-insensitive laminates this zone reaches a critical stage then it rapidly spreads completely across the specimen.

The motivation of this research was to incorporate both heterogeneity and orthotropy into a study of an edge crack or an edge notch in a unidirectional boron-epoxy composite to see what effect heterogeneity would have in the neighborhood of a crack. Tension tests were performed on notched specimens in order to determine the mode of failure and the failure load. A finite element model of this composite was made which took into account the effects of layering and heterogeneity in the neighborhood of the crack and orthotropy away from the crack. Certain preliminary results of this research project were previously reported in [13].

2. Experimental Work:

Test samples of Avco Rigidite 5505/4 boron-epoxy composite were provided by the Lockheed Georgia Company. Figure 1 shows all the dimensions. The percent of boron by volume in the specimens was 50.2. The boron had a tensile modulus of $58(10)^6$ psi (400 GN/m^2) and a Poisson's ratio of 0.208. The epoxy had a tensile modulus of $0.45(10)^6$ psi (3.10 GN/m^2) and a Poisson's ratio of approximately 0.351. The composite had a tensile modulus of $30.9(10)^6$ psi (213 GN/m^2) and a Poisson's ratio of 0.256 as given by the furnished data from Lockheed. A $3/8$ " diameter hole (9.5mm) was drilled through each end of the specimens in order to load them in axial tension with dowel pins. But it turned out

to be unsatisfactory because the first piece tested failed by debonding around the upper hole (Fig. 2). Consequently, tension grips were used for the remaining tests. 1/4" deep edge notches (6.4 mm) were cut by a carbon-phenolic abrasive wheel on a milling machine. Originally, it was planned to cycle all specimens in order to start the crack growing from the notches. One piece was cycled between 100 lb. (45.4 kg) and 1,200 lb. (544.3 kg) at a rate approximately 36 cycles per minute. Instead of starting a crack, the cycling served to debond the specimen vertically at the notch tip (Fig. 3). After about 30,000 cycles, it showed a clear line of debonding for about 1 5/16" (33 mm) long on both sides of the notch. This phenomenon indicated that the specimen was notch-insensitive, so the cycling plan was discontinued.

The specimens, including the cycled piece, were failed in simple tension using a universal testing machine with tension grips. It is interesting to note that the cycled piece failed in the same manner as the uncycled pieces. The first failure noted on all the notched specimens was a complete vertical debonding through the thickness at the notch tip (Fig. 4) at an average load of 3,200 lb. (1,470 kg). The average load at complete failure was 11,900 lb. (5,410 kg). For comparative purposes, three unnotched specimens were also failed in the same manner. Internal failures were seen at loads as low as 3,320 lb. (1,510 kg). Complete failure was in the same manner as for the notched specimens (Fig. 5) at an average load of 13,500 lb. (6,140 kg). Table 1 presents, for each specimen, the load at which notch debonding occurred (for the notched specimens), the smallest load at which internal failure (load-dropping point) was noted, and the load at total failure.

Table 1 Test Results

Piece	Notch Debonding	Earliest Internal Failure	Total Failure
1	4000 lb. (1814 kg)	6400 lb. (2903 kg)	12,580 lb. (5706 kg)
2	4000 (1814)	7000 (3175)	10,540 (4781)
3	3000 (1361)	6600 (2994)	12,320 (5588)
4	2400 (1089)	5400 (2449)	12,060 (5470)
5	2600 (1179)	7000 (3175)	11,940 (5416)
6*	----	9320 (4228)	13,800 (6260)
7*	----	4600 (2089)	13,120 (5951)
8*	----	3320 (1506)	13,620 (6178)

3. Finite Element Analysis

A finite element computer program capable of characterizing the crack-tip singularities was used to investigate the failure of a unidirectional boron-epoxy composite with an edge crack. Due to symmetry of the loading condition, only half of the specimen (2" x 4 1/2", or 55mm x 114mm)

needed to be modeled. This area was divided into constant strain triangles and material constants were assigned to each triangle. Away from the tip, the material constants of the composite were assigned to the triangle elements of the full thickness, 0.040" (1mm). In the vicinity of the crack tip, the boron and epoxy were modeled as separate entities and the layering was taken into account. This was accomplished by stacking eight triangles of 0.005" (0.13mm) thickness and 0.004" (0.1mm) width one on top of another in the crack tip region and alternating layers between boron and epoxy in sort of a three dimensional checkerboard fashion. The fibers, in other words, were approximated by rectangular prisms rather than circular prisms. This modeling was feasible because of the relatively large fibers (0.004" or 0.1mm in diameter). The purpose in modeling the composite in this fashion was to take into account heterogeneity in the crack tip region, the region in which it is felt most. The finite element grid is shown in Fig. 6. In the shaded area, the boron and epoxy were modeled separately and layering was taken into account. The crack element (8 elements actually) is centered at the bottom of the grid in the detailed diagram. A unit displacement was imposed along the top of the specimen and the resulting stresses along the top and the stress intensity factor were determined by the program. The relationship between the average mode-one stress intensity factor (K_I) and the applied stress (σ) was

$$K_I = 0.959 \sigma$$

for a 1/4 inch (6.4mm) crack. The stress intensity factor in the boron crack elements was

$$K_I = 1.904 \sigma$$

and in the epoxy elements it was

$$K_I = 0.014 \sigma$$

It should be noted that in practice, the strength of the composite will be governed by the strength of the boron and hence the stress intensity factor in the boron crack elements should be used as the governing stress intensity factor.

The stress results around the crack tip were also documented. Table 2 shows such data, where the origin is placed at the left free edge.

Table 2 Averaged Stress Around the Crack Tip

x	0.2453"	0.2473	0.2486	0.2500	0.2513	0.2526	0.2546
	(6.23mm)	(6.28)	(6.31)	(6.35)	(6.38)	(6.42)	(6.47)
σ	-290 psi	-220	+5850	+3830	+6640	+4850	+3700
at $y=0$	(-2.00MN/m ²)	(-1.52)	(+40.3)	(+26.4)	(+45.8)	(+33.4)	(+25.5)

It is interesting to note that the maximum value of σ_x , 6,640 psi (45.8 MN/_m²), due to an average load when the notch debonding was observed, is about 2/3 of the tensile strength of the epoxy, 10,000 psi (69.0 MN/_m²). Also, the zig-zag stress distribution would not have been obtained if the heterogeneity were not included.

4. Discussions and Conclusions:

Based on the results reported here, the following observations can be made:

- (1) The failure of the boron-epoxy composite is not by transverse fracture at the notch tip as in isotropic materials;
- (2) The failure of a dowel pin as observed here may mean that the stress concentration is higher there than at the notched tip. From the failure prevention point of view, a concentrated load in a hole would be of more concern than an edge notch;
- (3) The notch insensitivity as noted during the cycling operation, indicates that fracture criteria normally associated with isotropic materials does not adequately predict the failure of the composite studied here. The randomness of the failure as represented by Fig. 5 supports this assumption. It appears that the notch insensitivity and failure by debonding are due to the high fiber volume fraction and apparently low bond strength between the fibers and matrix;
- (4) The maximum stress $\sigma_x = 6,640$ psi (45.8 MN/_m²) occurred immediately to the right of the notch tip, and is about 2/3 of the tensile strength of the epoxy. This deviation may be caused by differences in the properties of the epoxy in bulk form compared to a small amount located between two boron fibers. From the fairly high value of σ_x , it is expected that longitudinal cracking is incipient in this investigation; and
- (5) Based upon the information on the average failure loads between the notched and unnotched specimens, 11,880 lb. versus 13,513 lb. (5,404 kg vs. 6,142 kg), it is interesting to note that the former value can be obtained by a proportion if the length of the crack is deducted from the width of the specimen. In other words, it can be concluded that the presence of the notch introduces no stress singularity in the remaining unnotched material.

Furthermore, a fracture toughness, or critical stress intensity factor, of the specimens tested may be calculated. Using the stress intensity factor in the boron cracked elements, $K_{IC} = 1.904\sigma$, and the average failure load of the notched specimens, 11,888 lb. (5,404 kg), the fracture toughness obtained is

$$K_{IC} = 283,000 \text{ psi } \sqrt{\text{in.}}$$

for a 2" (51 mm) by 0.040" (1 mm) cross-section. Using the failure load of the unnotched specimens tested, 13,513 lb. (6,132 kg), an ultimate tensile stress of 168,900 psi is obtained for the material based upon a 2" (51 mm) by 0.040" (1mm) cross-section. Following the example of Mandell et al [12], the ratio of fracture toughness to ultimate tensile stress for the material tested here is $1.68\sqrt{\text{in}}$. For the same material in a 90/0/0/90 ply configuration, they obtained a value of $0.32\sqrt{\text{in}}$. (Table 3, p. 283 of [12]). They also found that the subcrack length is generally greater for laminates with larger ratios of fracture toughness to ultimate tensile stress. The work performed in this investigation supports that finding, at least for the case of boron-epoxy composite since the subcrack length at fracture obtained here was a full 9" (229 mm), the length of the specimen, compared to a value of 0.2" (5mm) obtained in [12].

References

- [1] Rosen, B. W. and Dow, N. F., "Mechanics of Failure of Fibrous Composites," in Fracture (H. Liebowitz, ed.), vol. 7, Academic Press, 1972, pp. 611-674.
- [2] Zweben, C., "On the Strength of Notched Composites," J. Mech. Phys. Solids, vol. 19, 1971, pp. 103-116.
- [3] Sih, G. C., Paris, P. C., and Irwin, G. R., "On Cracks in Rectilinearly Anisotropic Bodies," J. Frac. Mech., vol. 1, no. 3, 1965, pp. 189-202.
- [4] Corten, H. T., "Failure Mechanics of Composites," in Fracture (H. Liebowitz, ed.), vol. 7, Academic Press, 1972, pp. 675-769.
- [5] Walsh, P. F., "Linear Fracture Mechanics in Orthotropic Materials," Eng. Frac. Mech., vol. 4, 1972, pp. 533-541.
- [6] Bowie, O. L. and Freese, C. E., "Central Crack in Plane Orthotropic Rectangular Sheet," Int. J. Frac. Mech., vol. 8, no. 1, March 1972, pp. 49-57.
- [7] Erdogan, F., "Fracture Problems in Composite Materials," Eng. Frac. Mech., vol. 4, 1972, pp. 811-840.
- [8] Olster, E. F. and Jones, R. C., "Effect of Interface on Fracture," in Composite Materials (L. J. Broutman and R. H. Krock, eds.), vol. 1, Academic Press, 1974, pp. 245-284.
- [9] Williams, M. L., "On the Stress Distribution at the Base of a Stationary Crack," J. Appl. Mech., March 1957, pp. 109-114.

- [10] Cooper, G. A. and Kelly, A., "Tensile Properties of Fibre-Reinforced Metals: Fracture Mechanics," J. Mech. Phys. Solids, vol. 15, 1967, pp. 279-297.
- [11] Hoover, W. R., and R. E. Allred, "The Effect of Crack Length and Bond Strength on the Delamination Process in Borsin-Al Composites", J. of Composite Materials, January 1974, pp. 55-64.
- [12] Mandell, J. F., Wang, S. S., and McGarry, F. J., "The Extension of Crack Tip Damage Zones in Fiber Reinforced Plastic Laminates", J. of Composite Materials, July, 1975, pp. 266-287.
- [13] Ueng, C. E. S., Aberson, J. A., and Lafitte, B. A., "Tensile Analysis of an Edge Notch in a Unidirectional Composites", J. of Composite Materials, April 1977, pp. 222-234.

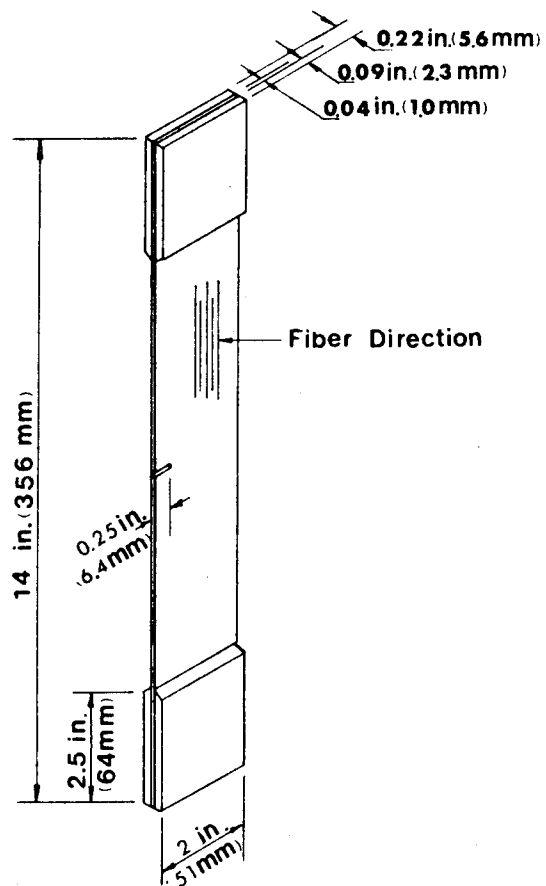


Fig. 1 Specimen Dimensions

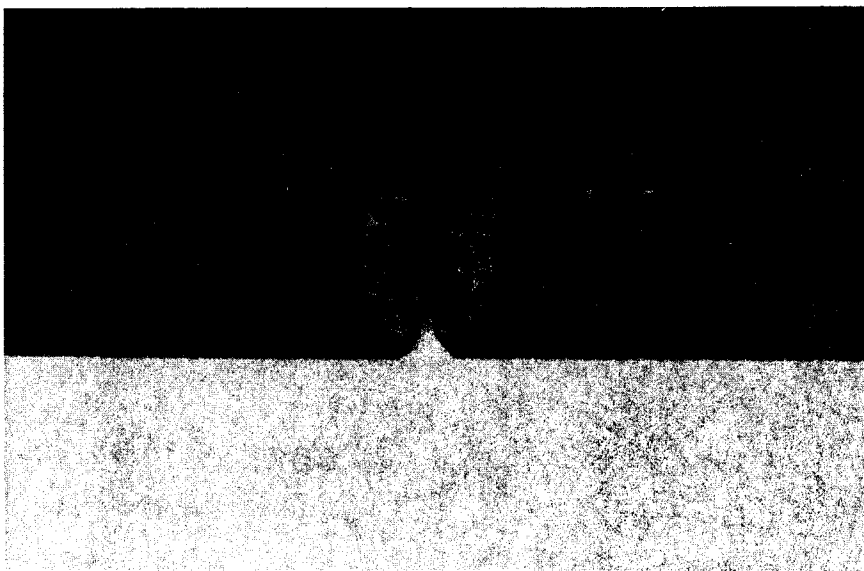


Fig. 3 Line of Vertical Debonding

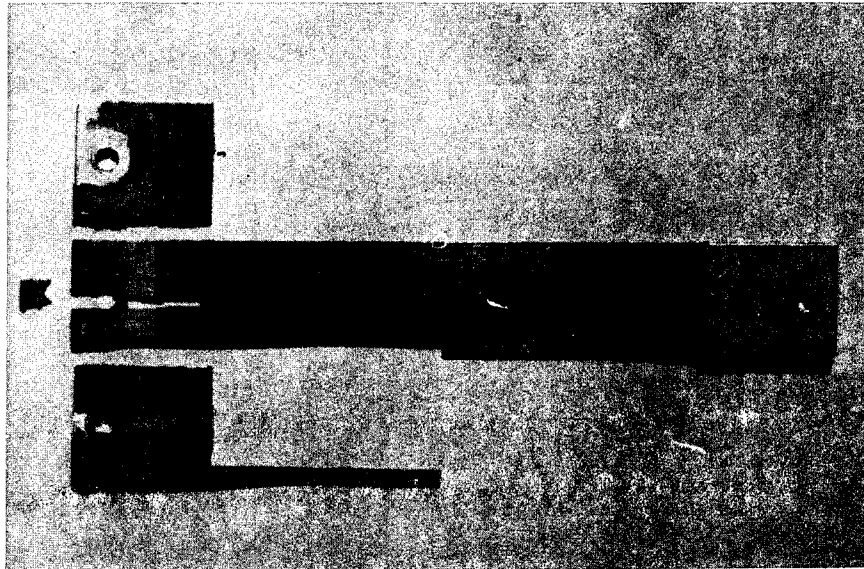


Fig. 2 Debonding at Dowel Pin Hole

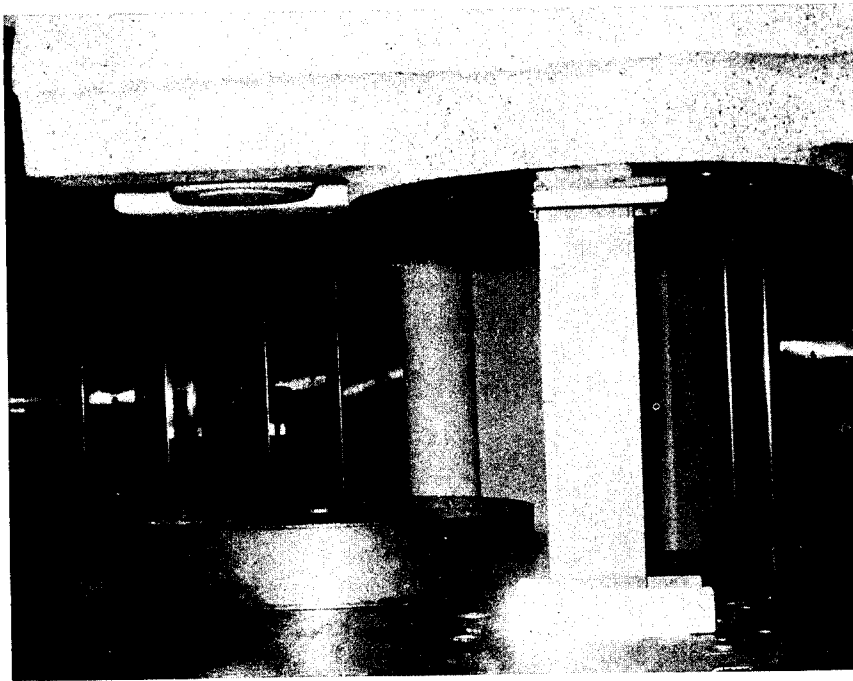


Fig. 4 Complete Vertical Debonding

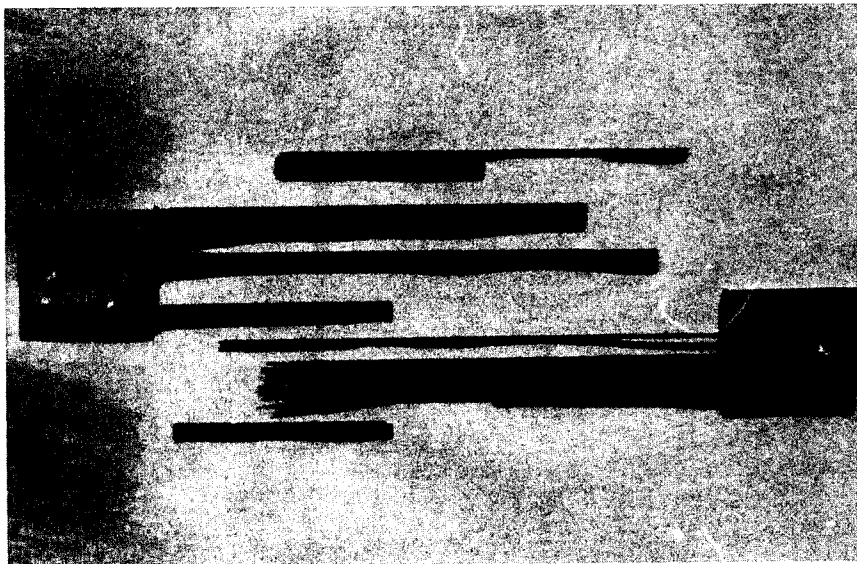


Fig. 5 Typical Failure

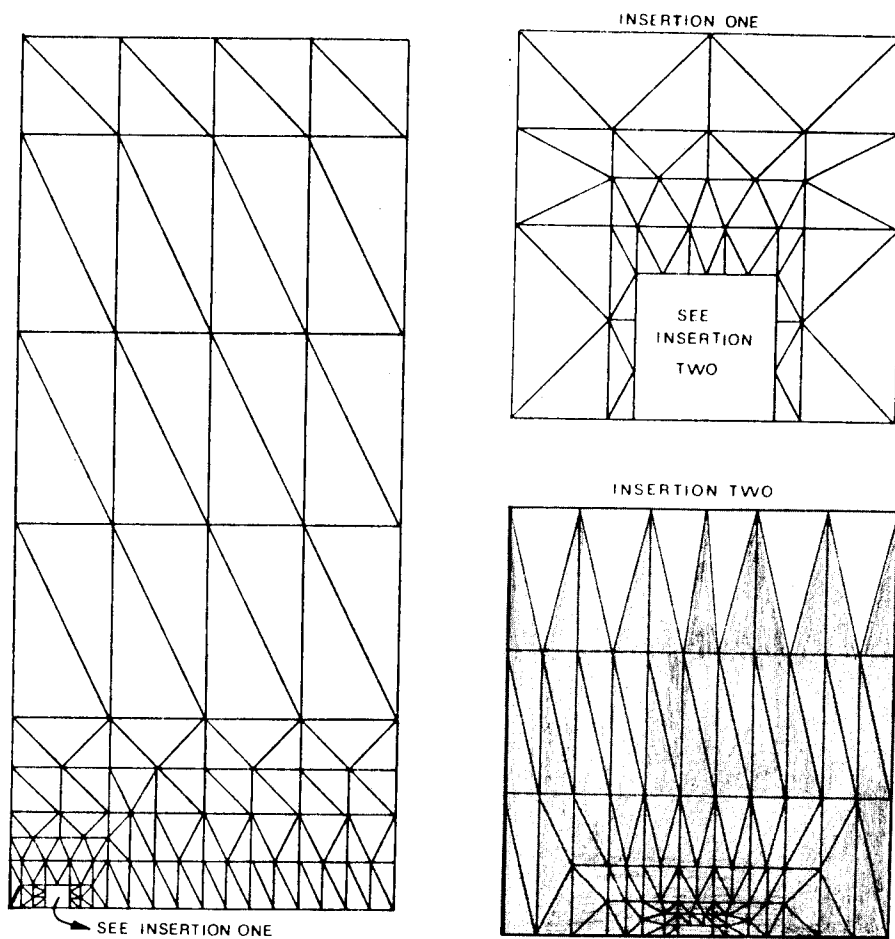


Fig. 6 Finite Element Grid

SESSION 9

FAILURE MODES IN ADVANCED COMPOSITES

Chairman: G. Kardos

Carleton University

Failure Criteria for Composites Under Complex Loading

P. W. Mast, L. A. Beaubien, D. R. Mulville, S. A. Sutton
R. W. Thomas, J. Tirosh, and I. Wolock
Naval Research Laboratory
Washington, D.C. 20375

Abstract

Studies are in progress to develop failure criteria for composites and bonded joints under a broad range of in-plane loads. Criteria for predicting the conditions under which a defect will grow in composites structural components, in such applications as Naval high performance craft, will be demonstrated. Validity of a new technique for determining failure criteria for composites has been verified in laboratory tests.

FAILURE ANALYSIS OF AN IDEALIZED COMPOSITE DAMAGE ZONE¹

Carl T. Herakovich and David A. O'Brien
Department of Engineering Science & Mechanics
Virginia Polytechnic Institute & State University
Blacksburg, Virginia 24061

Abstract: First failure of finite width laminates with an idealized composite damage zone is analyzed through the use of a linear elastic finite element stress analysis and the tensor polynomial failure criterion. Crossply and angleply [± 45]_s laminates are analyzed under tension and compression loading. It is shown that a boundary layer exists near the damage zone which is very similar to the boundary layer which has been shown previously to exist along free edges. Comparisons are made between predicted initial failure of damaged and undamaged laminates. Transverse tension is the dominate mode of failure for tensile loading, but compressive loading leads to a variety of failure modes depending upon the laminate configuration.

Key words: Laminated composites, failure, tensor polynomial, finite elements, stress concentrations, interlaminar stresses, tension, compression, graphite-epoxy.

INTRODUCTION

Failure of advanced composite materials has been the subject of many recent papers. Numerous failure theories have been proposed [1], and theoretical and experimental investigations have been conducted on notched and unnotched specimens. However, very little, if any, attention has been given to surface damage in which one or more layers have "peeled off" due to impact or other causes. This paper investigates the stress distribution around an idealized surface damage zone in composite laminates, and then uses the tensor polynomial failure criterion [2] to predict the initiation of failure. The idealized damage zone consists of a centered rectangular groove or cutout extending the entire length of a long symmetric composite laminate (Fig. 1). For symmetry reasons, both top and bottom surfaces of the laminate are considered to be damaged. This idealized "damage zone" was chosen as a tractable problem which would provide insight into the more general problem of the stress distribution around an irregularly shaped damage region.

¹Supported by The NASA-VPI&SU Composites Program, NASA Grant NGR 47-004-129.

The stress distributions are determined using a quasi-three-dimensional, linear elastic finite element stress analysis. The problem formulation includes the interlaminar stresses which are present in the vicinity of the idealized damage zone as well as those in the boundary layer along the laminate free edge [3-6]. Results are presented for $[0/90]_S$, $[90/0]_S$ and $[\pm 45]_S$ graphite-epoxy laminates under both tensile and compressive loading. The different character of initial failure in the three laminates is discussed.

PROBLEM FORMULATION

The Finite Element Problem

The laminates consist of layers of an orthotropic material with the principal axis of each layer aligned at an angle θ with the x axis (Fig. 1). Only balanced, symmetric laminates are considered. The constitutive equation for each layer can be written, in condensed notation, in the form

$$\{\sigma\}^k = [\bar{C}]^k \{\epsilon\}^k \quad (1)$$

where:

$[\bar{C}]^k$ is the transformed 6x6 stiffness matrix

$\{\sigma\}^k$ is a 6x1 stress vector

$\{\epsilon\}^k$ is a 6x1 strain vector

and k refers to the k^{th} layer of the laminate

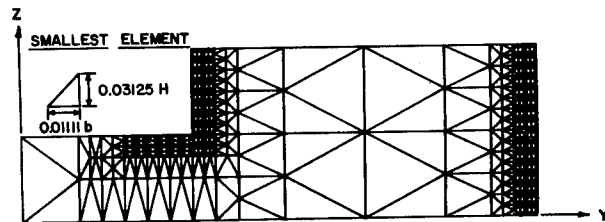
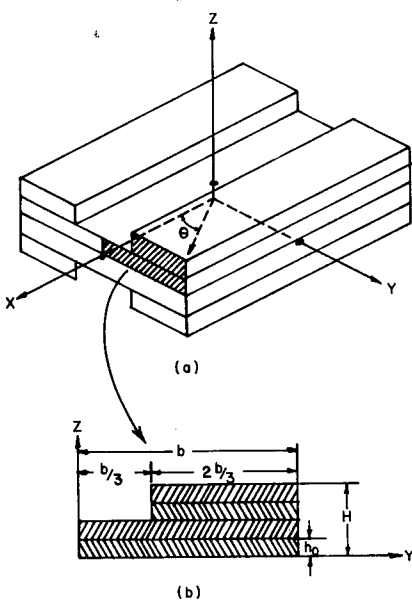


Fig. 2 - Finite Element Representation

Fig. 1 - Finite Width Laminate with Idealized Damage Zone

Since the laminate is long and the loads are applied at the ends, the states of stress and strain are independent of the axial coordinate x . The most general displacement field for this problem can be written in the form

$$\begin{aligned} u &= \xi x + U(y,z) \\ v &= V(y,z) \\ w &= W(y,z) \end{aligned} \quad (2)$$

where ξ is the applied uniform axial strain. Thus, the problem reduces to the determination of the unknown displacement functions $U(y,z)$, $V(y,z)$ and $W(y,z)$ over a cross section of the laminate. Symmetry allows the investigation to be limited to one-quarter of the cross section.

The finite element method of solution was chosen because of its versatility with irregular shaped geometries and material inhomogenities (including laminated materials). The region of interest is subdivided into a finite number of triangular elements as shown in Fig. 2. As indicated in the figure, a higher density of smaller elements was used in regions of suspected stress concentrations. The dimensions of the smallest element are shown in the figure.

The displacement fields (U,V,W) over each element were represented by linear interpolation functions expressed in terms of the unknown nodal displacements. The nodal values of the displacements were then the primary unknown of the problem. They were determined using minimum potential energy to establish the elemental force-displacement relationships in the form

$$[K]^{(\ell)} \{u\}^{(\ell)} = \{F\}^{(\ell)} \quad (3)$$

where

- $[K]^{(\ell)}$ is the elemental stiffness matrix
- $\{u\}^{(\ell)}$ are the elemental nodal displacements
- $\{F\}^{(\ell)}$ are the elemental nodal forces

The elemental relationships were then assembled into a set of simultaneous equations relating all unknown nodal displacements and known nodal forces. The simultaneous equations were solved for displacements after modification for boundary conditions. The strains and stresses in individual elements were then determined from the strain-displacement relations and constitutive equations. The linear interpolation function gives rise to constant stress and strain elements.

The problem formulation given here permits the determination of all six components of stress whenever present. It has been coded in FORTRAN for an IBM computing system and is documented more completely in references 7 and 8. The program uses the efficient in-core equation solver COLSOL [9].

Tensor Polynomial Failure Criterion

The availability of all six components of stress provides a unique opportunity to study the application of a three dimensional failure criterion. The tensor polynomial criterion was chosen as being representative of composite failure. The criterion postulates the existence of a failure surface of the form

$$F_i \sigma_i + F_{ij} \sigma_i \sigma_j = 1 \quad (4)$$

where F_i and F_{ij} are strength tensors whose components can be expressed in terms of the material principal strengths [2]. When (4) is expanded in principal material coordinates for an orthotropic material, it has the form

$$\begin{aligned} & F_1 \sigma_1^2 + F_2 \sigma_2^2 + F_3 \sigma_3^2 + F_{11} \sigma_1^4 + F_{22} \sigma_2^4 + F_{33} \sigma_3^4 \\ & + F_{44} \tau_{23}^2 + F_{55} \tau_{13}^2 + F_{66} \tau_{12}^2 + 2F_{12} \sigma_1 \sigma_2 + 2F_{13} \sigma_1 \sigma_3 + 2F_{23} \sigma_2 \sigma_3 = 1 \end{aligned} \quad (5)$$

Alternatively, the polynomial may be expressed in laminate coordinates. It then has the form

$$\begin{aligned} & F'_1 \sigma_x^2 + F'_2 \sigma_y^2 + F'_3 \sigma_z^2 + F'_6 \tau_{xy}^2 + F'_{11} \sigma_x^4 \\ & + F'_{22} \sigma_y^4 + F'_{33} \sigma_z^4 + F'_{44} \tau_{yz}^2 + F'_{55} \tau_{xz}^2 \\ & + F'_{66} \tau_{xy}^2 + 2F'_{16} \sigma_x \tau_{xy} + 2F'_{26} \sigma_y \tau_{xy} \\ & + 2F'_{36} \sigma_z \tau_{xy} + 2F'_{45} \tau_{yz} \tau_{xz} + 2F'_{12} \sigma_x \sigma_y \\ & + 2F'_{13} \sigma_x \sigma_z + 2F'_{23} \sigma_y \sigma_z = 1 \end{aligned} \quad (6)$$

where primed quantities are the transformed strength values.

The polynomial is evaluated for each constant stress element to determine which element will be the first to fail as the load is increased. Examination of the individual terms of the polynomial (5)

at failure provides insight into the mode of failure. Thus the form (5) is useful for failure mode determination. The form (6) is helpful when considering the stress free boundary conditions since individual terms may be set to zero. An interesting observation is the form of the failure criterion (6) for the intersection of a free edge with a free surface where boundary conditions require that, for any laminate, all components of stress with the exception of σ_x are zero. Equation (6) then reduces to:

$$F_1' \sigma_x + F_{11}' \sigma_x^2 = 1 \quad (7)$$

Material Properties and Geometry

All results presented in this paper have been obtained using material properties which are representative of Thornel 300/Narmco 5208 graphite-epoxy. The elastic properties used were:

$$\begin{aligned} E_{11}^t &= 27.6 \times 10^6 \text{ psi} & G_{12} &= G_{13} = G_{23} = 1.05 \times 10^6 \text{ psi} \\ E_{11}^c &= 18.9 \times 10^6 \text{ psi} & \nu_{12} &= \nu_{13} = \nu_{23} = 0.38 \\ E_{22}^t &= E_{33}^t = 1.6 \times 10^6 \text{ psi} & E_{22}^c &= E_{33}^c = 1.8 \times 10^6 \text{ psi} \end{aligned} \quad (8)$$

The principal strengths were taken to be:

$$\begin{aligned} X_t &= 218 \text{ ksi} & Y_t &= Z_t = 5.9 \text{ ksi} & F_{12} &= -0.58 \times 10^{-10} / (\text{psi})^2 \\ X_c &= -218 \text{ ksi} & Y_c &= Z_c = -36.3 \text{ ksi} & S_{12} &= S_{13} = S_{23} = 9.8 \text{ ksi} \end{aligned} \quad (9)$$

The resulting components of the strength tensors are:

$$\begin{aligned} F_1 &= 0 & F_{11} &= 0.00002 & F_{44} &= 0.0104 \\ F_2 &= 0.142 & F_{22} &= 0.00477 & F_{55} &= 0.0104 \\ F_3 &= 0.142 & F_{33} &= 0.00477 & F_{66} &= 0.0104 \end{aligned} \quad (10)$$

where the F_i and F_{ij} have units of $(\text{psi})^{-2}$.

Prediction of initial failure is of course dependent upon the elastic constants and principal strength values employed. As indicated above, some assumptions were made regarding the elastic properties in the 2-3 plane and the strength values. Thus, these predictions may require modification as more complete experimental results become available.

As indicated in Figure 1, the half-width of the damaged zone was taken to be $b/3$ where b is the laminate half-width. The depth of the damage zone was always equal to one ply thickness. The aspect ratio (b/H)

was 34.1 in all cases. Thus, the laminates under consideration are very wide. As shown in reference [10], the boundary layer width decreases with increasing aspect ratio.

RESULTS AND DISCUSSION

All three laminates were investigated under tensile and compressive loading, and both damaged and undamaged laminates were considered. The edge of the damage zone was sufficiently removed from the free edge to eliminate any possible interaction. It was verified that the classical laminate solution was recovered in the interior region between the free edge and the damage region.

The results of the failure analysis are summarized in Table 1. The table shows the contribution of the significant terms of the tensor polynomial, the strain at first failure and the location of first failure. In those cases where first failure occurred in the vicinity of the damage zone, the results for undamaged laminates are also presented. As indicated in the table, failure of crossply laminates is predicted to occur at the free edge for every case except compression of the $[90/0]_s$ laminate. First failure for this case is predicted at the corner of the damage zone. Unlike the crossply laminates, angleply $[\pm 45]_s$ laminates exhibit first failure at the damage zone for both tensile and compressive loading. The predicted failure strains are only a relative measure as they do not include residual thermal stresses or nonlinear material behavior.

All stress distributions presented in this paper were obtained using the two different stress averaging schemes depicted in Fig. 3. The interlaminar stresses σ_z , τ_{zx} and τ_{zy} must be continuous across any line $z = \text{constant}$ and hence the interlaminar stress at point H in the figure was taken to be the average of elements 14, 15, 16 and 17 which are on both sides of the interface. The inplane stress components σ_x , σ_y and τ_{xy} are not required to be continuous across an interface and, therefore, they were averaged along lines such as BB and DD in the figure. Thus, at point F, the stresses are the average of elements 8 and 9 while for point G elements 10 and 11 are averaged. The failure analysis was based upon the actual stress values in each element.

Crossply Laminates

Tensile loading of these laminates always resulted in first failure in the 90° ply at the intersection of the free edge and the $0/90$ interface. Failure is dominated by the transverse normal stress σ_2 with the linear term $F_2\sigma_2$ being the dominate term. The contribution from the interlaminar normal stress (σ_3) is small for both laminates, but it is much greater in the $[0/90]_s$ laminate which exhibits an 18 percent lower failure strain. The variable influence of the interlaminar normal stress is clearly shown by the stress distributions in figures 4 and 5. The $[0/90]_s$ laminate gives rise to a tensile σ_z at the free edge whereas

TABLE 1 TENSOR POLYNOMIAL CONTRIBUTIONS IN FAILED ELEMENT

Laminate	Load	F_{11}^2	F_{22}^2	F_{33}^2	F_{44}^2	F_{55}^2	F_{66}^2	Failure Strain (%)	Failure Location
<u>Damaged Laminates</u>									
[0/90] _s	T	-	0.120	0.155	-	-	-	0.2978	
[0/90] _s	C	1.065	-	-	-	-	-	-0.8146	
[90/0] _s	T	-	0.817	0.027	-	-	-	0.3643	
[90/0] _s	C	0.513	0.161	0.202	0.061	-	-	-0.5696	
[±45] _s	T	-	0.798	-	0.019	0.020	0.026	0.0905	
[±45] _s	C	-	-3.753	0.052	0.426	0.442	0.571	-0.4255	
<u>Undamaged Laminates</u>									
[90/0] _s	C	0.603	-	0.359	-	-	-	-0.6169	
[±45] _s	T	-	0.799	-	0.018	0.023	0.032	0.1037	
[±45] _s	C	-	-3.603	0.093	0.373	0.471	0.659	-0.4678	

NOTES: Insignificant terms not shown
T = Tension
C = Compression

it is negative there for the $[90/0]_S$ laminate. Close examination of these figures shows that the stress distributions are not merely a sign reversal and hence the laminates exhibit fundamentally different behavior. This result was first reported by Wang and Crossman [6]. (Results obtained in [11] with a much finer mesh show that σ_z is actually tensile at the free edge for both laminates, but is much higher for the $[0/90]_S$ laminate. These refined results did not alter the location of first failure.) These figures also show that stress concentrations exist in a boundary layer near the edge of the damage zone. The stress distributions in the damage zone boundary layer are similar in character to those in the free edge boundary layer, but the stress concentrations are of different strength.

Compression of these laminates indicates variable location and mode of failure. The $[0/90]_S$ laminate fails at the top outside corner of the laminate with failure being completely dominated by σ_1 as predicted by eqn. (7). The $[90/0]_S$ laminate fails in a combined mode with σ_1 , σ_2 and σ_3 all contributing significantly; however the major contribution is again from σ_1 . The compression failure strain for the damage zone failure of the $[90/0]_S$ laminate is 30 percent below the compressive failure strain of the $[0/90]_S$ laminates and 8 percent lower than first failure of an undamaged $[90/0]_S$ laminate. The primary reason for the different failure modes and locations is the value of σ_z near the damage zone. It is tensile for $[90/0]_S$ and compressive for $[0/90]_S$.

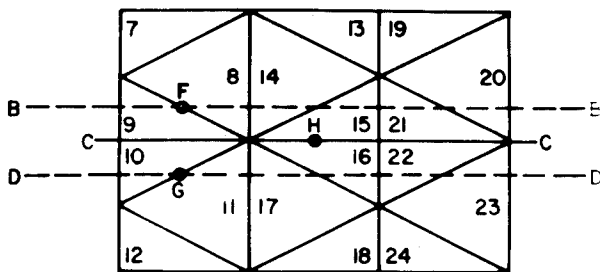


Fig. 3 - Stress Averaging

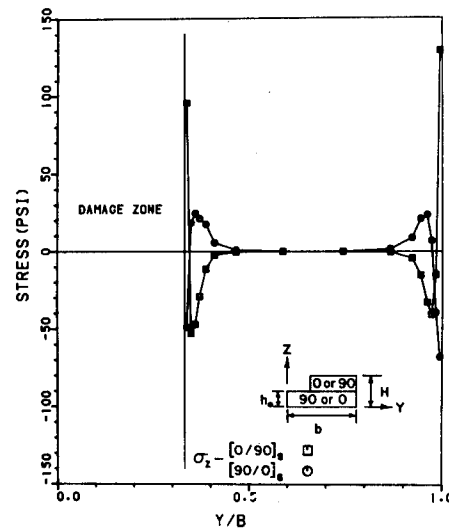


Fig. 4 - σ_z at $z=h_0$ for $[0/90]_S$ and $[90/0]_S$ ($\xi=0.1\%$)

(The stress distributions for compressive loading are reversed in sign from the tensile results in figures 4 and 5.) The different tensile and compressive failure stresses are due mainly to the different strengths in tension and compression (Eqn. 9). The undamaged $[90/0]_S$ laminate fails at the intersection of the midplane and the free edge in a combined σ_1, σ_3 failure mode when loaded in compression (Table 1).

The interrelationships between stresses can be explained by considering equilibrium of the free body diagrams shown in Fig. 6. The interlaminar normal stress τ_{yz} is related to σ_y by force equilibrium in the y direction. Since τ_{yz} is always zero along a center cut C-C (laminate solution), the interlaminar normal stress σ_z must be equivalent to a couple when σ_y is nonzero and must be equivalent to nonzero force and nonzero moment when $\sigma_y = 0$ (as in the case of the $[\pm 45]_S$ laminate). The interlaminar shear and normal stresses τ_{yz} and σ_z are of course always related through the point-wise equilibrium equation.

$[\pm 45]_S$ Angleply Laminate

As indicated in Table 1, first failure of damaged $[\pm 45]_S$ laminates occurs at the inside corner of the damage zone for both tensile and compressive loading. Tensile loading gives rise to a transverse σ_2 failure mode whereas compressive loading results in a mixed mode failure between σ_2 and all three shear components. The undamaged

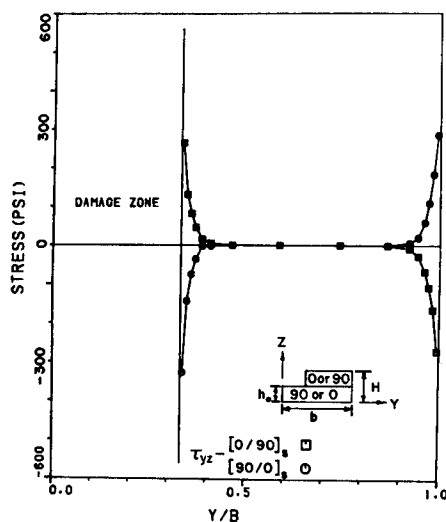


Fig. 5 - τ_{yz} at $z=h_0$ for $[0/90]_S$ and $[90/0]_S$ ($\xi=0.1\%$)

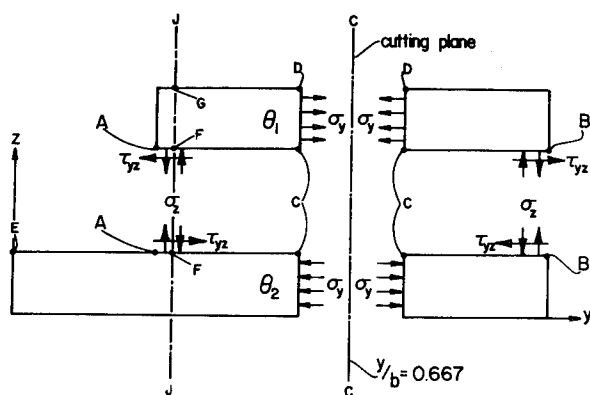


Fig. 6 - Partial Free Body Diagram

laminate fails on the midplane at the free edge when loaded in tension and on the ± 45 interface at the free edge when loaded in compression. The failure modes of the undamaged laminates are essentially the same as the damaged laminates. The failure strains of damaged laminates are approximately 10 percent lower than those of undamaged laminates.

Compression loading of both damaged and undamaged $[\pm 45]_s$ laminates shows an interesting result. The σ_2 terms of the tensor polynomial are both quite large, but of opposite sign at failure. However, the sum $F_2\sigma_2 + F_{22}\sigma_2^2$ is actually negative in both cases. Unlike the crossply laminates, shear plays an important role in first failure of the angleply laminate.

Stress distributions along the interface of $[\pm 45]_s$ laminates are presented in Figures 7 - 9. Again, we see that there are stress concentrations in a boundary layer near the free edge and the damage zone. Since σ_y is zero in interior regions of the $[\pm 45]_s$ angleply laminate, equilibrium considerations (Fig. 6) require that the integrals of τ_{yz} , σ_z and $y\sigma_z$ along the interface be zero in each boundary layer. Figure 7 shows that the stress distributions for these two stresses exhibit the proper number of oscillations about zero and, at least approximately, satisfy the equilibrium conditions. Invoking the stress boundary conditions and using the stress transformation equations gives

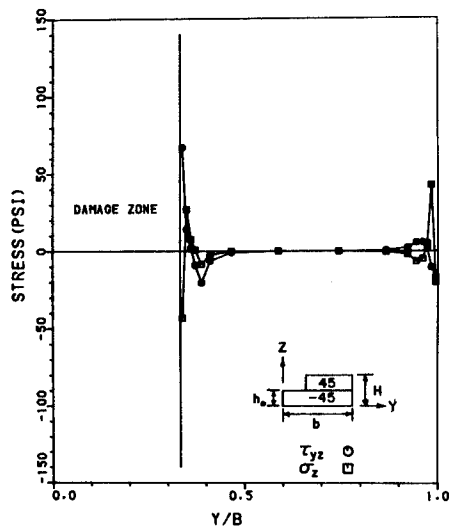


Fig. 7 - σ_z and τ_{yz} at $z=h_0$ for $[\pm 45]_s$ ($\xi=0.1\%$)

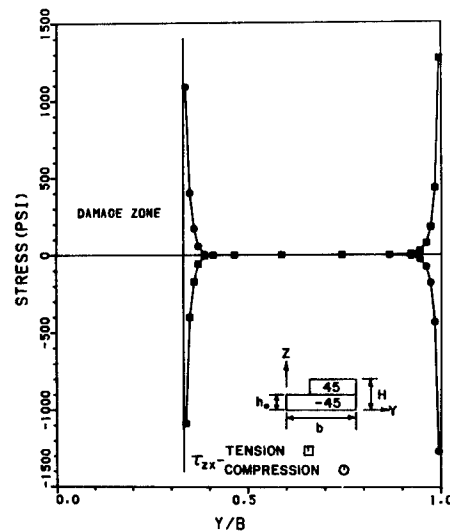


Fig. 8 - τ_{zx} at $z=h_0$ for $[\pm 45]_s$ ($\xi=\pm 0.1\%$)

the following equations for the stresses at the free edge, in material principal coordinates, in terms of the laminate stresses.

$$\begin{aligned}\sigma_1 &= \sigma_2 = \sigma_x/2 & \sigma_3 &= \sigma_z \\ \tau_{13} &= -\tau_{23} = \tau_{zx}/\sqrt{2} & \tau_{12} &= -\sigma_x/2\end{aligned}\quad (11)$$

These equations show that σ_x , σ_z and τ_{zx} control failure along free edges - including the free edges of the damage zone. As shown in Fig. 8, τ_{zx} exhibits a very high stress concentration at the corner of the damage zone and at the free edge. (The signs of shear stresses are not important since the shear stresses appeared only as "squared" terms in the tensor polynomial.) The distributions of σ_x above and below the interface $z = H$ are shown in Fig. 9. Stress concentrations are again present near the damage zone and the free edge. The highest concentration is near the damage zone where first failure occurs. Table 1, equations (11) and figures 8 and 9 indicate the first failure of $[\pm 45]_s$ laminates is primarily due to σ_2 (i.e. σ_x) for tensile loading, and is a mixed mode failure dominated by τ_{zx} and σ_x when loaded in compression.

The finite element formulation used in this investigation does not satisfy the stress-free boundary conditions exactly and hence equations (11) are only approximately satisfied. However, additional results for undamaged laminates with a much finer mesh have indicated that the location of failure does not shift [11].

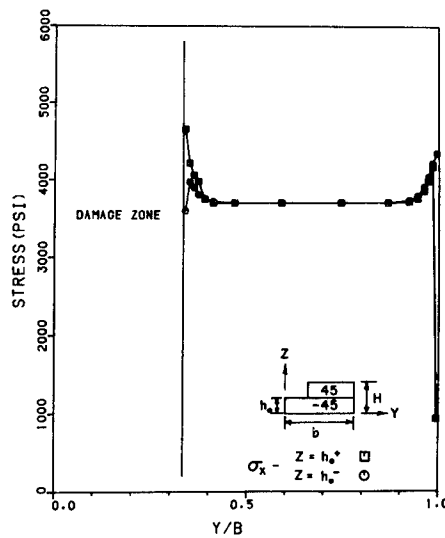


Fig. 9 - σ_x at $z=h_0$ for $[\pm 45]_s$
($\xi=0.1\%$)

CONCLUSIONS

Stress concentrations and interlaminar stresses are present in the vicinity of damage zones in laminated composites. The stress distributions near the damage zone are very similar to those which have been shown previously to exist along free edges. The tensor polynomial failure criterion predicts first failure to be transverse tension (σ_2) for tensile loading of all three laminates considered. Compressive loading leads to different failure modes depending upon the laminate configuration. Compressive failure of $[0/90]_s$ symmetric laminates is completely dominated by σ_1 normal stress, but the $[90/0]_s$ laminates fail in a combined mode involving all three normal stress components. The $[\pm 45]_s$ laminate fails in a combined mode when loaded in compression. Transverse σ_2 tension and all three shear components make significant contributions to the tensor polynomial for this case. With the exception of compression of the $[90/0]_s$ laminate, crossply laminates fail at the free edge before failing near the damage zone. The damage zone is more critical for $[\pm 45]_s$ with first failure occurring there for both tensile and compressive loading.

Future work in this area should include residual thermal stresses, moisture effects and nonlinear material behavior.

ACKNOWLEDGEMENT

The assistance of Mr. A. Nagarkar with some of the computational work is greatly appreciated as is the typing of Ms. Frances Carter.

REFERENCES

1. Inelastic Behavior of Composite Materials, (Herakovich, C. T., editor), ASME AMD Vol. 13, Am. Soc. Mechanical Engineers, 1975.
2. Wu, E. M., "Phenomenological Anisotropic Failure Criteria," in Composite Materials, Vol. 2, Mechanics of Composite Materials, (Broutman, L. J., Krock, R. H. and Sendeckyj, G. P., editors), Academic Press, 1974.
3. Pipes, R. B., and Pagano, N. J., "Interlaminar Stresses in Composite Laminates Under Uniform Axial Extension," J. Composite Materials, Vol. 4, 1970, 538-548.
4. Herakovich, C. T., Renieri, G. D., and Brinson, H. F., "Finite Element Analysis of Mechanical and Thermal Edge Effects in Composite Laminates," Army Symposium on Solid Mechanics, 1976, Composite Materials: The Influence of Mechanics of Failure on Design, Cape Cod, MA., Sept. 1976.

5. Wang, A. S. D. and Crossman, F. W., "Some New Results on Edge Effects in Symmetric Composite Laminates," J. Composite Materials, Vol. 11, 1977, 92-106.
6. Farley, G. L. and Herakovich, C. T., "Influence of Two-Dimensional Hygrothermal Gradients on Interlaminar Stresses Near Free Edges," Environmental Effects on Advanced Composite Materials, ASTM STP 658, Am. Soc. for Testing and Materials, 1978.
7. Renieri, G. D. and Herakovich, C. T., "Nonlinear Analysis of Laminated Fibrous Composites," VPI-E-76-10, also NASA CR-148317, June, 1976, 177 pages.
8. O'Brien, D. A. and Herakovich, C. T., "Finite Element Stress Analysis of Idealized Composite Damage Zones," VPI-E-78-6, also NASA CR-155923, February, 1978, 141 pages.
9. Bathe, K., Wilson, E. L., Numerical Methods in Finite Element Analysis, Prentice-Hall, Inc., Englewood Cliffs, N.J., 1976.
10. Hsu, P. W. and Herakovich, C. T., "Edge Effects in Angle-ply Composite Laminates," J. Composite Materials, Vol. 11 (Oct. 1977).
11. Herakovich, C. T., Nagarkar, A., and O'Brien, D. A., "Failure Analysis of Composite Laminates with Free Edges," submitted for publication.

INTERLAMINAR FAILURE IN EPOXY BASED COMPOSITE LAMINATES

A. S. Wang
Drexel University
Philadelphia, Pa. 19104

F. W. Crossman
Lockheed Palo Alto Research Laboratory
Palo Alto, Ca. 94304

G. E. Law, Jr.
Drexel University
Philadelphia, Pa. 19104

Abstract: One of the common failure modes in fibrous composite laminates involves interlaminar cracks which cause delamination. Several questions arise in the course of a delamination analysis. Notably these include (a) how is a delamination initiated? (b) under what condition will a delamination grow? and (c) what determines the stability of a delamination growth? Owing to the unusual complexity of composite laminate systems, there appears no simple way to answer these questions satisfactorily.

In this paper, a method is developed based on the energy principle of the classical linear fracture mechanics, in order to describe the various aspects of the delamination mechanisms. Specifically, free-edge induced delamination failure in some epoxy based composite laminates are investigated employing this method. And, the results obtained are compared with experiments. It will be shown that the energy method predicts well free-edge delamination in laminates under uniaxial tension, including the initiation, the growth and the growth stability of the delamination.

Key words: Delamination mechanisms; energy release rate; finite element method; free-edge stresses; graphite epoxy composites; interlaminar cracks; stability of cracks; virtual crack closure.

One of the common failure modes in fibrous composite laminates may involve the nucleation and propagation of interlaminar cracks. This will usually cause ply delamination. In some cases, delamination may lead to immediate failure of the laminate; and in other cases it may induce long-term property degradation resulting in a reduced structural reliability and durability. Delamination caused by free-edge stresses has frequently been encountered in laminates that have straight edges[1,3] or curved edges such as around cut-outs and holes[4,5]. It is known

that interlaminar stresses are highly localized near the laminate's free edge [6,7], and their sign and magnitude depend on the ply stacking sequence. Hence, some laminates may be more prone to delamination than others, depending on how the plies are stacked together.

Since free-edge delamination may cause immediate laminate failure, the ultimate strength of the laminate is therefore also sensitive to the stacking sequence of the plies. For example, reference [2] reported test results for a family of six different stacking sequences of T300/934 quasi-isotropic laminates that were tested under uniaxial tension. It was found that the tensile strength of the six differently stacked laminates ranged from 63 ksi to 87 ksi. When correlated with the free-edge interlaminar normal stress σ_z [7], the laminate of the lowest strength ($\pm 45/0/90$)s, was found to have the largest tensile σ_z ; the laminate of the highest strength ($90/\pm 45/0$)s, was found to have the largest compressive σ_z . Hence, in the case of the tensile σ_z , an opening mode delamination could be induced prematurely resulting in a lower laminate strength. This qualitative correlation however, could not be used as a failure criterion for the strength prediction.

In addition to the stacking sequence, free-edge delamination is found to depend on the thickness or the volume of the ply which is stressed interlaminarly. The characteristics of this effect is that the occurrence of ply delamination may be delayed by a decrease of the ply thickness, or it may be accelerated by an increase of the ply thickness. For example, reference [8] reported test results for a series of T300/5208 graphite epoxy quasi-isotropic laminates tested under uniaxial tension; the experimental data are summarized in Table I below:

TABLE I

<u>Laminate</u>	<u>Axial Stress At On-set of Delamination</u>	
($\pm 45/0/90$)s	45.3 ksi	
	45.3	45.4 (ave.)
	45.5	
($\pm 45_2/0_2/90_2$)s	38.3	
	38.6	38.2
	37.8	
($\pm 45_3/0_3/90_3$)s	28.7	29.7
	30.7	

It is seen that the applied axial stress at the on-set of delamination varies with the thickness of the material ply, even though the stacking sequence in all cases is the same. Furthermore, if a free-edge stress analysis [7] is performed for all the three laminates, one would find

an identical stress field for all three (under the same applied axial stress). Clearly, the observed ply volume effect cannot be explained adequately by a criterion based on stress alone. In particular, the conditions governing the on-set of delamination and the manner of its growth are not known.

In a recent paper by Rybicki, et al [9], the free-edge delamination problem was described by a stable crack growth procedure based on the energy release rate concept in classical fracture mechanics [10]. The quantity measuring the material resistance against ply delamination is the critical strain energy release rate G_c . It is reasoned that the stressed plies dissipate surface energy as new crack surface is created under the applied load; the rate of the available energy dissipation per newly created surface, G , is viewed as a driving force which can extend the crack further. Since the value of G depends on the level of the applied load, the crack can be extended when G exceeds the material resistance force G_c . Otherwise, the crack would remain stable until the applied load is increased, or the crack-tip conditions are altered. The crack-tip conditions can be altered at least by the size of the crack; hence the magnitude of G is a function of the crack length. A knowledge of the latter may determine the stability of the crack growth.

The energy release rate G is a quantity determined analytically, and it is in fact a complicated function of crack location, crack size, ply stacking sequence, ply properties, ply thickness and the applied load. To calculate G , a finite element procedure is suggested in conjunction with a crack-closure technique [9]. Specifically, G is computed from the work done in closing a known crack-tip extension. Because of the linear elasticity assumption, the work done in closing a crack is equivalent to the energy released when the same crack is opened [11].

In this paper, the energy release rate approach is further developed with the aid of a special finite element routine which models the free-edge delamination process in graphite epoxy laminates. Several laminates of practical interest are investigated by this method; and the results are compared with experiments. It will be shown that the energy method not only predicts the on-set of delamination, it also describes its growth behavior. The observed ply volume effect on delamination is explained explicitly by the analytical model.

Consider the laminate with a symmetric lay-up as shown in Fig. 1. Under the applied axial stress $\bar{\sigma}_x$, interlaminar normal stress $\bar{\sigma}_z$ and shearing stress $\bar{\tau}_{xz}$ and $\bar{\tau}_{yz}$ will be induced in the laminate free-edge region. These stresses are proportional to the applied laminate stress $\bar{\sigma}_x$, according to linear elasticity. Owing to these stresses, a free-edge delamination may be created as shown. It is assumed that some amount of surface energy, denoted by ΔE , is released creating the crack of size Δa . For elastic fracture, ΔE may be determined by the difference in the total stored strain energies of the laminate before and after the small

crack of size Δa . Thus, the energy release rate associated with the crack is given by:

$$G = \lim_{\Delta a \rightarrow 0} \left(\frac{\Delta E}{\Delta a} \right) \quad (1)$$

As the delamination crack grows incrementally in a self-similar manner, G is then calculated numerically as a function of the crack size a .

As is illustrated in Fig. 2a, the computational procedure is as follows: the cross-section of the laminate is represented by a net-work of finite elements with densely populated grids deployed near the intended interface crack region. To calculate G for a crack with crack-tip node k , see Fig. 2b, the nodal displacement components u_k , v_k and w_k are determined first in terms of the applied stress $\bar{\sigma}_x$. Next, by introducing a virtual crack extension Δa while maintaining the same applied stress, node k is then zipped open to two separate nodes k' and k'' as shown. A finite element solution then yields the displacements for nodes k' and k'' . And finally, nodes k' and k'' are forced to close so that the displacements of k' and k'' equal those of k . In this step, the finite element solution gives the nodal force components X_k , Y_k and Z_k which are needed to close the two open nodes. Thus, the energy release rate G for the crack of size a is given by the work done in closing the virtual crack extension Δa :

$$G(a) = [X_k(u_{k'} - u_{k''}) + Y_k(v_{k'} - v_{k''}) + Z_k(w_{k'} - w_{k''})] / 2\Delta a \quad (2)$$

The actual finite element net-work used in the computation reported in this paper differs from laminate to laminate. In general, the incremental crack extension Δa is set at 0.2 times the thickness of a single ply. For example, a typical graphite epoxy tape is approximately 0.005 inch thick; hence the incremental crack extension Δa is only 0.001 inch. The crack-tip elements typically contain about 10 (graphite) fiber cross-sections which is probably the smallest element size for which the effective continuum representation of the material ply is still applicable, see reference [12].

Since the finite element nodal forces and nodal displacements are solved in terms of the applied laminate stress $\bar{\sigma}_x$, the work done during the virtual crack closure process is then expressible in terms of $\bar{\sigma}_x^2 / \bar{E}_x$. Accordingly, the energy release rate G is expressed as

$$G(a) = g(a/t) t \bar{\sigma}_x^2 / \bar{E}_x \quad (3)$$

In the above expression, $\bar{\sigma}_x$ and \bar{E}_x are laminate stress and stiffness, respectively; t is a conveniently chosen characteristic length, such as the thickness of a single ply; g is a non-dimensional function of (a/t) , a being the delamination crack size, as shown in Fig. 1. Note that g is derived directly following Eq.(2).

Fig. 3 illustrates the general behavior of g as a function of (a/t) . It is seen that g increases sharply with (a/t) to reach a maximum, g_{\max} ,

at $a = a^*$; it then decreases slightly to a minimum, g_{\min} , at $a = a^{**}$. After this point, g increases again slowly and monotonically.

The physical interpretation of this behavior is that, under the applied stress $\bar{\sigma}_x$, the laminate is capable of releasing delamination energy depending on the ply interactions; there exists a unique maximum energy release rate g_{\max} , given the location of the delamination. It is then theorized that g_{\max} is associated with the on-set of delamination, an action that pops open a small crack of size a^* . Once this happens, the available energy release is somewhat reduced and a slightly higher load will be required to extend the crack further. This is a stable crack growth; but the process is rather short. The growth becomes unstable once the delamination crack reaches a size of a^{**} .

Suppose the criterion $G \rightarrow G_c$ for fracture is used. Then, it follows from Eq. (3) that the critical stress at the on-set of delamination is given by:

$$(\bar{\sigma}_x)_i = (G_c \bar{E}_x / g_{\max} t)^{\frac{1}{2}} \quad (4)$$

and the critical stress at unstable growth is given by:

$$(\bar{\sigma}_x)_f = (G_c \bar{E}_x / g_{\min} t)^{\frac{1}{2}} \quad (5)$$

Numerical calculation of g indicates generally that the value of a^* is approximately equal to the thickness of the material layer that is stressed the most by the interlaminar stresses. For instance, in the case of $(\pm 30/90_2)_s$, a^* is roughly the thickness of the 90-layer, or 2 ply thick; in the case of $(\pm 30/90_3)_s$, a^* is about 3 ply thickness. On the other hand, the value of a^{**} is usually 2 to 3 times the thickness of the laminate. It is also interesting to note that g_{\min} is about 90% of g_{\max} , making $(\bar{\sigma}_x)_i$ about 5% smaller than $(\bar{\sigma}_x)_f$.

For experimental comparison, two cases will be discussed in the following:

The first case concerns a T300/934 $(\pm 45/0/90)_s$ laminate which is tensile tested under step-loading. Micrographic examination is then performed to discern the damages that occurred at each load level. Detailed results of this study have been reported in reference [2]. It is found that edge delamination in the 90-layer first appeared at about 60 ksi; excessive delamination extending inside the laminate occurred at about 63 ksi. The laminate final strength was about 67 ksi.

To correlate these results with the energy release rate method, the finite element calculation for the function $g(a/t)$ is performed for the laminate using the following ply properties[2]:

$$E_L = 23.7 \text{ msi} \quad E_T = 1.72 \text{ msi}$$

$$\begin{aligned} G_{LT} &= 0.94 \text{ msi} & G_{TT} &= 0.5 \text{ msi} \\ \nu_{LT} &= 0.3 & \nu_{TT} &= 0.5 \end{aligned}$$

The individual ply thickness is 0.0055 in. and the overall laminate stiffness in the load direction is $\bar{E}_x = 9 \text{ msi}$.

Fig. 4 displays the calculated g function for delamination along the 90/90 interface. Here, $g_{\max} = 0.365$ and it occurs at about a^* equal to the ply thickness t . On the other hand, $g_{\min} = 0.33$ which occurs at about a^{**} equal to $15t$ (not shown in the figure).

Now, assume the on-set of delamination occurred at $\bar{\sigma}_x = 60 \text{ ksi}$. It then follows from Eq.(4) that the critical energy release rate G_c for ply delamination is 0.8 in-lb/in^2 , or 140 j/m^2 . This value is compared to $G_c = 150 \text{ j/m}^2$ found independently for similar material system[13], by a test method suggested in reference[14].

Using $g_{\min} = 0.33$ and $G_c = 0.8 \text{ in-lb/in}^2$, the critical stress for unstable delamination $(\bar{\sigma}_x)_f$ is found to be 63 ksi .

For the second case of experimental correlation, consider the test results reported in reference 8, where the ply-volume effect on edge delamination was observed experimentally. The three laminates with different ply volumes are $(\pm 45/0/90)_s$, $(\pm 45_2/0_2/90_2)_s$ and $(\pm 45_3/0_3/90_3)_s$; they are all made of T300/5208 graphite epoxy unidirectional tapes. The mechanical properties of the tape are given in the following[8]:

$$\begin{aligned} E_L &= 19.5 \text{ msi} & E_T &= 1.48 \text{ msi} \\ G_{LT} = G_{TT} &= 0.8 \text{ msi} & \nu_{LT} = \nu_{TT} &= 0.3 \end{aligned}$$

The individual ply thickness is 0.0057 in.

It is noted that the three laminates are identical in every aspect except the thickness of the material layer. In fact, under the same axial stress $\bar{\sigma}_x$, all three should develop identical laminate stress and strain fields. And, they all have the same axial stiffness $\bar{E}_x = 7.7 \text{ msi}$. Now, if we choose the thickness of the 90-layer to be the characteristic t in calculating the function g , then a common g can be generated. Fig. 5 displays this common function g for edge cracks along the 90/90 interface in all the three laminates. Here, $g_{\max} = 0.445$ and it happens at about a^* equal to t . Note that t equals to 0.0057 in. , 0.0114 in. and 0.0171 in. for the three respective laminates.

Again, assume $G_c = 0.8 \text{ in-lb/in}^2$. From Eq.(4) the critical stresses at the on-set of edge delamination for the three laminates are given by 49.3 ksi , 34.9 ksi and 28.5 ksi , respectively. These compare closely with the experimental values of 45.4 , 38.2 and 29.7 ksi as shown in

Table I.

It should be pointed out that Eq.(4) or (5) expresses explicitly the dependence of the critical stress on the characteristic length t . t , if properly chosen, represents the ply-volume effect.

In conclusion, the energy release rate approach developed in this paper appears to be useful for delamination analysis of composites. It not only predicts the on-set of delamination, it also describes its growth behavior. For all practical purposes, it gives a good estimate of the laminate's ultimate strength. Moreover, the observed ply-volume effect on delamination can be explained explicitly by the analytical model.

Reference:

1. K.L. Reifsnider, E.G. Henneke and W.W. Stinchcomb, 'Delamination of Quasi-isotropic Graphite Epoxy Laminates,' Composite Materials: Testing and Design. ASTM STP 617(1977), p. 93.
2. J.G. Bjeletich, F.W. Crossman and W.J. Warren, 'The Influence of Stacking Sequence On Failure Modes In Quasi-isotropic Graphite Epoxy Laminates,' Failure Modes In Composites-IV, AIME(1978).
3. G.P. Sendeckyj and H.D. Stalnaker, 'Effect of Time at Load on Fatigue Response of $(0/\pm 45/90)_2$ T300/5208 Graphite Epoxy Laminate,' Composite Materials: Testing and Design. ASTM STP 617(1977), p. 39.
4. J.M. Whitney and R.Y. Kim, 'Effect of Stacking Sequence on the Notched Strength of Laminated Composites,' Composite Materials: Testing and Design. ASTM STP 617(1977), p. 229.
5. M.S. Rosenfeld and S.L. Huang, 'Fatigue Characteristics of Graphite Epoxy Laminates Under Compressive Loading,' Jour. Aircraft, Vol. 15 (1978), p. 246.
6. R.B. Pipes and N.J. Pagano, 'Interlaminar Stresses in Composite Laminates Under Uniform Axial Extension,' Jour. Composite Materials, Vol. 4 (1970), p. 538.
7. A.S.D. Wang and F.W. Crossman, 'Some New Results on Edge Effects in Symmetric Composite Laminates,' Jour. Composite Materials, Vol. 11 (1977), p. 92.
8. B.T. Rodini, Jr. and J.R. Eisenmann, 'An analytical and Experimental Investigation of Edge Delamination in Composite Laminates,' 4th Conf. on Fibrous Composites, San Diego, Cal., Nov. 14-17 (1978).
9. E.F. Rybicki, D.W. Schmueser and J. Fox, 'An Energy Release Rate Ap-

proach for Stable Crack Growth in the Free Edge Delamination Problem' Jour. Composite Materials, Vol. 11 (1977), p. 470.

10. A.S. Tetelman and A.J. McEvily, Jr., 'Fracture of Structural Materials,' John Wiley and Sons, New York (1967).
11. G.R. Irwin, 'Handbuch der Physik,' Vol. 6 (1958), Springer-Verlag. p. 551.
12. E.F. Rybicki and N.J. Pagano, 'A Study of the Influence of Micro-Structure on the Modified Effective Modulus Approach for Composite Laminates,' Proc. Internatl. Conf. Composite Materials, AIMPE (1976).
13. M.G. Bader and P.T. Curtis, 'The Micromechanics of Fibre Composites-Carbon Programme,' 1st Report, July (1977), and 2nd. Report, Dec. (1977), Dept. Met. and Matls. Tech., Univ. Surrey.
14. J.E. Srawley and W.F. Brown, 'Fracture Toughness Testing and Its Applications,' ASTM STP 381 (1964).

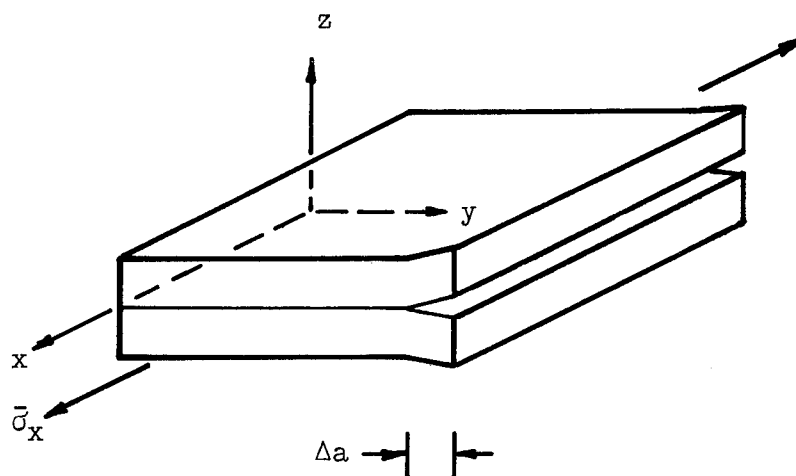


Fig. 1 Isometric View of Free Edge Delamination

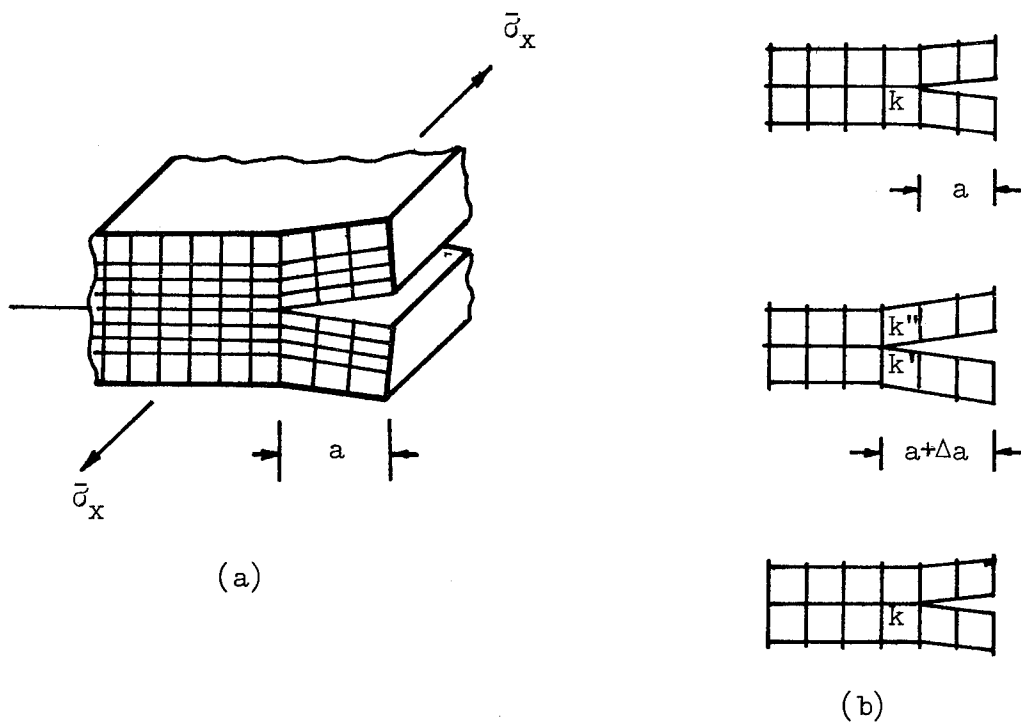


Fig. 2 (a) Finite Element Grid-work in the Crack-tip Region.
 (b) The Finite Element Virtual Crack Closure Procedure.

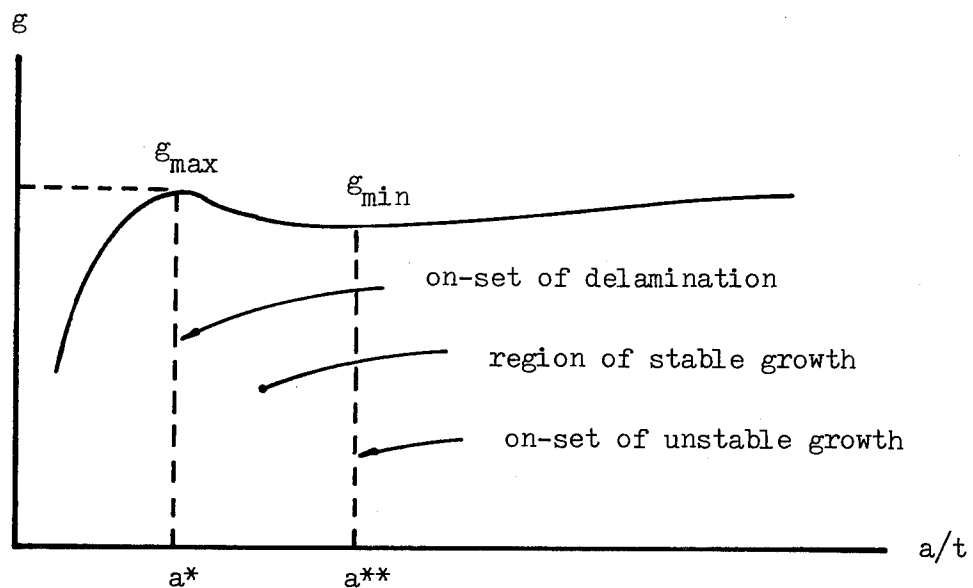


Fig. 3 Energy Release Rate Function g vs. Delamination Size a/t

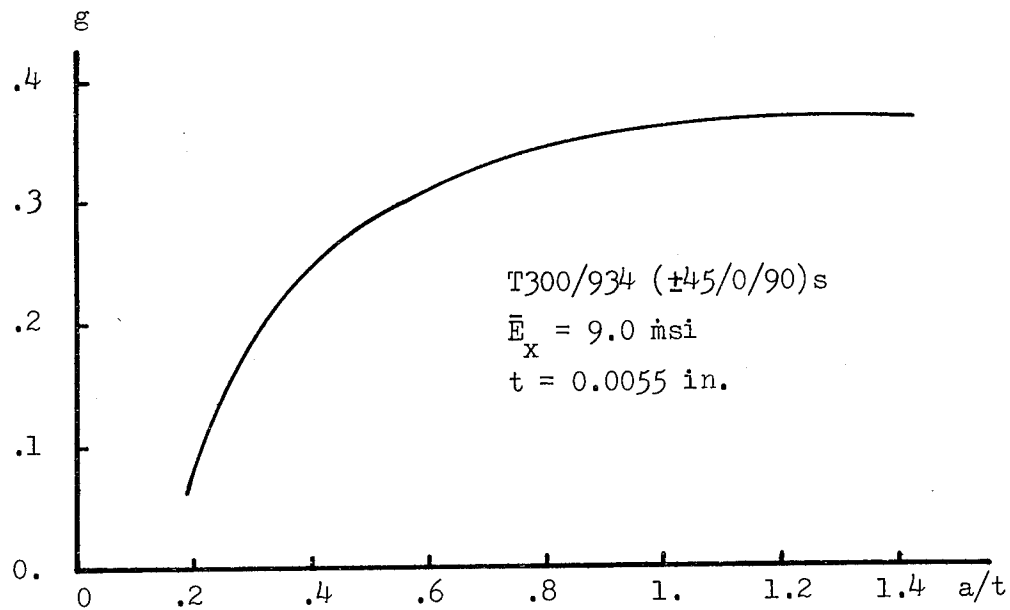


Fig. 4 Energy Release Rate Function g for Crack Along 90/90 Interface. T300/934.

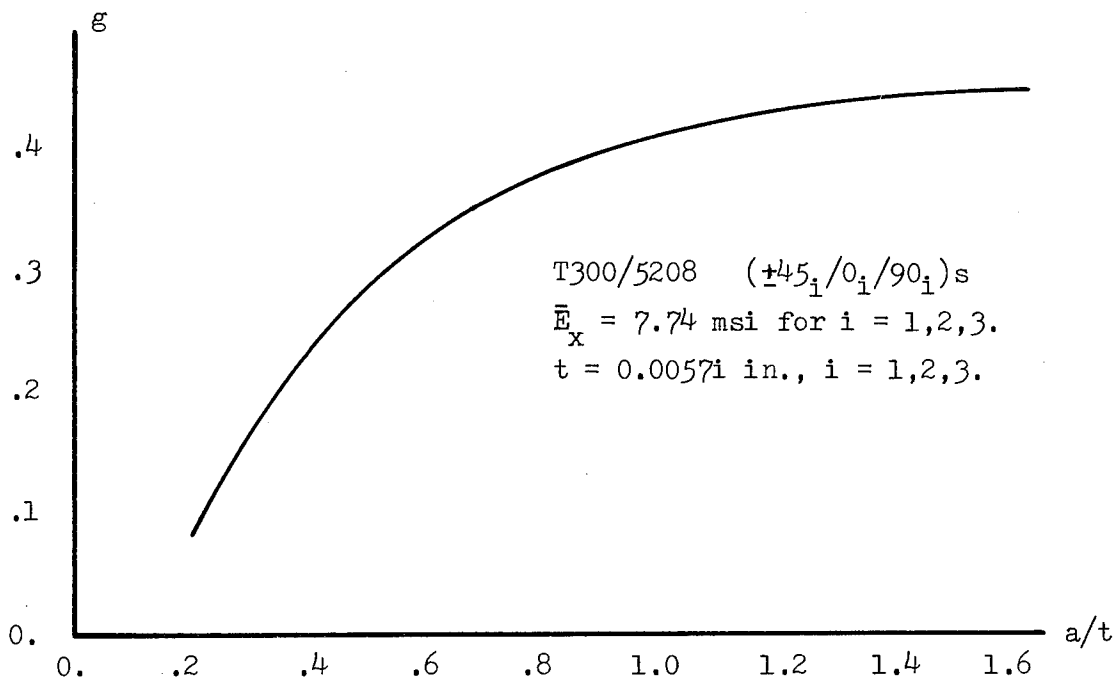


Fig. 5 Energy Release Rate Function g for Crack Along 90/90 Interface. T300/5208.

SESSION 10

MARINE APPLICATIONS AND DESIGN

Chairman: M. Silvergleit

**David W. Taylor Naval Ship
Research & Development Center**

CURRENT DEVELOPMENTS IN ADVANCED COMPOSITES
FOR NAVAL SHIP APPLICATION

J.J. Kelly
David W. Taylor Naval Ship R&D Center
Annapolis, MD. 21402

H.H. Vanderveldt
Naval Sea Systems Command
Washington, D.C. 20362

Abstract: The reasons for and the limitations on the use of composites for ship applications are described. The current exploratory development program in advanced composites for Navy ship applications emphasizes high performance craft such as hydrofoils. The future program will complete these efforts and stress broader applications for composites. Development of fire resistant composites, survivable structural concepts and materials which reduce maintenance requirements will be emphasized.

Introduction

The purpose of this paper is to provide an overview of the Navy's R&D Program in composite technology for ship application. Prior to describing the current program and its future directions, the reasons for both the Navy's interest and its hesitation in all-out adaptation of these materials should be clearly understood. The major reasons for the Navy's interest are:

- These materials offer the potential of reducing structural weight with little or no sacrifice in strength.
- The materials can be "designed" to meet the requirements of a specific application.
- Past experience in applications such as small boats, submarine sonar domes, superstructure, ladders and piping by the U.S. Navy has generally been good.
- Use of composite materials by both foreign navies and commercial/private ships has been extensive and generally exhibited good, reliable performance.

- The capacity of these materials to "fail" gradually rather than suddenly without warning is a highly desirable characteristic.
- The noncorrosive nature of most of these materials can lead to a significant reduction in shipboard maintenance requirements.
- For some applications such as minesweepers, the non-magnetic features of most of these materials are important.

In spite of these desirable features, the Navy is cautious in the use of these materials in ship applications. The following factors have limited and delayed the use of composites:

- The effect of long-term marine environment exposure on mechanical and physical properties of composite materials and configurations is not well known.
- The cost of the materials and subsequent fabrication are relatively high.
- Composites require the addition of fire retardants or protective coatings to survive and not contribute in a fire environment. Most of these materials will emit large quantities of smoke and toxic products in a fire, even if not contributing to supporting the fire. This is a serious problem, especially in the confined spaces of a ship at sea.
- Lack of detailed knowledge on all loads and conditions which can effect a specific application.
- At the present time, the shipbuilding industry, Navy shipyards and fleet support activities are not geared to handle these materials.
- In contrast to the Air Force, Army and the Navy's Air Fleet, there are only a limited number of ships available for testing new materials/concepts in a real environment.
- The funding levels for R&D in composites do not permit investigation for a large number of applications.

Program Management and Selection

The R&D programs currently directed by the Naval Sea Systems Command are all aimed at either eliminating or reducing the impact of these limitations so that the fleet's performance can be increased and/or the cost of ownership can be reduced. These programs are carried out by in-house design personnel, Navy laboratories and industrial contractors. For clarity, the R&D programs can be viewed as being conducted in two distinct phases. In one case, the risk is held to a minimum by using accepted design practices and materials with well established properties and behavior. In general, these efforts are in response to a specific fleet need, such as design and evaluation of composite antenna masts. In contrast, the exploratory development phase not only addresses advanced materials such as graphite and boron fiber reinforced epoxies, thermoplastics, metal matrix composites but concepts such as isogrid structures. The primary purpose of this latter R&D phase is to identify areas where composites can have a significant impact, and develop both the materials and/or data necessary to support design for a marine environment application. In general, with this information in hand, a test component is fabricated to develop cost data and for testing both in the laboratory and on a ship if possible. The results of these efforts are incorporated in a specification guidance document and report to support follow-on advanced development, manufacturing technology or direct use by the fleet.

As mentioned earlier, the available resources for these programs and especially the exploratory development efforts are limited. In order to obtain maximum use of these resources, developments successfully completed or currently underway in the Air Force, Army, NASA and Navy Air Systems are carefully reviewed for use in this program.

Current Programs

The current Exploratory Development is shown in Table I with the lead performing activity identified. For the most part, the program shown here had its genesis back in 1973/74 when there was a fairly high emphasis on advanced ships such as hydrofoils. Since many of these ships and craft were weight critical, the use of composites for structural and equipment applications was a high priority item.

Studies were conducted to determine where composites could be employed and how much benefit could be derived.^{1,2} Since most of these tasks are discussed in detail in other

papers today, only a brief synopsis of each will be provided here.

- The composite flap is a control surface for a hydrofoil ship. The flap was designed and fabricated by Boeing Marine Systems and installed on the Navy hydrofoil "High Point" in late 1978. The flap is actually a hybrid consisting of a titanium structure to which graphite/epoxy skins are attached. These skins are overlaid with a thin titanium sheet for erosion protection. Evaluation of the flap should be completed in early FY1980.
- The hybrid Box Beam is a test element which represents a ship structure. The hybrid Box Beam consists of a HY-130 steel frame with graphite/epoxy skins attached. It was designed and fabricated by the McDonnell Douglas Astronautics Company. This element has been received by the Navy and examined nondestructively by a pulse echo ultrasonic test method. The element has failed in the area of load application twice and an in-depth analysis of the failure and the necessary corrective action is currently underway.
- The all composite Box Beam is again a test element and represents an extension of the technology for the Navy's data base. McDonnell Douglas Astronautics Company is currently doing the preliminary design and testing for this element.
- The Silicon Carbide/Aluminum metal matrix composite has been developed by the Naval Surface Weapons Center, White Oak Laboratory. The composite can be readily made with 2000, 6000 and 7000 series aluminum alloys. Current investigations are aimed at extending this capability to the 5000 series marine grade aluminum alloys. Investigations of joining methods, corrosion behavior and mechanical properties are currently underway.
- Failure Analysis and Nondestructive Evaluation methods are currently being developed and evaluated by the Naval Research Laboratory. In particular, the analysis effort is investigating failure behavior of composites and bonded joints under both static and fatigue spectrums representative of the loading induced on box beam and hydrofoil structures. The use of ultrasonic test techniques with the ability to provide permanent records is the

primary thrust of the NDE effort.

- Structural Evaluation is the Navy's planned effort to evaluate box beams under full spectrum loading; analyze the results of the shipboard tests of the instrumented foil flap and develop the necessary analytical methods for future evaluations and materials developments.
- Marine properties are determined for a number of composite materials and configurations that are being used or contemplated for use in box beams, flaps, etc. In addition, studies of other promising composite materials such as fiber-reinforced thermoplastics, metal matrix composites and joint designs are also investigated.
- GRP piping systems for shipboard service investigation involved an extensive amount of testing of actual pipe, joints, and complete assemblies for fatigue, fire resistance, fouling behavior, erosion resistance, and shock resistance. This program will be completed this fiscal year and has already produced a draft specification for GRP piping systems that is currently being reviewed by industry.

Future Directions

As can be seen on Table II, for the near term, the emphasis in the exploratory development program will be to complete the current underway efforts directed to advanced ship applications. As shown in Table III, the process of identifying specific shipboard areas of potential composite application will be continued and items which can contribute to reduced maintenance requirements will be stressed. Development of fire retardant composite materials with low smoke and toxic product evolution will be initiated. For the longer term, the use of composite materials for applications such as propellers or impellers will be investigated. This effort will draw on a new independent in-house Navy laboratory effort in this area. Isogrid or similar concepts using composite materials will be investigated for application to ship and especially advanced craft structures such as Air Cushion Vehicle propeller shrouds where they can offer improved maintenance requirements. The combination of ceramic fibers and foam as well as organic composites for structural ballistics and fire protection

will also be examined. The SiC/Al composites and other metal matrix composites will be investigated for specific ship application. These applications will be determined when a proper trade-off between existing materials, organic and metal matrix composites has been conducted.

References

1. Greszezuk, L.B. and Hawley, A.W.; Application of Advanced Composites to Patrol Craft Hydrofoils; Final Report, Contract No. N00024-72-C-5536, McDonnell Douglas Astronautics Company, April 1973.
2. Greszezuk, L.B. and Hawley, A.V.; Application of Advanced Composites to Hydrofoil Strut; Final Report, Contract No. N00024-72-C-5536, McDonnell Douglas Astronautics Company, December 1973.

TABLE I

CURRENT EXPLORATORY DEVELOPMENT PROGRAM

ADVANCED COMPOSITES MATERIALS

FOR

SURFACE SHIPS AND SUBMARINES

COMPOSITE FLAP FOR HYDROFOIL	BOEING MARINE SYSTEMS
HYBRID BOX BEAM (Composite Over HY130 Frame)	MCDONNELL DOUGLAS ASTRONAUTIC COMPANY
ALL COMPOSITE BOX BEAM	MCDONNELL DOUGLAS ASTRONAUTIC COMPANY
FAILURE ANALYSIS/NDE	NRL
STRUCTURAL EVALUATION	DTNSRDC
MARINE PROPERTIES/JOINT DESIGN	DTNSRDC
SILICON CARBIDE/ALUMINUM	NSWC/WO
GRP PIPING SYSTEMS	DTNSRDC

TABLE II

FUTURE DIRECTIONS OF THE ADVANCED COMPOSITES MATERIALS
FOR SURFACE SHIP AND SUBMARINE PROGRAM

NEAR TERM:

- COMPLETE CURRENT ADVANCED SHIP APPLICATIONS
- IDENTIFY SHIPBOARD AREAS FOR COMPOSITE APPLICATION
- INITIATE DEVELOPMENT OF FIRE RESISTANT COMPOSITE MATERIALS

LONG TERM:

- INVESTIGATE COMPOSITES FOR APPLICATIONS SUCH AS
PROPELLERS AND IMPELLERS
- DEVELOP ISOGRID-LIKE STRUCTURE TECHNOLOGY FOR SHIP APPLICATION
- INVESTIGATE FEASIBILITY OF COMBINED FIRE/BALLISTIC PROTECTION
- INVESTIGATE METAL MATRIX COMPOSITES FOR SPECIFIC SHIP APPLICATIONS

TABLE 3 - ACV SPECIFIC APPLICATIONS

GROUP	COMPONENTS	APPLICATION CRITERIA									
		LOW COST FAB	MAINT REDUCTION	SPECIFIC STRENGTH	SPECIFIC STIFFNESS	FATIGUE SPECTRUM	ENVIRON. FACTORS	CORROSION	WEAR RESIST.	IMPACT RESIST.	OTHER
	BOW AND STERN RAMPS		X	X	X	X	X	X	X	X	
	CARGO DECK		X	X	X			X	X	X	
	CARGO DECK OVERLAY		X					X	X	X	
	PROPULSOR SHROUD	X	X	X	X	X		X	X	X	ACOUSTIC SMOOTHNESS
	PROPULSOR BLADES			X	X	X			X	X	
	MASTS		X		X	X	X	X			
	LIFT FAN HOUSING	X	X		X			X	X	X	ACOUSTIC SMOOTHNESS
	LIFT FAN BLADES		X	X	X	X		X	X	X	
	LIFT FAN CORE STRUCTURE			X	X						
	GEAR BOXES (HOUSINGS)	X		X	X	X					
	GEARS, LIFT AND PROPULSION	X		X	X	X			X		

ENVIRONMENTAL EFFECTS ON FIBER REINFORCED
ORGANIC MATRIX COMPOSITES

M. Silvergleit

A.B. Macander

F.A. Brauer

H.P. Edelstein

David W. Taylor Naval Ship Research and Development Center
Annapolis, Maryland 21402

Abstract: A review is presented on the effects of the marine environment on fiber reinforced organic matrix composites. In addition to the effects of extended immersion in seawater on composite properties, the limiting utility of composites due to cavitation erosion, flammability and smoke spread evolution and damage due to impact are discussed. In general, high quality, low void content glass reinforced plastics (GRP) and graphite epoxy composites retain over 90% of their initial strength after three years immersion in seawater. Organic matrix composites, which are subjected to high speed fluid flow are degraded by erosion due to the collapse of the cavitation cloud, however, erosion resistance can be improved by using elastomeric or thin metallic overlays. With the exception of polyimides, organic matrix composites have poor resistance to flammability and emit large quantities of dense smoke. Impact resistance of composites is a function of fiber/resin properties and composite orientation. Incorporation of high toughness flexible matrices and/or high strength, low modulus fibers will increase composite impact resistance.

Key words: Graphite epoxy; glass reinforced plastics; advanced composites; extended immersion; marine environment; cavitation erosion; flammability; impact.

Emphasis in the Navy is being directed to reduce ship subsystem weights while maintaining or increasing lifetime reliability. Reductions in weight can be achieved through the development and use of low weight, high strength/stiffness fiber reinforced organic matrix composites. Glass reinforced plastics (GRP) which are currently being used and graphite epoxy composites which are contemplated for use in Navy ship structural applications are the two typical composites discussed. The

literature abounds with information on fabrication procedures and physical and mechanical properties of GRP and graphite epoxy composites. However, for Naval structural use information is required on the response of these materials to the marine environment. It may be expected that composites used in surface ship applications may be subjected to prolonged exposure to seawater. Under these conditions the effect of water on strength retention and response of composites under fatigue loading conditions will be of extreme importance. In sub-surface applications, similar information is required except that the effect of pressure on composites would be the dominant factor. Application of composites in high speed areas, such as propellers, foils, etc....may be subjected to degradation by cavitation erosion. Conventional organic matrices support combustion and evolve large quantities of smoke while burning. Information on the response of composites to flammability is essential since recent shipboard fires have placed severe restrictions on materials which support combustion and evolve smoke. Damage may be induced in composites by impact during docking procedures or maneuvers. This type of damage can result in cracking of the matrix which may permit ingress of water into the structure, thereby reducing its efficiency, or in the main, cause significant loss in strength or stiffness. These major aspects of the Navy's program on the effects of the environment and flammability and damage on fiber reinforced organic matrix materials are delineated in this paper.

EFFECT OF EXTENDED IMMERSION

The effects of extended exposure to seawater on GRP laminates which are used in surface ship applications are shown in Figure 1. The response is quite typical of GRP materials, in that if degradation occurs it will occur in a relatively short time after which the rate slows down with no further loss in strength.¹ There have also been periodic surveys conducted by the Navy to evaluate the laminate properties and to assess the durability of Navy small boat GRP hulls. A study² conducted for the Navy showed no indication of degradation in GRP hulls due to aging or extended immersion in the marine environment.

GRP materials have also been used in submarine applications. Submarine fairwaters which are used to minimize

turbulent flow have performed satisfactorily for over 11 years. Fried and Graner³ report that after 11 years service there was no evidence of deterioration and the material met the original specification requirements, Figure 2. Studies⁴ were conducted to assess the effects of extended seawater immersion at various pressures up to 13,000 psig (30,000 foot depth) on glass reinforced filament wound epoxy materials. It was observed that these materials were unaffected by hydrostatic pressure and retained over 90% of their initial strength provided that the laminates were of good quality and had void contents of less than 1%. Other compositional factors, such as type of resin and hardener system, could markedly influence response of the material to extended immersion. It was also demonstrated that the fatigue strength in the "wet" state was somewhat lower than the "dry" condition. A concept⁵ was developed wherein the fatigue life of fiber reinforced plastics was expressed as a percentage of the ultimate static stress.

The weight critical nature of the Navy's high performance ships, i.e., hydrofoils, air cushioned vehicles, and surface effect ships, impose design limitations on ship size and operational efficiencies. Graphite epoxy composites which are lightweight and have high strength and stiffness characteristics meet the design requirements of high performance ships and are actively being considered for structural applications. As in the case of GRP, it was observed⁶ that the properties of a high quality graphite epoxy composite (void content < 1%) were not adversely affected by extended immersion in seawater, Figure 3. It was also noted that there was no relation between amount of water absorbed and strength retention and that the maximum rate of water absorption occurred during the initial phase of the immersion period.

CAVITATION EROSION

The phenomenon of cavitation erosion is associated with high velocity systems, such as propellers, pumps and foils. It results in local damage and removal of material due to the cavitating environment. The mechanism of cavitation erosion has been proposed as occurring when vapor bubbles form in a rapidly moving liquid and grow until they reach a higher pressure and then collapse. Energy created by the collapsing bubbles damage the material with resultant erosion. Studies of this phenomenon have shown⁷ that high yield steels, titanium

and stainless steel are most resistant to cavitation erosion, while fiber reinforced organic matrix composites are affected to a greater degree, Figure 4. Measurements were made using the vibratory cavitation erosion apparatus, ASTM G-32. The initial effect of the cavitation phenomenon on fiber reinforced organic matrix composites is to erode and degrade the matrix. Continued implosions crack the matrix and the exposed fiber becomes unstable. In the extreme case the fiber is eroded and can be fractured. Elastomeric type coatings are available which are resistant to cavitation erosion but difficulties have been noted in adhering large sections to the coatings.

FLAMMABILITY

Under exposure to a flame, polyester and epoxy matrices will support combustion and evolve large quantities of smoke. Recent shipboard fires have resulted in placing severe restrictions on the utilization of materials which support combustion and evolve smoke. These restrictions may severely limit the use of organic matrix materials, particularly in ships habitability spaces. The effect of resin, fiber and fire retardant additives on the flammability characteristics of organic matrix composites were evaluated.⁸ Flame spread index was determined by the radiant panel test, ASTM E-162, the amount of smoke and products of combustion were determined using the National Bureau of Standards Smoke Density Apparatus, while the amount of oxygen required to support combustion was determined using the Oxygen Index Method, ASTM D2863. Polyimide/glass laminates, which have the highest thermal resistance of fiber reinforced organic matrix composites, had the greatest resistance to burning as exemplified by a flame spread index of 1. A comparison of the flammability characteristics of various composites is shown below:

TABLE 1
Flame Spread of Fiber Reinforced
Organic Matrix Composites

<u>Composite</u> <u>(Matrix/Reinforcement)</u>	<u>Flame Spread</u> <u>Index</u>
Polyimide/Glass	1
Polyester/Glass	31

TABLE 1 (cont)

<u>Composite (Matrix/Reinforcement)</u>	<u>Flame Spread Index</u>
Epoxy/Glass	38
Epoxy/Graphite	32

Addition of fire retardants to the polyester and epoxy matrices resulted in significant reductions in flame spread index. For example, the flame spread index of the polyester glass composite, Table 1, was reduced from 31 to 5, after the addition of antimony trioxide and hydrated alumina fire retardants. However, this also resulted in a substantial increase in the amount of smoke evolved. The amount of smoke generated, as determined by the National Bureau of Standards Smoke Density Apparatus is shown below:

TABLE 2

<u>Composite (Matrix/Reinforcement)</u>	<u>Maximum Specific Optical Density</u>
Polyimide/Glass	29
Polyester/Glass	469
Polyester/Glass*	634
Epoxy/Glass	364
Epoxy/Glass*	565
Epoxy/Graphite	313
Epoxy/Graphite*	678

*Resin system contains fire retardants

The high thermal capabilities of the polyimide system is evidenced by its having the lowest smoke generation (maximum specific optical density). The addition of fire retardants showed significant increases in smoke generation for both the polyester and epoxy systems. Ceramic type barriers when added to the polyester or epoxy systems were found to effectively reduce the flame spread index and increased the time required to develop maximum smoke accumulation.

IMPACT

Fiber reinforced composite materials used in Naval structural applications may be damaged by impact induced

in docking procedures, by falling tools or equipment during ship overhaul procedures and by striking submerged logs or other debris during high speed maneuvers. Studies are being conducted at the Center to determine the influence of fiber, matrix, matrix flexibility and fiber orientation on the impact resistance of composites. GRP materials, incorporating an elastomeric modified epoxy resin, exhibited significantly higher impact resistance than conventional polyester or epoxy resin systems. Similar studies on graphite epoxy composites have indicated that normal impact strength is a function of fiber tensile strength and modulus, fiber orientation and resin ductility.

A summary of the data for graphite epoxy composites is shown in Table 3. For example, a composite fabricated with high tensile strength, intermediate modulus graphite fiber subject to normal impact had greater impact resistance than a lower strength ultra-high modulus graphite fiber. Use of a thermoplastic resin system, which has higher ductility than the conventional rigid epoxy resin, in a composite reinforced with graphite fibers also produced improved impact resistance characteristics.

TABLE 3

Impact¹ Strength of 1/4" Thick Composites

<u>Material</u>	<u>Impact Energy (ft-lbs)</u>
Ultra High Modulus Graphite Fiber/Epoxy ² Matrix (0°/90° Fiber Orientation)	4
High Tensile Strength Medium Modulus Graphite Fiber/Epoxy ² Matrix (0° Fiber Orientation)	16
High Tensile Strength, Medium Modulus Graphite Fiber/Epoxy ² Matrix (0°/90° Fiber Orientation)	18
High Tensile Strength, Medium Modulus Graphite Fiber/Flexibilized Epoxy Matrix (0°/90° Fiber Orientation)	22

TABLE 3 (cont)

<u>Material</u>	<u>Impact Energy (ft-lbs)</u>
High Tensile Strength, Medium Modulus Graphite Fiber/Thermoplastic Matrix ³ (0°/90° Fiber Orientation)	32

- 1) Impact Normal to Surface
- 2) Rigid Epoxy Matrix
- 3) Composite Thickness - 1/8"

Observation by ultrasonic nondestructive evaluation of damage induced by impact and correlation with mechanical properties showed that damage is confined to a local area. Additionally, impact resistance of graphite epoxy composites can be improved by incorporation of fibers of high strain characteristics, such as, glass or Kevlar. Another possible alternative to improve impact resistance may be the use of an elastomeric or metallic overlay.

SUMMARY

- o GRP and graphite epoxy composites, void content less than 1%, have not been degraded by extended immersion in the marine environment.
- o Fiber reinforced organic matrix composites are eroded and degraded by cavitation erosion. Effects of cavitation erosion can be reduced by utilization of an elastomeric coating or thin metallic overlay.
- o Polyimide resin matrix composites exhibit the greatest resistance to flammability and evolution of smoke. In general, polyester and epoxy matrices have poor resistance to flammability and generate large quantities of dense smoke.
- o Ceramic type barriers are effective in reducing flame spread and smoke evolution.
- o Fiber/resin properties and composite orientation influence impact resistance of composite materials.

References:

1. Silvergleit, M., "Historical Review - Navy Programs," Center for Composite Material, University of Delaware, Newark, Delaware, 30-31 March 1976.
2. Graner, W.R. and R.V. Della Rocca, "Evaluation of U.S. Navy GRP Boats for Material Durability," Society of the Plastics Industry, Reinforced Plastics/Composites Division, 26th Annual Technical Conference, February 1971.
3. Fried, N., and W.R. Graner, "Durability of Reinforced Plastic Structural Material in Marine Service," Marine Technology, Vol. 3, Nov 3, 1966.
4. Silvergleit, M., J. Kaminetsky and N. Fried, "Filament Wound Glass Reinforced Plastics for Deep Sea Vehicles - the Present-State-of-the-Art," Society of Aerospace Materials and Process Engineers, 1967.
5. Freund, J.F. and M. Silvergleit, "Fatigue Characteristics of Glass Filament Reinforced Plastic Material," Society of the Plastics Industry, Reinforced Plastics Division, 21st Annual Technical Conference, February 1966.
6. Macander, A. and M. Silvergleit, "The Effect of the Marine Environment on Stressed and Unstressed Graphite/Epoxy Composites," Naval Engineers Journal, August 1977.
7. Silvergleit, M., R. Deppa and H.P. Edelstein, "Potential Application of Advanced Composites for High Performance Craft," National SAMPE Technical Conference Series, Vol. 5, October 1973.
8. Silvergleit, M., J. S. Morris, and C. N. LaRosa, "Flammability Characteristics of Fiber Reinforced Organic Matrix Composites," Polymer Engineering and Science, Vol 18, No. 2., February 1978.

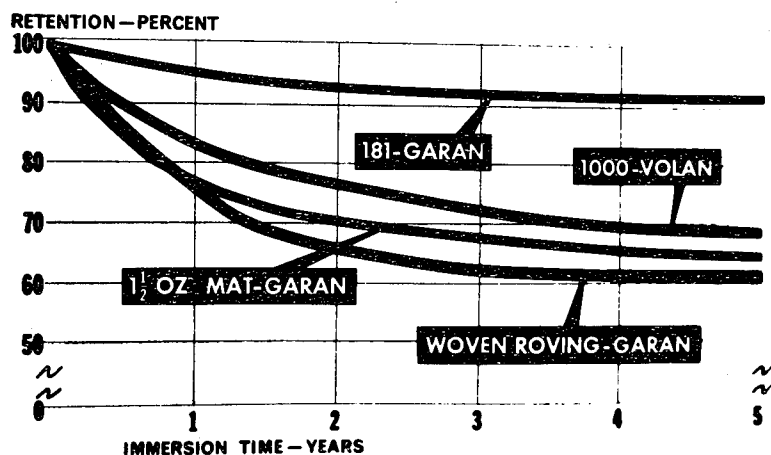
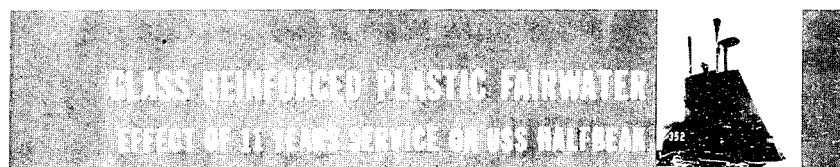


Figure 1 - Effect of Extended Immersion in the Ocean on the Compressive Strength of Glass Reinforced Polyester Laminates.



PROPERTY	CONDITION	ORIGINAL DATA	CURRENT DATA (11 YRS. SERV.)	SPECIFICATION ^(a) REQUIREMENT
FLEXURAL STRENGTH, PSI	DRY	52,400	51,900	50,000
	WET ^(b)	54,300	46,900	45,000
FLEXURAL MODULUS, PSI x 10 ⁻⁶	DRY	2.54	2.52	2.50
	WET	2.49	2.37	2.30
COMPRESSIVE STRENGTH, PSI	DRY	-	39,100	33,000
	WET	-	35,600	28,000

(a) MIL-P-17549

(b) TWO HOUR BOIL

Figure 2

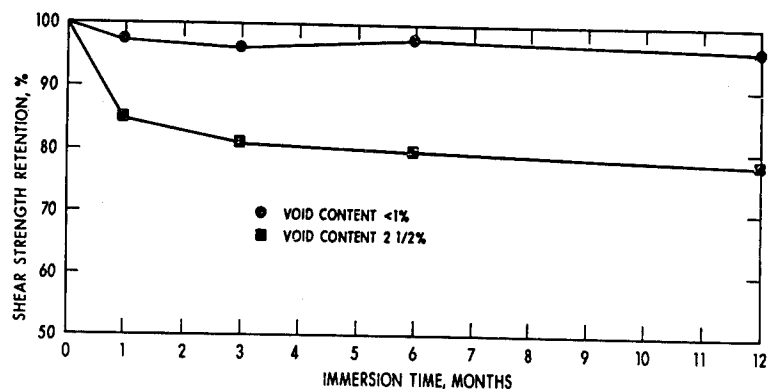


Figure 3 - Effect of Extended Immersion on the Inter-laminar Shear Strength of Graphite Epoxy Composites

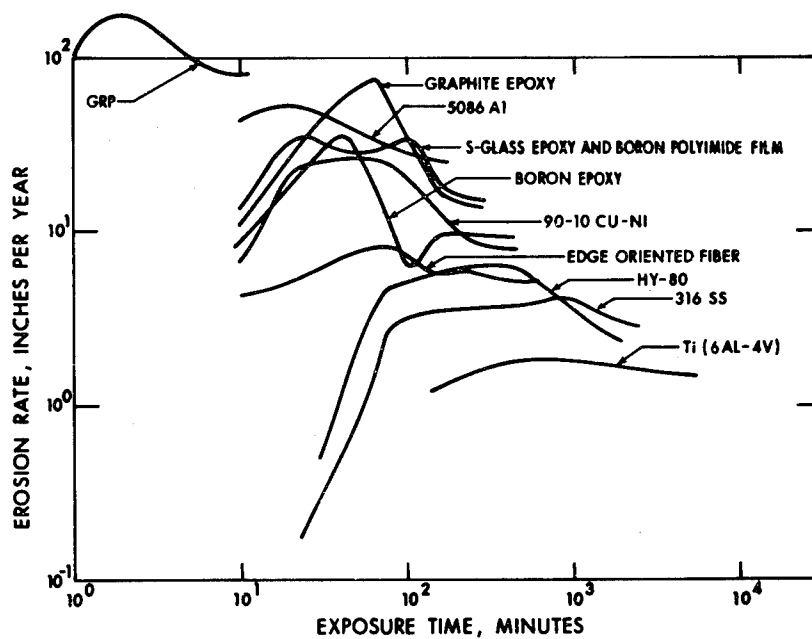


Figure 4 - Cavitation Erosion Rate for Various Materials

COMPOSITE TECHNOLOGY FOR MARINE APPLICATION

W. P. Couch

David W. Taylor Naval Ship R&D Center
Bethesda, MD 20084

Abstract: Under the sponsorship of the Naval Sea Systems Command (NAVSEA 035), the David W. Taylor Naval Ship Research and Development Center (DTNSRDC) has been conducting a program to assess the current technology status of advanced composites, and to determine the feasibility of application to marine structures. The approach being utilized to achieve this objective involves a coordinated structures/materials community effort seeking input from private industry and other government agencies. As a result of feasibility studies performed by the McDonnell Douglas Astronautics Company and the Grumman Aerospace Corporation and a review of high payoff areas for structural application of advanced composites by the Naval Ship Composites Community, the hydro-foil strut/foil system was selected as the primary structural element to evaluate the use of advanced composites for advanced naval ship structures. Two subcomponents were selected for this evaluation; a foil test component (tapered box beam), and a hydrofoil control flap. Concurrently, analytical methods incorporating composite mechanics developed by the aerospace composites program are reviewed, modified and utilized when applicable to determine the structural behavior for marine, load-carrying components. In addition, preliminary design studies are conducted on other naval ship structures to determine the feasibility of composite construction. The following text describes the current effort under investigation related to the four program subtasks: box beam validation, foil flap validation, analytical methods and design application studies.

Key Words: Advanced composites, structural analysis, advanced ships, nondestructive tests, fatigue tests, elastic properties, ultimate strength.

Box Beam Validation: The objective of the box beam subtask is to assess the fatigue behavior of a typical graphite/epoxy (gr/ep) structure under simulated sea loads, and compare its behavior with current metal designs. The McDonnell Douglas Astronautics Company has designed and fabricated^{1,2} two box beams consisting of T-300/GY-70 hybrid skins and HY-130 steel spars. This design represents a strut/foil system having an approximate weight savings of 25% compared to current metallic strut/foil systems fabricated entirely of steel with a yield strength of 130 ksi. Figure 1 shows schematically the development of the box beam configuration from the forward foil of the hydrofoil, PCH-1 (HIGH POINT).

During the Preliminary Design Phase, several concepts were developed and the subject design was selected for further investigation. The laminate skins consist of 53 plies ($\sim 58\%$) of T-300/5208 at 0° orientation and 32 plies ($\sim 42\%$) of GY-70/5208 at $\pm 45^\circ$ orientation. The 85 plies making up the 1/2 inch thick hybrid composite were dispersed according to the following layup:

$$[0^\circ, (0_3^\circ, \pm 45^\circ)_8, 0_3^\circ, (\pm 45^\circ, 0_3^\circ)_8, 0^\circ]$$

During the Design Verification Phase, the laminate was characterized to validate the theory used to predict the elastic and ultimate strength properties for a hybrid laminate. All averaged experimental data agreed with predicted properties within 7.4%. An in-depth joint evaluation was conducted as the next step of design verification. Both the scarf transition joint and the steel spar to gr/ep skin joint were modeled and evaluated under static and fatigue loading, which led to a 33% reduction in the design ultimate strength of the hybrid laminate. However, this reduction did not significantly sacrifice the efficiency of the overall box beam design since the steel spars are loaded to 90% of yield strength when the hybrid laminate is stressed to the reduced design ultimate strength.

Following the static and fatigue testing of joint models, the box beam design was finalized; see Figure 2. Even though the strength of the adhesive was adequate to transmit the shear stress from the skins to the stiffeners without failure of the adhesive, the design included bolting of the skins to the internal metal structure. The bolted/bonded design was based on reliability considerations of both the box beam and of the full size foil or strut. A NASTRAN finite element analysis was performed on the final design, and compared with the strength of materials analysis performed on the preliminary design; Figure 3 shows the maximum fiber stress in the composite skins and steel spars along the longitudinal centerline of the box beam as a result of the NASTRAN and strength of materials analyses.

The Fabrication Phase included cocurring the steel transition scarf and composite skins, and a thru-transmission ultrasonic C-scan inspection; machining, welding and radiographic inspection of the steel spars and load plate; and bolting/bonding the composite skins to the steel spars, and pulse-echo ultrasonic and Fokker Bond Inspection after assembly. The nondestructive evaluation of the components and finished assembly, see Figure 4, revealed no detectable defects as a result of laminate fabrication or box beam assembly.

The first box beam was scheduled to undergo a static proof test to a maximum load of 60,000 lbs which would induce an extreme fiber stress in the composite skins of 44 ksi (Design Ultimate Strength/Factor of

Safety). Although the box beam incurred delaminations in the load application area at 80% of maximum operating load, elastic strains measured by electrical resistance strain gages agreed with those predicted by the NASTRAN finite element analysis; see Figure 3. The area of delamination was inspected using radiographic and pulse-echo ultrasonic test techniques, and the suspected areas of defects repaired. The load area was also "stiffened" in an attempt to help distribute the shear in this area. A second static proof test was conducted; a similar failure occurred in the same area at a load of 47,500 lbs. It is currently awaiting repair and additional testing while a 3-dimensional finite element analysis (SAP 4) is being performed on the load application detail to explain the cause of failure.

Foil Flap Validation: The second structural component to be addressed is one of the aft inboard control flaps on the PCH-1. The aim in developing a composite flap was to obtain in-service performance data relative to operational loads in the marine environment. An aft inboard flap was chosen because it is the least likely of the flaps to see extreme load conditions, such as impact, for which the program has not yet developed design/analysis techniques. The original plan was to fabricate two flaps; one to be evaluated in the laboratory under full lifetime simulated service loading, and the second to be put into fully instrumented service on the ship. However, the phase out schedule for the PCH-1 prevented following this approach; the first flap will be evaluated in service, to be followed by the laboratory test.

The Boeing Company was awarded a 3-phase contract to design and fabricate an advanced composite flap completely interchangeable with the present metal design. Seven conceptual designs were evaluated during the Preliminary Design Phase; the baseline design was selected for further study. This concept was composed of titanium-clad, variable thickness gr/ep skins and a titanium crank-spar assembly. T-300/934 bi-directional preimpregnated gr/ep fabric oriented at $\pm 45^\circ$ to the flap span and 6Al4V ELI-grade Ti were incorporated into the design. The titanium cladding (.010-inch thick on both sides of each gr/ep skin) was added to protect the composite from water penetration, cavitation erosion, and small-particle impact. The ELI-grade Ti was selected for the crank-spar assembly in order to protect against corrosion fatigue and stress-corrosion cracking. The gr/ep fabric was oriented at $\pm 45^\circ$ to take advantage of its torsional and shear characteristics in that layout. Since the variable thickness skins appeared inadequate to carry the evenly-distributed 6300 psf design load, DTNSRDC conducted a NASTRAN analysis of the baseline design. The results led to constant 0.5-inch thick skins including the Ti cladding; see Figure 5. Once the skin design was finalized, a full range of static and fatigue tests were conducted for mechanical property and salt water exposure data; see Table 1. The results of these tests indicated no significant degradation in material performance after exposure up to 270 days.

In order to verify the design and fabrication processes and to evaluate joints, a full-scale portion of the flap was built and tested. This feasibility component incorporates the first 20 inches of the flap, end joint and crank fitting. The feasibility component sustained a static proof test to maximum operation load or 40% of design ultimate. The component failed after approximately 12,000 cycles (safe life = 16×10^6 cycles) due to a debond along the leading edge, which changed the load path and resulted in a catastrophic failure of the titanium end fitting. A more detailed NASTRAN analysis was conducted, and the component was repaired and beefed up in the leading edge joint and end fitting areas. A second fatigue test resulted in catastrophic failure of the titanium end fitting after 145,000 cycles. The results of these tests led to a removal of all blind fasteners due to their poor fatigue performance and a redesign of the crank-spar assembly for the final design.

A full scale component has been fabricated using the techniques developed during the fabrication of the feasibility component. The covers were made by laying up 36 plies of gr-ep cloth and cured at 350°F and 100 psi in an autoclave. The titanium cladding was bonded to the covers using EA9628 adhesive at 250°F and 100 psi. The crank and spar details were cut to approximate shape with a plasma torch, rough machined to their approximate final configuration, electron beam welded into a single assembly, and milled and bored to final configuration. The composite flap details were stacked for final assembly, bolted with titanium fasteners, and bonded using the EA9628 adhesive at 250°F for 90 minutes and 50 psi. The 52 internal strain gages were calibrated in the laboratory, the flap was installed and actuated on the PCH-1 while on blocks (see Figure 6), the instrumentation was hooked up to the ship's data acquisition system, and the gages again calibrated. Both calibrations indicated that the gages are operating accurately, and that no major performance deficiencies currently exist. The ship is scheduled to go back into the water this summer, with calm and rough water trials scheduled to be completed by the end of 1979. Following the in-service evaluation, the flap will be shipped to DTNSRDC for a full lifetime fatigue evaluation in salt water.

Analytical Methods: Because of the anisotropic nature of fiber-reinforced plastics, strength of material and classical fracture/fatigue methods for analyzing their structural behavior are approximations at best. Instead, a thorough understanding of composite mechanics is required to perform an accurate analysis of complex structures. This includes micro and macro mechanics, lamination theory and failure mechanics. Much of this work has been developed by academia and industry under aerospace sponsored programs. Often, the application of this theory for the design/analysis of marine structures subjected to the unique loads and environment of the ocean requires extension and modification.

A basic knowledge of the stress-strain and transformation relations of an orthotropic, multi-directional laminate was required to develop the

extensional and bending stiffness matrices for the NASTRAN finite element analyses of the box beam and foil flap. In addition to the stress-strain and transformation relations, both the distortion energy and maximum strain failure theories were utilized to predict the elastic and strength properties of the hybrid laminate during the design phase of the box beams. Both the material characterization of the box beam laminate and the static strain-gage evaluation of the box beam structure agreed with the theoretical methods described above. It should be noted that the aforementioned analyses have all been 2-dimensional, i.e., the thru-thickness elastic stiffness and strength properties were not considered. However, the in-plane analyses have not explained the reasons why the box beam has incurred two failures; both of which may well have been interlaminar in nature as opposed to in-plane. It is for this reason that a 3-dimensional analysis is under way; an analysis that is an order of magnitude more complex to perform.

Because graphite/epoxy has demonstrated a very low resistance to impact loading when compared to metals and even glass or kevlar/epoxy, a new study has been initiated to develop design/analysis techniques for this extremely complex dynamic phenomenon. As presently envisioned, a combined material/structural dynamic response computer code will be developed that would give the designer/analyst an effective tool in predicting the behavior of a composite structure under a variety of impact loads such as tools, logs, etc.

Design Application Studies: Although the hydrofoil strut/foil system was selected as the primary structural element to validate the current technology base of advanced composites for marine application, feasibility studies are conducted on other structures with respect to reduced weight and life-cycle costs and increased reliability. Several potential components have been evaluated on SES and ACV type advanced ships including longitudinal hull girder reinforcement, masts, ramps and lift fans. Unless a larger emphasis is placed on making these advanced ships an important part of the fleet, the potential weight savings and increased reliability do not warrant the increase in initial costs associated with research and development of advanced composite materials.

References:

1. Greszczuk, L. B., A. V. Hawley and W. P. Couch, "Application of Hybrid Composites to Hydrofoil Structures," Presented to AIAA/SNAME Advanced Marine Vehicle Conference, San Diego, CA, 17-19 April, 1978.
2. Greszczuk, L. B. and W. P. Couch, "Design, Fabrication, and Non-destructive Evaluation of an Advanced Composite Foil Test Component (Tapered Box Beam)," ASTM STP 674, Composite Materials: Testing and Design (Fifth Conference), June, 1979.

ITEM NO.	EXPOSURE BEFORE TEST	TEST ENVIRONMENT	LOAD TYPE	SPECIMEN CONFIGURATION	NUMBER OF SPECIMENS	TEST OBJECTIVES	NOTES
1	NONE	RT/AIR	STATIC COMPR.	D6-4671-341	5	E_c, F_{cu}, F_{cy} G, F_{su}, F_{sy} E, F_{tu}, F_{ty} F_{isu} S-N CURVE FRACTURE STR.	6 EA 5/16 DIA HOLES. 6 W/O HOLES GOUGES DENTS
2			RAIL SHEAR		5		
3			STATIC TENSION		5		
4			INTERLAMINAR SHR.		5		
5			COMPR. FATIGUE		12		
6			RAIL SHR. FATIGUE		12		
7			TENSION FATIGUE		12		
8			FRACTURE		3		
9			FRACTURE		3		
10	90-DAY EXPOSURE TO SALT WATER	RT/AIR	STATIC COMPR.	D6-4671-341	3	E_c, F_{cu}, F_{cy} G, F_{su}, F_{sy} E, F_{tu}, F_{ty} F_{isu}	
11			RAIL SHEAR		3		
12			STATIC		3		
13		RT/SALT WATER	INTERLAMINAR SHR.	D6-4671-341	3	S-N CURVE	
14			COMPR. FATIGUE		12		
15			RAIL SHR. FATIGUE		12		
16			TENSION FATIGUE	D6-4671-341	12	FRACTURE STR.	
17			FRACTURE		3		
18			FRACTURE		3		

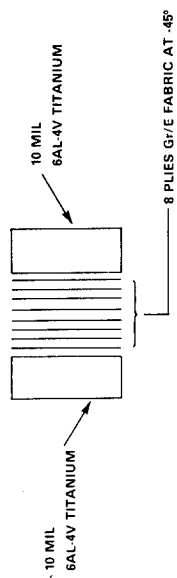


TABLE 1 - COMPOSITE HYDROFOIL FLAP MATERIAL PROPERTY TESTS TITANIUM CLAD GRAPHITE FABRIC/EPOXY ($\pm 45^\circ$)

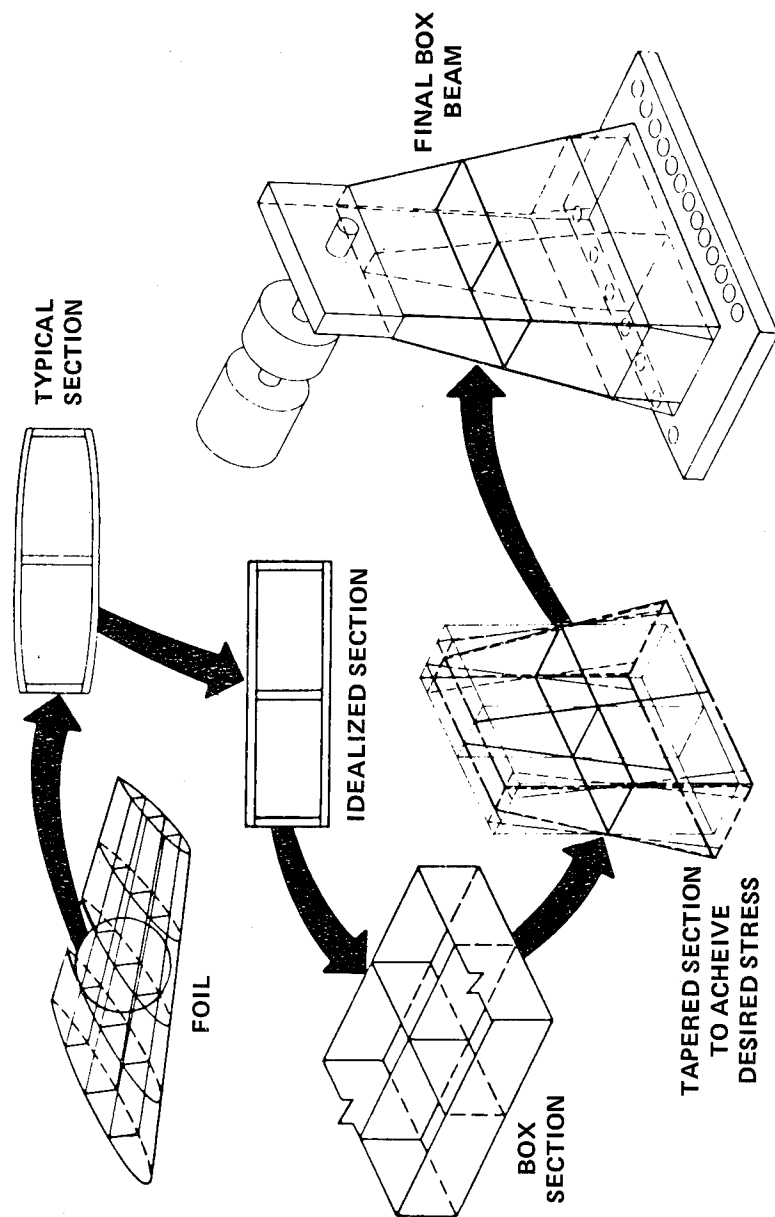


Figure 1 - Development of Box Beam Configuration

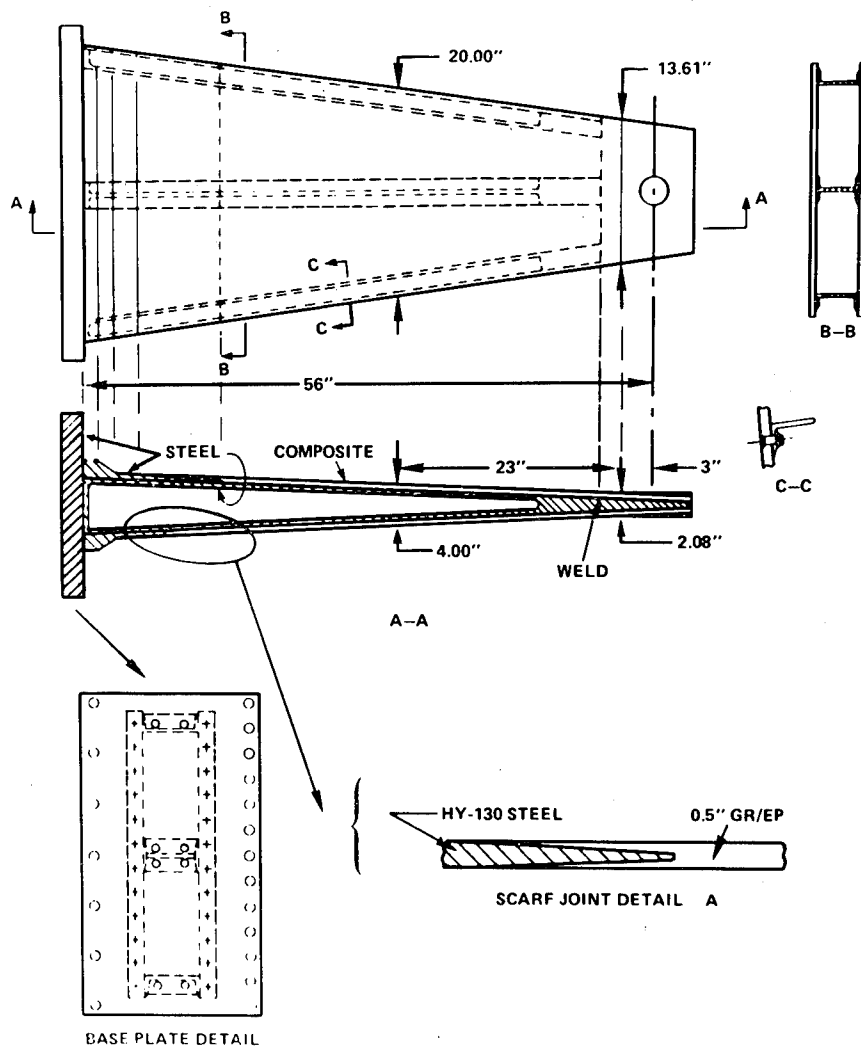


Figure 2 - Schematic of Hybrid Graphite/Epoxy Skin-Skeleton Box Beam

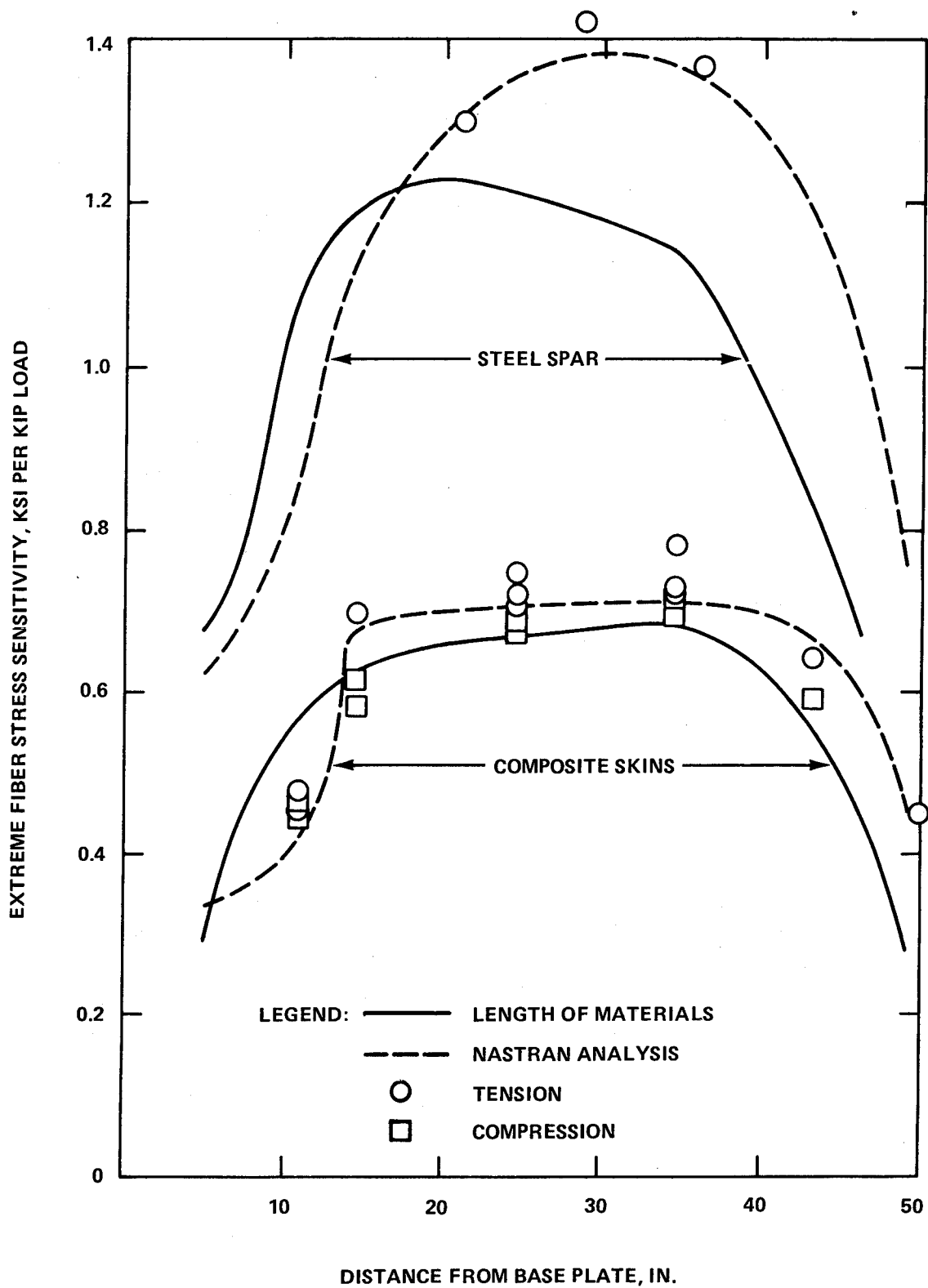


Figure 3 - Comparison of Longitudinal Bending Stresses in Composite Skin and Steel Spar between Strength of Materials and NASTRAN Analyses

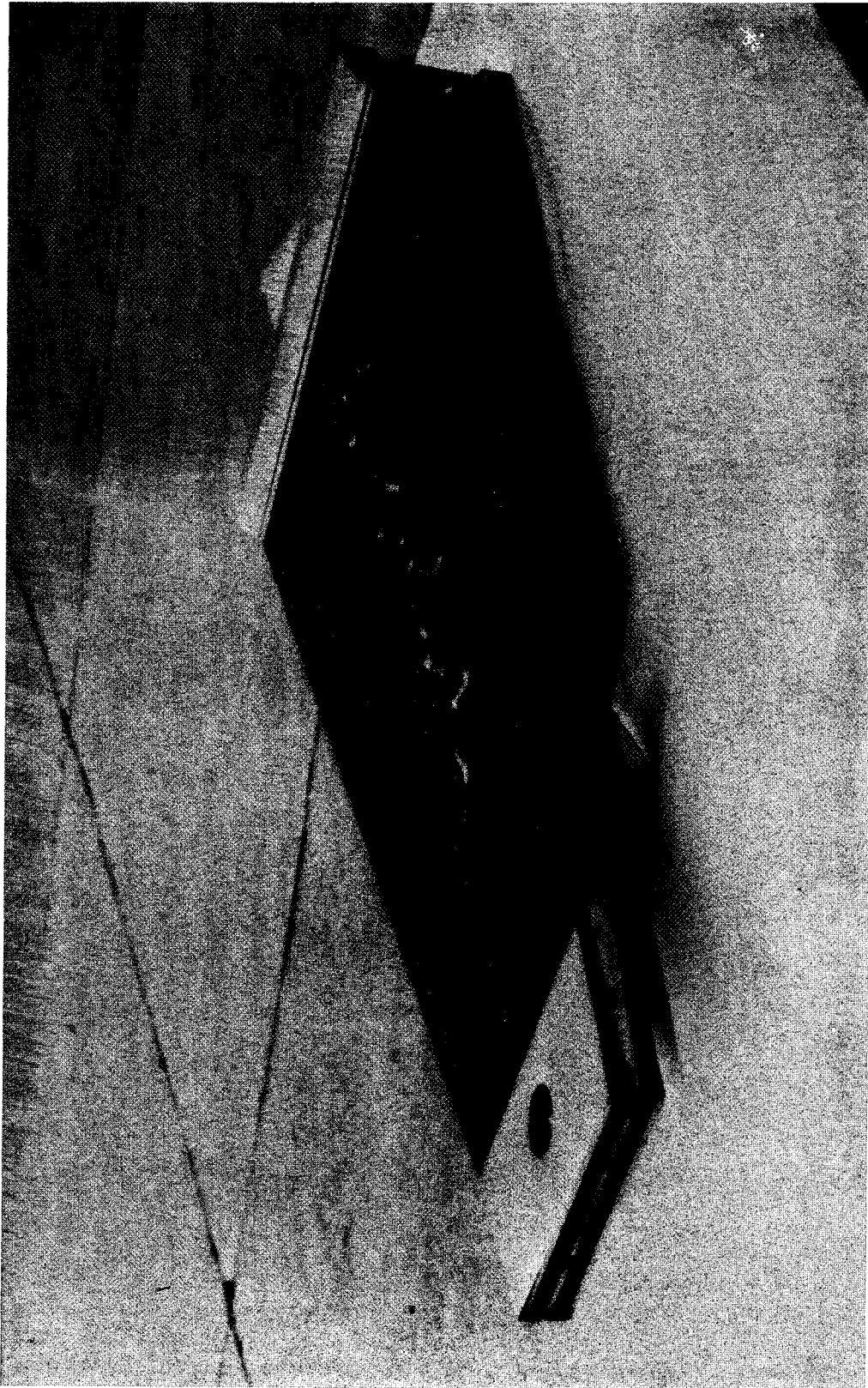


Figure 4 - Photograph of Assembled Box Beam

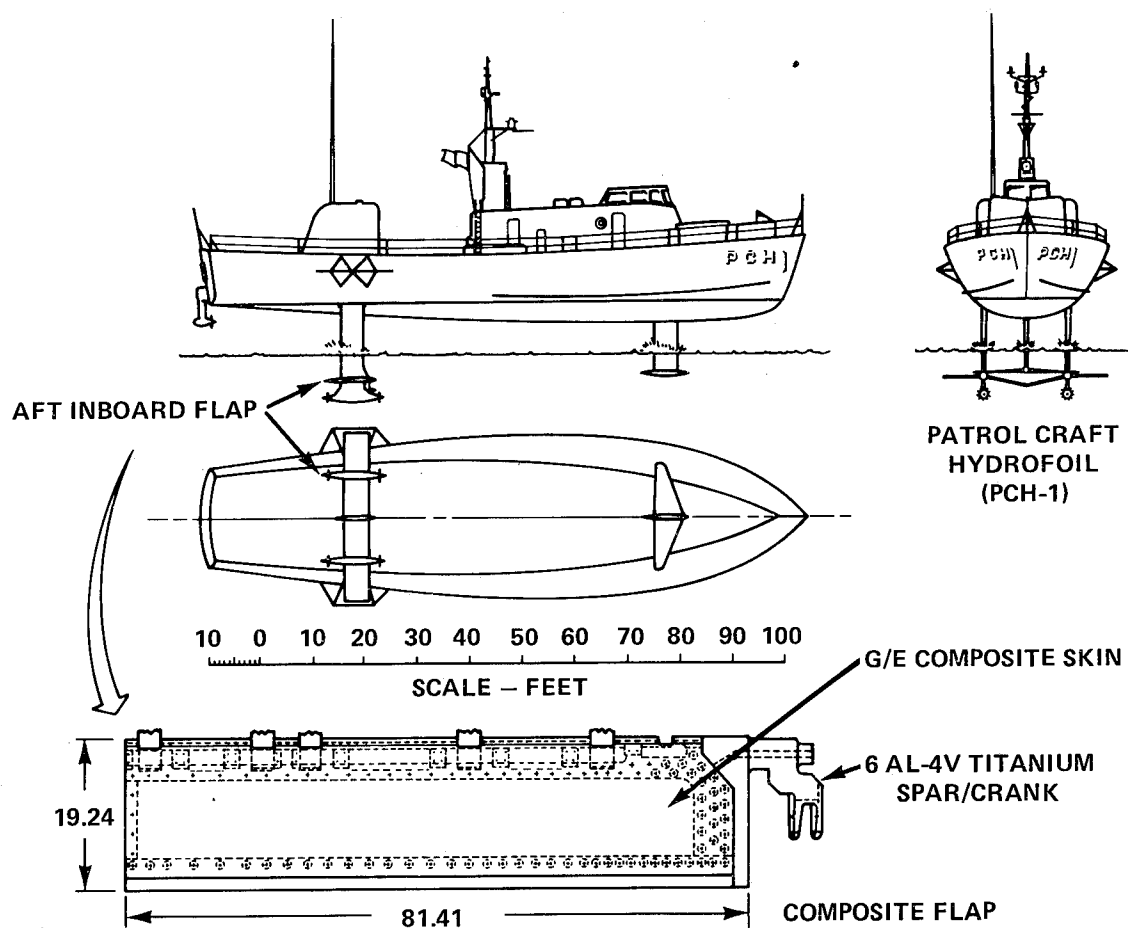


Figure 5 - Patrol Craft Hydrofoil (PCH-1) - Composite Flap

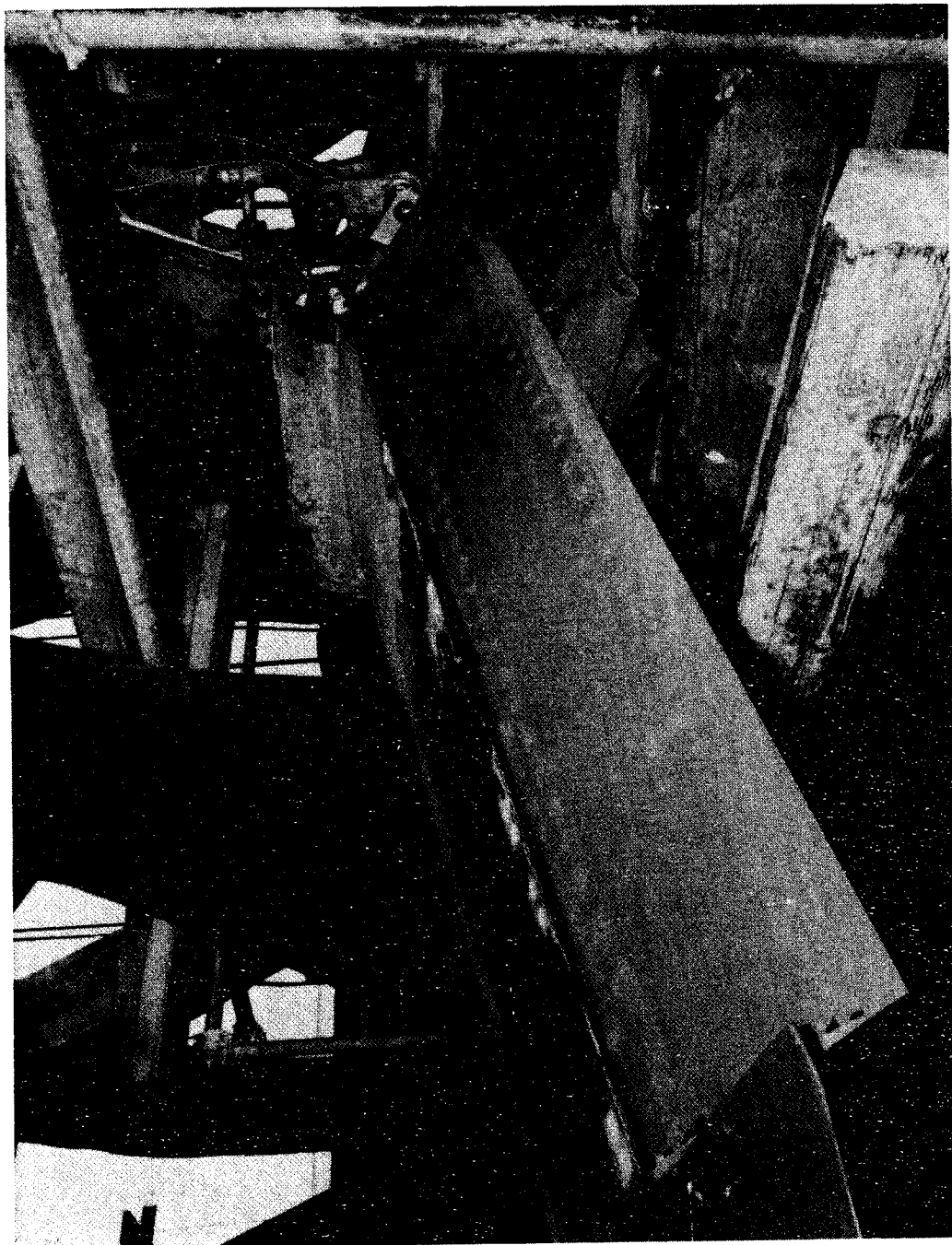


Figure 6 - Photograph of Installed Foil Flap

APPENDIX

MECHANICAL FAILURES PREVENTION GROUP

ADVANCED COMPOSITES:
DESIGN AND APPLICATIONS

29th MEETING

May 23-25, 1979

ATTENDANCE LIST

Jamil A. Abbasi
Federal Aviation Administration
800 Independence Avenue, SW
Washington, DC 20591

N. Ahmed
Perkin Elmer Co.
100 Wooster Heights
Mail Stop 823
Danbury, CT 06810

Arnold Anderjaska
Federal Aviation Administration
800 Independence Avenue, SW
Washington, DC 20591

Alfred J. Babecki
NASA/Goddard
Code 313
Greenbelt, MD 20771

D. M. Boyd
Lawrence Livermore Labs.
P. O. Box 808
Livermore, CA 94550

W. H. Browne, Jr.
NASA/Goddard
Code 731
Greenbelt, MD 20771

Harry C. Burnett
National Bureau of Standards
Materials Bldg., Room B264
Washington, DC 20234

James M. Candela
Naval Air Rework Facility
Naval Air Station
Norfolk, VA 23511

Frank J. Cepollina
NASA/Goddard
Greenbelt, MD 20771

F. H. Chang
General Dynamics, Ft. Worth Division
P. O. Box 748
Fort Worth, TX 76101

Stanley L. Channon/STD
Institute for Defense Analyses
400 Army-Navy Drive
Arlington, VA 22202

Rustam Chinoy
Mechanical Technology Inc.
968 Albany/Shaker Road
Latham, NY 12110

Peter J. Cloud
LNP Corp.
412 King Street
Malvern, PA 19355

J. A. Corrado
David W. Taylor Naval Ship
R&D Center
Code 1702
Bethesda, MD 20084

W. P. Couch
David W. Taylor Naval Ship
R&D Center
Annapolis, MD 21402

Clifford K. Deakyne
E. I. DuPont de Nemours & Co.
Chestnut Run, Bldg. 701
Wilmington, DE 19898

Jerry D. Deans
Naval Air Rework Facility
4361 Gadwall Pl.
Virginia Beach, VA 23462

Wallace J. Downs
General Electric Space Division
Valley Forge, PA 19481

Harold P. Edelstein
David W. Taylor Naval Ship
R&D Center
Code 2823
Annapolis, MD 21402

Gerard Emptoz
French Scientific Mission
2129 Wyoming Avenue, NW
Washington, DC 20008

Joseph D. Feko
Owens Corning Fiberglass Corp.
2075 W. Big Beaver Road
Suite 500
Troy, MI 48084

David S. Fine
Chevrolet Engineering Center
30003 Van Dyke, C-2-232
Warren, MI 48090

Aaron Fisher
NASA/Goddard
Code 313
Greenbelt, MD 20771

David R. Geise
Naval Air Engineering Center
GSED 92623
Lakehurst, NJ 08733

Joseph G. Gerber
General Dynamics-Fort Worth Div.
P. O. Box 748
Fort Worth, TX 76101

R. F. Gilby
E. I. DuPont de Nemours & Co.
Textile Fibers Dept.
Chestnut Run
Wilmington, DE 19898

Robert Gordon
Structural Composites Industries, Inc.
6344 N. Irwindale Avenue
Azusa, CA 91702

W. W. Gunkel
General Motors Inc.
Warren, MI 48090

Frank Guzzetta
Armco-Research Center
Curtis Street
Middletown, OH 45043

Steven G. Hackett
NASA/Goddard
Greenbelt, MD 20771

S. L. Hanlein
NASA/Goddard
Code 731
Greenbelt, MD 20771

James F. Haskins
General Dynamics, Convair Div.
P. O. Box 80847
San Diego, CA 92138

Henry R. Hegner
Mantech of New Jersey Corp.
2341 Jefferson Davis Highway
Suite 930
Arlington, VA 22202

Carl T. Herakovich
Virginia Polytechnic Inst. and
State University
120 Norris
Blacksburg, VA 24061

Robert R. Holden
Hughes Aircraft Co.
Bldg. 117, Mail Station 1
P. O. Box 90515
Los Angeles, CA 90009

G. H. Honeycutt
NASA/Goddard
Code 731
Greenbelt, MD 20771

W. D. Humphrey
Brunswick Corp., Defense Division
4300 Industrial Avenue
Lincoln, NB 68504

S. E. J. Johnsen
Detroit Diesel Allison Division
General Motors Corporation
Plant 8, T9
Indianapolis, IN 46206

Michael David Judd
Materials Section
Product Assurance Division
European Space Technology Center
Noordwijk, The Netherlands

Geza Kardos
Carleton University
Ottawa, Canada

S. D. Karmarkar
Metallic Materials Branch
Naval Surface Weapons Center
Dahlgren, VA 22448

J. J. Kelly
David W. Taylor Naval Ship
R&D Center
Annapolis, MD 21402

Ronald Khol
Machine Design
Penton Plaza
Cleveland, OH 44114

E. Kirchman
NASA/Goddard
Greenbelt, MD 20771

E. E. Klaus
133 Chemical Engineering Bldg.
The Pennsylvania State University
University Park, PA 16802

Karyn Knoll
2/LT, USFF
Air Force Materials Lab.
Wright Patterson Air Force Base
Ohio 45433

Hari Kulkarni
Ford Motor Co.
Scientific Research Labs
P. O. Box 2053
Dearborn, MI 48121

Arthur Lazarow, Jr.
Naval Air Engineering Office
Naval Air Station, Code 343
Norfolk, VA 23511

W. A. Leavy
NASA/Goddard
Code 731
Greenbelt, MD 20771

C. L. Leung
Rockwell Intl Science Center
1045 Camino Dos Rios
P. O. Box 1085
Thousand Oaks, CA 91360

Richard Margolis
Plastics Division, Rockwell Intl
1049 Camino Dos Rios
P. O. Box 1085
Thousand Oaks, CA 91360

R. E. Maringer
Battelle Columbus Labs
505 King Avenue
Columbus, OH 43201

Frank T. Martin
NASA/Goddard
Code 753
Greenbelt, MD 20771

P. W. Mast
Naval Research Laboratory
Washington, DC 20375

Robert H. McDonnell
NASA/Goddard
6407 McCahill Drive
Laurel, MD 20810

Ernest W. Mielke
NASA/Goddard
Code 313
Greenbelt, MD 20771

D. R. Mulville
Naval Research Laboratory
Washington, DC 20375

Robert L. Mumper
Trident Engineering Associates
48 Maryland Avenue
Annapolis, MD 21401

D. E. Murray
NASA/Goddard
Code 731
Greenbelt, MD 20771

H. C. Nash
Naval Research Laboratory
Washington, DC 20375

Earl Nicewarner
Fairchild Space & Electronics Co.
20301 Century Blvd., A-7
Germantown, MD 20760

Bryan R. Noton
Battelle Columbus Labs.
505 King Avenue
Columbus, OH 43201

Maurice A. Nygaard
NASA/Goddard
Code 741.2
Greenbelt, MD 20771

James S. O'Brien
NASA/Goddard
Greenbelt, MD 20771

Derek J. Palmer
Defense Equipment, Staff Matls
Officer
British Embassy
3100 Massachusetts Avenue, NW
Washington, DC 20008

John J. Park
NASA/Goddard
Code 313
Greenbelt, MD 20771

Elio Passaglia
National Bureau of Standards
Materials Bldg., Room B308
Washington, DC 20234

Chris Passerello
Michigan Tech. Univ.
Dept. of ME.-EM.
Houghton, MI 49931

William L. Phillips
Naval Research Laboratory
Washington, DC 20375

John A. Philosophos
Allis-Chalmers
P. O. Box 512
Milwaukee, WI 53201

R. D. Pistole
GTR Reinforced Plastics Co.
P. O. Box 966
Southfield, MI 48037

Chet Poranski
Naval Research Laboratory
Code 6110
Washington, DC 20375

J. Howard Powell
Rockwell International-Tulsa Div.
2000 N. Memorial Drive
Tulsa, OK 74151

Mark R. Probst
Harry Diamond Labs
U.S. Army, Branch 36200
2800 Powder Mill Road
Adelphi, MD 20783

Yapa D. S. Rajapakse
Naval Research Laboratory
Code 6371
Washington, DC 20375

Marwood E. Rand
Wyman-Gordon Company
Worcester Street
North Grafton, MA 01536

James J. Rast
NASA/Goddard
Greenbelt, MD 20771

Verlyn Reneau
Cessna Aircraft Co.
Wallace Division
P. O. Box 7704
Wichita, KS 67277

James Rinde
Lawrence Livermore Lab.
P. O. Box 808, L-338
Livermore, CA 94550

A. W. Ruff
National Bureau of Standards
Materials Bldg., Room B264
Washington, DC 20234

Depsek Sanghani
Perkin Elmer Corp.
100 Wooster Heights Road
Danbury, CT 06810

Donald K. Saylor
Union Carbide Corp.
12900 Snow Road
Parma, OH 44136

W. W. Schmidt
Brunswick Corp.
Defense Division
4300 Industrial Avenue
Lincoln, NB 68504

S. J. Schneider
National Bureau of Standards
Materials Bldg., Room B308
Washington, DC 20234

John J. Scialdone
NASA/Goddard
Code 725
Greenbelt, MD 20771

James N. Scott
NASA/Goddard
Code 302
Greenbelt, MD 20771

T. R. Shives
National Bureau of Standards
Materials Bldg., Room A111
Washington, DC 20234

M. Silvergleit
David W. Taylor Naval Ship
R&D Center
Annapolis, MD 21402

Charles O. Smith
Univ. of Nebraska
College of Engineering
60th & Dodge
Omaha, NE 68182

Joseph R. Soderquist
Federal Aviation Administration
800 Independence Avenue, SW
Washington, DC 20591

Lawrence R. Sparrow
COMSAT Labs.
P. O. Box 115
Clarksburg, MD 20734

Charles L. Staugaitis
NASA/Goddard
Greenbelt, MD 20771

Robert Stedfeld
Editor, Materials Engineering
1111 Chester Avenue
Cleveland, OH 44114

B. H. Stephenson
NASA/Goddard
Code 731
Greenbelt, MD 20771

J. E. Stern
NASA/Goddard
Code 721
Beltsville, MD 20771

L. D. Strege
NASA/Goddard
Code 731
Greenbelt, MD 20771

John L. Tarpley
NASA/Goddard
Code 313
Greenbelt, MD 20771

David F. Thompson
TM Development Inc.
Chester, PA 19013

Robert Y. Ting
Naval Research Laboratory
Chemistry Division
Washington, DC 20375

Charles E. S. Ueng
Georgia Institute of Technology
225 North Avenue, NW
Atlanta, GA 30332

Alfred F. Vargas
Acoustic Emission Technology Corp.
P. O. Box 408
Stratford, CT 06497

Charles E. Vest
NASA/Goddard
Code 313
Greenbelt, MD 20771

J. B. Wachtman
Director, Center for Matls Science
National Bureau of Standards
Washington, DC 20234

Jim Wadin
Dunegan/Endevco
Rancho Viejo Road
San Juan Capistrano, CA 92675

A. S. Wang
Drexel University
Dept. of Mechanical Engineering
and Mechanics
Philadelphia, PA 19104

Tony K. Wang
General Motors Corp.
GM Technical Center
Bldg. MD-A, #96
Warren, MI 48090

J. B. Webb
NASA/Goddard
Code 731
Greenbelt, MD 20771

W. A. Willard
National Bureau of Standards
Materials Bldg., Room B120
Washington, DC 20234

Irvin Wolock
Naval Research Laboratory
Washington, DC 20375

George Wuerch
Northwest Alaskan Pipeline Co.
1801 K Street, NW
Washington, DC 20036

H. W. Zussman
CIBA-GEIGY Corporation
Ardsley, NY 10502

MFPG PUBLICATIONS

Both printed and microfiche copies of the following MFPG publications (1-11) whose catalog numbers start with "AD" or "COM" may be obtained from the NTIS.

National Technical Information Service
5285 Port Royal Road
Springfield, VA 22151

1. Glossary of Terms AD 721 354
2. Proceedings of Meetings 1-9 (set of 5) AD 721 359

Meeting Nos. 1-5 Papers and discussion on failure
analysis and control.

Meeting No. 6 "Detection, Diagnosis and Prognosis",
December 6, 1968.

Meeting No. 7 "Failure Mechanisms as Identified
with Helicopter Transmissions",
March 27, 1969.

Meeting No. 8 "Critical Failure Problem Areas in
the Aircraft Gas Turbine Engine",
June 25-26, 1969.

Meeting No. 9 "Potential for Reduction of Mechanical
Failure Through Design Methodology",
November 5-6, 1969.
3. Proceedings of Meeting No. 10 AD 721 912
"Vibration Analysis Systems"
January 21-22, 1970
4. Proceedings of Meeting No. 11 AD 724 475
"Failure Mechanisms: Fatigue"
April 7-8, 1970
4. Proceedings of Meeting No. 12 AD 721 913
"Identification and Prevention of Mechanical
Failures in Internal Combustion Engines"
July 8-9, 1970

6. Proceedings of Meeting No. 13 AD 724 637
"Standards as a Design Tool in Surface
Specification for Mechanical Components
and Structures"
October 19-20, 1970
7. Proceedings of Meeting No. 14 AD 721 355
"Advances in Decision-Making Processes
in Detection, Diagnosis and Prognosis"
January 25-26, 1971
8. Proceedings of Meeting No. 15 AD 725 200
"Failure Mechanisms: Corrosion"
April 14-15, 1971
9. Proceedings of Meeting No. 16 AD 738 855
"Mechanical Failure Prevention Through
Lubricating Oil Analysis"
November 2-4, 1971
10. Proceedings of Meeting No. 17 AD 750 411
"Effects of Environment Upon Mechanical
Failures, Mechanisms and Detection"
April 25-27, 1972
11. Proceedings of Meeting No. 18 AD 772 082
"Detection, Diagnosis and Prognosis"
November 8-10, 1972
12. Proceedings of Meeting No. 19 (NBS SP 394) COM-74-50523
"The Role of Cavitation in Mechanical Failures"
October 21 - November 2, 1973

Printed copies of the following MFPG publications (catalog numbers starting with SN) may be obtained from the Government Printing Office.

Superintendent of Documents
U. S. Government Printing Office
Washington, DC 20402

Microfiche copies of these publications (catalog numbers starting with NBS-SP) may be obtained from NTIS.

13. Proceedings of Meeting No. 20 (NBS SP 423)
"Mechanical Failure - Definition of the Problem"
May 8-10, 1974
Cost: Printed copy \$6.10 SN003-003-01451-6

14. Proceedings of Meeting No. 21 (NBS SP 433)
"Success By Design: Progress Through
Failure Analysis"
November 7-8, 1974
Cost: Printed copy \$3.50 SN003-003-01639-0
Microfiche copy \$2.25 NBS-SP-433

15. Proceedings of Meeting No. 22 (NBS SP 436)
"Detection, Diagnosis and Prognosis"
April 23-25, 1975
Cost: Printed copy \$4.25 SN003-003-01556-3
Microfiche copy \$2.25 NBS-SP-436

16. Proceedings of Meeting No. 23 (NBS SP 452)
"The Role of Coatings in the Prevention
of Mechanical Failures"
October 29-31, 1975
Cost: Printed copy \$2.65 SN003-003-01664-1

17. Proceedings of Meeting No. 24 (NBS SP 468)
"Prevention of Failures in Coal
Conversion Systems"
April 21-24, 1976
Cost: Printed copy \$3.00 SN003-003-01760-4

18. Proceedings of Meeting No. 25 (NBS SP 487)
"Engineering Design"
November 3-5, 1976
Cost: Printed copy \$5.25 SN003-003-01829-5

19. Proceedings of Meeting No. 26 (NBS SP 494)
"Detection, Diagnosis and Prognosis"
May 17-19, 1977
Cost: Printed copy \$4.50 SN003-003-01844-9

20. Proceedings of Meeting No. 27 (NBS SP 514)
"Product Durability and Life"
November 1-3, 1977
Cost: Printed Copy \$3.75 SN003-003-01935-6

21. Proceedings of Meeting No. 28 (NBS SP 547)
"Detection, Diagnosis and Prognosis"
November 28-30, 1978
Cost: Printed Copy \$7.00 SN003-003-02083-4

U.S. DEPT. OF COMM. BIBLIOGRAPHIC DATA SHEET		1. PUBLICATION OR REPORT NO. SP 563	2. Gov't Accession No.	3. Recipient's Accession No.
4. TITLE AND SUBTITLE Advanced Composites: Design and Applications. Proceedings of the 29th Meeting of the Mechanical Failures Prevention Group, held at the National Bureau of Standards, Gaithersburg, Maryland, May 23-25, 1979			5. Publication Date October 1979	
			6. Performing Organization Code	
7. AUTHORS EDITORS T. Robert Shives and William A. Willard			8. Performing Organ. Report No.	
9. PERFORMING ORGANIZATION NAME AND ADDRESS NATIONAL BUREAU OF STANDARDS DEPARTMENT OF COMMERCE WASHINGTON, DC 20234			10. Project/Task/Work Unit No.	
			11. Contract/Grant No.	
12. SPONSORING ORGANIZATION NAME AND COMPLETE ADDRESS (Street, City, State, ZIP) Center for Matls Science, NBS, Washington, DC 20234; ONR, Arlington, VA 22217; NAVAIRSYSCOM (A.J. Koury), Washington, DC 20360; NASA, Greenbelt, MD 20771; DoE, Fossil Energy, Washington, DC 20545			13. Type of Report & Period Covered Final	
			14. Sponsoring Agency Code	
15. SUPPLEMENTARY NOTES Library of Congress Number 79-600151 <input type="checkbox"/> Document describes a computer program; SF-185, FIPS Software Summary, is attached.				
16. ABSTRACT (A 200-word or less factual summary of most significant information. If document includes a significant bibliography or literature survey, mention it here.) These proceedings consist of a group of thirty one submitted entries (twenty one papers and ten abstracts) from the 29th meeting of the Mechanical Failures Prevention Group which was held at the National Bureau of Standards in Gaithersburg, Maryland, May 23-25, 1979. The subject of the symposium was the design and application of advanced composites. Special emphasis was directed to aerospace, aircraft, automotive, marine, and industrial applications and design. Failure modes in advanced composites were also discussed.				
17. KEY WORDS (six to twelve entries; alphabetical order; capitalize only the first letter of the first key word unless a proper name; separated by semicolons) Advanced composites; applications of composites; composites; composite structures; design using composites; fiber composites; fiber glass; filament wound composites.				
18. AVAILABILITY <input checked="" type="checkbox"/> Unlimited <input type="checkbox"/> For Official Distribution. Do Not Release to NTIS <input checked="" type="checkbox"/> Order From Sup. of Doc., U.S. Government Printing Office, Washington, DC 20402, SD Stock No. SN003-003-02120-2 <input type="checkbox"/> Order From National Technical Information Service (NTIS), Springfield, VA, 22161		19. SECURITY CLASS (THIS REPORT) UNCLASSIFIED		21. NO. OF PRINTED PAGES 304
		20. SECURITY CLASS (THIS PAGE) UNCLASSIFIED		22. Price \$7.00

There's
a new
look
to...

DIMENSIONS

... the monthly magazine of the National Bureau of Standards. Still featured are special articles of general interest on current topics such as consumer product safety and building technology. In addition, new sections are designed to . . . **PROVIDE SCIENTISTS** with illustrated discussions of recent technical developments and work in progress . . . **INFORM INDUSTRIAL MANAGERS** of technology transfer activities in Federal and private labs. . . **DESCRIBE TO MANUFACTURERS** advances in the field of voluntary and mandatory standards. The new DIMENSIONS/NBS also carries complete listings of upcoming conferences to be held at NBS and reports on all the latest NBS publications, with information on how to order. Finally, each issue carries a page of News Briefs, aimed at keeping scientist and consumer alike up to date on major developments at the Nation's physical sciences and measurement laboratory.

(please detach here)

SUBSCRIPTION ORDER FORM

Enter my Subscription To DIMENSIONS/NBS at \$11.00. Add \$2.75 for foreign mailing. No additional postage is required for mailing within the United States or its possessions. Domestic remittances should be made either by postal money order, express money order, or check. Foreign remittances should be made either by international money order, draft on an American bank, or by UNESCO coupons.

Send Subscription to:

NAME-FIRST, LAST																													
COMPANY NAME OR ADDITIONAL ADDRESS LINE																													
STREET ADDRESS																													
CITY															STATE					ZIP CODE									

PLEASE PRINT

- ☐ Remittance Enclosed
(Make checks payable
to Superintendent of
Documents)
- ☐ Charge to my Deposit
Account No.

MAIL ORDER FORM TO:
Superintendent of Documents
Government Printing Office
Washington, D.C. 20402

U.S. DEPARTMENT OF COMMERCE
National Bureau of Standards
Washington, D.C. 20234

OFFICIAL BUSINESS

Penalty for Private Use, \$300

POSTAGE AND FEES PAID
U.S. DEPARTMENT OF COMMERCE
COM-215



SPECIAL FOURTH-CLASS RATE
BOOK